Peter J. Irvine

Climatic Effects of Solar Radiation Management Geoengineering

A dissertation submitted to the University of Bristol in accordance with the requirements of the degree of Doctor of Philosophy in the Faculty of Science.
School of Geographical Sciences, May 2012

Summary

Geoengineering, intentional large-scale manipulation of the Earth-system, has been proposed as a means to ameliorate the impacts of global warming. There are two approaches; Carbon Dioxide Removal (CDR) geoengineering which would reduce CO_2 concentrations and address the cause of climate change, and Solar Radiation Management geoengineering which would cool the planet by reducing the amount of sunlight absorbed by the planet without affecting CO_2 concentrations. This thesis reviews geoengineering and investigates the direct and indirect climate effects of SRM geoengineering.

The sunshade geoengineering scheme, which would reduce the solar insolation, is investigated in depth in this thesis. Sunshade geoengineering may be implemented at a range of CO_2 concentrations and it would also offer control over the amount of insolation that reaches the planet. Both of these aspects of sunsahde geoengineering are investigated using a climate model and it is found that sunshade geoengineering would ameliorate most of the effects of elevated CO_2 but would cause heterogeneous changes in climate; globally reducing precipitation and leaving many regions with a climate markedly different from the pre-industrial. The regional climate effects of sunshade geoengineering are found to vary linearly with both the solar insolation reduction and the CO_2 forcing applied.

An off-line ice-sheet model is used to investigate the indirect climate effects of different strengths of sunshade geoengineering on the Greenland Ice-Sheet at quadrupled CO_2 levels, to determine whether sunshade geoengineering could stabilize the ice-sheet and reduce sea-level rise. It is found that the ice-sheet would eventually collapse at quadrupled CO_2 levels but that strong sunshade geoengineering can stabilize the entire ice-sheet or at weaker implementations, part of the ice-sheet could be maintained.

A comparison is made between the urban, crop and desert surface albedo geoengineering schemes, which would have a highly heterogeneous radiative forcing effect, and sunshade geoengineering, which would have a more homogeneous radiative forcing effect. This comparison shows that regional geoengineering forcing, if it

is relatively weak, may provide local and regional cooling and other benefits but for stronger land albedo forcing there are large shifts in precipitation, including substantial reductions in monsoon precipitation, which could prove to be more harmful than the effects of global warming.

Finally, to determine the robustness of the results in this thesis, a perturbed parameter ensemble is developed, tested and then used to investigate the effects of parametric uncertainty on the sunshade geoengineering climate effects. The perturbed parameter results agree with much of what was found in other parts of the thesis about sunshade geoengineering but finds that there is uncertainty in the residual warming at the poles, the magnitude of the northward shift of the ITCZ, and that the standard climate model may have overestimated the effectiveness of sunshade geoengineering at maintaining the Greenland Ice-Sheet.

Overall, I find that SRM geoengineering could offer a considerable amelioration of the impacts of global warming; however, the climate would differ substantially from a low-CO_2 climate, and there would be winners and losers as a result. Regional SRM geoengineering would have very heterogeneous climate impacts, potentially causing large problems but could offer a large degree of control over the climate. Whether the political risks that control over the climate could bring would outweigh the potential climate benefits, is an open question.

Acknowledgements

I'd like to thank my supervisors, Andy Ridgwell and Dan Lunt, for all the help and support they offered over the course of the PhD. Thanks to all those who helped directly with the content of this PhD: Andy Ridgwell, Dan Lunt, Paul Valdes, Joy Singarayer, Emma Stone, Lauren Gregoire, Klaus Keller, and Ryan Sriver. I'd also like to thank my other collaborators: Toby Svodoba, Elena Couce, Nany Tuana, Roman Olson, and Jacob Haqq-Misra. This thesis was funded by a NERC studentship and part of the work was supported by a Worldwide Universities Network Research Mobility Program grant.

I'd also like to thank the members of my annual progress panels; John Bamber, Sandy Harrison, and Joy Singarayer, for their advice. Thanks to Gethin Williams and Greg le Tourte who helped resolve a number of technical computing problems, Ed Thomas and Duncan Baldwin for managing the computer resources, and the HPC team for maintaining the supercomputer. I'd like to thank Emma Stone for helping me to get started with the PhD, Jonny Day, Lauren Gregoire, and many other PhD students for their expertise and advice over the course of the PhD. I'm grateful to Paul Valdes and Jonty Rougier for the various discussions on climate modelling and uncertainty that we've had.

My thanks go out to Klaus and Irene Keller, Ryan Sriver, Nancy Tuana, Toby Svodoba and Roman Olson for making my time at Penn State University productive, interesting and enjoyable. Thanks must be given to Andy Heaps for developing the IDL routines used for all the figures. I'd also like to thank my proof readers: Catherine Bradshaw, Claire Lopston, Sarah Jones and Mathieu depoorter.

Carly, thanks for all the support you gave me during the PhD and for making my time in Bristol fantastic. Dad, thanks for answering all my daft questions when I was younger and getting me interested in science in the first place. Mum, thanks for the support and understanding you've given me through the years. Mike and Jenny, thanks for being there and making things more fun.

Author's Declaration

I declare that the work in this dissertation was carried out in accordance with the Regulations of the University of Bristol. The work is original, except where indicated by special reference in the text, and no part of the dissertation has been submitted for any other academic award. Any views expressed in the dissertation are those of the author.

SIGNED: ..... DATE:.....

Contents

List of Figures **10**

List of Tables **12**

Chapter 1 : Introduction **13**

1.1 General aims and methodology of thesis 13

1.2 Background 13

1.3 Solar Radiation Management geoengineering overview 18

1.3.1 Sunshade geoengineering 23

1.3.2 Stratospheric aerosol geoengineering 26

1.3.3 Cloud albedo geoengineering 28

1.3.4 Urban albedo geoengineering 29

1.3.5 Crop albedo geoengineering 31

1.3.6 Desert albedo geoengineering 32

1.3.7 Micro-bubble geoengineering 32

1.3.8 Cirrus cloud modification geoengineering 33

1.4 Carbon Dioxide Removal geoengineering overview 33

1.4.1 Afforestation and reforestation 34

1.4.2 Biochar and bioenergy with carbons sequestration (BECS) . 36

1.4.3 Air capture geoengineering 36

1.4.4 Ocean fertilization geoengineering 37

1.4.5 Enhanced weathering 38

1.4.6 CDR summary 39

1.5 Methodological approach 39

1.6 Aims and objectives 40

1.7 Thesis structure 42

Chapter 2 : Methodology and sunshade geoengineering **45**

2.1 Cover sheet 45

2.2 Introduction 47
2.3 Modelling approach 51
2.4 Experimental approach 55
2.5 Assessing the regional disparities in geoengineering impacts 58
2.5.1 Abstract 58
2.5.2 Introduction 58
2.5.3 Methodology 59
2.5.4 Results 60
2.5.5 Discussion and conclusions 66
2.5.6 The linearity of the climate response to a range of strengths of sunshade geoengineering 68
2.6 The fate of the Greenland Ice Sheet in a geoengineered, high CO_2 world 70
2.6.1 Abstract 70
2.6.2 Introduction 71
2.6.3 Methodology 72
2.6.4 Results 74
2.6.5 Discussion and conclusions 79
2.7 Sunshade geoengineering at diverse CO_2 levels with HadCM3 and HadCM3L 82
2.7.1 Introduction 82
2.7.2 Comparison of HadCM3 and HadCM3L 83
2.7.3 Sunshade geoengineering at different CO_2 concentrations . . 86
2.7.4 Response of ENSO to sunshade geoengineering 88
2.7.5 Temperature and sea-level response of an EMIC to a range of sunshade geoengineering scenarios 93
2.8 Summary and conclusion 93

Chapter 3 : Climatic effects of surface albedo geoengineering 96

3.1 Cover sheet 96
3.2 Abstract 97
3.3 Introduction 98
3.3.1 Summary and chapter outline 99
3.4 Methodology 100

3.4.1 Urban albedo modification . . . 103
3.4.2 Crop albedo modification . . . 104
3.4.3 Desert albedo modification . . . 105
3.5 Results . . . 106
3.5.1 Global effects . . . 107
3.5.2 European summertime changes . . . 114
3.5.3 Monsoon changes . . . 117
3.5.4 Arctic changes . . . 123
3.6 Discussion and conclusion . . . 125

Chapter 4 : Development of a perturbed parameter ensemble with an application to SRM geoengineering 129

4.1 Cover sheet . . . 129
4.2 Abstract . . . 130
4.3 Introduction . . . 131
4.3.1 Motivation for SRM geoengineering application . . . 135
4.4 Methodology . . . 135
4.4.1 HadCM3 model description . . . 135
4.4.2 Ensemble design . . . 136
4.4.3 Experimental setup . . . 139
4.5 Results . . . 140
4.5.1 Basic performance . . . 140
4.5.2 Pre-industrial control . . . 142
4.5.3 Elevated CO_2 experiments . . . 150
4.5.4 Sunshade geoengineering results . . . 158
4.6 Discussion . . . 162
4.7 Conclusion . . . 169
4.8 Implications for thesis . . . 170

Chapter 5 : Conclusion 173

5.1 Introduction . . . 173
5.2 Summary of work . . . 173
5.2.1 Sunshade geoengineering . . . 173

5.2.2 Greenland Ice Sheet and sea-level rise response to sunshade geoengineering . . . 175
5.2.3 Comparison of surface albedo modification and sunshade geoengineering . . . 176
5.2.4 Development and testing of a perturbed parameter ensemble of HadCM3 . . . 178
5.2.5 Sunshade geoengineering parametric uncertainty . . . 180
5.3 Contribution of thesis . . . 181
5.4 Future work . . . 182
5.5 Final thoughts . . . 185

Bibliography **188**

Appendix A : Appendix A **221**
A.1 IRVINE, P. & RIDGWELL, A. 2009. 'Geoengineering' - taking control of our planet's climate. Science Progress, **92**, 139-162. . . . 221

Appendix B : Appendix B **222**
B.1 SINGARAYER, J. S., RIDGWELL, A. & IRVINE, P. 2009. Assessing the benefits of crop albedo bio-geoengineering. Environmental Research Letters, **4**, 8. . . . 222

Appendix C : Appendix C **223**
C.1 IRVINE, P. J., SRIVER, R. L. & KELLER, K. 2012. Tension between reducing sea-level rise and global warming through solar radiation management. Nature Clim. Change, **2**, 2. . . . 223

List of Figures

1.1 IPCC SRES temperature projections. 16
1.2 IPCC 'reasons for concern' 17
1.3 Global mean temperature response to volcanic eruptions. 21
1.4 Diagram showing a number of SRM geoengineering schemes. 22
1.5 Regions of SRM geoengineering application. 23
1.6 Diagram showing a number of CDR geoengineering schemes. 34

2.1 Zonal climate anomaly at different sunshade levels. 60
2.2 Regional precipitation response to different sunshade levels. 62
2.3 Global-mean and 'novel' climate response to sunshade geoengineering. 65
2.4 novel climate diagram 66
2.5 Climate anomaly at different sunshade levels. 69
2.6 Greenland climate anomalies at different sunshade levels 75
2.7 Seasonal Greenland-mean climate anomalies. 76
2.8 Greenland Ice-Sheet state in pre-industrial and at high-CO_2. 77
2.9 Greenland Ice-Sheet state at different sunshade levels. 78
2.10 Change in Greenland Ice-Sheet volume in response to sunshade geoengineering. 79
2.11 Evolution of the Greenland Ice-Sheet volume. 80
2.12 Comparison of the climates of HadCM3 and HadCM3L. 85
2.13 Global-mean climate response to sunshade geoengineering at different CO_2 levels. 87
2.14 Temperature anomaly response to sunshade geoengineering at high-CO_2. 89
2.15 Precipitation anomaly response to sunshade geoengineering at high-CO_2. 90
2.16 ENSO response to sunshade geoengineering. 92

3.1 Surface albedo geoengineering regions. 102

3.2 Temperature anomaly for a range of surface albedo geoengineering schemes. 110
3.3 Precipitation anomaly for a range of surface albedo geoengineering schemes. 112
3.4 Histogram of European summer temperatures for different surface albedo geoengineering schemes. 116
3.5 Seasonality of precipitation for surface albedo geoengineering. 119
3.6 Desert albedo geoengineering circulation and precipitation changes. . 120
3.7 Histogram of Indian precipitation for surface albedo geoengineering. 122
3.8 Snow and sea-ice cover response to surface albedo geoengineering. . 124

4.1 Projected temperatures for initial ensemble members. 141
4.2 Evolution of climate variables during pre-industrial control. 143
4.3 Relationship of pre-industrial temperature and two parameters. . . . 144
4.4 Relationship between cloud fraction and ice-fall speed. 145
4.5 Effect of vertical ocean diffusivity on temperature and ocean heat flux. 145
4.6 Ocean profiles for PPE. 146
4.7 Atlantic overturning strength of PPE. 147
4.8 Zonal plots comparing PPE and CMIP3 ensemble. 148
4.9 Vertical plots comparing PPE and CMIP3 ensemble. 149
4.10 Change in vertical profile of PPE at high-CO_2. 152
4.11 Relationship between high-altitude humidity and the entrainment rate coefficient. 154
4.12 Evolution of climate at high-CO_2. 155
4.13 Relationship between pre-industrial temperature and climate sensitivity. 156
4.14 Gregory plots of PPE at high-CO_2. 156
4.15 Histograms of climate sensitivity and other metrics for PPE. 158
4.16 Evolution of climate variables at high-CO_2 with sunshade geoengineering. 159
4.17 Zonal mean anomalies of PPE for sunshade geoengineering. 161
4.18 Ensemble-mean climate anomalies for sunshade geoengineering. . . . 163
4.19 List of parameter values and climate indicators for PPE. 164

List of Tables

1.1 List of the pros and cons of SRM and CDR geoengineering 18

1.2 Summary of the pros, cons, risks and costs of SRM geoengineering. . 24

1.3 Summary of the pros, cons, risks and costs of CDR geoengineering. . 35

3.1 Area affected and albedo increase for geoengineering schemes. 103

3.2 Annual average aurface air temperature and precipitation change. . . 108

3.3 Surface air temperature change in Western Europe 115

3.4 Precipitation change in monsoon regions. 120

4.1 Parameter values for PPE members. 138

CHAPTER 1

Introduction

1.1 General aims and methodology of thesis

The aim of this thesis is to investigate the climatic effects of Solar Radiation Management (SRM) geoengineering using a General Circulation Model (GCM). There are two types of geoengineering, Carbon Dioxide Removal (CDR) geoengineering and SRM geoengineering, the first would lower CO_2 concentrations, addressing the cause of global warming, and the second would cool the climate by altering the Earth's energy balance, addressing some of the effects of elevated CO_2 concentrations. CDR geoengineering would lower CO_2 concentrations and is similar to traditional mitigation; the success or failure of CDR geoengineering would thus be determined by the magnitude of the CO_2 drawn down and the cost of doing so. SRM geoengineering would alter the climate and its success or failure must be determined by analyzing its potential climate effects to determine whether they are beneficial or harmful. SRM geoengineering is analyzed in this thesis as little is known about the climatic effects of SRM geoengineering, whereas much is known about the climatic effects of CDR geoengineering, i.e. changing concentrations of CO_2. Using GCM models to estimate the climatic consequences of SRM geoengineering will help to determine whether it may be an appropriate measure to reduce the harms of global warming.

1.2 Background

The extent of man-made land-surface changes, deliberate and unintentional extinctions, and industrial emissions have led some to suggest that we have entered a new geological period, the Anthropocene, one in which human influence dominates natural factors in determining the geology of our planet (Steffen *et al.*, 2007). Humans have been affecting the Earth's climate for thousands of years by clearing and burning forests and developing agricultural lands (Taylor *et al.*, 2002; Betts *et al.*, 2007a); changing the albedo of the land surface (Pongratz *et al.*, 2011); and releasing carbon stored in soils and emitting methane from paddy fields (Watson *et al.*, 2000;

Etheridge *et al.*, 1998). Since the industrial revolution the emission of anthropogenic greenhouse gases, particularly from the burning of fossil fuels, has become the dominant driver of anthopogenic climate change (Steffen *et al.*, 2007; IPCC, 2007). These historical anthropogenic influences unknowingly shaped our planet but now we are in a position to understand our influence on the planet and to act on that knowledge.

The anthropogenic influence on the concentrations of the most important greenhouse gases (GHGs) is clear: CO_2 concentrations were 385 ppm in 2008 up from ∼280 ppm in the pre-industrial (Le Quere *et al.*, 2009); methane levels were 1774 ppb in 2005 up from ∼700 ppb (Etheridge *et al.*, 1998); and N_2O levels were 319 ppb up from ∼275 ppb (Machida *et al.*, 1995; IPCC, 2007). Anthropogenic aerosol emissions have also risen dramatically since the pre-industrial, most notably sulphate aerosols which are exerting a large, but uncertain, cooling on the climate (Kiehl, 2007; Hansen *et al.*, 1997; Quaas *et al.*, 2009; Ramanathan *et al.*, 2001). To limit the anthropogenic influence on the climate, emissions of these radiatively active species need to be cut. Of all of the GHGs CO_2 poses the greatest challenge; it exerts the greatest total radiative forcing of any greenhouse gas today and it has a very long lifetime in the atmosphere as it does not rain out or chemically decompose, like many other anthropogenic emission species (Archer *et al.*, 2009). The fate of CO_2 emissions is determined by the carbon cycle which initially redistributes the surplus CO_2 from the atmosphere into the land surface and ocean, and eventually into the lithosphere. CO_2 which is dissolved in the ocean will increase the acidity of the surface waters; since the pre-industrial the pH of the ocean surface waters has dropped by ∼0.1 units and may drop by a further 0.3 - 0.4 units by 2100 with unknown consequences on ocean ecosystems (Doney *et al.*, 2009). Simulations of the lifetime of fossil fuel CO_2 find that 20 - 35% of the CO_2 remains in the atmosphere after equilibration with the ocean which takes hundreds of years. Mineralization, which draws the atmospheric fraction down further, takes thousands of years and brings the CO_2 concentration back into equilibrium (Archer *et al.*, 2009). Due to the longevity of CO_2 in the atmosphere, the CO_2 emissions of the few generations since the industrial era will leave a legacy which will last for thousands of years.

These historical emissions are already having an observable effect on the planet, which has warmed by 0.76 +/- 0.19 °C between the periods 1850-1899 and 2001-2005 (IPCC, 2007). Future changes are likely to be much greater; the IPCC's 4th

Assessment Report concluded that the global temperature change by 2100 would likely range from 1.1 to 6.4 °C, depending on the climate sensitivity of the Earth and on the emissions pathway followed (IPCC, 2007), see figure 1.1. Temperatures will not rise uniformly and larger temperature increases are expected at higher latitudes due to sea-ice and snow-cover change feedbacks (Johannessen *et al.*, 2004; Hinzman *et al.*, 2005; Arndt *et al.*, 2011). The hydrological cycle is also expected to intensify with evaporation and precipitation increasing (Bala *et al.*, 2010b; Andrews *et al.*, 2010; Arndt *et al.*, 2011), and with precipitation events becoming more intense (Pall *et al.*, 2011). There will also likely be shifts in the patterns of precipitation, with dry regions becoming drier and wet regions becoming wetter on the whole (IPCC, 2007; Trenberth, 2011). Some extreme climate events such as heatwaves, floods and droughts are expected to become more frequent and more intense, whereas others such as extremes of cold are expected to become less frequent and less intense (Stott *et al.*, 2004; Schar *et al.*, 2004; Meehl and Tebaldi, 2004; Tebaldi *et al.*, 2006; IPCC, 2007). These kinds of climate changes could have a large impact on human health and wellbeing, and cause great damage to ecosystems and biodiversity (Leemans and Eickhout, 2004; Schar *et al.*, 2004; Held *et al.*, 2005; IPCC, 2007).

The effects of agriculture, industry and other human activities on the composition of the atmosphere have grown to such an extent that without serious action dangerous changes in the climate may occur in the next century (Hansen *et al.*, 2007). To limit global warming to 2°C or less, a target proposed by the European Union (CEC, 2007), some authors predict that emissions reductions of 90% by 2050 may be required (Weaver *et al.*, 2007). However, efforts to mitigate CO_2 emissions so far have been relatively ineffectual; global emissions of GHGs increased by 29% between 2000 and 2008 to 8.7 PgC yr^{-1}, reduced in 2009 by 1.3% as a result of the economic crisis and are projected to have grown during 2010 by more than 3% (Le Quere *et al.*, 2009; Friedlingstein *et al.*, 2010). The lack of concerted action on emissions of GHGs and the potentially dire consequences of unmitigated climate change, has led some to suggest that an alternative is needed (Crutzen, 2006).

If serious action to reduce emissions is not taken within the next few decades then the planet will likely warm by more than 2 °C, a level some have defined as being the threshold for dangerous climate change (Weaver *et al.*, 2007; Schneider, 2001; Vaughan *et al.*, 2009). Figure 1.2 shows 'reasons for concern' identified in

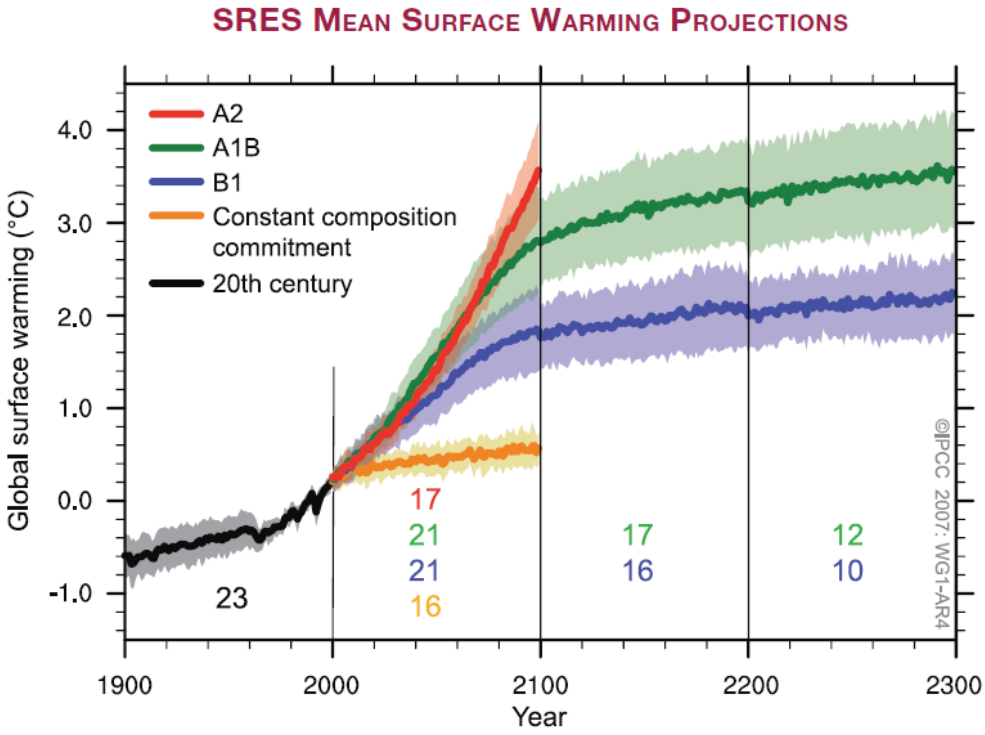

Figure 1.1: Multi-model means of surface warming (compared to the 1980-1999 base period) for the SRES scenarios A2 (red), A1B (green) and B1 (blue), shown as continuations of the 20th-century simulation. The latter two scenarios are continued beyond the year 2100 with forcing kept constant (committed climate change as it is defined in Box TS.9). An additional experiment, in which the forcing is kept at the year 2000 level is also shown (orange). Linear trends from the corresponding control runs have been removed from these time series. Lines show the multi-model means, shading denotes the ± 1 standard deviation range. Discontinuities between different periods have no physical meaning and are caused by the fact that the number of models that have run a given scenario is different for each period and scenario (numbers indicated in figure). For the same reason, uncertainty across scenarios should not be interpreted from this figure (see Section 10.5 for uncertainty estimates). figure 10.4 (Reproduced with permission from Climate Change 2007: Technical Summary. Contribution of Working Group I to the Fourth Assessment Report of the Intergovernmental Panel on Climate Change. Figure TS.32. Cambridge University Press.)(IPCC, 2007)

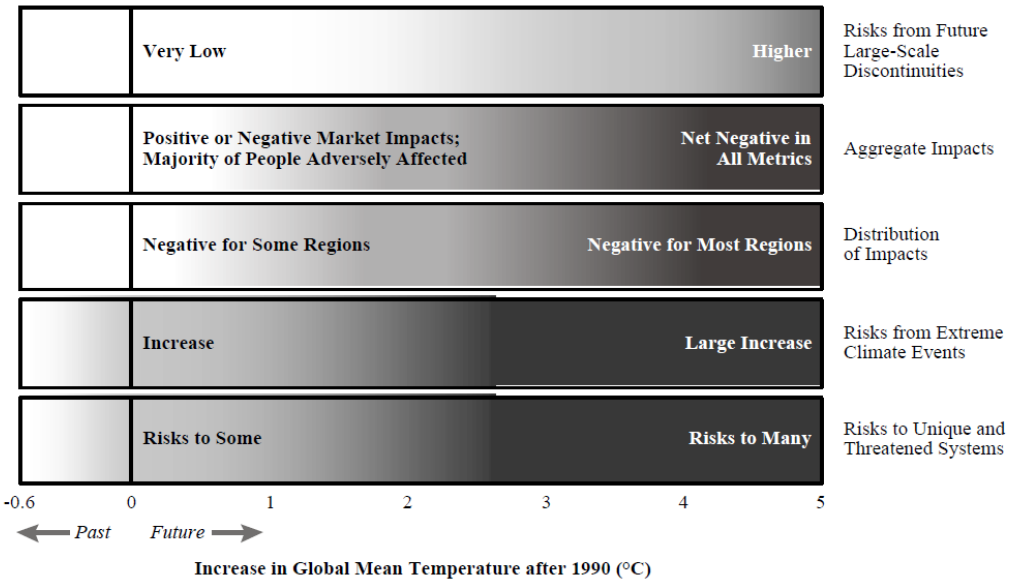

Figure 1.2: Impacts of or risks from climate change, by reason for concern. Each row corresponds to a reason for concern; shades correspond to severity of impact or risk. White means no or virtually neutral impact or risk, light fray means somewhat negative impacts or low risks, and gray means more negative impacts or higher risks. Global average temperatures in the 20th century increased by 0.6°C and left to some impacts. Impacts are plotted against increases in global mean temperature after 1990. This figure addresses only how impacts or risks change as thresholds of increase in global mean temperature are crossed, not how impacts or risks change at different rates of change in climate. Temperature should be taken as approximate indications of impacts, not as absolute thresholds. (Reproduced with permission from Climate Change 2001: Impacts, Adaptation and Vulnerability. Contribution of Working Group II to the Third Assessment Report of the Intergovernmental Panel on Climate Change. Figure 19-7. Cambridge University Press.)(Smith *et al.*, 2009)

the third Intergovernmental Panel on Climate Change (IPCC) (Smith *et al.*, 2009). If action is not taken on mitigating GHG emissions soon enough; we could turn to a radical alternative: 'geoengineering, the intentional large-scale manipulation of the environment, particularly manipulation that is intended to reduce undesired anthropogenic climate change' (Keith, 2000).

There are two types of geoengineering; Carbon Dioxide Removal (CDR) schemes, which would reduce the concentrations of CO_2 in the atmosphere; and Solar Radiation Management (SRM) schemes, which would reduce the amount of solar energy absorbed by the planet and lower temperatures. CDR geoengineering addresses the cause of climate change, elevated GHG concentrations, whereas SRM geoengineering would cool the planet and alter the climate. Table 1.1 gives a summary of the general pros and cons of the two approaches. There are many different CDR and SRM geoengineering schemes with their own properties which are described below.

The rest of this chapter overviews the main SRM and CDR geoengineering

	SRM geoengineering	CDR geoengineering
Pros	- Fast-acting - Potentially cheap - Large cooling effect	- Addresses the cause (CO_2) - Few negative consequences - Many low-tech solutions
Cons	- Potential direct and unanticipated negative consequences - Unknown climate effects - Elevated CO_2 levels and ocean acidification	- Slow-acting - Expensive - Potentially energy intensive

Table 1.1: List of the pros and cons of SRM and CDR geoengineering

schemes in Sections 1.3 and 1.4. Section 1.5 describes the general methodological approach of this thesis. Section 1.6 lists the aims and objectives of the thesis, and Section 1.7 details the structure of the thesis. Some of the material in Section 1.3 and 1.4 adapts text used in a general overview of geoengineering that I wrote with Andy Ridgwell (Irvine and Ridgwell, 2009) that is included as Appendix A, and the urban, crop and desert geoengineering subsections of Section 1.3 appear in Irvine *et al.* (2011). The full details of the contributions of myself and other authors to these sections appear in Appendix A and in Section 3.1 of Chapter 3.

1.3 Solar Radiation Management geoengineering overview

Instead of reducing the human influence on the climate, SRM geoengineering would alter the Earth's energy budget; the increase in longwave radiative forcing of elevated greenhouse gas concentrations would be counteracted by a reduction in the shortwave or longwave radiative forcing. Many of the SRM schemes that have been proposed could be cheap, could exert a large cooling effect and could halt or reverse warming within years of deployment (Robock *et al.*, 2009; Lenton and Vaughan, 2009). This potential for SRM geoengineering schemes to offer control over the magnitude and rate of global temperature change at relatively little cost, has made it seem like an attractive solution to global warming for some and a potentially dangerous threat to our future for others (Jamieson, 1996; Robock, 2008; Barrett, 2008). In either case, if SRM geoengineering is realized it would constitute a great shift in the relation between mankind and the natural environment.

Large volcanic eruptions provide a natural analogue for shortwave SRM geoengineering as they cause an increase in aerosol optical depth in the atmosphere, reducing the amount of sunlight reaching the surface and cause cooling and other

climate changes (Trenberth and Dai, 2007). Reviewing the climate response to volcanic eruptions will provide some information which will be relevant to the potential climate response to SRM geoengineering. Figure 1.3 shows that large volcanic eruptions, those which inject substantial amounts of material into the stratosphere, have played a large role in 20th century climate, causing cooling of a few tenths of a degree Celsius for a number of years (IPCC, 2007; Trenberth and Dai, 2007). The 1815 Tambora eruption and another large eruption in 1809 caused an unusually cold decade, the coldest in 500 years in some regions, and is responsible for the 'year without a summer' (1816) which affected Europe and other regions (Stothers, 1984; Cole-Dai *et al.*, 2009). Model simulations have found a simple relationship between volcanic aerosol optical depth and the maximum cooling after a large explosive eruption which injects material into the stratosphere, finding that cooling does not scale linearly with eruption size and instead that the global annual-mean cooling may saturate at around 11.5 K (Harris and Highwood, 2011). Simulations of Laki and other high-latitude volcanic eruptions find that they cause a reduction in the intensity of the African and Asian monsoons (Oman *et al.*, 2006, 2005). Following the 1783-1784 Laki eruption, the largest high-latitude volcanic eruption in 1000 years (Thordarson and Self, 2003), there was a large reduction in the flow of the Nile causing a severe drought and famine in Egypt (Oman *et al.*, 2006). Studies of the 1991 Pinatubo eruption find that continental precipitation and runoff were reduced after the eruption (Trenberth and Dai, 2007). Simulations also show that monsoon intensity is reduced after such eruptions, perhaps driven by the greater cooling over the land, setting up a land-sea temperature contrast (Joseph and Zeng, 2011). Trenberth and Dai (2007) warn that as SRM geoengineering may cause changes similar to volcanic eruptions and that it could lead to drought and reduced freshwater resources across the globe. However, volcanic eruptions only exert a short-lived effect on the climate system whereas SRM geoengineering would exert a continuous effect. MacMynowski *et al.* (2011) investigated the effects of periodic solar insolation reductions and found a large reduction in the intensity of the Asian monsoon for annual variations but not for longer period variations and continuous forcing. The climate response to volcanic eruptions provides some insights into the climatic effects that SRM geoengineering may have. Hoewever, the analogy is not perfect and robust conclusions about all of the effects of continuous SRM geoengineering cannot

be drawn from these volcano-analogy studies due to the transitory nature of the forcing from volcanic eruptions.

SRM geoengineering, like volcanic eruptions, would cool the planet but would not alter other effects of elevated CO_2 on the planet. CO_2, being one of the inputs for photosynthesis can boost the productivity of plants and may increase the strength of the terrestrial carbon sink (Le Quere *et al.*, 2009). Elevated CO_2 levels cause plants to produce fewer stomata, pores which allow the passage of gas and moisture into and out of the leaf, which results in plants losing less moisture (Cao *et al.*, 2010). This CO_2-induced physiological response has an effect on regional scale evapotranspiration, latent heat flux, and can reduce the recycling of precipitation over land and raise temperatures (Cao *et al.*, 2010; Betts *et al.*, 2007b; Boucher *et al.*, 2009). Ocean acidification would remain largely unaffected by geoengineering (Matthews *et al.*, 2009), and is expected to harm shelled sea-creatures and coral reefs (Doney *et al.*, 2009). CO_2 is also known to cause a cooling of the stratosphere whilst warming the troposphere which will change the chemistry of the stratosphere and affect ozone concentrations (Tilmes *et al.*, 2008; Govindasamy *et al.*, 2003).

SRM geoengineering would create a negative shortwave or longwave radiative forcing and would cool the planet but would not directly affect the longwave radiative forcing from GHGs or alter other effects of elevated CO_2 concentrations on the planet. Thus the climatic consequences of SRM geoengineering are central to understanding whether SRM geoengineering is an appropriate response to climate change. There are many proposed SRM geoengineering schemes and the nature of their climate consequences will be very different; taken together they offer an inherently limited, but still great, possibility of control over the climate. The Anthropocene so far has been shaped by an unknowing human influence on the planet, today it is largely being shaped by the known but unintended consequences of our activities, and in the future SRM geoengineering and other technologies may offer the possibility of a truly man-made planet.

This thesis aims to explore the consequences of SRM geoengineering on the climate and its effect on other Earth-system processes, i.e. sea-level rise and ice-sheet stability. The focus is on SRM geoengineering because its purpose is to alter the energy budget in response to elevated CO_2 levels thus creating novel boundary conditions for the climate. CDR geoengineering is not analysed becuase it would

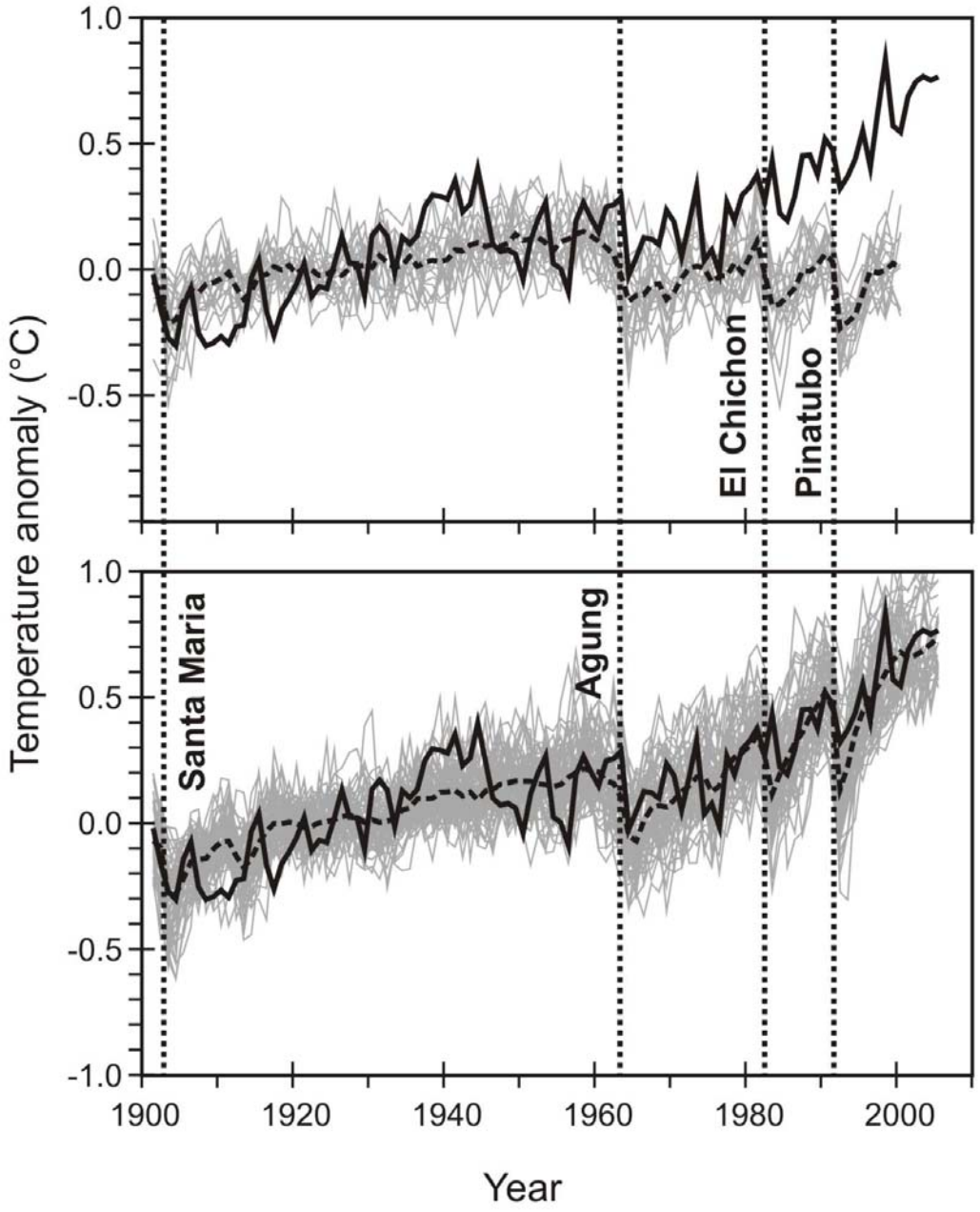

Figure 1.3: Diagram showing a comparison between observed and model-predicted global mean surface temperatures since 1900. The upper panel shows the individual predictions of a range of atmospheric GCMs (thin grey lines) when including only solar variability and volcanic eruptions as external forcings, with the mean of the models as a black dashed line. The lower panel shows the individual predictions of the same GCMs but with the effect of increasing greenhouse concentrations in addition to solar variability and volcanic eruptions and with the model mean. In both panels the instrumental observations from 1900 to present are indicated by a continuous black line. All temperatures are plotted as anomalies relative to the period 1901-1950. Major eruptions are marked with dotted lines and labeled. Adapted from IPCC (2007) and Irvine and Ridgwell (2009)

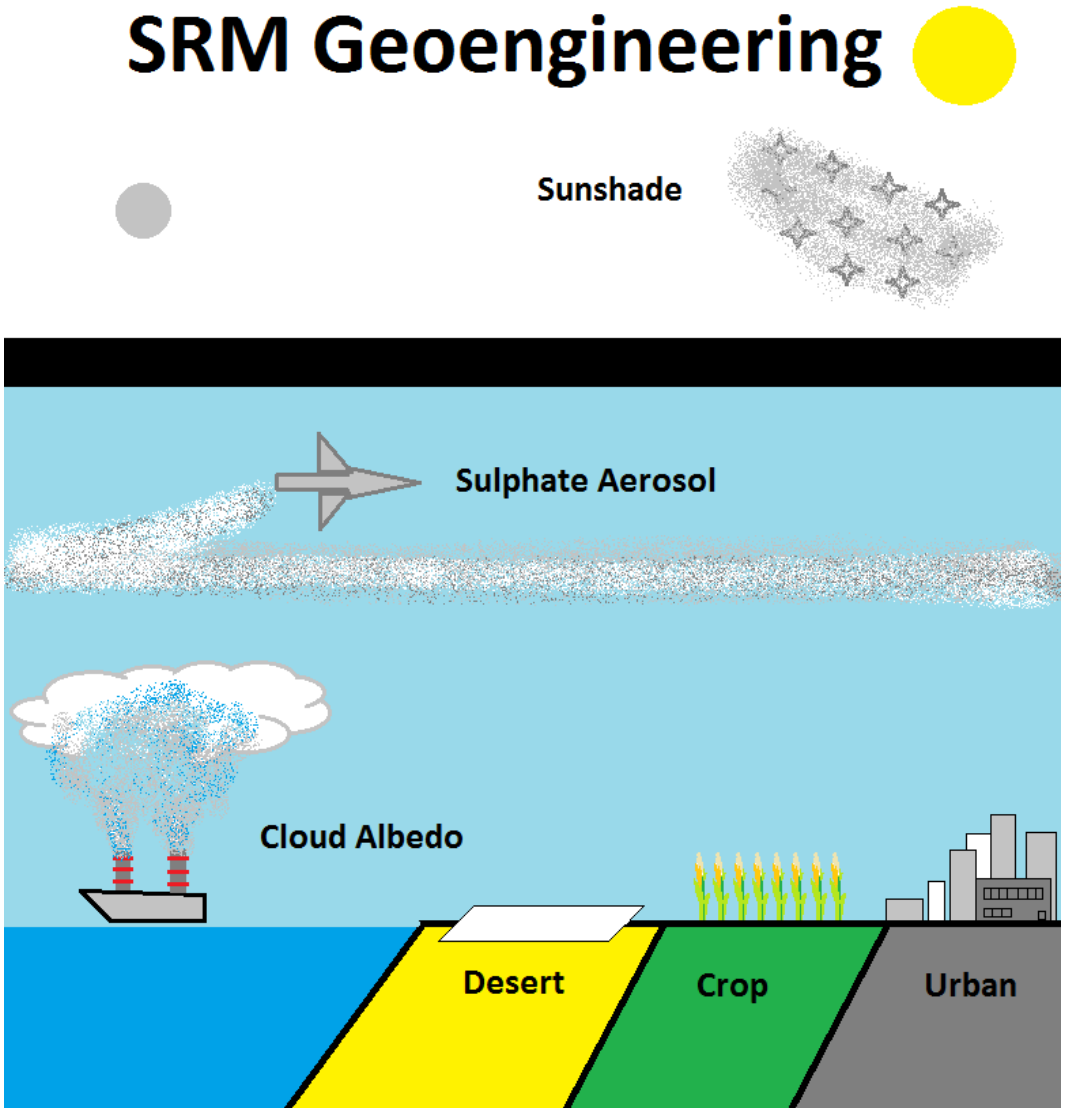

Figure 1.4: Diagram showing a number of SRM geoengineering schemes.

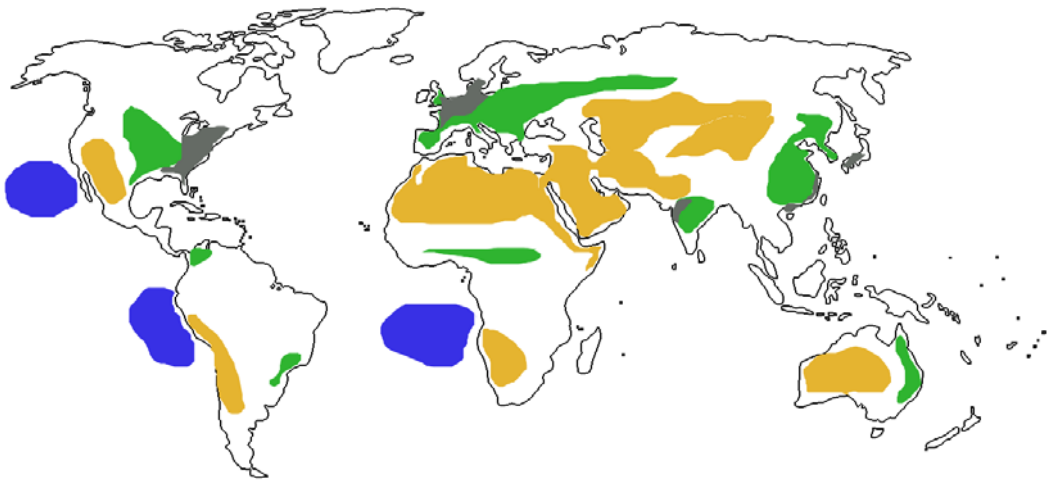

Figure 1.5: Diagram showing approximate locations where regional SRM geoengineering could be applied. Desert (yellow), crop (green), urban (grey), and cloud albedo geoengineering (blue) shown. Other SRM geoengineering schemes do not exert highly regional forcing, and it may be possible to apply cloud albedo geoengineering more broadly in ocean areas.

reduce CO_2 concentrations which would have the same effect as mitigation, effectively altering the greenhouse gas pathway, and the effects of different greenhouse gas pathways have been studied thoroughly (Johns *et al.*, 2003; IPCC, 2007; Meehl *et al.*, 2007a). Different SRM geoengineering schemes will also cause very different climate effects and knowing the details of these effects is essential to understanding whether a scheme is appropriate. The sunshade, urban, crop and desert geoengineering schemes are investigated in this thesis and the climate effects of different forcing strengths and regions of application considered. Here, I review several SRM schemes which are examined in this thesis as well as the other leading SRM geoengineering schemes. Figure 1.4 shows a diagram of the SRM geoengineering schemes reviewed below and figure 1.5 shows the regional areas of application for SRM geoengineering schemes that have limited areas of application. Table 1.1 provides a summary of the pros and cons of the major SRM geoengineering schemes.

1.3.1 Sunshade geoengineering

The most direct way to reduce the amount of sunlight absorbed at the Earth's surface is to intercept incoming sunlight in space. It has been proposed that a cloud of reflective satellites positioned near the L1 Lagrange Point, a point in space where the gravitational pull of the Earth and Sun balance, some 1.5 million Km from the Earth (almost 4 times the distance between the Earth and the Moon), could be used

Scheme	Pros	Cons	Risk	Cost
Sunshade	- Large cooling effect - Can be stopped quickly - Simple modification	- Advanced technologies required - Very costly - Uncertain climate effects	High	Very high
Sulfur aerosols	- Large cooling effect - Can be stopped quickly - Technologies avialable	- Efficacy somewhat uncertain - Ozone damage - Uncertain climate effects	High	Low / medium
Cloud albedo	- Large cooling effect - Can be stopped quickly - Regional deployment	- Efficacy uncertain - Highly heterogeneous - Uncertain climate effects	Medium	Low / medium
Crop albedo	- Regional cooling - Easily implemented	- Globally small effect - Only benefits some regions	Very low	Low
Urban albedo	- Mitigate some effects - Reduces heat-island effect	- Globally small effect - Only benefits some regions	Very low	Low / medium
Desert albedo	- Large cooling effect - Can be applied within national boundaries	- Significant maintenance and cost - Uncertain climate effects	High	Very high
Micro-bubbles	- Large cooling effect - Regional deployment	- Feasibility uncertain - Unknown ocean ecosystem impact	Medium	Low / high
Cirrus cloud modification	- Large cooling effect - Addresses longwave radiation	- Uncertain climate impacts - Unknown environmental impact	Medium	Low / high

Table 1.2: Summary of the pros, cons, risks and costs of SRM geoengineering.

to deflect a percentage of the sunlight heading for Earth (Angel, 2006). To create a pre-industrial global temperature in a world with doubled CO_2 in the atmosphere (compared to the year 1765), it has been estimated that 1.8% less sunlight would have to reach Earth (Govindasamy and Caldeira, 2000). A design by Angel (2006) envisages ∼16 trillion satellites with a total mass of ∼20 million tons achieving this. To make this geoengineering scheme feasible, the current cost to put 1 Kg in space of ∼$20000 would need to drop to $50 per kg (Angel, 2006). This may be achieved by using electric rail guns to launch the satellites into position, with the main cost then being the generation and storage of the electricity. On this basis, the total estimated cost of the system is less than 5 trillion dollars and that it could be in orbit in 25 years (Angel, 2006). Averaged over the lifetime of the system (50 years), this is only 0.2% of predicted global GDP (Angel, 2006). This scheme is ambitious; as the author notes it would arguably require equal or greater efforts as the challenge of decarbonizing the world economy.

Despite the technical challenges of this scheme, sunshade geoengineering is very easy to model because it involves a simple reduction in the strength of solar energy reaching Earth. Climate models (e.g., Govindasamy *et al.* (2003) and Lunt *et al.* (2008b)) show that the Equator of a world with elevated CO_2 levels and with a sunshade would be cooler, and the poles warmer, compared to the Pre-industrial. This is because the radiative forcing from a reduction in the solar constant is greatest at the equator and least at the poles (e.g. ranging from -17Wm^{-2} to -7Wm^{-2} in Lunt *et al.* (2008b)) and although the radiative forcing from CO_2 is greatest at low latitudes and reduced at high latitudes, the latitudinal gradient is less steep than for the solar forcing resulting in a net negative radiative forcing in the tropics and a net positive radiative forcing at high latitudes (Lunt *et al.*, 2008b). Winter temperatures are also higher than for the pre-industrial as the effect of a reduction in incoming solar radiation is less effective in the winter (Schmidt *et al.*, 2012). Precipitation is also reduced in sunshade geoengineering simulations as the reduction in solar radiation leads to a change in the surface energy budget which is made up by a reduction in the latent heat flux to the atmosphere thus to a reduction in evaporation and precipitation (Bala *et al.*, 2008). Knock-on effects include a reduction in some ocean and atmosphere circulation intensity and a global drop in precipitation as evaporation is reduced as a result of lower solar heating (Lunt *et al.*,

2008b; Govindasamy *et al.*, 2003).

1.3.2 Stratospheric aerosol geoengineering

Reflective aerosols are known to exert a cooling effect on the climate by scattering light and affecting cloud properties (Albrecht, 1989; Twomey, 1977; Lohmann and Feichter, 2005). It has been suggested that by deliberately injecting reflective aerosols into the stratosphere the planet could be cooled (Crutzen, 2006; Keith, 2000). Many different species of aerosol could potentially be used for SRM geoengineering; black carbon (Kravitz *et al.*, press), lime stone, titania, and sulphate aerosols (Ferraro *et al.*, 2011). There are even suggestions that 'smart' aerosols composed of engineered, controllable nano-particles may be possible (Keith, 2010). Global stratospheric aerosol geoengineering and sunshade geoengineering should have a similar effect on climate as both would globally reduce the amount of sunlight reaching the surface. However one important difference is that scattering aerosols do not just reflect light but scatter a large fraction of the incoming light, converting direct light into diffuse light (Rasch *et al.*, 2008b), which would reduce the effectiveness of concentrating solar power generation (Murphy, 2009), but may boost plant productivity (Mercado *et al.*, 2009; Gu *et al.*, 2003). Aerosols added to the stratosphere would increase the surface area for heterogeneous chemical reactions, which is expected to lower ozone concentrations (Tilmes *et al.*, 2008, 2009; Rasch *et al.*, 2008b).

The most feasible stratospheric aerosol approach is the sulphate aerosol geoengineering scheme, which has the proven natural analogue of large volcanic eruptions which have been observed to exert a strong global cooling caused by the injection of sulphate aerosols into the stratosphere (IPCC, 2007; Wigley, 2006; Cole-Dai *et al.*, 2009). Anthropogenic sulphate aerosols in the troposphere are known to exert a direct light-scattering cooling effect and a larger (Andreae *et al.*, 2005; IPCC, 2007), less certain, indirect effect on clouds (Lohmann and Feichter, 2005; Feichter and Leisner, 2009; Ramanathan *et al.*, 2001). Sulphate aerosols have been targeted by clean-air legislation due to the risks they pose to human health and their contribution to acid rain (Dockery *et al.*, 1993; Likens *et al.*, 1996). Crutzen (2006) suggested that stratospheric sulphate aerosol geoengineering should be used to replace the lost cooling effect caused by the reductions in tropospheric sulphate aerosol which are

motivated by the human health concerns. Aerosol lifetimes in the stratosphere are much longer than in the troposphere so the cooling effect of the tropospheric aerosols could be achieved with a much smaller injection of sulphate. The geoengineered sulphate would also cause only a small increase in sulphate deposition at the surface (Kravitz *et al.*, 2009; Rasch *et al.*, 2008b; Crutzen, 2006).

Initial investigations into the cost and effectiveness of lofting sulphate aerosol precursors into the stratosphere suggested that it was likely to work and could be relatively cheap compared to mitigation (Robock *et al.*, 2009; Rasch *et al.*, 2008b). Further research has provided more information on the potential effectiveness of this scheme and the climate consequence (Niemeier *et al.*, 2011). Transport in the lower stratosphere will tend to move particles from lower latitudes to higher latitudes where they will be removed (Rasch *et al.*, 2008b). This means that it is possible to restrict an aerosol cloud to one hemisphere or the other or to restrict an aerosol cloud to high latitudes only (Robock *et al.*, 2008). It has been found that emissions of aerosols at high altitudes and low latitudes produce the greatest radiative forcing (Eliseev and Mokhov, 2009; Niemeier *et al.*, 2011). Small aerosol droplets are found to be preferable to large aerosol droplets as small droplets fall more slowly and take longer to rain out (Rasch *et al.*, 2008a). It has also been found that the radiative forcing does not scale linearly with the injection rate of sulphate aerosols as the higher concentrations of sulphates cause the aerosol particles to grow larger and fall out more quickly (Niemeier *et al.*, 2011). It has also been found that injecting H_2SO_4 (sulphuric acid) rather than SO_2 can increase the aerosol burden for the same injected mass (Niemeier *et al.*, 2011; Pierce *et al.*, 2010). These studies have shown that stratospheric sulphate aerosol geoengineering is feasible. The natural analogue of volcanic aerosols guarantees to some extent that it would work (Kirchner *et al.*, 1999).

The climate effects of sulphate aerosol geoengineering would be similar to sunshade geoengineering (Kravitz *et al.*, press; Ammann *et al.*, 2010), with a large cooling effect causing an overcooling in the tropics and an under-cooling in the polar regions, and a large reduction in global average precipitation (Robock *et al.*, 2008). Studies attempting to reproduce a pre-industrial climate with sulphate aerosol geoengineering have found that it is not possible (Ban-Weiss and Caldeira, 2010; Ricke *et al.*, 2010). If sulphate aerosols were deployed in the Arctic only, the greatest

cooling effect would occur there but the climate changes would not be limited to the region of deployment, with changes in climate occurring across the world (Robock *et al.*, 2008). Sulphate aerosol geoengineering offers the potential for a cheap, effective, strong and controllable cooling of the climate but with all the limitations inherent to SRM geoengineering.

1.3.3 Cloud albedo geoengineering

Cloud albedo geoengineering aims to raise the albedo of maritime clouds via the Twomey or first indirect effect, by lofting sea-salt aerosol from the ocean surface to act as cloud condensation nuclei (CCN) (Twomey, 1977; Latham, 1990). Increasing CCN concentrations increases the number of cloud droplets for the same moisture content making clouds more reflective (the first indirect effect) and also increases the residence time and the longevity of clouds (the second indirect effect) (Albrecht, 1989). One embodiment of this scheme envisages a fleet of wind powered 'spray vessels' pumping out micron-sized droplets of sea-salt into the air in regions with suitable clouds (Salter *et al.*, 2008). Low-level marine clouds in regions with a low background level of CCN, i.e. unpolluted regions, are most suitable for cloud albedo geoengineering (Pringle *et al.*, 2012; Salter *et al.*, 2008). To offset the warming produced by a doubling of CO_2, Latham *et al.* (2008), calculated that a doubling of the natural cloud droplet number globally would be sufficient, however whether such an increase in cloud droplet number is feasible is a topic of current research (Pringle *et al.*, 2012; Korhonen *et al.*, 2010).

Research has shown that only some precursor clouds would be appropriate for cloud albedo geoengineering (Pringle *et al.*, 2012; Rasch *et al.*, 2009), generally low-lying and relatively un-polluted clouds, such as the stratocumulus decks off of the African South Atlantic coast, and the American North Pacific and South Pacific coasts (Jones *et al.*, 2009). Uncertainty in the aerosol indirect effect is large and it is an area of climate modelling that needs significant development (Chen *et al.*, 2010; Penner *et al.*, 2011; Quaas *et al.*, 2009; IPCC, 2007), and so the effectiveness of cloud albedo geoengineering is uncertain (Pringle *et al.*, 2012). To simulate cloud albedo geoengineering many early studies simply increased the cloud droplet number to 375 cm^{-3} for all clouds (Jones *et al.*, 2009), but aerosol modelling suggest that reaching such a level may be difficult or impossible to achieve in some regions (Korhonen

et al., 2010; Pringle *et al.*, 2012). In fact it is possible to cause a reduction in the cloud droplet number by adding sea-salt aerosols in some regions (Korhonen *et al.*, 2010). To achieve an increase in cloud albedo the cloud regions must have sufficient updraught, a low background concentration of CCN (i.e. low levels of pollution) and the injected sea-salt aerosols must be of a small diameter (Pringle *et al.*, 2012; Wang *et al.*, 2011).

Climate model simulations of cloud albedo geoengineering suggest that it could have a large cooling effect; however the resultant climate would differ substantially from the pre-industrial (Latham *et al.*, 2008; Bala *et al.*, 2010a; Jones *et al.*, 2009). Simulations conducted by Bala *et al.* (2010a) doubled CO_2 levels and raised cloud albedo ocean-wide. They found that global precipitation was reduced strongly relative to the pre-industrial, however a larger fraction of the total precipitation fell over the continents, which returned continental precipitation close to the pre-industrial state (Bala *et al.*, 2010a). Cloud albedo geoengineering need not be implemented pseudo-globally but certain regions could be seeded with sea-salt and others left undisturbed. A study which investigated cloud albedo modification in three regions which were suitable found that there were large differences in the patterns of regional precipitation and temperature change, with one cloud albedo region triggering a large reduction in precipitation over the Amazon (Jones *et al.*, 2009). Cloud albedo geoengineering is of uncertain effectiveness but offers a potentially strong and potentially highly regionally differentiated control over forcing and hence climate effects.

1.3.4 Urban albedo geoengineering

The idea of urban albedo geoengineering has been around for a number of years in the guise of reducing the heat island effect and helping improve air quality in cities (Taha *et al.*, 1999; Pomerantz *et al.*, 1999). Urban albedo geoengineering involves enhancing the albedo of urban areas by replacing standard building materials, for roofs and paving, etc., with alternative more reflective (higher albedo) materials or by adding a more reflective coating (Bretz *et al.*, 1998; Akbari *et al.*, 2009). Achievable increases to albedo from 0.1 to 0.4 and from 0.15 to 0.25 have been estimated for roofing and paving, respectively (Akbari *et al.*, 2009). Implementation of these changes would be costly unless incorporated into the building materials of

new builds and refurbishment, although there may still be additional costs associated with maintaining and cleaning the high reflectance surfaces. There would be energy savings in air conditioning for cities during summer months, but potentially offset by increased heating requirements in winter as less sunlight would be absorbed (Akbari *et al.*, 2009). Calculations by Oleson *et al.* (2010) show that the net effect on energy consumption would likely be negative in higher latitudes. Implementation across all major human settlements would be required to achieve any significant cooling effect globally (Akbari *et al.*, 2009; Hamwey, 2007).

There have been several previous analyses of the potential impact (and benefits) of global urban albedo enhancement. Most have applied a 0-D global mean radiative forcing approach (Lenton and Vaughan, 2009; Akbari *et al.*, 2009; Hamwey, 2007). The negative radiative forcing, due to urban albedo enhancement (and hence climatic impacts), depends strongly on the assumptions of the total urban area and the degree to which the albedo could be enhanced. Hamwey (2007) assumed a value for an average urban area per capita which totalled to 0.64% of the Earth's surface and that the albedo of urban areas could be doubled from 0.15 to 0.3. Akbari *et al.* (2009) assumed that 0.29% of the Earth's surface was urban and suitable for albedo increase, based on the Global Rural-Urban Mapping Project (GRUMP) urban extent dataset which places the fraction at 0.7% (GRUMP, 2005), and that the albedo of urban areas could be increased by 0.1. Lenton and Vaughan (2009) cautioned that other satellite data indicated the urban fraction to be much lower, at 0.051% of the Earth's surface (Hansen *et al.*, 2000; Loveland *et al.*, 2000).

In a recent study climate model simulations and urban modelling were used to investigate the effects of urban geoengineering (Oleson *et al.*, 2010). In that study, Oleson *et al.* (2010) use a coupled urban canyon model, taking the (LandScanTM) 2004 data to define urban areas, and applied a roof albedo of 0.9 to all buildings in the urban canyon model. Oleson *et al.* (2010) did not find any statistically significant changes to global climate as a result of the urban albedo modification they applied. These results indicate that urban albedo geoengineering does not offer a global-scale solution to climate change but may offer regional or local amelioration of some of the impacts.

1.3.5 Crop albedo geoengineering

Bio-geoengineering or crop albedo geoengineering would involve growing crop plant varieties with a higher albedo than currently grown as a means to affect a cooling of the planet. Crop albedo is often higher than the albedo of natural vegetation, for example barley at European latitudes has a higher albedo (0.23) than deciduous (0.18) or coniferous (0.16) woodland (Monteith and Unsworth, 1990). Hence the spread of agriculture historically has already led to modification of the albedo properties of the Earth's surface (Costa *et al.*, 2007; Betts *et al.*, 2007a), which has cooled the Earth by an estimated 0.17 °C (Matthews *et al.*, 2003). The albedo of different varieties of a single crop species also differs, depending on, for example, the properties of the leaf wax, the 'hairiness' of the leaves, and the morphology of the leaf canopy (Febrero *et al.*, 1998; Hatfield and Carlson, 1979; Holmes and Keiller, 2002). It has been proposed that these properties could be managed to increase the overall albedo of both grassland (pasture) and cropland (Hamwey, 2007; Ridgwell *et al.*, 2009).

Initial assessments of crop albedo modification again used calculations of the global mean annual radiative balance (Hamwey, 2007; Lenton and Vaughan, 2009). Based on the estimate of Hamwey (2007) that grassland albedo could be increased by 25% (+0.0425), Lenton and Vaughan (2009) calculated that when applied to all grassland (∼7.5% of the Earth's surface) a radiative forcing of $-0.51 W m^{-2}$ would be achieved. Fully coupled climate models have been used to assess the effectiveness of bio-geoengineering (Ridgwell *et al.*, 2009; Singarayer *et al.*, 2009). Singarayer *et al.* (2009) used the UK Hadley Centre climate model HadCM3 (Gordon *et al.*, 2000) and applied an increase in albedo of +0.04 to all cropland (∼2.8% of the Earth's surface (Lenton and Vaughan, 2009)), achieving a global cooling of ∼0.1°C. One of the advantages of a GCM rather than a global mean annual radiative balance approach is that it is possible to determine regional and seasonal effects, accounting for cloud and other feedbacks. In the case of crop albedo geoengineering it was found that the cooling effect was most pronounced in the summer and around a belt of northern latitudes that included central Europe, North America and Russia, with a cooling of up to ∼1°C (Ridgwell *et al.*, 2009; Singarayer *et al.*, 2009). Crop albedo geoengineering like urban geoengineering offers the potential for a regional

reduction in climate change magnitude but does not have a large global effect.

1.3.6 Desert albedo geoengineering

Desert albedo geoengineering involves the laying of highly reflective material across the extensive desert areas of the world to increase the average planetary albedo (Gaskill, 2004). Suggestions for achieving this include laying and cleaning some form of reinforced plastic sheeting by automated vehicles, covering an estimated 11.7 million km^2 of suitable desert (Gaskill, 2004). The area of deserts which could be suitable for this type of geoengineering cover $\sim$2% of the Earth's surface and the albedo increase proposed is from $\sim$0.36 to $\sim$0.8. This modification would give a total radiative forcing of -2.12 Wm^{-2} (Lenton and Vaughan, 2009). This would go some of the way to offsetting the $+3.71$ Wm^{-2} for a doubling of CO_2, making it the most effective (by impact) of the different surface albedo schemes (Lenton and Vaughan, 2009). There has been no analysis of desert albedo geoengineering using a spatially resolved climate model but due to the highly regional nature of the radiative forcing this scheme would produce, it is likely to have complex, inhomogeneous climate effects.

1.3.7 Micro-bubble geoengineering

Injecting micron-sized bubbles of air into seawater, causing it to scatter light in a way similar to aerosols in the atmosphere, could raise ocean albedo and provide a means to cool the planet (Seitz, 2011). It may require little energy to produce large quantities of micron-sized bubbles and air is free (Seitz, 1958). The lifetime of micron-size bubbles is uncertain but is critical to the feasibility of this scheme. Surfactants may be able to boost the lifetime of bubbles substantially but would add considerable cost to the scheme (Johnson and Cooke, 1981). If optimistic assumptions are made then it may be possible to counter the warming effect of a doubling of CO_2 concentrations by injecting 50 $Tgyr^{-1}$ of air into the ocean surface (Seitz, 2011). An ocean wide application of this micro-bubble scheme would likely cause similar changes as an increase in ocean-wide cloud albedo, i.e. greater cooling over ocean regions with a large reduction in ocean-wide precipitation and a much smaller change in continental precipitation (Bala *et al.*, 2010a). If this scheme is feasible it would offer the greatest control over regional shortwave forcing of any of the SRM

geoengineering schemes; patches of micro-bubbles could be produced in any body of water, limited only by advection, diffusion and bubble lifetime (Seitz, 2011).

1.3.8 Cirrus cloud modification geoengineering

Cirrus clouds have the greatest longwave top-of-atmosphere radiative forcing of any cloud type (Chen *et al.*, 2000), and cirrus cloud modification would aim to reduce this radiative forcing by increasing the ice-fall speed of cirrus clouds (Mitchell and Finnegan, 2009). Cirrus cloud modification is the only type of SRM geoengineering that aims to produce a negative longwave radiative forcing but it fits into the SRM category because the climate effects of this scheme would differ from a reduction in GHG concentrations and would thus be important in determining whether this scheme would be beneficial or not. Increasing the ice-fall speed in climate models has been found to reduce the climate sensitivity and cool the planet (Mitchell and Finnegan, 2009; Sanderson *et al.*, 2008b). An increase in ice-fall speed in cirrus clouds could be achieved by increasing the ice nucleation rates by introducing very efficient heterogeneous ice nuclei, such as bismuth tri-iodide, which would cause larger ice crystals to form which would precipitate more quickly than smaller crystals (Mitchell and Finnegan, 2009). Mineral dust and some types of soot have also been observed to have this effect on cirrus clouds (Mitchell and Finnegan, 2009). Simulations of cirrus cloud modification find that it could offset the warming produced by a doubling of CO_2 concentration but the climate effects have not yet been studied (Mitchell and Finnegan, 2009).

1.4 Carbon Dioxide Removal geoengineering overview

This thesis focuses on the climate consequences of SRM geoengineering but for completeness I review the leading CDR geoengineering schemes, describing the details of these schemes and some of the consequences. CDR geoengineering would complement traditional mitigation efforts by reducing concentrations of CO_2 in the atmosphere. The means by which the different CDR geoengineering schemes would achieve their aim of capturing CO_2 differ greatly but the global-scale effects of all the schemes would be similar, i.e. a greater or lesser reduction in CO_2 concentrations over time. Figure 1.6 shows a diagram of the leading CDR geoengineering

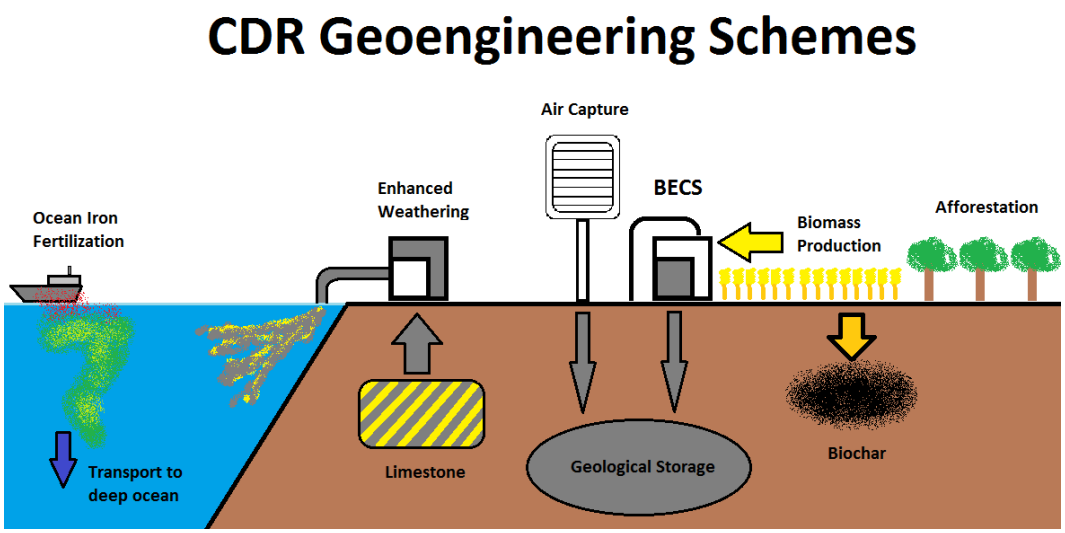

Figure 1.6: Diagram showing a number of CDR geoengineering schemes.

schemes described below and Table 1.3 gives a summary of the pros and cons of these schemes.

1.4.1 Afforestation and reforestation

Forest ecosystems store more than twice the carbon contained in the atmosphere (Canadell and Raupach, 2008), and with appropriate changes in management practice it may be possible to double the carbon storage of some managed forests, by increasing the standing biomass and soil carbon content (Nelson *et al.*, 2009). This increase in carbon storage could be achieved whilst simultaneously achieving biodiversity and ecosystem services goals with appropriate land management (Paquette and Messier, 2010). Despite concerns about the reduced albedo of forests compared to grassland, it is possible to have a net cooling effect on the planet by reforesting temperate regions (Pongratz *et al.*, 2011). There are difficulties in measuring carbon fluxes into and out of forest ecosystems which will make it hard to assess how much carbon is being stored but with appropriate governance this could be managed (Fahey *et al.*, 2010). The main obstacle to widespread afforestation and reforestation is competition with other land uses such as for agriculture and growing biofuels (Shepherd *et al.*, 2009). Overall afforestation and reforestation would be cheap to deploy and may bring some co-benefits but will compete with other land uses and have a limited effect on CO_2 concentrations which will take a long time to realize (Lenton and Vaughan, 2009; Shepherd *et al.*, 2009).

Scheme	Pros	Cons	Risk	Cost
Afforestation and reforestation	- Low cost and low tech - Few negative side-effects	- Little effect on CO_2 levels - Competition with other land uses	Very low	Low
Biomass with carbon sequestration (BECS)	- permanent sequestration - Fairly large potential	- Competition with other land uses - Slow acting - Limited rate of drawdown	Low	Medium
Biomass sequestration and Biochar	- Low-tech	- competition with other land uses - slow acting	Low	Low / medium
Air capture	- No limit to amount of CO_2 captured - Few negative side-effects	- Unproven technologies - High cost - Slow acting	Low	High / Very High
Ocean iron fertilization	- Cheap - Easy to implement	- Limited effectiveness - Unknown side-effects	Medium / High	Low
Enhanced weathering	- Large potential effectiveness - Mitigates ocean acidification locally	- High energy costs - Slow acting - Unknown side-effects	Medium	Medium

Table 1.3: Summary of the pros, cons, risks and costs of CDR geoengineering.

1.4.2 Biochar and bioenergy with carbons sequestration (BECS)

In addition to afforestation and reforestation there are a number of uses of biomass that could draw down CO_2 concentrations: creating and burying charcoal in soils (biochar), biomass sequestration, or bioenergy with carbon sequestration (BECS) (Shepherd *et al.*, 2009). Creating biochar transforms plant-produced carbon by pyrolysis into a much less labile and thus long-lived form (Lehmann *et al.*, 2006). This could be used to raise the carbon content of soils more or less permanently but the long term effects of adding large quantities of biochar to soils is unknown (Shepherd *et al.*, 2009; Lenton and Vaughan, 2009). Biomass sequestration like biochar prevents biomass from decomposing and releasing CO_2 and methane into the atmosphere but would achieve this by burying the raw biomass deep underground or disposing of it in the deep ocean (Strand and Benford, 2009). Biomass sequestration would require monitoring schemes to determine whether carbon is escaping from the storage reservoirs and would also require substantial expenditures of energy on transport and potentially earth-moving operations (Strand and Benford, 2009). BECS would use standard carbon sequestration techniques, which have been applied on a number of small scale projects at power plants (Obersteiner *et al.*, 2001), but with a biomass fuel source. The biomass whilst it is growing would be a sink of carbon and as the emissions are sequestered geologically, the whole process is carbon negative (Azar *et al.*, 2010). It has been argued that burying biomass would be a waste as it could be more fruitfully employed in displacing carbon-intensive energy sources, this may be valid but these biomass burial schemes are carbon negative allowing CO_2 levels to be gradually reduced (Shepherd *et al.*, 2009). All biomass schemes would require substantial appropriations of land to be effective, competing with other land uses, and although these schemes offer the potential for long-term draw-down of CO_2 it would only be at a limited rate (Shepherd *et al.*, 2009).

1.4.3 Air capture geoengineering

Air capture and storage, describes a range of potential engineering schemes to capture CO_2 from ambient air and sequester it in geologic reservoirs. There are a number of approaches to capturing CO_2 from ambient air or waste gas plumes; adsorption on solids (Lackner, 2009; Gray *et al.*, 2008), absorption into highly alkaline

solutions (Mahmoudkhani and Keith, 2009), and absorption into a moderately alkaline solution with a catalyst (Bao and Trachtenberg, 2006). The energy costs to capture CO_2 from ambient air will be higher than from waste fluxes as in Carbon Capture and Storage (CCS) as the fraction of CO_2 is much lower (Shepherd *et al.*, 2009). Unlike CCS air capture should have little difficulty in getting concentrated carbon to areas where geological storage is possible, as it will be possible to site air capture adjacent to the geological storage sites (Shepherd *et al.*, 2009). If an appropriate air capture scheme can be found then the limiting factors on air capture are mainly financial and energy cost (Keith *et al.*, 2006), which may be prohibitively large (Shepherd *et al.*, 2009; Lenton and Vaughan, 2009). Air capture could also be used to recycle the captured CO_2 as the source for carbon-neutral hydrocarbons by reacting CO_2 with carbon-neutral hydrogen (Zeman, 2007). Overall air capture could provide any scale of carbon capture limited only by the potentially very high energy and financial costs (Keith, 2009; Dessler, 2009; Lackner, 2009).

1.4.4 Ocean fertilization geoengineering

The atmosphere, surface ocean and land surface contain most of the anthropogenic carbon emitted to date but the deep ocean is the eventual destination of the vast majority of anthropogenic carbon (Archer *et al.*, 2009). Photosynthesis in the surface waters draws carbon into the surface ocean ecosystems and some of this captured carbon is exported downwards through the ocean column by the sinking of debris. Most of this downward flux is recycled below the surface waters but some is transported to the deep ocean. This process is known as the 'biological pump' and the intensity of the pump controls how quickly carbon is removed from the surface to the deep ocean (Ridgwell, 2011). If this biological pump could be sped up then it is hoped that more carbon can be transferred from the surface ocean to the deep ocean and atmospheric CO_2 concentration will fall (Shepherd *et al.*, 2009). Biological activity in large areas of the world's oceans is limited by a lack of macro or micro nutrients. Ocean fertilization with iron, nitrogen or phosphorous aims to provide the limiting nutrient to an area of ocean that would otherwise be productive and thus cause plankton blooms which would carry carbon to depth (Glibert *et al.*, 2008; Boyd, 2008; Lenton and Vaughan, 2009). Although many iron fertilization studies have been conducted it is very difficult to assess how well they have worked

at transporting carbon to depth, due to a lack of understanding of the iron cycle in the ocean and the difficulty in tracking the fate of the initial carbon captured (Boyd *et al.*, 2007). Nitrogen and phosphorous fertilization would aim to provide a missing macro-nutrient to ocean regions again with the aim of stimulating plankton blooms and hopefully sequestering carbon to depth (Shepherd *et al.*, 2009). The ecosystem consequences of ocean fertilization are highly uncertain and concerns over a test of urea fertilization (a source of nitrogen) potentially causing a bloom of toxic dinoflagellates led to an emergency warning from some scientists (Glibert *et al.*, 2008). Overall ocean fertilization offers the potential for a cheap way to reduce atmospheric CO_2 levels somewhat but its effectiveness is highly uncertain and it may cause negative ecosystem impacts (Shepherd *et al.*, 2009).

1.4.5 Enhanced weathering

Carbon dioxide is naturally removed from the atmosphere and oceans by weathering carbonate and silicate rocks and this weathering acts to stabilize CO_2 levels in the very long term (Archer *et al.*, 2009). These rocks react with CO_2 to form carbonates (vary stable carbon containing minerals) and thus draw CO_2 into a very stable and long-lived state. Artificially elevating the rate at which weathering occurs could provide a permanent means of drawing anthropogenic CO_2 from the atmosphere (Shepherd *et al.*, 2009). Carbonate rock, such as limestone, could be ground up and either scattered directly onto the ocean where it would react with CO_2 (Harvey, 2008) or could be treated with solutions containing high concentrations of CO_2 in chemical processing plants and then be flushed into the sea (Rau, 2008). Adding this alkaline solution to the oceans would reduce acidity locally and counter the effects of ocean acidification (Shepherd *et al.*, 2009). The environmental consequences of these schemes would be fairly severe as large mining and processing operations would be required and the ecosystem effects of adding alkaline minerals to the ocean is unknown (Shepherd *et al.*, 2009). These schemes have the potential to draw down considerable quantities of CO_2 but would require large quantities of minerals to be mined, processed and distributed and thus would be energy intensive and costly (Lenton and Vaughan, 2009).

1.4.6 CDR summary

CDR geoengineering offers the most complete solution to climate change but many proposals have potentially high costs or require vast amounts of land to operate effectively, and these schemes could only lower CO_2 levels slowly, making CDR of limited use in a 'climate emergency' (Keith, 2009; Lenton and Vaughan, 2009). CDR geoengineering would lower CO_2 concentrations and as such there has been little research on the global-scale environmental consequences of CDR geoengineering (there are some examples, e.g. Moore *et al.* (2010) and Cao and Caldeira (2010)). Most CDR geoengineering research focuses on the technical details of the land-use management, chemistry, engineering, etc. that would be required to achieve carbon capture.

This thesis investigates the climate consequences of geoengineering using an atmosphere-ocean GCM and as CDR geoengineering would have a very simple effect on the climate, i.e. it would only alter the evolution of the CO_2 concentration, it is not investigated. A full earth system model, including bio-geo-chemistry and a full carbon cycle, would be needed to investigate CDR geoengineering well.

1.5 Methodological approach

Efforts to assess and understand SRM geoengineering were initially limited to energy-balance models which have been used to calculate the radiative effectiveness of different SRM geoengineering schemes (Lenton and Vaughan, 2009). However, to get an idea of the full consequences of any SRM geoengineering scheme requires more complex climate models known as general circulation models (GCMs). GCM studies of the SRM geoengineering have generally confirmed the radiative effectiveness calculations made by energy-balance models but due to cloud and other feedbacks, only represented in the more complex model, some schemes have been found to be more or less effective than supposed (Lenton and Vaughan, 2009; Schmidt *et al.*, 2012).

The real value of GCM models comes from their ability to represent the full climate response to SRM geoengineering and their ability to resolve changes in regional and seasonal climate (Ricke *et al.*, 2010; Lunt *et al.*, 2008b). As described above SRM geoengineering would not match the longwave radiative forcing of an-

thropogenic greenhouse gases, instead a reduction in the shortwave radiative forcing would be made, which, even when fine-tuned, would result in a radiative balance that differs significantly from the pre-industrial (Schmidt *et al.*, 2012; Ban-Weiss and Caldeira, 2010). This unbalanced radiative forcing would give rise to complex regional climate responses, changes in seasonality, and changes in circulation which must be analyzed to determine whether SRM geoengineering would have a beneficial effect on the climate. For these reasons a GCM model is used in this thesis to assess the climate effects of SRM geoengineering schemes.

There are many aspects of the Earth-system that will be affected by SRM geoengineering that are not represented in GCMs, however these models can provide input to other off-line models and assessments of the impacts of SRM geoengineering. In this thesis the response of the Greenland Ice-Sheet to SRM geoengineering is investigated using data from the GCM to drive an off-line ice-sheet model. This will help determine whether SRM geoengineering may help to stabilize the Greenland Ice Sheet, preventing it from collapsing and contributing up to 7.3m to global sea-levels (Bamber *et al.*, 2001). A simpler Earth System Model of Intermediate Complexity (EMIC) is also used to simulate the global-mean surface air temperature and sea-level response to a large number of different geoengineering scenarios, a task that would require too much computing time with a GCM model.

1.6 Aims and objectives

This thesis aims to investigate the climate effects of a number of SRM geoengineering schemes. SRM geoengineering offers control over shortwave radiative forcing, or over longwave cloud forcings, potentially countering the increase in longwave radiative forcing due to rising greenhouse gas concentrations, and cooling the planet. However, this will not lead to a return to the climate of the pre-industrial. Global mean analyses of SRM geoengineering, such as those with energy balance models, do not capture many of the important aspects of SRM geoengineering and so GCM models are needed to analyse these schemes. Some SRM geoengineering schemes, such as desert albedo geoengineering, have not been analyzed by GCM models and as yet different schemes have not been compared using the same modelling framework. GCM models are not perfect representations of the climate system and different

models will yield SRM results that differ in some ways. To provide a more thorough assessment of the climate effects of SRM geoengineering the parametric and structural uncertainties of GCMs need to be considered.

The specific objectives of this thesis are:

1. GCM simulation of the climate effects of sunshade geoengineering to determine how the effects differ for different solar insolation reductions and whether partial sunshade geoengineering may be preferable. Simulation of sunshade geoengineering to determine whether the climate effects differ over a range of CO_2 concentrations. A range of different analysis approaches will be developed to provide insight into the consequences of the sunshade geoengineered climate.

2. Using the results of the initial GCM simulations to evaluate the ice-sheet response to sunshade geoengineering for a range of solar reductions using an offline ice-sheet model. The surface air temperature and sea-level rise response to a broader range of sunshade geoengineering scenarios will also be investigated using a simpler climate model (EMIC).

3. Representation of the urban, crop, desert and sunshade geoengineering schemes together in a GCM model using the same methodology for each scheme. This will allow a comparison of the urban, crop, desert and sunshade geoengineering schemes in the same modelling framework for the first time. A detailed assessment of the climate effects of these schemes will be made building on the achievements of objective 1.

4. Development of a perturbed parameter ensemble of the fully-coupled GCM HadCM3 without the use of flux-adjustment to determine the parametric uncertainty of some of the results in this thesis. Testing the pre-industrial climatology and the response to elevated CO_2 levels of the ensemble and determining which members of the ensemble show appropriate responses.

5. Assessment of sunshade geoengineering using the perturbed parameter ensemble created to achieve objective 4. This will help determine which aspects of the climate response to sunshade geoengineering are more or less certain and which are in doubt. These findings will be used to assess the robustness of the findings from objectives 1-3.

1.7 Thesis structure

This thesis is primarily composed of work published by myself in collaboration with other authors. This approach was taken as the majority of the work conducted during the thesis had been published or was in preparation for submission to a scientific journal. For the most part these papers have been included verbatim with the contributions of each of the authors clearly stated in a cover section. In Chapter 2 two short papers dealing with the same sunshade geoengineering runs are included, with only minor changes, along with additional material covering the methodology followed in this thesis and additional sunshade geoengineering results not covered in these two papers. A supplementary sunshade geoengineering study, which is discussed in Chapter 2, is not included within Chapter 2 as it follows a very different methodology but is included in appendix C. Chapter 3 presents one long paper on surface albedo geoengineering with a cover sheet explaining the author contributions and its place in this thesis. The material in Chapter 4 consists of a manuscript which is being prepared for submission and which has been modified to include additional sunshade geoengineering results and discussion relevant to the thesis. Chapter 5 is a summary, discussion and conclusion of the thesis. This approach, of presenting chapters composed of papers with necessary additions, has been followed to preserve the work that went into producing publication-quality studies and to make explicit the contributions of others to the studies that make up this thesis.

Chapter 2 develops a range of approaches for assessing the impacts and effectiveness of SRM geoengineering. The GCM modelling methodology applied in this thesis is developed and results on sunshade geoengineering presented. The effects of a range of different insolation reductions for sunshade geoengineering are investigated to determine whether partial sunshade geoengineering may be preferable to fully offsetting the CO_2-induced warming. Sunshade geoengineering is investigated to determine whether the climate effects differ for a range of CO_2 concentrations. The two versions of the GCM used in this chapter, HadCM3 and HadCM3L (Gordon *et al.*, 2000; Cox *et al.*, 2000), are compared to determine whether they respond in the same way to SRM geoengineering. To determine the effects of sunshade geoengineering on the long-term fate of the Greenland Ice-sheet, and hence sea-levels, output from the GCM is input to the off-line ice-sheet model GLIMMER (Rutt

et al., 2009). To provide a broader picture of the effects of SRM geoengineering on sea-level additional analysis is conducted on a large number of sunshade geoengineering scenarios is conducted using the UVic mofrl and is presented in appendix C.

Chapter 3 provides an intercomparison of the effectiveness and climate impacts of a range of different SRM geoengineering schemes using an identical GCM setup. The urban, crop and desert geoengineering schemes are reviewed and the schemes are implemented as regional albedo changes in the HadCM3 model. These surface albedo geoengineering schemes are compared with the sunshade geoengineering scheme discussed in Chapter 2 using a range of analyses to investigate changes in the global climate, the occurrence of warm summers in Europe, changes in the monsoon and in circulation, and changes in Arctic conditions. Conclusions are drawn about the consequences of the climate impacts of the schemes, and the value of the schemes for offsetting global climate change and for regional amelioration of impacts.

Chapter 4 investigates the uncertainty in climate model estimates of the effectiveness and impacts of SRM geoengineering and discusses the implications for the results in this thesis. The effects of parametric uncertainty on the climate effects of SRM geoengineering is investigated through the application of a perturbed parameter ensemble, i.e. an ensemble of versions of the HadCM3 model with different values for important but uncertain parameters. A 27 member non-flux adjusted perturbed parameter ensemble of the GCM HadCM3 is created and the methodology for its development is presented. The ensemble performance is tested by simulating the pre-industrial and comparing this ensemble climatology against the climatologies of the GCM models of the third Climate Model Intercomparison Project (CMIP3) (Meehl *et al.*, 2007b). The ensemble is then applied to two elevated CO_2 and two sunshade geoengineering experiments which are part of the Geoengineering Model Intercomparison Project (geoMIP) (Kravitz *et al.*, 2011), an attempt to compare the geoengineering results of many different GCMs. The geoengineering results of the ensemble are analyzed to determine the role of parametric uncertainty in the climate response to sunshade geoengineering and comparisons are made to a study comparing four GCMs climate response to one of the geoMIP experiments. On the basis of this evaluation of the effects of parametric uncertainty and inter-model differences on sunshade geoengineering, conclusions are drawn about the robustness of

the results presented in the preceding chapters.

Finally, Chapter 5 summarizes the material presented in the thesis, discusses some of the limitations of this thesis, draws some conclusions, suggests some avenues for future work, and presents some final thoughts.

CHAPTER 2

Methodology and sunshade geoengineering

2.1 Cover sheet

Sunshade geoengineering is the simplest form of SRM geoengineering and there have been a number of assessments of the climate effects of this scheme (Govindasamy and Caldeira, 2000; Govindasamy *et al.*, 2003; Lunt *et al.*, 2008b; Schmidt *et al.*, 2012); however, these studies have only investigated a single CO_2 concentration with a single insolation reduction. CO_2 levels are rising and if sunshade geoengineering is implemented CO_2 levels will still be changing over the time it is in place. Sunshade geoengineering also offers control over how much the solar insolation is reduced by which will greatly change the impact of this scheme on the climate. This chapter explores the climate effects of sunshade geoengineering for a range of different insolation reductions and CO_2 concentrations using GCM models and also investigates the effects of sunshade geoengineering on the Greenland Ice-Sheet. The methodology and experimental setup used in these studies is justified and explained in this chapter and then applied in the work in the following chapters. This chapter presents a combination of published and unpublished material produced by the author and collaborators; the contribution of the collaborating authors to the published work is explained here. Unless otherwise stated the work presented in this chapter is the author's own.

It is found that the regional and seasonal changes in climate that Sunshade geoengineering causes vary linearly with the insolation reduction. A similar linear response to sunshade geoengineering at different CO_2 forcings is found to hold at the global level and seems to hold at the regional level as well. The climate of the sunshade geoengineering simulation is found to differ substantially from both the pre-industrial and elevated CO_2 simulations. There is also evidence that sunshade geoengineering would reduce the intensity of the El Niño Southern Oscillation

(ENSO) but this conclusion is tentative. Results from an off-line ice-sheet model coupled to a GCM indicate that sunshade geoengineering could help stabilize the Greenland Ice-Sheet, and that a return to the pre-industrial global mean temperature is not necessary to achieve this.

Section 2.5 presents a sunshade geoengineering study with different insolation reductions that I was first author of, Irvine *et al.* (2010), with additional material produced by me that was not included in the published study. This study uses the HadCM3L model (Cox *et al.*, 2000), analyses the regional effects and develops a novel approach to the analysis of SRM geoengineering. It is worth noting that whilst this work was being conducted a very similar study with HadCM3L was being conducted by another group and was published prior to this study (Ricke *et al.*, 2010). These studies were carried out independently and the authors were not aware of each other's work. The contributions of the authors of this study are as follows. I conducted all simulations, analysis and authored the first draft of the paper. Dr. Dan Lunt, Prof. Andy Ridgwell and I all jointly developed the project goals and chose the analysis included in the paper. Dr. Dan Lunt made suggestions for changes to the manuscript text and Prof. Andy Ridgwell provided input on the structure and wording of the text. I arranged the corrections to the text and figures and prepared the article for submission. Two anonymous reviewers are to be thanked for their comments and suggestions. The reviews were jointly discussed by all authors, but answers to the reviews were written by me, as were changes implemented in the manuscirpt. The material presented in Section 2.5.6 was prepared solely by the author. The published paper is available here:

DOI:10.1029/2010GL044447

Section 2.6 presents a study of the effects of sunshade geoengineering on the Greenland Ice-Sheet that I was first author of, Irvine *et al.* (2009). This section investigates the response of the Greenland ice-sheet to different levels of sunshade geoengineering at quadrupled CO_2 levels using the HadCM3L model and the off-line GLIMMER ice-sheet model (Cox *et al.*, 2000; Rutt *et al.*, 2009). I carried out the HadCM3L and GLIMMER simulations, conducted the analysis and wrote the first draft. However, significant work on the background to the ice-sheet model and the relevant caveats to the ice-sheet results were provided by Dr. Dan Lunt and Dr. Emma Stone. The ice-sheet coupling method was developed by Dr. Dan Lunt and

Dr. Emma Stone and they also provided scripts that were used to generate the ice-sheet plots in figures 2.8 and 2.9 (figures 3 and 4 in the published paper). The project goals and approach were developed by Dr. Dan Lunt, Prof. Andy Ridgwell and me. Dr. Dan Lunt made suggestions for changes to the manuscript text, Dr. Emma Stone added some corrections, and Prof. Andy Ridgwell provided input on the structure and wording of the text. I arranged the corrections to the text and figures and prepared the article for submission. Two anonymous reviewers are to be thanked for their comments and suggestions. The reviews were jointly discussed by all authors, but answers to the reviews were written by me, as were changes implemented in the manuscirpt. This study provides insights into the indirect climate effects of geoengineering that off-line models can provide. However, ice-sheet modelling is not the focus of this thesis and this study would not have been possible without the expertise of the co-authors. The published paper is available here:

DOI:10.1088/1748-9326/4/4/045109

Two other studies that I was involved in are referred to in the course of this chapter; Singarayer *et al.* (2009) and Irvine *et al.* (2012), these are included in Appendix B and C, respectively, with the contribution of the authors outlined there.

2.2 Introduction

Simple energy balance calculations show that SRM geoengineering, by increasing planetary albedo or reducing incoming insolation, will cool the planet but these calculations can only show roughly how effective different SRM proposals would be (Lenton and Vaughan, 2009). Global mean temperature change is used as the headline metric of climate change but it is the climate consequences of this warming that worries scientists and policy makers (Smith *et al.*, 2009; Hansen *et al.*, 2007; Schneider, 2001). The anticipated climate effects of global warming differ greatly from one region to the next, with warming expected in all regions but a much greater warming at high latitudes (Johannessen *et al.*, 2004), and some regions expecting large increases in precipitation and others large decreases in precipitation (Burke *et al.*, 2006; Piani *et al.*, 2007; Burke and Brown, 2008). Similarly global warming will cause seasonal changes which will affect the strength of the monsoons (Kripalani *et al.*, 2007), the intensity of heatwaves (Schar *et al.*, 2004; Tebaldi *et al.*,

2006), and the timing and strength of peak river flows (Betts *et al.*, 2007b; Palmer *et al.*, 2008). These climate changes are expected to raise sea-levels substantially by melting glaciers and ice-caps (Wigley and Raper, 2005; Meier *et al.*, 2007; Radic and Hock, 2011), threatening the stability of the Greenland and Antarctic ice-sheets (Ridley *et al.*, 2005; Gregory and Huybrechts, 2006; Rignot *et al.*, 2011), and causing thermosteric expansion of the oceans (Peltier, 2009; Domingues *et al.*, 2008). These regional and seasonal climate changes will affect human populations by raising sea-levels (Tol *et al.*, 2006); affecting agriculture (Lobell and Field, 2007); pests and disease vectors (Costello *et al.*, 2009; Kyle and Harris, 2008); and changing the exposure to weather extremes (Tebaldi *et al.*, 2006). To assume that because an SRM geoengineering scheme would lower global mean temperature it would therefore reduce the climate risk facing mankind would ignore the fact that SRM geoengineering will alter the climate in ways that do not necessarily reverse the effects of elevated greenhouse gas concentrations (e.g. Lunt *et al.* (2008b), Jones *et al.* (2009), Robock *et al.* (2008)). To determine whether any particular SRM geoengineering scheme is a good idea much more needs to be known about the regional and seasonal climate effects of these schemes and the effects that these changes would have on humans and ecosystems.

In this thesis the regional and seasonal climate consequences of SRM geoengineering are investigated and to do this, sophisticated climate models, known as general circulation models (GCMs), are needed. GCMs include representations of the atmosphere, ocean and land surface, that discretize and parameterize the known physics of these systems onto a three dimensional grid. This GCM representation simplifies some aspects of the physics and applies empirical equations to represent other aspects that cannot be resolved by the model. GCM models attempt to replicate the behaviour of the climate system from first principles and are now fairly successful at capturing many of the first-order features of the climate system (Gordon *et al.*, 2000; IPCC, 2007). GCMs are not perfect simulators of the Earth's climate and their results must be interpreted with caution but they are the best tools for assessing future climate change (IPCC, 2007). This thesis also investigates the effect of SRM geoengineering on the Greenland Ice-Sheet and on sea-level rise to determine whether SRM geoengineering would be able to halt sea-level rise or stabilize the Greenland Ice-Sheet. To achieve these goals I used an off-line ice-sheet model

that uses GCM output to calculate the surface mass-balance and ice-sheet dynamic response; and an EMIC model with a simple off-line model (Weaver *et al.*, 2001), based on the methods used in the IPCC AR4 (IPCC, 2007; Wigley and Raper, 2005; Gregory and Huybrechts, 2006), that represents the contributions of thermosteric expansion, glacier melt and ice-sheet to sea-level rise.

SRM geoengineering research is a relatively new field but there have been many GCM studies of SRM geoengineering to date. The simplest SRM geoengineering scheme, sunshade geoengineering (Angel, 2006), and the two most feasible types of SRM geoengineering, stratospheric sulphate aerosol geoengineering and cloud albedo modification geoengineering (Crutzen, 2006; Latham, 1990), are being thoroughly investigated. Sunshade geoengineering is simple to model and provides a first approximation to the climate effects of sulphate aerosol geoengineering (Kravitz *et al.*, 2011), as such many studies have been conducted into the climate effects of sunshade geoengineering to see whether SRM geoengineering may offer a way to address global warming (Lunt *et al.*, 2008b; Govindasamy and Caldeira, 2000; Schmidt *et al.*, 2012). To fully represent the climate effects of sulphate aerosol geoengineering a climate model needs a sophisticated representation of aerosols, the stratosphere, and atmospheric chemistry; and a number of studies with sophisticated GCMs with just these components have been published over the course of this thesis (Robock *et al.*, 2008; Rasch *et al.*, 2008a,b; Tilmes *et al.*, 2009; Jones *et al.*, 2010; Heckendorn and et al., 2009; Niemeier *et al.*, 2011). Similarly for cloud albedo geoengineering a sophisticated representation of tropospheric aerosols and their interaction with clouds is needed and this has been investigated as well (Pringle *et al.*, 2012; Korhonen *et al.*, 2010; Wang *et al.*, 2011). Approximations of sulphate aerosol and cloud albedo geoengineering are possible but have already been investigated; i.e. applying an optical depth increase to represent sulphate aerosol geoengineering (Ricke *et al.*, 2010), and simply increasing the number of cloud condensation nuclei to represent cloud albedo modification (Jones *et al.*, 2009; Latham *et al.*, 2008; Rasch *et al.*, 2009). Neither the sulphate aerosol or cloud albedo geoengineering schemes are examined in this thesis as it was judged that additional work with a last-generation GCM would add little to what is being carried out by the latest generation of GCMs.

In this chapter the sunshade geoengineering scheme is investigated in detail using two versions of a fast GCM climate model, an Earth-system model of intermediate

complexity (EMIC), and an off-line ice sheet model. Section 2.3 outlines the modelling approach followed and Section 2.4 presents the experimental setup used in this chapter. Sunshade geoengineering would involve reducing the solar insolation so that the planet's temperature can be lowered. To date all simulations of sunshade geoengineering have only simulated a reduction in solar insolation sufficient to return global-mean temperature to the pre-industrial value (Lunt *et al.*, 2008b; Govindasamy *et al.*, 2003; Schmidt *et al.*, 2012). However, as sunshade geoengineering causes a large reduction in global precipitation compared to the pre-industrial (Lunt *et al.*, 2008b; Schmidt *et al.*, 2012), partial sunshade geoengineering may be preferable as it could cool the planet somewhat without reducing precipitation by so much. To investigate this, a set of simulations with different strengths of solar insolation reduction and with CO_2 levels quadrupled from their pre-industrial concentration are run. The regional climate effects and the occurrence of 'novel' climate conditions for these runs are analysed in Section 2.5 and the effects of different strengths of sunshade geoengineering on the stability of the Greenland ice-sheet is analyzed in Section 2.6. Sunshade geoengineering would offer control over the magnitude of the solar insolation reduction but it would also offer control over the timing and rate at which it would be applied and, if it was deemed necessary, the rate at which it would be phased out. The consequences of this range of control are investigated in appendix C. It is likely that if SRM geoengineering were deployed it would be whilst CO_2 concentrations are still rising, and as such knowing whether the climate effects of sunshade geoengineering, or any other scheme, would change at different CO_2 levels is important (Singarayer *et al.*, 2009). Section 2.7 investigates the climate effects of sunshade geoengineering for a range of CO_2 levels and investigates the effect one of the strongest modes of variability in the climate system (Collins *et al.*, 2010b), the El Niño Southern Oscillation (ENSO). A comparison is also made between the two GCM models used in this thesis to determine whether they respond in the same way to sunshade geoengineering. Section 2.8 summarizes the results of this chapter and discusses their implications.

2.3 Modelling approach

There are a number of simpler modelling tools that have been applied to geoengineering which are not capable of determining all of the relevant climate effects of geoengineering. The simplest tool to assess SRM geoengineering are energy balance models and other 0D or 1D models, however these models can only give basic information about the radiative effectiveness of proposed geoengineering schemes (Lenton and Vaughan, 2009) and some aspects of the global mean response to warming such as rates of temperature change and empirically-based estimations of sea-level rise (Wigley, 2006; Moore *et al.*, 2010). Earth system models of intermediate complexity (EMICs) are models of the Earth system which have simplified representations of the atmosphere, ocean and usually the carbon cycle, and are useful for modelling the response of the Earth-system on timescales of thousands to tens of thousands of years (Lenton *et al.*, 2006; Weaver *et al.*, 2001). These models have been used to investigate the effect of geoengineering on the carbon cycle (Matthews and Caldeira, 2007; Matthews *et al.*, 2009), the rate of temperature change (Goes *et al.*, 2011), and on the joint behaviour of temperature and sea-level rise (Irvine *et al.*, 2012), presented as appendix C to this PhD.

GCM models are the most complete representations of the Earth's climate with a 3D physical atmosphere and land surface scheme (Cox *et al.*, 1999) perhaps additionally coupled to a 3D ocean (Gordon *et al.*, 2000), carbon cycle (Cox *et al.*, 2000), atmospheric chemistry (Collins *et al.*, 2011) and/or other modules. These models are used for century-scale future climate projections (Meehl *et al.*, 2007b; IPCC, 2007), paleo-climate reconstructions (Lunt *et al.*, 2007), and for theoretical work such as geoengineering (Govindasamy *et al.*, 2003; Lunt *et al.*, 2008a; Jones *et al.*, 2009). They are used to generate a first-order estimate of the response of the climate system to perturbations such as rising CO_2 levels and SRM geoengineering (Meehl *et al.*, 2007a; Schmidt *et al.*, 2012). GCM models produce all the relevant climatic variables, e.g. surface air temperature, precipitation, humidity, etc., needed to diagnose the climatic effects of SRM geoengineering and are thus the only tool appropriate for the goals of this thesis.

The climate, and more broadly the Earth-system, is immensely complex with important processes occurring from the smallest to the largest scale, from chemical

reactions and ice-crystal formation, to the growth of rainforests and changes in the Atlantic overturning circulation. Due to limits of spatial resolution, understanding and computing resources, GCMs must approximate the physics of the Earth-system and cannot represent all processes. Additionally the equations representing the flows of air, moisture and energy through the climate system must be discretized and the model must be run at a coarse grid resolution, typically with gridcells with edges 100s of kilometres long. Parameterizations of processes must be made and empirical relations are found to represent processes that occur on small scales, derived either from observations or from higher resolution models (Xu and Randall, 1999; Khairoutdinov *et al.*, 2005; Hohenegger *et al.*, 2008). The equations that govern a GCM are determined by a mix of directly observable quantities such as the heat capacity of water and on parameters which cannot be determined by direct observation. An example of such a parameter is the critical relative humidity in HadCM3 which is the relative humidity at which cloud formation begins in a gridbox.

These properties of GCM models give rise to a number of problems that need to be understood for climate model results to be properly interpreted. The higher the resolution of a GCM, the more processes can be resolved, and the fewer processes require empirical parameterizations. Cloud and convective processes for example operate on scales below the current generation of GCMs (Xu and Randall, 1999; Khairoutdinov *et al.*, 2005), but efforts are being made to achieve the higher resolutions needed to remove the need for parameterization (Hohenegger *et al.*, 2008). Higher resolution orography can improve local climatology (Jacob *et al.*, 2007), particularly for precipitation (Kimoto *et al.*, 2005), and can result in significant improvements 'downwind' of features (Sakamoto *et al.*, 2004). Resolution also affects emergent phenomena with high resolutions required to resolve hurricanes and ocean eddies correctly (Yoshimura *et al.*, 2006; Sakamoto *et al.*, 2004; Liu *et al.*, 2004). Another resolution-dependent problem is that of two-way flow through a narrow opening, e.g. the Mediterranean (Bryden *et al.*, 1994), grid cells can only permit flow in one direction at any time and so if only one grid cell is present at the opening it is not possible to have a two-way flow. This problem forces model groups to be careful with defining the land-sea mask and orography and sometimes forces model groups to remove land masses to allow more realistic flows (Cox *et al.*, 2000). Discretization causes some numerical diffusion in most numerical methods resulting in

sharp gradients in a tracer becoming smoothed out (Stenke *et al.*, 2008).

One of the major limiting factors on climate models is computational cost and a trade-off must be made between the length of simulations, the number of processes included, and the resolution of the model. Including more processes and running the model at a higher resolution improves GCM performance which is why each generation of GCM is at a higher resolution and includes more processes, e.g. compare HadCM3 with HadGEM2-ES (Gordon *et al.*, 2000; Collins *et al.*, 2011). However each additional model component slows the GCM down and complicates the climate response to a forcing, adding additional feedback processes that are hard to disentangle. Higher resolution also comes at the cost of speed, for example if the horizontal and vertical resolution are doubled then 8 times as many calculations will be required. In fact, the time-step would likely need to be halved as well due to the Courant-Friedrichs-Lewy constraint which in the simplest case, requires that the timestep for numerical solutions must be short enough that the speed of propagation or advection of the properties calculated does not exceed the speed at which information can travel on the grid, i.e. one gridcell in one timestep. Therefore the computational cost of increasing resolution scales as resolution to the power 4. Another problem is that some Earth-system components respond to altered conditions in an inherently slow way such as the ocean which can take many thousands of years to reach equilibrium (IPCC, 2007). The appropriate GCM model setup depends on the nature of the processes of interest, the computational resources available, and the length of runs required.

The GCM models that were compared in the third Climate Model Intercomparison Project (CMIP3) reproduced many of the first-order features of the global climate system but GCMs are far from perfect representations of the Earth's climate (Meehl *et al.*, 2007b; IPCC, 2007). Although they perform relatively well on the large scale, they do not match observations well on small spatial and temporal scales (IPCC, 2007). GCMs are particularly poor at reproducing regional precipitation observations and have large regional biases, for example the South Pacific Convergence Zone extends farther and in a more easterly direction than observed (the 'double ITCZ' problem)(Meehl *et al.*, 2007a; IPCC, 2007). The CMIP3 GCMs also fail to reproduce the temporal structure of observed precipitation with simulated precipitation occurring too frequently and at lower intensity than observed (Kimoto

et al., 2005). Jiang *et al.* (2005) assessed some of the models used in the CMIP3 for their performance at reproducing the East-Asian monsoon and found that all models had difficulties reproducing the observed behaviour. As outlined above the coarse resolution of coupled GCM models prevents certain phenomena from being represented, e.g. hurricanes, and this has an effect on climatology. GCM models produce a reasonable representation of the climate system but are not perfect and so the results must be treated with caution.

The GCM chosen for this thesis is the HadCM3 model (Gordon *et al.*, 2000), which was part of the CMIP3 ensemble and contributed to the IPCC AR4 assessment (Meehl *et al.*, 2007b,a; IPCC, 2007), and the lower ocean resolution version HadCM3L (Cox *et al.*, 2000). Although HadCM3 has been superseded by the HadGEM2-ES model (Collins *et al.*, 2011) as the official UK climate model (Jones *et al.*, 2011b), it is still widely used in climate process (Boucher *et al.*, 2009), perturbed parameter ensemble (Collins *et al.*, 2010a; Brierley *et al.*, 2010; Piani *et al.*, 2007), paleo-climate (Lunt *et al.*, 2007; Dowsett *et al.*, 2011) and SRM geoengineering studies (MacMynowski *et al.*, 2011; Ricke *et al.*, 2010; Singarayer *et al.*, 2009). HadCM3 is a fully-coupled GCM and was one of the better performing models of the CMIP3 ensemble (Meehl *et al.*, 2007a; IPCC, 2007), and it runs relatively fast allowing many thousands of years of computer simulations for a single experiment. HadCM3 does not include a atmospheric chemistry scheme, interactive vegetation or a carbon cycle, this limits the types of simulations and analysis which can be conducted but it simplifies the climate response to SRM geoengineering, removing certain interactions and feedback which make it more difficult to determine the cause of changes. For Chapters 3 and 4 which make use of HadCM3, the MOSES 1 land surface scheme with fixed vegetation is employed (Cox *et al.*, 1999), which accounts for terrestrial surface fluxes of temperature, moisture and radiation. The combination of HadCM3 with MOSES 1 is the most widely used and is the most robustly tested HadCM3 setup (Gordon *et al.*, 2000; Martin *et al.*, 2006; Johns *et al.*, 2003) and for this reason this combination is used for most of this thesis. A full model description of HadCM3 and MOSES1 can be found in Section 3.4 of Chapter 3.

However, for the results in this chapter HadCM3L with the MOSES 2.2 land surface model with fixed vegetation is employed (Essery and Clark, 2003). HadCM3L has half the ocean resolution of HadCM3 and runs approximately twice as fast

allowing more simulations to be conducted. This combination of HadCM3L and MOSES 2.2 has been used previously in a paleo-climate study (Lunt *et al.*, 2007) and a number of geoengineering studies (Lunt *et al.*, 2008b; MacMynowski *et al.*, 2011; Ricke *et al.*, 2010). The work in this chapter was developed from the Lunt *et al.* (2008b) study which used HadCM3l with MOSES 2.2 and so applies the same methodology, however HadCM3 with MOSES 1 was judged to be more appropriate for the other experiments in Chapters 3 and 4 because it is the most widely used and most robustly tested HadCM3 setup. A full model description of HadCM3L and MOSES2.2 can be found in Section 2.6.3 of Chapter 2.

As two different versions of the HadCM3 model are used in this thesis, a comparison between them is needed to determine how they differ and whether they respond in similar ways to elevated CO_2 and SRM geoengineering. To test whether the results of the sections which used HadCM3L would differ if the HadCM3 model was used instead, the two models are directly compared on a number of identical simulations in Section 2.7.2. The similarity of the response of these models will have implications for comparisons between the chapters and the robustness of conclusions drawn from one model or the other.

2.4 Experimental approach

This section describes the equilibrium experimental approach adopted in this work and some of the limitations which affect the choice of experimental approach. The purpose of this thesis is to investigate the climate effects of SRM geoengineering and as such a simple approach is taken where only the CO_2 concentration is elevated and the SRM geoengineering modification is made. This equilibrium response approach takes a pre-industrial control run and instantaneously changes conditions at the beginning of the experiment, the model is then run for decades or centuries to allow the climate to adjust to these new conditions, and the equilibrium conditions are recorded and analysed. Few equilibrium studies allow the ocean to fully adjust which would take millennia and instead allow an adjustment time of a few centuries, or wait until the rate of temperature change drops below a certain threshold (Lunt *et al.*, 2008b; Govindasamy *et al.*, 2003; Govindasamy and Caldeira, 2000). Other geoengineering studies have used future anthropogenic emissions scenarios and ap-

plied SRM geoengineering to these changing conditions (Ricke *et al.*, 2010; Kravitz *et al.*, 2011; Jones *et al.*, 2010); these transient studies present more realistic future scenarios but many factors are changing simultaneously and there is a changing trend over time.

The climate system has a large degree of natural variability and GCM models similarly have a large degree of internal variability which needs to be accounted for when analysing GCM results. There is a large degree of interannual variability even for global-mean variables such as temperature which varies by up to 0.5°C from year-to-year (Brohan *et al.*, 2006), and larger variability at the regional scale, e.g. the central England temperature record varies by up to 2°C year-to-year (Parker *et al.*, 1992). For shorter averaging periods, interannual variability is a major problem but it is possible to approximate the effect of this climate noise and determine whether a change in climate has occurred or not. The Student t-test is an approach that is commonly applied in GCM modelling studies to test whether a change in the climate is greater than a threshold based on the climate variability. The Student t-test assumes a normal distribution and tests the likelihood that two samples are drawn from the same distribution, i.e. that no change has occurred. I adopt the common approach of masking out all regions that fail a 5% t-test, i.e. the only regions considered are those which have a 95% or higher probability of having changed.

The variability in the climate system is not limited to the interannual timescale, longer timescale effects such as ENSO (Trenberth, 1997) and ocean circulation variations can introduce decadal to centennial variability in models (Manabe and Stouffer, 1996; Mann and Park, 1994). Climate model simulations of the pre-industrial show such large internal variability on longer timescales that many of the regional decadal trends and distinct climate periods, such as the little ice age, are now suspected to be purely a result of natural variability (Bengtsson *et al.*, 2006). The short term and long term internal variations in the climate of GCM models necessitate decades-long, or even centuries-long, averaging periods to minimize, but unfortunately not negate, the effects of these variations on the results, see appendix B for an example of the effects of longer term variability on the results of GCM experiments.

The availability of computing resources and secure data storage capacities affect what kinds of experiments are possible and the kinds of analyses that can be conducted. The HadCM3 model runs at about 20 years a day using 16 cores on Bris-

tol's supercomputer Bluecrystal phase 2, and HadCM3L runs approximately twice as fast. This means that the same number of simulations 'cost' about half as much with HadCM3L. The speed of the models and the availability of computing resources limit the studies in this thesis to tens of model runs, hundreds of years long. EMIC models can consist of many times the number of simulations thus many different SRM geoengineering scenarios can be investigated at once, as in appendix C. There are limits on the data processing and storage of climate model output because if all variables were output for all timesteps on all gridcells a single simulation would generate tens of terabytes of data. Although it is possible to generate and store daily data if this were done for the tens of simulations of hundreds of years that the studies in this thesis require, it would constitute a vast amount of data and be challenging to analyze.

Standard control simulations were prepared for this chapter; a pre-industrial control and a simulation with instantaneously increased CO_2 concentration. These are standard experiments that are used in many model intercomparisons and SRM geoengineering is applied as a modification to the elevated CO_2 simulations to allow comparison to these standard controls (Meehl *et al.*, 2007b; IPCC, 2007; Kravitz *et al.*, 2011). All the simulations in this chapter consist of a 300 year spinup which allows the model to adjust to the altered conditions and a 100 year averaging period which allows a large signal-to-noise ratio to be achieved. Quadrupled CO_2 is used as the baseline in this chapter for the HadCM3L sunshade experiments as sunshade geoengineering has a potentially unlimited cooling effect and with a larger initial CO_2 forcing there will be a greater sunshade induced signal. Three different CO_2 concentrations, doubled, tripled and quadrupled from the pre-industrial control, are investigated with HadCM3 to determine whether the effects of sunshade geoengineering change at different CO_2 concentrations.

In all the sunshade experiments in this chapter the sunshade geoengineering is implemented by reducing the solar constant, i.e. reducing the constant which sets the incoming top-of-atmosphere shortwave radiation in the model. The insolation reduction required to offset the effects of elevated CO_2 concentrations was estimated from simple energy balance calculations and then iterated to achieve the pre-industrial global mean temperature within 0.1 K. The iteration is required as an insolation reduction based on a simple energy balance calculation fails to account for feedbacks

in the climate system which reduces the effectiveness of sunshade geoengineering (Schmidt *et al.*, 2012; Lunt *et al.*, 2008b).

2.5 Assessing the regional disparities in geoengineering impacts

2.5.1 Abstract

Solar Radiation Management (SRM) Geoengineering may ameliorate many consequences of global warming but also has the potential to drive regional climates outside the envelope of greenhouse-gas induced warming, creating 'novel' conditions, and could affect precipitation in some regions disproportionably. Here, using a fully coupled climate model we explore some new methodologies for assessing regional disparities in geoengineering impacts. Taking a $4 \times CO_2$ climate and an idealized 'sunshade' SRM strategy, we consider different fractions of the maximum theoretical, $4 \times CO_2$-cancelling global mean cooling. Whilst regional predictions, particularly in relatively low resolution global climate models, must be treated with caution, our simulations indicate that it might be possible to identify a level of SRM geoengineering capable of meeting multiple mitigation targets. It may be possible to maintain a stable mass balance of the Greenland ice sheet and lower the global mean temperature without reducing global precipitation below pre-industrial levels or exposing significant fractions of the Earth to 'novel' climate conditions.

2.5.2 Introduction

General Circulation Model (GCM) studies of large scale SRM geoengineering schemes, such as the creation of a solar 'sunshade' (Angel, 2006) or stratospheric sulphate aerosol injection (Crutzen, 2006) have revealed that a globally uniform intervention cannot cancel out the pattern of warming that elevated CO_2 creates (Brovkin *et al.*, 2009; Govindasamy *et al.*, 2003; Lunt *et al.*, 2008b). Even for a perfect correction for the global mean surface air temperature, the poles are left relatively warmer and the equator cooler due to differences in the zonal distributions of short and long wave radiation budget (Govindasamy *et al.*, 2003; Lunt *et al.*, 2008b). Adverse impacts of SRM geoengineering on the hydrological cycle may be more serious, with most

simulations indicating a global reduction in precipitation with more acute changes regionally (Bala *et al.*, 2008; Lunt *et al.*, 2008b). The potential to exacerbate droughts (or floods) beyond the effects of elevated CO_2 alone makes the consideration of SRM geoengineering technologies controversial (Bala *et al.*, 2008; Robock *et al.*, 2009).

The nature and patterns of the climatic (and ultimately, socio-economic) impact of geoengineering must hence be understood for adequately informed decision making on potential SRM implementation. In this paper we explore different ways in which regional disparities in geoengineering impacts can be assessed in a fully coupled climate model. However, it must be borne in mind that GCMs, whilst being the best available tools (short of large-scale field trials and partial deployment) to assess the likely impacts of SRM geoengineering, currently do not perform well on the regional scale and particularly not for precipitation (IPCC, 2007).

2.5.3 Methodology

We used the fully coupled atmosphere-ocean UK Met Office GCM, HadCM3L (Cox *et al.*, 2000) in a configuration identical to that described by (Lunt *et al.*, 2008b). With this, we carried out 12 400-year climate model simulations, all initialized from the end of a (pre-industrial) spin-up totaling more than 1000 years, with the final 100 years used to calculate the climatological averages. Of these, 3 followed Lunt *et al.* (2008b) a pre-industrial control ('Pre'), a simulation with atmospheric CO_2 set at 1120 ppmv, i.e., 4 times the pre-industrial value ('0%Geo'), and a simulation with 1120 ppmv but reduced solar constant ('100%Geo'). In 100%Geo (full SRM), the reduction in the solar constant is chosen such that the global annual mean 2m air temperature is as close as possible to that of the Pre simulation and determined iteratively (Lunt *et al.*, 2008b). For 100%Geo, the solar constant is reduced by 57 Wm^{-2} from the standard value used in Pre, a reduction of 4.2%. A further 9 simulations were carried out; all at 1120ppmv CO_2 but differing in that the solar constant is reduced by a fraction of the maximum 100%Geo value from 10% to 90% in increments of 10%. It should be recognized that these simulations are not intended to represent realistic scenarios of future climate or geoengineering mitigation per se, but instead are designed to illustrate the effect of degrees of SRM geoengineering on a high-CO_2 world and how the spatial patterns of impact might change.

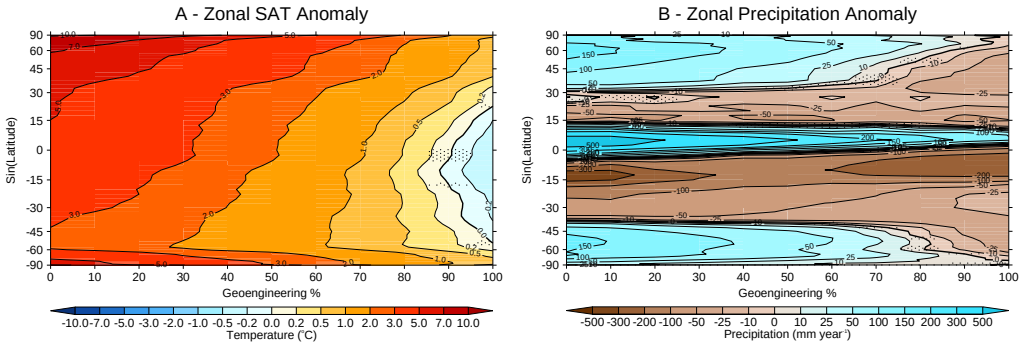

Figure 2.1: Zonally averaged anomaly with pre-industrial control, a: mean annual surface air temperature (SAT) and b: precipitation. Plots show the sine of latitude (to facilitate comparison on a per-area impacted basis) against the level of SRM geoengineering. Stippling indicates areas which fail a 5% student t-test.

2.5.4 Results

As previously noted (e.g., Govindasamy *et al.* (2003); Brovkin *et al.* (2009); Lunt *et al.* (2008b)), we find that SRM does not perfectly cancel the warming due to elevated CO_2 levels, even when prescribing a reduction in the solar constant sufficient to return the global average surface temperature to pre-industrial (Figure 2.1a). With an increasing degree of SRM geoengineering deployment, surface air temperatures (SAT) decrease, with higher latitudes cooling more than lower latitudes. For full SRM deployment (100%Geo), annual SAT at the equatorial regions becomes cooler than pre-industrial (~ -0.5°C) while the poles remain warmer ($\sim +1$°C). The radiative forcing from a reduction in the solar constant is greatest at the equator and diminishes towards the poles, the same is true for the radiative forcing from CO_2 but the meridional gradient is less steep, resulting in a net negative radiative forcing in the tropics and a net positive forcing at the poles (Lunt *et al.*, 2008b). This produces a temperature difference between the Polar Regions and the equatorial regions which is amplified by the operation of temperature feedbacks involving snow cover and sea-ice extent.

The response of the zonal average precipitation anomaly as a function of the level of SRM is more complex (Figure 2.1b). In the simulated unmitigated $4 \times CO_2$ climate (0%Geo), we find substantial changes in hydrology which are broadly consistent with other fully coupled climate models (IPCC, 2007) increases in precipitation in the tropics and high latitudes and decreases in the sub-tropics. For the three wetter bands (Tropical, extra-tropical, and Polar), increasing the level of SRM de-

creases precipitation, and in the 100%Geo experiment, the extra-tropical regions end up drier and the tropics wetter than in the pre-industrial. In the southern subtropical zone between 10S and 15S, we observe a maximum in precipitation at ∼50% deployment and reduced precipitation at 0%Geo and 100%Geo.

However, aggregating geoengineering climatic changes into zonal and annual averages hides a more complex and heterogeneous pattern of geoengineering impacts. To visualize this we have defined a series of averaging regions, consisting of grouped national boundaries (but which are further subdivided to avoid averaging over disparate climate conditions) and based on those from the FUND model (Figure 2.2f). For illustration, here we show the change in annual and seasonal (Northern Hemisphere seasons, e.g. June, July and August for summer, etc.) precipitation for five different regions (Figure 2.2).

We find that the United States mainland region shows the closest match to global average values in precipitation; starting from a positive anomaly in annual precipitation of +7.7% at 0%Geo and decreasing with progressive application of SRM to −11.8% at 100%Geo. Annual precipitation reaches pre-industrial values between 40% and 50% of SRM deployment (Figure 2.2a), although the seasonality of rainfall has changed with relatively more rainfall in Autumn and Winter than Spring and Summer at 40-50%. The East Chinese (Figure 2.2b) region experiences a +28.6% increase in annual precipitation under unmitigated greenhouse warming (0%Geo) compared to pre-industrial which decreases under SRM geoengineering, returning to close to the pre-industrial annual average (−0.9% reduction) and seasonality (aside from a slightly drier spring) at 100%Geo. The Brazilian and Australian regions (Figure 2.2c and 2.2d) display large reductions in annual precipitation at 0%Geo which is ameliorated, to a greater or lesser extent, by increasing levels of SRM. The Australian region shows a complete recovery from a 28.0% reduction in annual precipitation and returns to the pre-industrial average under 100%Geo. The Brazilian region shows a lesser recovery from −34.8% to −9.5%. In the Western European region (figure 2.2e) there is a shift to a much drier summer and a wetter winter at 0%Geo and under increased levels of SRM this shifts and the pre-industrial seasonality is restored however, overall the Western European region shows relatively little response in annual average precipitation to SRM deployment. It should be noted that despite using 100 year averages to calculate the climate state there will

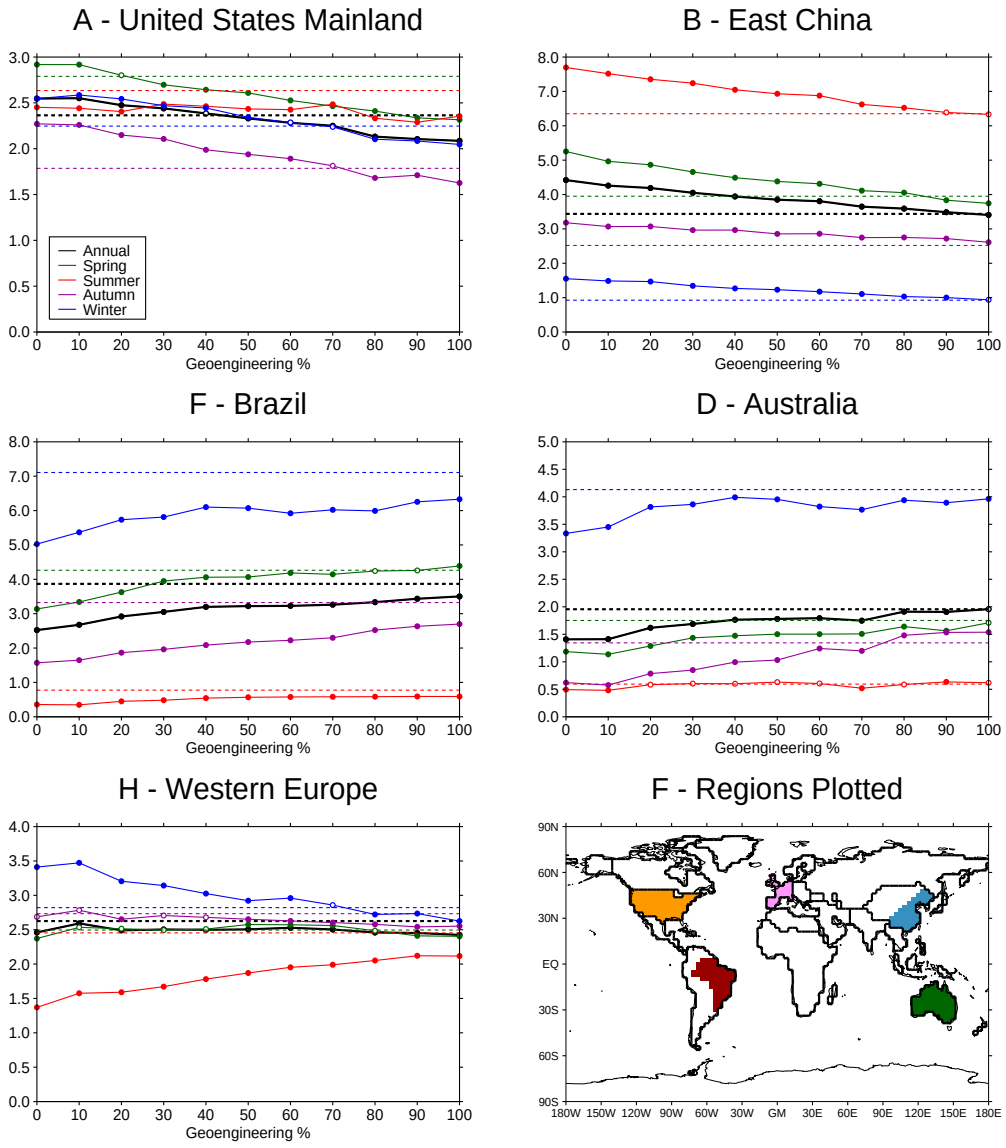

Figure 2.2: Panels a to e display the average daily rainfall in mm per day, both seasonally and annually, as a function of the level of geoengineering. The pre-industrial average is shown with a thick dashed line for the annual average and with thin dashed lines for each season. Unfilled circles show which values failed a 5% student t-test. Panel f shows the regions plotted and the borders of the FUND regions on which they are based (Anthoff *et al.*, 2009).

still be a degree of natural variability in these results.

Even at the aggregation level of the regions discussed above, important smaller scale impacts may still be obscured. Moreover, geoengineering impacts will differ substantially in socio-economic terms according to the relationship between climatic change and for example, distributions of population and cropland. As we have shown in figure 2.1 the climate effects of sunshade geoengineering differ depending on latitude and between regions, the global mean response will not necessarily characterize the impacts on cropland or urban areas as a whole. We have thus explored an alternative means of assessing the regionality of the climate response to geoengineering, retaining the impacts calculated at the native resolution of the climate model (3.75° longitude by 2.5° latitude (Cox *et al.*, 2000)), but calculating a single index by weighting the impacts according to specific 'recipients'. To illustrate, we present analysis weighted on a cropland fractional area and population density (per capita) basis, e.g.:

$$\Delta T_{crops} = \sum F_{crops,i} \cdot \Delta T_i \tag{2.1}$$

where ΔT_i is the change in temperature in gridcell i, $F_{crops,i}$ is the fraction of all cropland that is in gridcell i, and ΔT_{crops} is the weighted total change in temperature over cropland areas. This means that the impact on a small, highly cultivated region would be equal to the same impact on a large expanse of lightly cultivated land if they contained the same total area of crops, whilst two regions with the same intensity of cultivation would be weighted in direct proportion to their area. Figures 2.3e and 2.3f show the fraction of global crop area and population, at the resolution of the GCM model, used to generate this weighting.

Figure 2.3a summarizes the changes in global average temperature and precipitation as well as average changes over crop area and populated areas. The crop area is calculated from the distribution of C3 and C4 grasses in managed regions derived from the Wilson and Henderson-Sellers vegetation cover dataset (Wilson and Henderson-Sellers, 1985) and the population distribution is derived from the LandScan 2007 population dataset (LandScanTM, 2007). At 0%Geo, compared to pre-industrial, globally there is a 4.87°C warming and a 5.8% increase in precipitation whereas at 100%Geo there is a return to the pre-industrial temperature and a 5% reduction in the average precipitation (Lunt *et al.*, 2008b). To return average annual precipitation to the pre-industrial value globally would require ∼55% of full

geoengineering deployment. However, this figure is ∼75% for crop regions and ∼85% for populated areas.

Even weighting by crop area/population density will mask disparities in regional precipitation and hence 'winners' and 'losers' of SRM geoengineering. We therefore introduce the concept of a 'novel' climate, which we define as the existence of a climatic state, measured by either surface temperature or rainfall (annual or seasonal), that lies outside the continuum of climatic states bounded by the pre-industrial and an unmitigated ($4 \times CO_2$) greenhouse. Figure 2.4 illustrates this novel climate definition. Of the 3 geoengineered climates shown in figure 2.4 two would be classed as novel, B and C, as they produce a climate state outside of the bounds defined by the unmitigated global warming case. For example, for a full SRM deployment, we would class the cooler-than-pre-Industrial tropics (Brovkin *et al.*, 2009; Govindasamy *et al.*, 2003) as constituting a 'novel' climate. However, to give a reasonable margin of error and to account for inter-annual variability we require the mean geoengineered climate state to exceed a threshold, based on the standard deviation of pre-industrial or unmitigated ($4 \times CO_2$) climate variability, before it is classed as 'novel'.

Figures 2.3 b, c, d show the fraction of the global area (b), crop area (c) and population (d) which are affected by a novel climate at each level of SRM for 3 different thresholds, i.e. a climate state that is beyond 0.25, 0.5 and 1.0 standard deviations of the upper/lower bound. For global aggregation (figure 2.3b), we find, using the lowest threshold (± 0.25 SD), that for all levels of geoengineering some regions are affected by a novel precipitation, with 67% of the world affected at 100%Geo. With a more stringent threshold for a novel precipitation, the fractions affected are much lower, 33% for the moderate threshold (± 0.5 SD) 5% for the highest threshold (± 1.0 SD). For crop area aggregation (figure 2.3c) there is little change from the global picture but for population aggregation (figure 2.3d) there is an increase in the affected fraction at higher levels of geoengineering for all threshold levels. Novel (cool) temperature conditions occur in the global analysis at around 70-80%Geo with 61% of the Earth affected at the lowest threshold, dropping somewhat to 35% affected at the highest threshold. For both crop area (figure 2.3c) and population (figure 2.3d) aggregation a smaller fraction is affected by the cooler temperatures, this is due to the cooling mainly occurring in tropical and ocean areas.

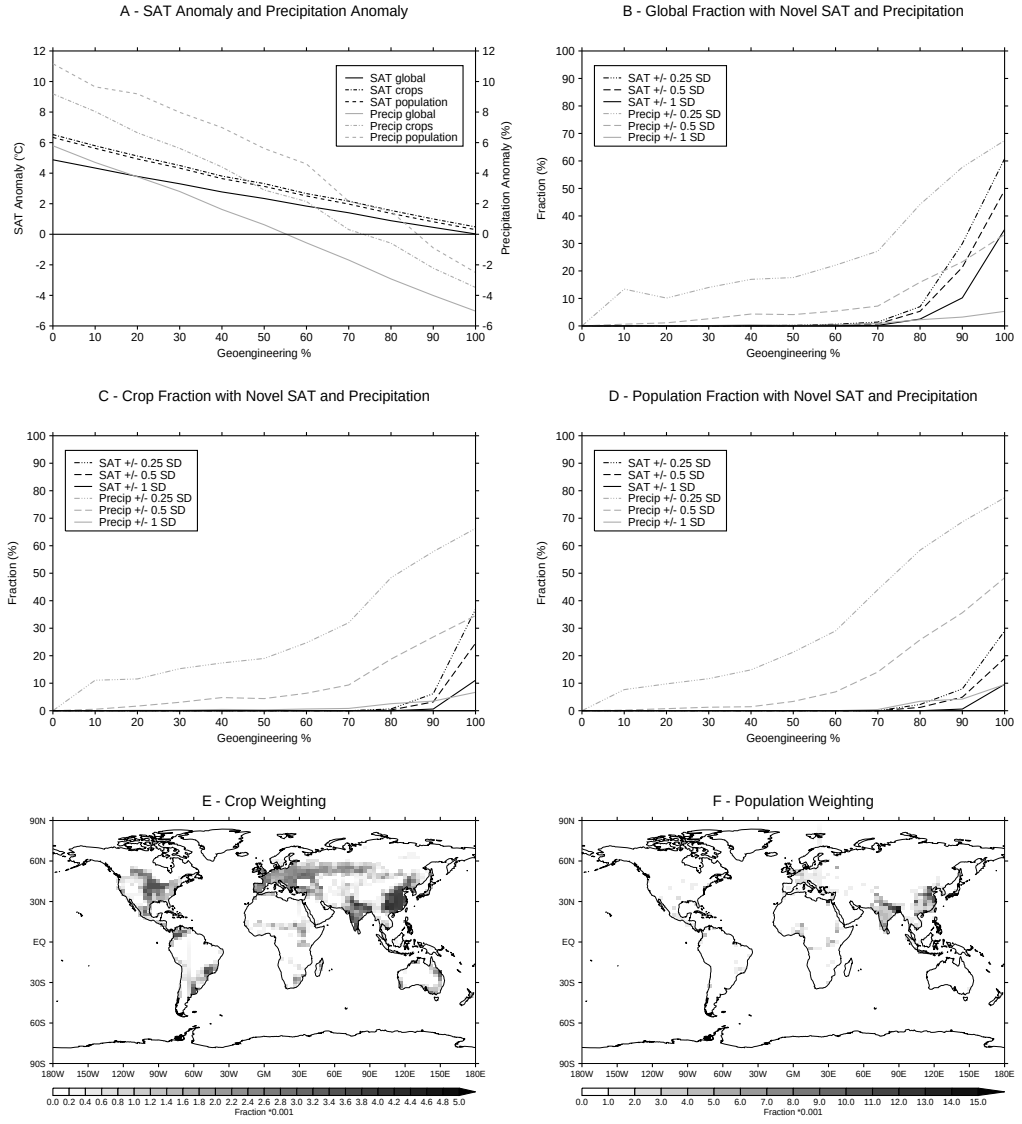

Figure 2.3: Panel a shows the average surface air temperature (SAT) and precipitation (Precip) anomaly with the pre-industrial control as a function of the level of geoengineering, for the global average, weighted by crop area or by population. Panels b-d show the fraction of the global area (b), crop area (c) or population (d) which experience novel SAT and precipitation conditions as a function of the level of SRM geoengineering (see text for description). Panels e and f show the crop area and population weighting applied to calculate the above.

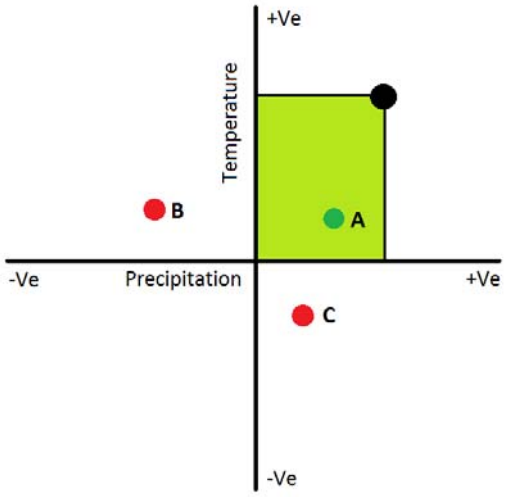

Figure 2.4: Shows illustrative pre-industrial anomalies for unmitigated global warming (black spot) and for 3 geoengineering cases (red and green spots). the unmitigated global warming anomaly defines an acceptable space (green rectangle); A is within the acceptable region and so is not classed as novel whereas B and C are outside the region and so are classed as novel.

2.5.5 Discussion and conclusions

GCMs have model-specific biases, particularly with respect to precipitation changes at the regional and seasonal scales, and this will be reflected in assessments of geoengineering impacts. Even at the global scale, it is noticeable that models differ in the percentage (or absolute Wm^{-2}) reduction in the solar constant needed to cancel out a given concentration of CO_2 (e.g., $4 \times CO_2$). For instance, Govindasamy *et al.* (2003) find that to offset the warming of a quadrupling of CO_2 compared to pre-industrial, a 3.6% reduction in insolation is required, compared to our estimate of 4.2%. This difference likely reflects inter-model differences in climate sensitivity, because many of the same climate feedbacks will operate in response to both changes in incoming shortwave radiations and CO_2. The warming of 4.02°C reported by Govindasamy *et al.* (2003) at $4 \times CO_2$ compared to 4.87°C in this study is in approximately the same proportion as the solar constant change, supporting our interpretation. For full sunshade geoengineering the negative solar forcing is greatest at the equator and least at the poles and although the longwave forcing from CO_2 is greatest at low latitudes and reduced at high latitudes, the latitudinal gradient is less steep than for the solar forcing resulting in a net negative radiative forcing in the tropics and a net positive radiative forcing at high latitudes which causes the equator to be overcooled and the poles undercooled. Sunshade geoengineering

reduces precipitation because the reduction in solar radiation leads to a change in the surface energy budget which is made up by a reduction in the latent heat flux to the atmosphere thus to a reduction in evaporation and precipitation (Bala *et al.*, 2008). Beyond the global scale, precipitation patterns are not as well modeled in GCMs as temperature patterns and so our results should be viewed with this in mind (IPCC, 2007). The GCM ensemble used in the IPCC's 4^{th} report reproduced the observed zonal mean distribution of precipitation well and captured the major regional precipitation patterns (e.g. maxima over rainforests), but there were deficiencies in the ensemble's estimates for tropical precipitation, particularly in the tropical Atlantic and around the Bay of Bengal and the Maritime continent (IPCC, 2007). When predicting precipitation changes as a result of global warming by the end of the 21^{st} century, the magnitude of the change varies between GCMs with agreement on the sign of the change in most regions, with most of the disagreement in the mid-latitudes (IPCC, 2007).

Furthermore, although the coupled GCM we used, HadCM3L, has been used in studies of future and past climates (e.g., (Cox *et al.*, 2000; Lunt *et al.*, 2007)), it has a relatively low resolution compared to many models used in the 4^{th} Assessment Report (IPCC, 2007). We have also chosen to keep vegetation fixed at pre-industrial values in the simulations in this study, therefore neglecting vegetation-climate feedbacks.

If SRM geoengineering were to be implemented, it is apparent that it need not be deployed fully (i.e., to return global average temperatures to the pre-industrial value) and alternative mitigation objectives such as ensuring a neutral surface mass balance of the Greenland ice sheet (Oppenheimer and Alley, 2005) might be considered, see section 2.6. Restricting to only partial deployment may also avoid the occurrence of a significant area being affected by novel climates and hence adverse impacts.

Although the results presented here are illustrative rather than predictive per se, and need to be replicated with higher resolution GCMs and ideally in multi-model ensembles, they indicate that it might be possible to identify a level of SRM geoengineering sufficient to cool the climate significantly via SRM, but without a large reduction in global precipitation and exposing only a small fraction of the Earth to novel climates. Clearly, a comprehensive cost-benefit analysis covering the impacts on agriculture, biodiversity, human health and other factors would also be

required to assess adequately any proposed SRM geoengineering intervention.

2.5.6 The linearity of the climate response to a range of strengths of sunshade geoengineering

Irvine *et al.* (2010) is a short study and as such there was little space to present all the results from the investigation into the climate effects of full and partial sunshade geoengineering. This section presents climate anomaly plots, to assess whether there is evidence that the linear climate response to sunshade geoengineering strength seen at the global and regional level also hold at the gridcell level. Figure 2.5 shows surface air temperature (SAT) and Precipitation anomalies for $4 \times CO_2$ and $4 \times CO_2$ with 2 different sunshade levels; 50% and 100%. The SAT anomaly is higher than the global mean at high latitudes, particularly in the Northern Hemisphere, and over continental regions for the unmitigated and both geoengineered cases (see panels a, c and e). For 100% sunshade some regions are cooled below their pre-industrial temperatures with most of the tropical and southern ocean cooler and some tropical continental regions cooler too. For 50% sunshade geoengineering the global-mean temperature anomaly from the pre-industrial is half that of $4 \times CO_2$ and the global-mean precipitation is only 1% higher than in the pre-industrial. These global-mean figures are reflected in the SAT and precipitation anomalies for 50% sunshade geoengineering with the pattern of temperature anomalies similar to the $4 \times CO_2$ response but substantially reduced and precipitation anomalies are similar to $4 \times CO_2$ but with mid-latitude precipitation close to the pre-industrial state. For all simulations there are large shifts in patterns of precipitation and all simulations show a northward shift in the ITCZ perhaps as a result of the warming of the northern hemisphere relative to the southern hemisphere (see panels b, d and f).

Figure 2.2 and 2.3 showed a near-linear climate response, at the global and regional level of aggregation, to changes in sunshade strength and these anomaly plots provide some insight into whether this linearity extends to the gridcell level. The results of figure 2.5 (above) reflect the zonal climate anomaly changes seen in figure 2.1, and show nothing that would contradict the assumption that the near-linear change in climate anomaly seen at the regional scale may extend to the gridcell level. A truly robust assessment of the linearity of the climate response to sunshade geoengineering is difficult to achieve due to the fact that the data is essentially four

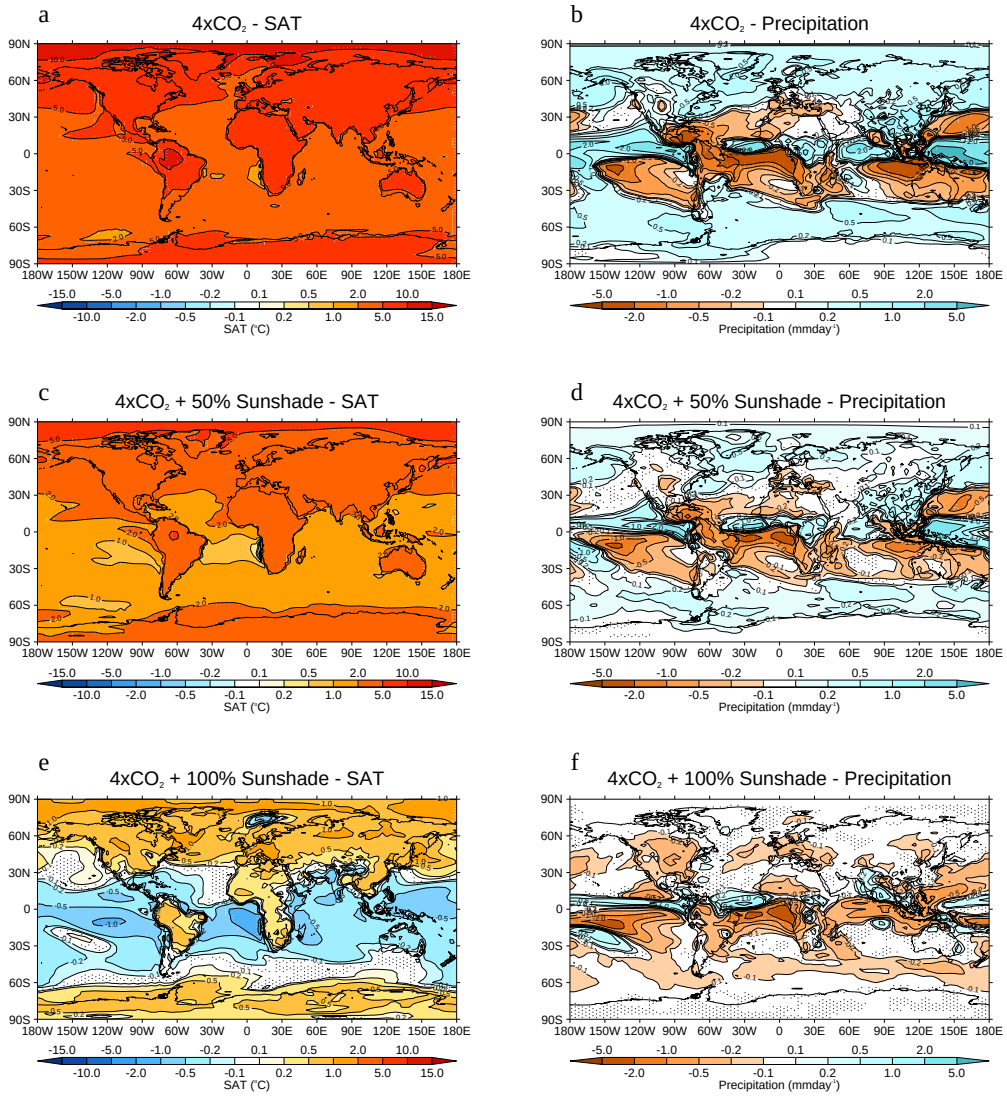

Figure 2.5: Surface air temperature (SAT) and Precipitation anomalies for $4 \times CO_2$ (a, b), $4 \times CO_2$ with 50% sunshade (c, d), and $4 \times CO_2$ with 100% sunshade (e, f), relative to the pre-industrial. Stippling indicates which areas failed a 5% student t-test.

dimensional; with model variability in the hundred year averaging period affecting the climate signal of the eleven different sunshade geoengineering strength experiments (0% to 100%). These results show that HadCM3 responds linearly to the strength of sunshade geoengineering at the global and regional level and there are indications that this linearity may hold down to the gridcell-scale.

2.6 The fate of the Greenland Ice Sheet in a geoengineered, high CO_2 world

2.6.1 Abstract

SRM Geoengineering has been proposed as one means of helping avoid the occurrence of dangerous climate change and undesirable state transitions ('tipping points') in the Earth system. The irreversible melting of the Greenland Ice Sheet is a case in point - a state transition that could occur as a result of CO_2-driven elevated global temperatures, and one leading to a large rise in sea-level. SRM schemes such as the creation of a 'sunshade' or injection of sulphate aerosols into the stratosphere could reduce incoming solar radiation, and in theory balance, on a global mean, the greenhouse warming resulting from elevated concentrations of CO_2 in the atmosphere. Previous work has highlighted that a geoengineered world would have: warming towards the poles, cooling in the tropics, and a reduction in the global hydrological cycle, which may have important implications for the Greenland Ice Sheet. Using a fully coupled global climate model in conjunction with an ice sheet model, we assess the consequences for the mass balance of the Greenland Ice Sheet of the reorganization of climate patterns by the combination of high CO_2 and geoengineering. We find that Greenland surface temperature and precipitation anomalies compared to pre-industrial, decrease almost linearly with increasing levels of SRM geoengineering, but that these combine to create a highly non-linear response of the ice sheet. The substantial melting of the Greenland Ice Sheet predicted for four times pre-industrial CO_2 levels is prevented in our model with only a partial application of SRM, and hence without having to fully restore the global average temperature back to pre-industrial levels. This suggests that the degree of SRM geoengineering required to mitigate the worst impacts of greenhouse warming, such as sea-level rise,

need not be as extensive as generally assumed.

2.6.2 Introduction

It is expected that by the end of the century, global average surface temperatures will have risen by a further 1.5-4°C, depending on emissions pathway (IPCC, 2007). To avoid 'dangerous' climate change (Hansen *et al.*, 2006) and the occurrence of undesirable and rapid and/or discontinuous state transitions in the Earth system (known loosely as 'tipping points' (Lenton *et al.*, 2008)), many authors and international bodies are calling for efforts to limit the temperature rise to a maximum of 2°C (Hansen *et al.*, 2006). However, efforts to secure the necessary reductions in CO_2 emissions have so far been mostly unsuccessful and a recent study showed that even relatively ambitious CO_2 reduction targets may fail to prevent an eventual 2°C temperature rise (Weaver *et al.*, 2007).

One of the already observable consequences of greenhouse warming is a reduction in the volume of the Greenland Ice Sheet (GrIS) (Alley *et al.*, 2005; Krabill *et al.*, 2004; Rignot *et al.*, 2008) and an associated sea-level rise. For a sustained atmospheric CO_2 concentration of 550 ppm, Alley *et al.* (2005) estimate that a near-total melting of the GrIS would eventually occur, albeit highly unlikely to occur in the next century (Pfeffer *et al.*, 2008). Although there are uncertainties regarding where the CO_2 threshold for complete melting lies (e.g. Lunt *et al.* (2009)) as well as the timescale at which the melting would take place, the extreme social and economic consequences of even a fraction of the maximum potential sea-level rise of 7.3m occurring (Bamber *et al.*, 2001), clearly warrant an urgent assessment of whether mitigation strategies exist for melting of the GrIS and whether they would be effective.

SRM geoengineering has been proposed as a means to avoid dangerous levels of climate change and tipping points (such as large-scale melting of the GrIS) being crossed (Shepherd *et al.*, 2009; Irvine and Ridgwell, 2009). however, returning global mean temperatures to pre-industrial does not *a priori* imply that the GrIS would be safeguarded. This is because these types of solar radiation management (SRM) do not provide a perfect cancellation of global warming and restoration of a pre-industrial climate. Instead, due to latitudinal differences in the radiative forcing of sunshade geoengineering and CO_2, the tropics tend to end up cooler and the

poles warmer than pre-industrial, even when temperature is restored at the global mean (Lunt *et al.*, 2008b; Govindasamy and Caldeira, 2000; Matthews and Caldeira, 2007). As such, it is possible that SRM would not be effective against sea-level rise, as both the Greenland and Antarctic ice sheets would likely remain significantly warmer than pre-industrial.

In this paper, we investigate the efficacy of SRM geoengineering in mitigating against sea-level rise from the GrIS and specifically in the context of its long-term mass balance. We also estimate the minimum level of SRM geoengineering required to avert a potential tipping point associated with the GrIS and the associated sea-level rise. However, our analysis excludes contributions to sea-level rise from the Antarctic ice sheet and from the thermal expansion of the oceans.

2.6.3 Methodology

To assess the response of climate to greenhouse forcing and SRM geoengineering, we use the fully coupled atmosphere-ocean UK Met Office GCM, HadCM3L (Cox *et al.*, 2000). HadCM3L has a horizontal resolution of 3.75° longitude by 2.5° latitude in the atmosphere and ocean, 19 vertical levels in the atmosphere and 20 vertical levels in the ocean. It consists of a hydrostatic primitive-equation atmosphere, with parameterizations for sub-gridscale processes such as convection (Gregory and Rowntree, 1990). The ocean includes parameterizations of eddy mixing (Gent and McWilliams, 1990), and a dynamic-thermodynamic sea ice scheme (Cattle and Crossley, 1995). The configuration of the climate model we use is identical to that described by (Lunt *et al.*, 2008b). A version of the model with increased ocean resolution (HadCM3) has been extensively tested (Gordon *et al.*, 2000) and performs well relative to other GCMs according to a variety of metrics (IPCC, 2007; Covey *et al.*, 2003).

Using this model we carried out twelve 400-year climate model simulations, all initialized from the end of a spin-up totaling more than 1000 years, with the final 100 years used to calculate the climatological averages. The first is a pre-industrial control ('Pre'), the second has atmospheric CO_2 set at 1120 ppmv, 4 times the pre-industrial value ($4 \times CO_2$) , and the other ten simulations have $4 \times CO_2$ and a reduced solar constant scaled according to the assumed degree of SRM geoengineering. The pre-industrial climate has been chosen as the reference state as the GrIS was stable under these conditions and is beginning to melt under modern conditions

(van den Broeke *et al.*, 2009). For the reduced solar constant simulations; full SRM geoengineering ('100%Geo') has the solar constant reduced such that the global annual mean 2m air temperature was as close as possible to that of the Pre simulation, the other nine simulations have the solar constant reduced by a fraction of this value from 10% to 90% in increments of 10%. The reduction in solar constant for 100% SRM geoengineering was found by carrying out a number of preparatory simulations with improving estimates of the required reduction, as in Lunt *et al.* (2008b). As a result, simulation 100%Geo has a solar constant 57 Wm^{-2} less than that of Pre, a reduction of 4.2%. For comparison, Govindasamy *et al.* (2003) found that they required a reduction of 3.6% to offset a 4 times increase in CO_2. The radiative effect of stratospheric sulphate aerosols on the climate can also be approximated fairly well using a global reduction in insolation. For instance, Brovkin *et al.* (2009) find small differences in the radiative forcing effect for an even distribution of aerosol, while (Robock *et al.*, 2008) observe that a fairly even distribution of aerosols is possible for a constant injection of sulphates into the tropical stratosphere.

From the GCM simulations, we calculate the temperature and precipitation anomalies relative to the control simulation, and combine these anomalies with an observed climatology to drive an off-line ice sheet model - Glimmer (Rutt *et al.*, 2009). Glimmer (v. 1.0.4) is a three-dimensional thermomechanical ice-sheet model, configured over the Greenland region. The core of the model is based on the ice-sheet model described by (Payne, 1999). The model resolution is 20 km, and is configured as described in (Lunt *et al.*, 2008a, 2009). Glimmer performs well against established EISMINT benchmarks and against other analytical solutions for ice flow (Rutt *et al.*, 2009). However, due to the use of the shallow-ice approximation (Hutter, 1983), it does not well simulate fast-flowing ice streams and has a relatively simple treatment of basal sliding, basal hydrology, and calving at marine margins. The implications of some of these shortcomings are discussed later in the paper. The last 100 years of the climate simulations are used to generate an annual mean and half-range climatology - Glimmer then applies a sinusoidal seasonal and diurnal cycle to this climatology and this drives the ice sheet model for the duration of the experiment. The Glimmer ice sheet model uses an anomaly method to accommodate for biases in the driving climatology; the pre-industrial is the control simulation with all other simulations applying an anomaly to the standard (i.e., observed) climatology. For

each GCM simulation, the ice sheet model is run for 50,000 years, allowing most of the simulations to come to equilibrium with the driving climatology. Three simulations required more time to reach equilibrium; these were run for a further 50,000 years. A full description of the offline coupling of the climate model and ice sheet model can be found in (Lunt *et al.*, 2008a, 2009).

2.6.4 Results

The mass balance of an ice-sheet depends on the net difference between the rate of snow accumulation and the melt rate, and hence the balance between precipitation and temperature across the region and season of ablation. Increases in summer temperatures have the largest impact on the mass balance of ice sheets as this is the time when air temperatures are highest, the ablation zone largest, and surface ice melt rates most rapid. The total amount of snow, and the amount of rain that subsequently freezes, that falls on the ice-sheet throughout the year determines the accumulation of ice mass.

In the absence of SRM geoengineering and hence an un-mitigated $4 \times CO_2$ climate, the centre of the GrIS has a summer average temperature over 6°C warmer than in the pre-industrial with no region experiencing a temperature less than 4°C warmer (Figure 2.6a). However, annual precipitation also increases across Greenland, with increases of over 6m per year along some of the eastern coast and towards the southern tip (Figure 2.6d).

Both the patterns as well as magnitude of temperature and precipitation anomalies change as a function of the degree of SRM geoengineering (Figure 2.6). Figures 2.6b and 2.6c show the annual average temperature anomalies for the 50%Geo and 100%Geo simulations, illustrating how climatological patterns respond to the degree of SRM geoengineering intervention. The annual mean surface air temperature anomalies in Greenland are significantly reduced with the application of 100% SRM geoengineering, although the island remains warmer than in the pre-industrial. A temperature increase of at least 0.5°C persists across Greenland with the northern and southern coasts experiencing a warming of 0.75°C and the southern tip has over 1°C of warming. The 50%Geo simulation shows an approximately intermediate warming compared with pre-industrial and 100%Geo, with at least 3°C of warming across most of the island. For both 50%Geo and 100%Geo, Greenland experiences

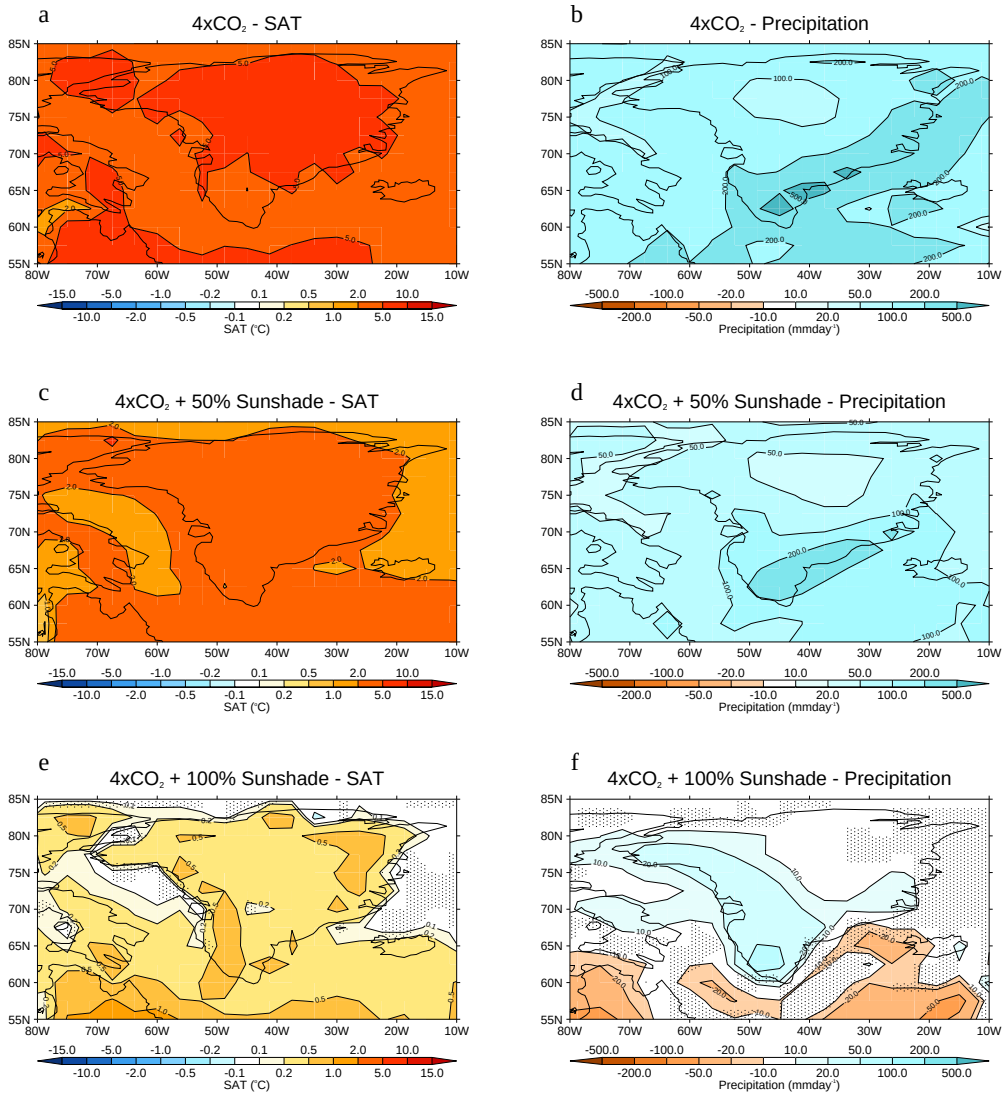

Figure 2.6: a, b and c shows the summer temperature anomaly with pre-industrial for the $4 \times CO_2$, 50%Geo and 100%Geo simulations respectively. d, e and f show the annual precipitation anomalies for the same simulations. Stippling indicates which regions failed a 5% student t-test.

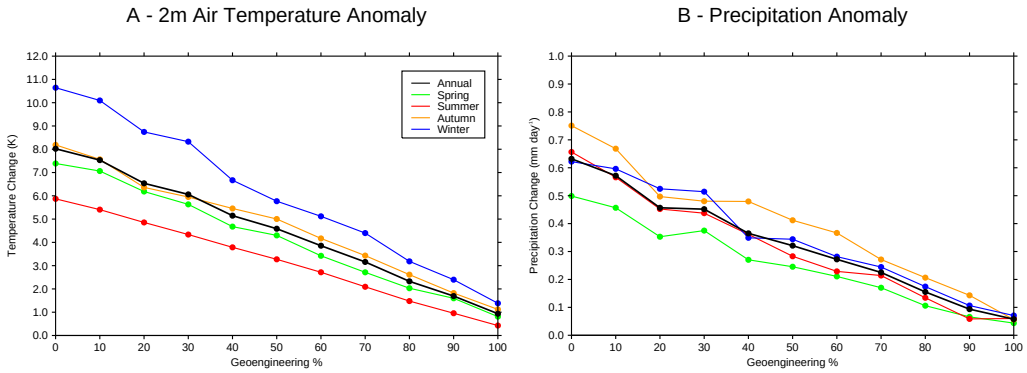

Figure 2.7: Seasonal and annual anomalies relative to pre-industrial for different levels of SRM geoengineering, averaged over Greenland. a: 2m air temperature anomaly, b: precipitation anomaly. All values passed a 5% student t-test.

a smaller increase in precipitation than temperature. This increase in precipitation over Greenland for 100%Geo is despite the global mean reduction in precipitation found in this study and other studies of sunshade and stratospheric aerosol geoengineering (Lunt *et al.*, 2008b; Robock *et al.*, 2008; Bala *et al.*, 2008) in which on a global scale, the reduced insolation causes a reduction in latent heat flux, and consequently evaporative flux, from the land and sea surfaces reducing the intensity of the global hydrological cycle. The regional precipitation increases we find in all of the simulations are focused to the south of the island.

Averaging the temperature anomalies over the area of Greenland, we find an approximate linear relationship with the level of SRM geoengineering (Figure 2.7a). For temperature, the annual average is 8°C warmer for $4 \times CO_2$, decreasing almost linearly to a 1°C positive anomaly for the 100%Geo simulation. This relationship also holds for the individual seasonal changes although the slope varies. The increase in summer temperature is 6°C at $4\times CO_2$, which is below the annual average warming whereas the spring temperature shows the greatest departure from pre-industrial with an anomaly of 10.5°C. The climate changes in the Arctic are affected by the ice-albedo effect, as sea-ice cover and snow cover is reduced; there is an increased absorption of sunlight and so regional warming (Johannessen *et al.*, 2004). There is also a reduction in the insulation of the Arctic Ocean as sea-ice cover retreats, this leads to an increased heat flux from the ocean in the autumn, which warms the atmosphere (Serreze *et al.*, 2000).

Similar responses to the degree of SRM geoengineering are apparent for the precipitation anomalies (Figure 2.7). With no SRM geoengineering the annual change

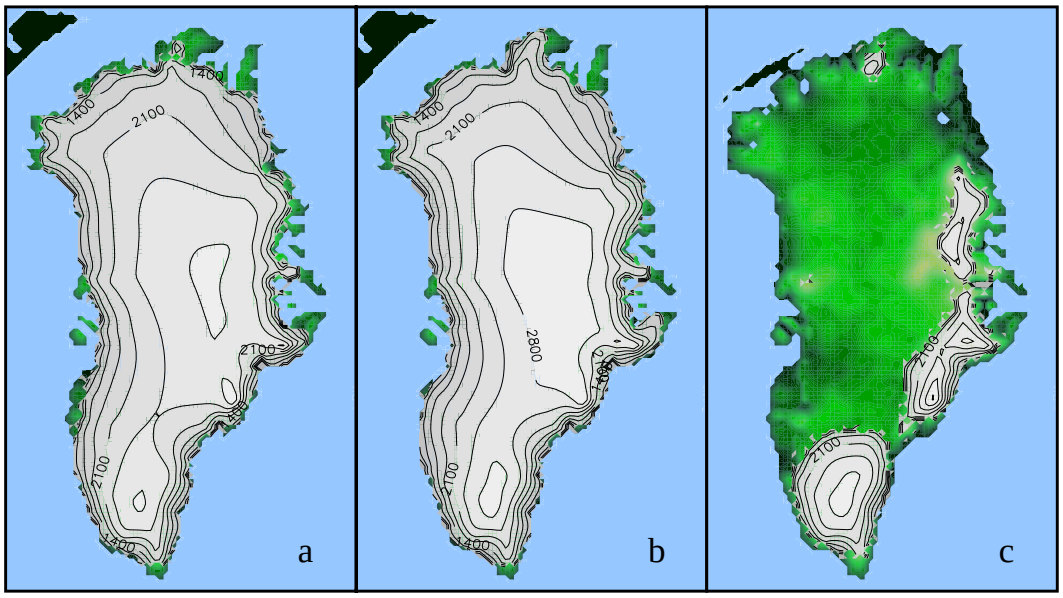

Figure 2.8: a: observed modern ice sheet, b Simulated pre-industrial ice sheet, c: ice-sheet at $4 \times CO_2$

in precipitation is 0.63 mm day^{-1} or 228 mm year^{-1}, which decreases roughly linearly with increasing SRM geoengineering level, with a positive anomaly of 21 mm year^{-1} for 100%Geo (Figure 2.7b). The greatest increase in precipitation occurs in the autumn with 76 mm year^{-1} more in the un-geoengineered case than in the pre-industrial. Winter and spring precipitation anomalies closely track the annual mean.

To assess the implications of a change in climate over Greenland on the global sea-level an ice sheet model must be used. Simply inferring sea-level changes from just the climate model output is insufficient as it is impossible to capture important properties of ice sheets like the altitude-temperature feedback, where an ice sheet which is accumulating/losing mass gains/loses altitude which lowers/raises the temperature of the ice sheet surface which lowers/raises ablation and helps to accumulate/lose more mass. The response of the GrIS mass to changes in the climate also has the potential to be non-linear with possible hysteresis due to the large positive altitude-temperature feedback.

Figure 2.8 shows the predicted ice sheet response, calculated by running Glimmer to equilibrium, for the pre-industrial and $4 \times CO_2$ simulations, as well as the observed modern ice sheet. In the pre-industrial control experiment (Figure 2.8b), the ice volume is over-estimated compared with observations (Figure 2.8a), giving a sea-level equivalent of 8.6m compared with the literature value of 7.3m (Bamber *et al.*,

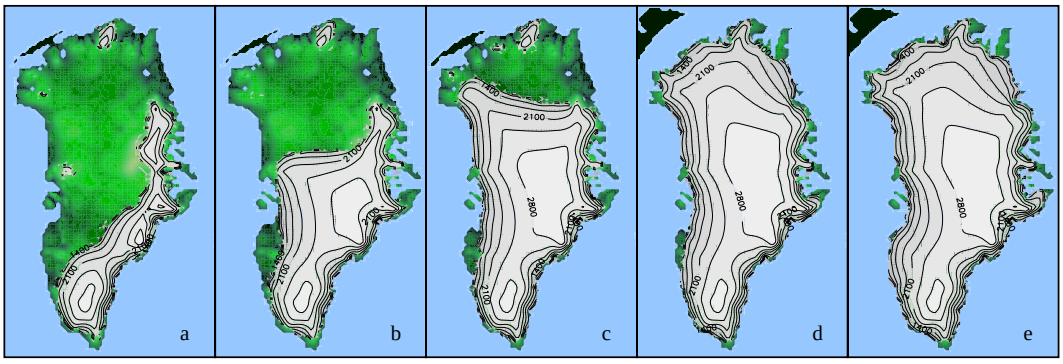

Figure 2.9: Shows the equilibrium ice sheet extent predicted for different levels of geoengineering: (a) 20%Geo, (b) 30%Geo, (c) 40%Geo, (d) 60%Geo, (e) 100%Geo. For b, d and e the ice sheets reach equilibrium after 50,000 years, For a and c 100,000 years were run to reach equilibrium.

2001). This is a common deficiency in current ice sheet models due, in part, to the lack of an accurate representation of ice dynamics (Ridley *et al.*, 2005; Huybrechts and de Wolde, 1999; Ritz *et al.*, 1997; Greve, 2000). Sea-level equivalents given here are estimated using the fractional ice sheet mass difference to calculate a sea-level rise equivalent and hence account for this systematic overestimation. Figure 2.8c shows the ice sheet height and extent at equilibrium after being forced by the $4 \times CO_2$ climatology; the ice sheet is only 12.8% of its original mass, equivalent to a sea-level rise of 6.4 m. The remnants of the ice-sheet are located at the high altitude regions on the eastern coastline and on the southern tip. Other authors have noted that a similar, near total, melting of the GrIS at 4 times pre-industrial CO_2 is likely (Gregory *et al.*, 2004a). However, the pattern of ice sheet remnants differs from others in that ice is present in the southern tip of the island (Alley *et al.*, 2005; Ridley *et al.*, 2005).

We now turn to the predicted extent and height of the ice sheets generated under different levels of SRM geoengineering (Figure 4). At 20% SRM Geoengineering (Figure 2.9a), the extent and coverage of the ice sheet is slightly larger than the un-geoengineered case, with the remnants of the ice sheet more inter-connected and larger. At 30% (2.9b) and 40% (2.9c) SRM geoengineering there is a partial ice sheet with losses in extent to the north of the island and losses in altitude for the 30%Geo case. The ice sheet is effectively at full height and coverage for 60% SRM geoengineering and above (figure 2.9d-e), and a pre-industrial ice sheet is maintained.

In contrast to the temperature and precipitation anomalies (Figure 2.7), the equilibrium response of the volume of the GrIS to the level of SRM geoengineering

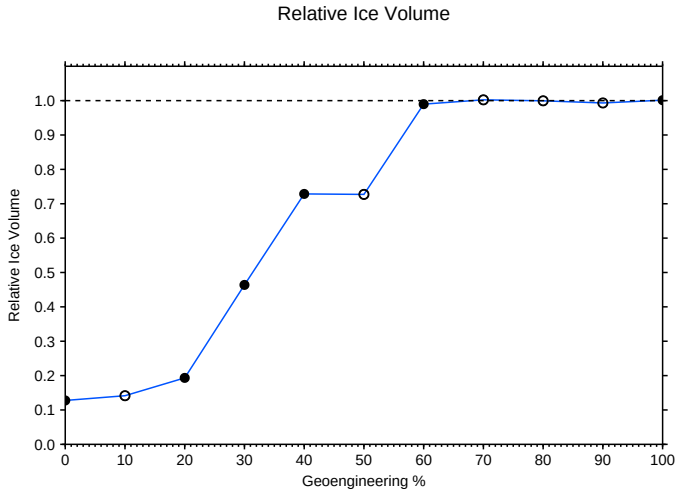

Figure 2.10: Fraction of ice volume, relative to pre-industrial, at different levels of SRM geoengineering. The filled circles highlight the ice sheets which are shown in figure 2.8 and in figure 2.9, unfilled circles are not displayed in other figures.

is highly non-linear and displays a step like behavior (Figure 2.10). The ice volume is only slightly increased for 10%Geo and 20%Geo compared with $4 \times CO_2$, increasing for 30%Geo and again at 40%Geo; 50%Geo produces the same ice sheet volume as 40%Geo, and in 60%Geo and at greater degrees of SRM geoengineering, the ice sheet volume remains at roughly the pre-industrial value.

2.6.5 Discussion and conclusions

For all of the SRM geoengineering simulations and the $4 \times CO_2$ case, the climate of Greenland is warmer and wetter than the pre-industrial. Averaged over Greenland, the temperature and precipitation anomalies decrease almost linearly with increases in the level of SRM geoengineering but with residual warming and wetting of Greenland at full SRM geoengineering. This contrasts with the global picture, in which average surface air temperature is exactly the same as in the pre-industrial for full SRM geoengineering and there is a net global reduction in precipitation (Lunt *et al.*, 2008b).

In agreement with previous work (Ridley *et al.*, 2005), the consequence of unmitigated ($4 \times CO_2$) climate change to the mass balance of the GrIS are drastic enough to eventually melt it almost entirely. By applying increasing degrees of SRM geoengineering and hence reductions in the incoming solar radiation, climate change under $4 \times CO_2$ is progressively mitigated at the global mean and over Greenland.

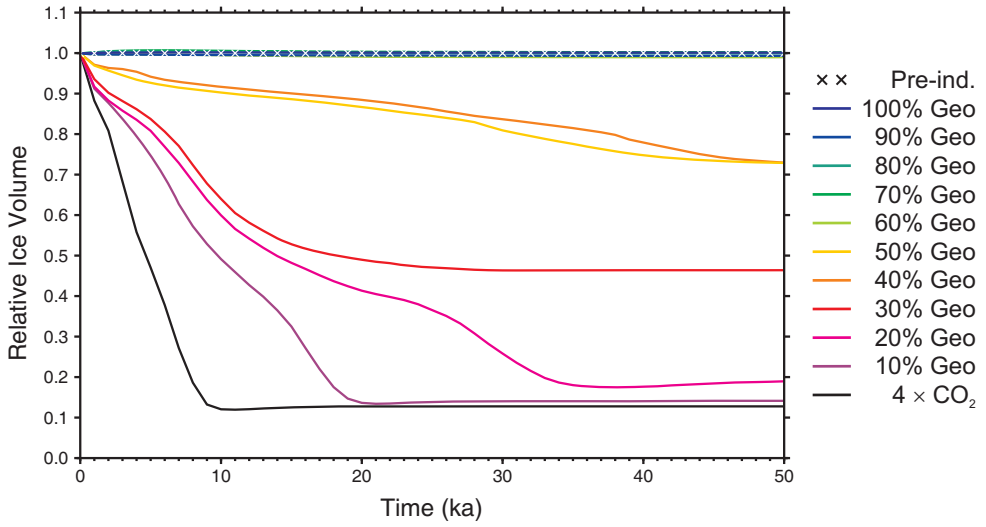

Figure 2.11: Evolution of the ice sheet volume, for all the simulations, relative to the equilibrium volume of the pre-industrial control ice-sheet. Only the first 50 ka are shown, as the ice sheets have mostly reached equilibrium by this point.

However, the approximately linear change in the climate conditions over Greenland are not reflected in the ice sheet response.

We interpret the varying responses to the degree of SRM geoengineering as reflecting the existence of multiple thresholds and stable states in the ice sheet, illustrated by the time-dependent behavior of ice sheet volume in Figure 2.11. For 20%, 40% and 50% SRM geoengineering the ice sheet has not quite reached equilibrium by 50,000 years however they are all within 0.5% of their volume after an additional 50,000 years. For 60%Geo and above a similar evolution is seen as for the pre-industrial. The 40%Geo and 50%Geo ice sheets follow similar trajectories, with 40%Geo having a greater volume than 50%Geo, but with both stabilizing at a relative ice volume of just over 70% of the pre-industrial ice sheet. The 20%Geo and 30%Geo cases follow similar trajectories until around 20,000 years at this point the ice-sheet in the 20% SRM geoengineering climate begins to collapse, ending slightly larger than the $4 \times CO_2$ case; the 30%Geo case stabilizes and a partial ice-sheet remains. The 10%Geo and the $4 \times CO_2$ cases both collapse rapidly leaving a residual ice-sheet with just over 10% of the pre-industrial control volume.

The ice sheet hence responds in a step-like manner to the SRM geoengineered changes in the climate; for low levels the ice sheet almost completely melts, for 30-50% SRM geoengineering a partial ice sheet remains and at levels of SRM geoengineering of 60% or above the ice sheet remains fully intact. We interpret the

bifurcation of the evolution of the 20% and 30% SRM geoengineering ice-sheets in terms of a positive altitude-temperature feedback, which amplifies the small difference in input climates and causes a run-away melting. Without further simulations it is hard to tell whether the 30% SRM geoengineering ice sheet represents a third stable level or whether it forms part of a continuum of partial ice sheets between 20%Geo and 40%Geo.

Our results suggest that a full SRM geoengineering intervention would prevent the melting of the GrIS and stop the resultant ice-induced sea-level rise. At $4 \times CO_2$ the melting of the GrIS would contribute 6.4 m to sea-level, for 30%Geo the sea-level rise would be 3.9m, for 40%Geo and 50%Geo 2m and at 60%Geo and above no sea-level increase from the GrIS is observed. The changes in sea-level that occur in the first 100 years of the simulations are strongly dependent on the level of SRM geoengineering: for $4 \times CO_2$ there would be 24cm, for 40%Geo 6cm, for 60%Geo 2cm and for 100%Geo there would be 0.1cm of sea-level increase. This dramatically non-linear response of the ice sheet highlights the necessity of detailed analysis of the regional impacts of SRM geoengineering schemes.

In interpreting the results presented here it must be borne in mind that the climate and ice sheet models available today have flaws and do not exactly reproduce observed modern climate and ice sheet extent. Many climate models agree on the broad changes in the temperature that would occur at high levels of CO_2 but there is a large degree of disagreement for regional climate change and for other aspects of climate such as cloud cover and precipitation. The UK Met Office Model (HadCM3), which is used in this paper, has a cold bias towards the poles over the Northern Hemisphere land masses (IPCC, 2007). However, the Glimmer model uses an anomaly method to calculate the climate to force the ice sheet and hence minimizes the consequences of the cold bias in the climate model.

It is also important to be aware that our simulations are performed without interactive coupling between the ice sheet model and GCM and hence neglecting in particular the ice-albedo feedback and any circulation changes from changes in orography, although the ice-altitude feedback is taken into account using a lapse-rate correction. Current ice sheet models also generally lack higher order physics and although able to simulate slow moving ice dynamics adequately they are not yet able to represent the dynamics of fast moving ice streams. Deficiencies of ice

sheet models in these areas is currently being addressed, with improvements to ice dynamics (Pattyn, 2003), representations of the fast ice streams and ice shelves (Schoof, 2006, 2007; Pattyn *et al.*, 2006), more realistic modeling of the surface mass balance (Bougamont *et al.*, 2007), and treatments of basal sliding which take into account positive feedbacks (Parizek and Alley, 2004; Price *et al.*, 2008). Recent work has indicated that current loss of mass from the Greenland ice sheet is roughly equally partitioned between surface mass balance changes and changes in dynamics (van den Broeke *et al.*, 2009). Given the large uncertainties in quantifying future dynamic ice losses at Greenland's marine terminating outlet glaciers, the thresholds determined in this paper for effective SRM geoengineering in the context of the GrIS should be regarded with some caution. In particular, it is likely that ice loss will be greater than predicted by the ice sheet model, resulting in a higher level of SRM geoengineering needed to avert a given sea-level rise.

It has been argued that the predicted changes in the climate caused by SRM geoengineering are not benign. For example, the reduction in global precipitation could have an adverse effect on agriculture, and so partial geoengineering could potentially be a more favourable proposition (Robock *et al.*, 2008; Bala *et al.*, 2008). From this study, we find that a partial SRM geoengineering intervention might also prevent the melting of the GrIS and avoid the sea-level rise that this would cause. However, the existence of thresholds and multiple states in sub-systems such as the GrIS cautions that regional impacts and climate teleconnections need be studied in detail when assessing SRM geoengineering and determining its efficacy.

2.7 Sunshade geoengineering at diverse CO_2 levels with HadCM3 and HadCM3L

2.7.1 Introduction

Sunshade geoengineering may be deployed whilst CO_2 levels are increasing or decreasing, and knowing whether the climate effects will change at different CO_2 levels is important. Section 2.7.3 compares sunshade geoengineering at doubled, tripled and quadrupled CO_2 concentrations relative to the pre-industrial using HadCM3 with MOSES 1 (Gordon *et al.*, 2000; Cox *et al.*, 1999), to determine whether the

global-mean and regional climate effects vary linearly with the CO_2 forcing that is being counteracted. If the effects of sunshade geoengineering vary linearly with CO_2 forcing then this would indicate that no 'tipping points' or shifts in the climate occur for sunshade geoengineering at different CO_2 levels, which would imply that results found at one CO_2 concentration can be extrapolated to another (Lenton *et al.*, 2008). The climate responses of the two different versions of the HadCM3 model used in this thesis are compared in section 2.7.2 to determine how they differ and whether they respond in similar ways to elevated CO_2 and SRM geoengineering.

SRM geoengineering will change the global mean and regional climates of the world but it will also have an impact on the modes of climate variability, which can shift mean climate conditions and dominate climate variability in some regions (Terray and Cassou, 2002; Seager *et al.*, 2005; Joseph and Nigam, 2006; Collins *et al.*, 2010b). The example of the El Niño Southern Oscillation is taken as it is a major mode of variability in the climate system which can affects global temperature evolution, ecosystems, agriculture and severe weather events across the world (Collins *et al.*, 2010b; Trenberth *et al.*, 2002). Using HadCM3 and HadCM3L simulations at different CO_2 concentrations, with and without sunshade geoengineering, the climatology and response of ENSO is investigated in Section 2.7.4. The pre-industrial ENSO 3.4 timeseries is compared to observations for the HadCM3 and HadCM3L models to determine whether either model simulates ENSO well, and the response of ENSO to elevated CO_2 levels and sunshade geoengineering is discussed.

Additional work on the global-mean temperature and sea-level response to a range of sunshade geoengineering scenarios carried out with the EMIC UVic is presented in appendix C and is discussed in Section 2.7.5.

2.7.2 Comparison of HadCM3 and HadCM3L

As two different versions of the HadCM3 model, HadCM3 and HadCM3L (which has half the ocean resolution of HadCM3), are used in this thesis, I investigate the differences in their control state and climate response to elevated CO_2 levels and sunshade geoengineering. A set of HadCM3 sunshade geoengineering experiments were set up as in Lunt *et al.* (2008b) and Sections 2.5.3, 2.6.3 and 2.3, i.e. with elevated CO_2 concentration and a reduction in insolation to maintain pre-industrial temperature.

Figure 2.12 shows the difference between HadCM3 and HadCM3L for the pre-industrial control, and the differences between the anomalies of quadrupled CO_2, and quadrupled CO_2 with sunshade simulations from the pre-industrial control. There are large differences in the pre-industrial control climates of these two models. HadCM3 is generally cooler at high latitudes, with the exception of the northern Atlantic, and warmer in the tropics, there are also large differences in precipitation world-wide. HadCM3 seems to have a stronger Hadley circulation than HadCM3L with greater precipitation near the equator and reduced precipitation elsewhere in the tropics, and the ITCZ in HadCM3 is farther north than in HadCM3L perhaps as a result of the Northern Hemisphere being warmer in HadCM3. HadCM3 also has greater precipitation at high northern latitudes perhaps as a result of the far higher temperatures in the North Atlantic and generally higher temperatures across the Northern Hemisphere.

At $4 \times CO_2$ HadCM3 warms more than HadCM3L with the greatest positive anomaly in temperature in the Arctic and the Northern land masses, although some ocean regions, scattered across the world warm more in HadCM3L than HadCM3. The precipitation response at $4 \times CO_2$ is also markedly different, with greater precipitation increases at high latitudes in HadCM3, a reflection of the greater increases in temperature in these regions, and large differences in tropical precipitation between the two models.

For sunshade geoengineering the temperature differences are smaller, with HadCM3 around half a degree warmer than HadCM3L over most of the Northern Hemisphere land masses and cooler by about half a degree across Africa, with little difference in the ocean responses except in the Atlantic. The sunshade geoengineering precipitation responses of the two models are fairly different across the tropics but there are few differences outside the tropics but this may be due to the small magnitude of the precipitation changes in these regions.

Directly comparing HadCM3 and HadCM3L simulations shows that they have substantial differences in their pre-industrial control climate and in their response to $4 \times CO_2$ and the differences in their response to sunshade geoengineering are smaller but still considerable. The models share the same atmospheric model HadAM3 but use different land surface models, HadCM3 uses MOSES 1 (Cox *et al.*, 1999) and HadCM3L uses MOSES 2.2 (Essery and Clark, 2003), HadCM3L also has a lower

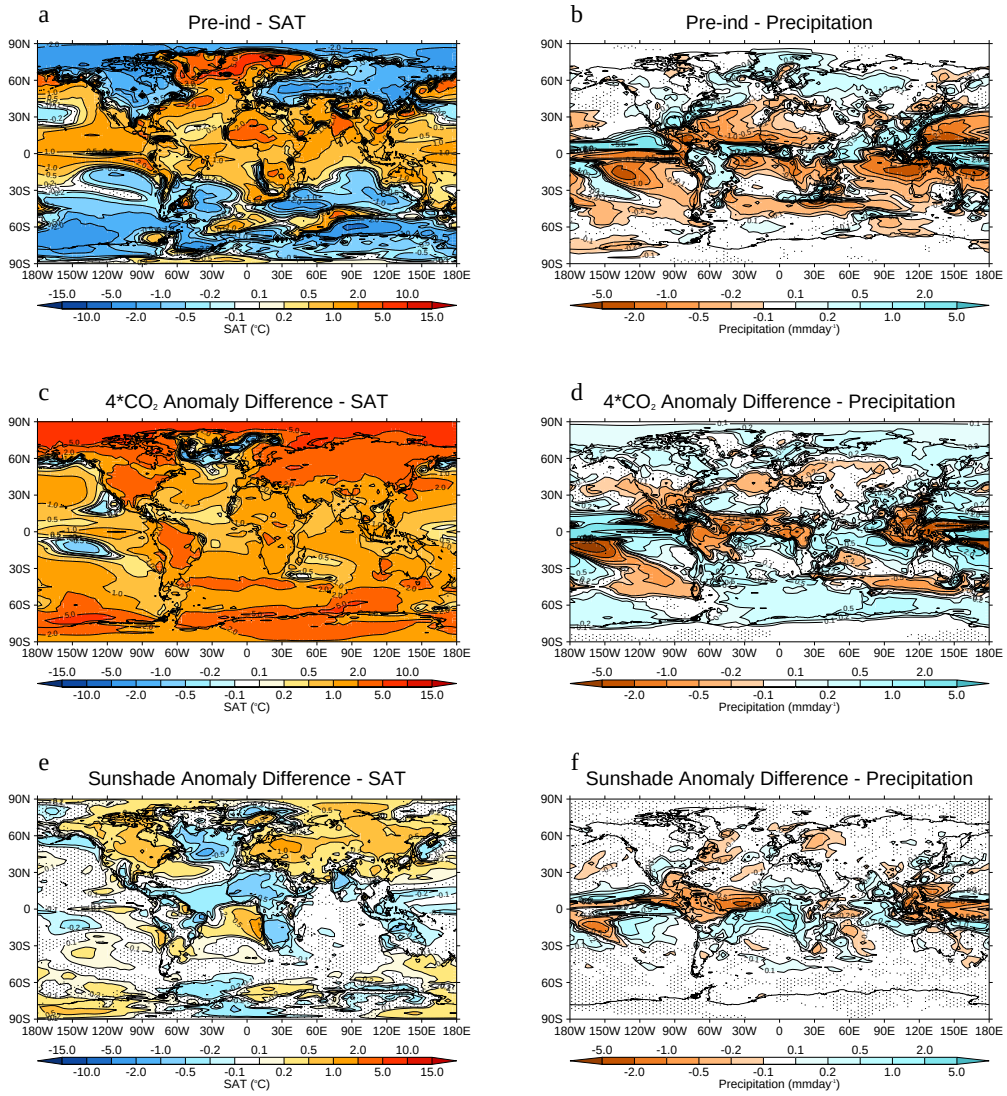

Figure 2.12: Compares the temperature and precipitation of the HadCM3 and HadCM3L model, showing the difference for the preindustrial control (a,b), the difference in the anomalies between quadrupled CO_2 levels and the pre-industrial (c,d), and the difference in the anomalies between quadrupled CO_2 levels with sunshade geoengineering and the pre-industrial (e,f). Stippling indicates which regions failed a 5% student t-test.

resolution version of the same ocean model (Gordon *et al.*, 2000; Cox *et al.*, 1999). The fact that the $4 \times CO_2$ simulation causes a greater warming in HadCM3 than HadCM3L suggests that the ocean of HadCM3 is absorbing less energy than the ocean of HadCM3L but the different land surface scheme may also be having an effect. Although for sunshade geoengineering there are smaller differences between the model responses these are still relatively large compared with the magnitude of the climate signal for sunshade geoengineering, i.e. figure 2.5 shows the tropics as roughly half a degree cooler and the Arctic around a degree warmer than the pre-industrial. Two seemingly small changes in model setup have clearly caused large changes in the pre-industrial control state and also in the response to changes in boundary conditions. These results suggest that care must be taken when comparing the results of HadCM3 and HadCM3L simulations, and that the results of Sections 2.5 and 2.6 would have differed quite substantially if HadCM3 with MOSES 1 was used in place of HadCM3L with MOSES 2.2. These results also suggest that there may be large differences between the results of any single model and another, and that to get a more complete picture the results of many GCMs should be combined.

2.7.3 Sunshade geoengineering at different CO_2 concentrations

If SRM geoengineering is deployed it may be deployed whilst CO_2 levels are still increasing and so determining whether the climate effects of SRM geoengineering differ at different CO_2 concentrations is important to know. Section 2.5 showed that some of the global and regional climate effects of sunshade geoengineering vary near-linearly with the reduction in insolation at a fixed CO_2 concentration. Figure 2.13 shows how global-mean temperature and precipitation vary for sunshade geoengineering at different CO_2 concentrations. For global-mean, land-area-mean and ocean-mean aggregation both temperature and precipitation vary linearly with the log of CO_2 concentrations, i.e. linearly with CO_2 forcing. Elevated CO_2 levels cause a larger warming over land areas than over ocean areas and sunshade geoengineering does not fully cancel the warming over land, and ocean areas are slightly cooler that in the pre-industrial. Precipitation increases globally for increases in CO_2 concentration and is reduced, but by less, for elevated CO_2 with sunshade geoengineering. The largest precipitation changes occur over the ocean but averaged over the land area sunshade geoengineering reduces precipitation more than CO_2 alone raises it.

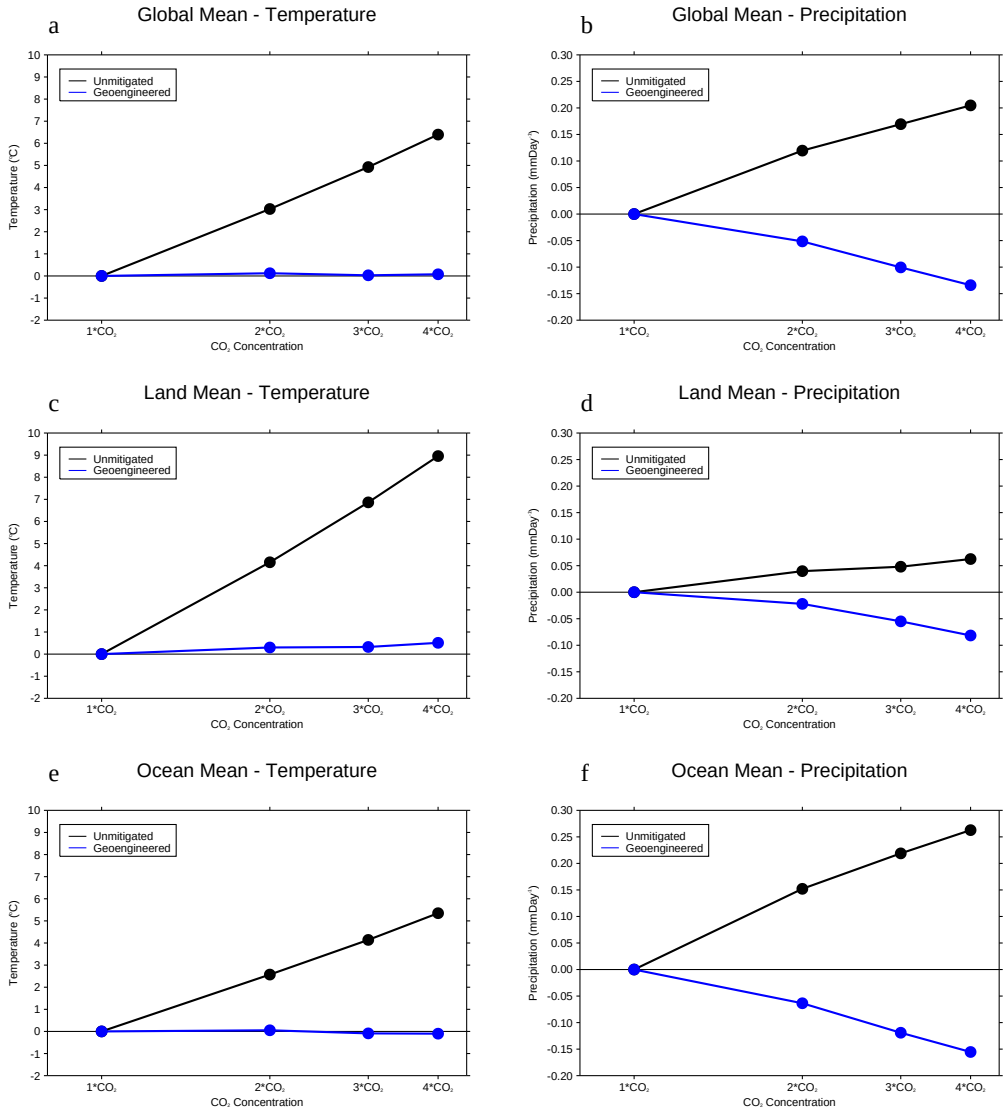

Figure 2.13: Shows the global-mean, land-area-mean and ocean-mean surface air temperature and precipitation for pre-industrial ($1 \times CO_2$) and a range of elevated CO_2 levels with and without sunshade geoengineering. All values passed a 5% student t-test.

At the global-scale at least a linear relation is found between the joint climate effects of elevated CO_2 levels and sunshade geoengineering. This suggests that sunshade geoengineering causes the same kinds of global-scale changes at different CO_2 concentrations and that the response at other CO_2 concentrations not investigated here can be predicted.

Figure 2.14 shows the surface air temperature (SAT) response to elevated CO_2 concentrations with and without sunshade geoengineering. A similar pattern of warming can be seen in all of the simulations without sunshade geoengineering (a, c and e), showing continents and higher latitudes warming more than other regions.

The pattern of temperature change for all of the sunshade geoengineering experiments (b, d and f) are similar too, showing a cooling in the topics and that some continental and high latitude regions remain warmer than in the pre-industrial. In fact, the spatial pattern of the temperature anomalies of the three sunshade experiments are very similar but, of course, with different magnitudes. Figure 2.15 shows the precipitation response to elevated CO_2 concentrations with and without sunshade geoengineering. Again the patterns of change are very similar for both the elevated CO_2 and sunshade experiments. The most notable aspects of the sunshade precipitation response are the general reduction in precipitation, which is marked in Europe and North America, and the northward shift of the ITCZ. The great similarity between the patterns of the climate response at different CO_2 concentrations suggests that regional climate change may also vary linearly or near linearly with CO_2 concentration, as it was found to do for the strength of sunshade forcing in Section 2.5. These results also suggest that if the climate effects of two studies of sunshade geoengineering with different GCMs and different CO_2 concentrations differ, this is likely to be mainly as a result of model differences and not the differences in CO_2 concentration.

2.7.4 Response of ENSO to sunshade geoengineering

ENSO is one of the key modes of natural variability in the climate system affecting climate conditions across the world and even the global mean temperature (IPCC, 2007; Trenberth *et al.*, 2002; Joseph and Nigam, 2006). ENSO is a joint atmosphere-ocean phenomenon and coupled oceans are required for GCM models to have a chance of simulating ENSO (Philip *et al.*, 2010; Trenberth and Caron, 2000; IPCC, 2007). The ENSO 3.4 region has been used to monitor the ENSO signal and is defined as being within ± 5 degrees of the equator and extending from 190° to 240° East (Trenberth, 1997). The timeseries in figure 2.16 shows the anomaly from the monthly mean climatology with a 5 month running backward mean applied (this classification is used for observations which explains the use of a backward mean). To be classed as an el niño / la niña event the smoothed timeseries must exceed ± 0.4°C for 6 months or longer (Trenberth, 1997). We apply the same criteria for defining the ENSO 3.4 timeseries as is used for observations to allow for direct comparison between the models and the observations. Panels a and b show the

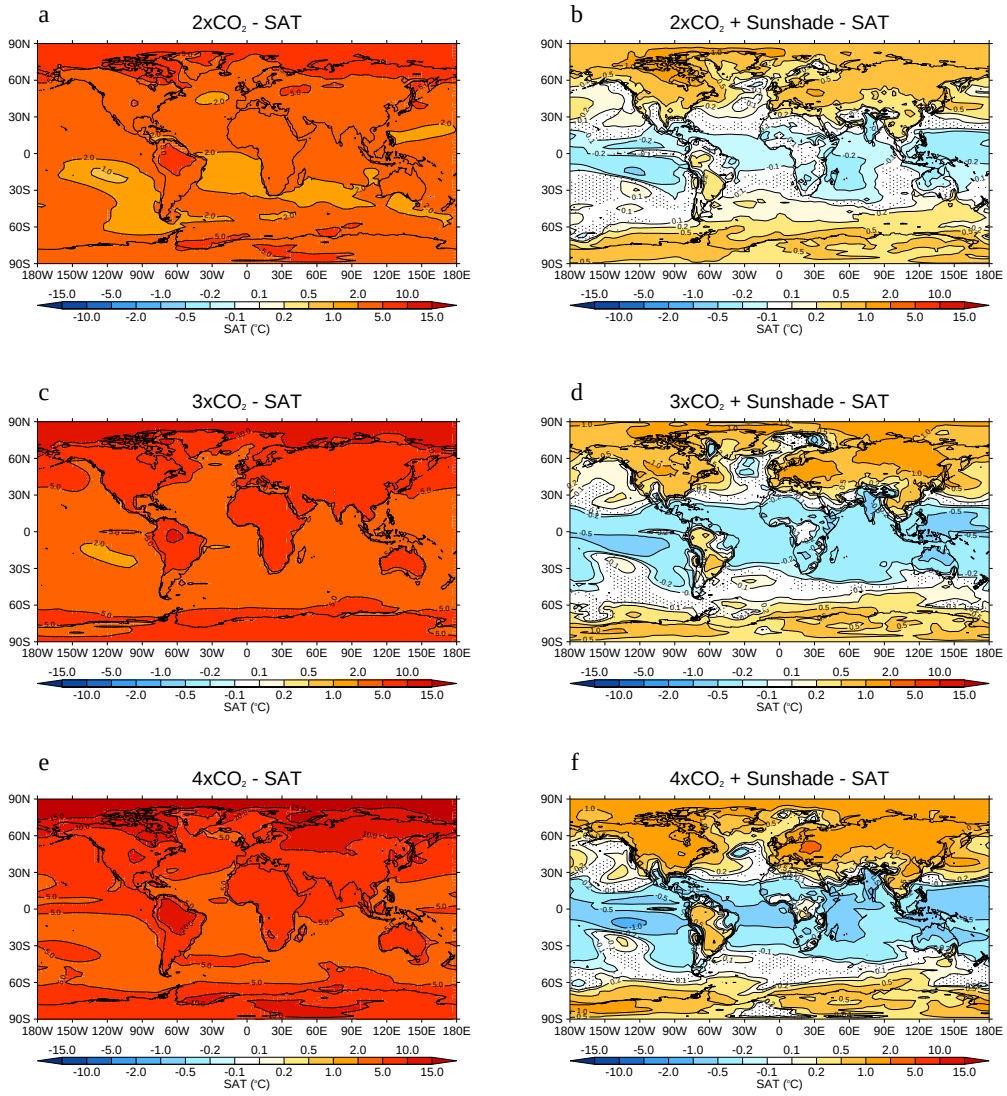

Figure 2.14: Shows the surface air temperature response of $2 \times CO_2$ (a and b), $3 \times CO_2$ (c and d), and $4 \times CO_2$ (e and f), without and with sunshade geoengineering respectively. Anomalies are plotted relative to a pre-industrial control simulation. Stippling indicates which regions failed a 5% student t-test.

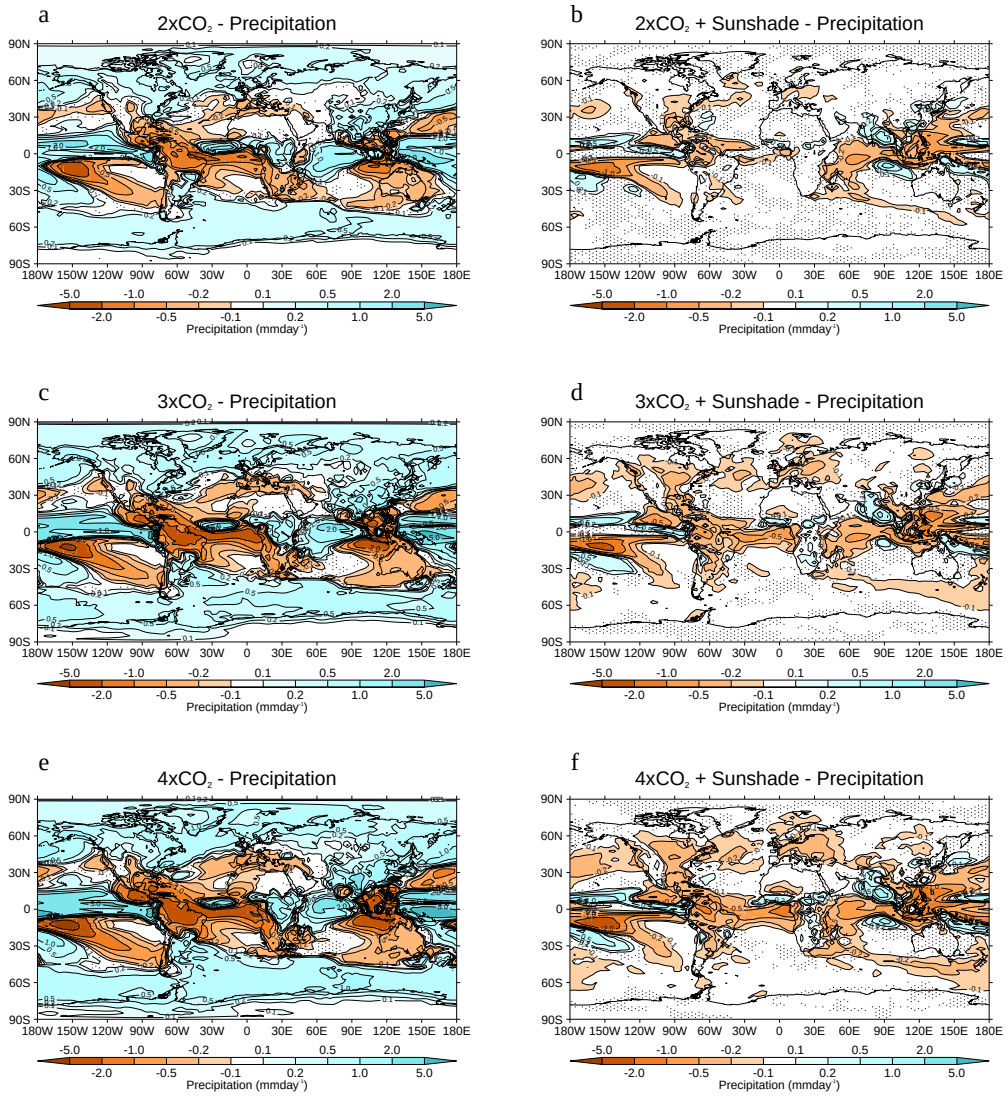

Figure 2.15: Shows the precipitation response of $2 \times CO_2$ (a and b), $3 \times CO_2$ (c and d), and $4 \times CO_2$ (e and f), without and with sunshade geoengineering respectively. Anomalies are plotted relative to a pre-industrial control simulation. Stippling indicates which regions failed a 5% student t-test.

pre-industrial HadCM3 and HadCM3L ENSO 3.4 timeseries, and compared against figure 1 of Trenberth (1997) which shows the timeseries of ENSO 3.4 temperatures between 1950 and 1997, HadCM3 performs much better than HadCM3L. HadCM3 shows clear el niño events with a magnitude of up to 3°C (although most events have an anomaly below 2°C), La niña events of a smaller magnitude, and quiescent periods. The length of the el niño and la niña events in HadCM3 are between 1 and 3 years on average, similar to observations (Trenberth, 1997). HadCM3L performs very poorly in comparison and has only a few el niño and la niña events over a century and remains mostly quiescent, in fact the SST signal appears to be just noise, without any coherent cycles or ENSO events. ENSO is a coupled atmosphere-ocean phenomena and it appears that the reduced ocean resolution of HadCM3L has affected some of the ocean processes involved in ENSO and thus reduced its ability to spontaneously generate ENSO variability. Due to this poor performance, the ENSO response of HadCM3L is not investigated further.

Figure 2.16 panels c and e show the HadCM3 ENSO 3.4 timeseries for $2 \times CO_2$ and $4 \times CO_2$, respectively. Compared to the pre-industrial, at $4 \times CO_2$ there seems to be an increase in ENSO variability but a change is less clear at $2 \times CO_2$. However comparing the sunshade results, panels d and f, with the $2 \times CO_2$ and $4 \times CO_2$ results, panels c and e, seems to show that sunshade geoengineering would reduce the variability of ENSO. Comparing the $4 \times CO_2$ sunshade results with the pre-industrial control would also seem to suggest that ENSO intensity is reduced below pre-industrial levels. It is very difficult to draw concrete conclusions as to the model response with only a century of data as ENSO is highly variable, as comparing any two multi-decadal periods on the same panel will show. Additionally it is not clear whether HadCM3 or other GCMs captures the way in which ENSO operates correctly (Collins *et al.*, 2010b; IPCC, 2007). The study of Lunt *et al.* (2008b) using the HadCM3L model suggested that sunshade geoengineering would reduce ENSO intensity however as we reported earlier HadCM3L performs poorly at reproducing the ENSO 3.4 climatology, having effectively no periodic, organized variation in SSTs and so these results are probably not to be trusted. The relative performance of HadCM3L and HadCM3 on this key mode of climate variability also suggests that HadCM3 is a more suitable model for investigating the joint atmosphere and ocean response to SRM geoengineering. Overall, these results suggest that ENSO

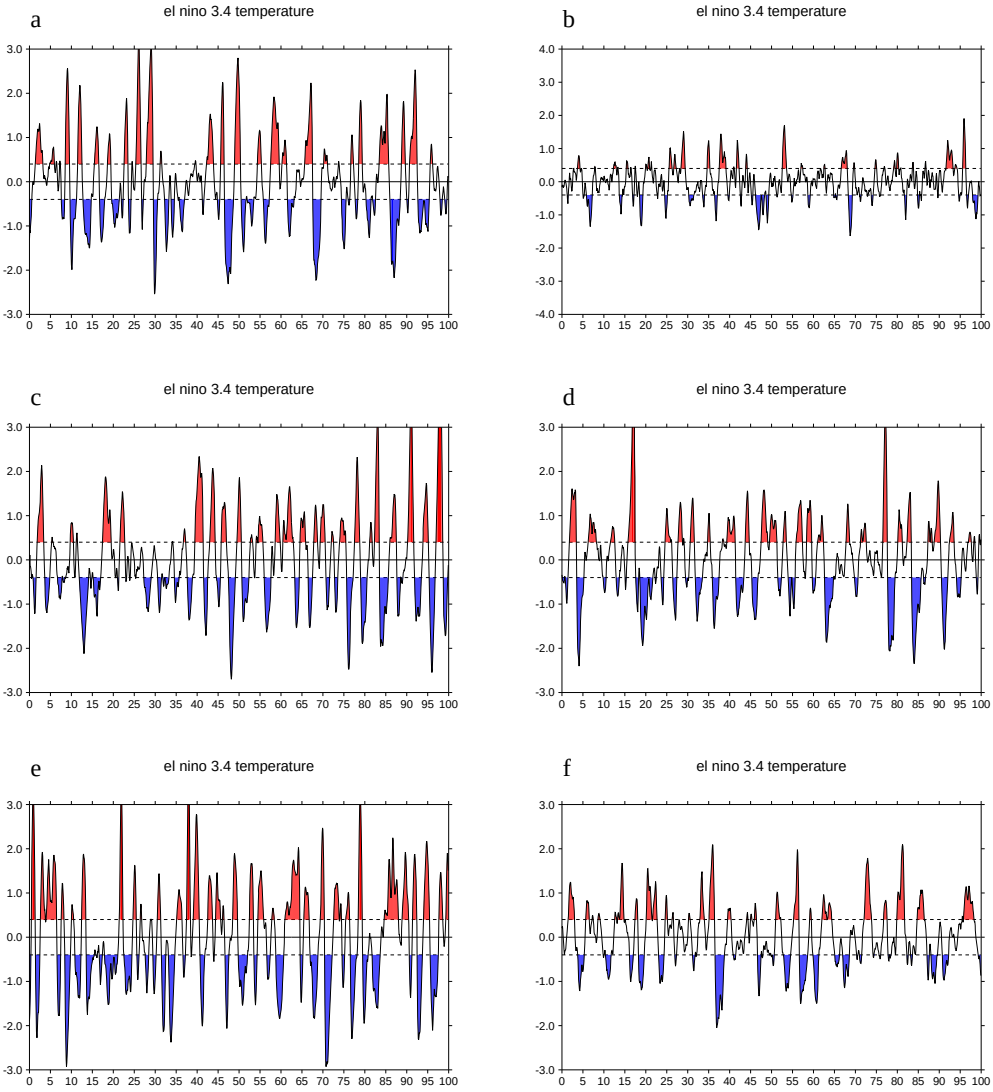

Figure 2.16: Shows the ENSO 3.4 mean sea-surface temperature timeseries for pre-industrial with HadCM3 (a) and HadCM3L (b), and for doubled and quadrupled CO_2 levels without (c and e) and with (d and f) sunshade geoengineering for the HadCM3 model.

intensity may be reduced by sunshade geoengineering however this result must be treated with caution.

2.7.5 Temperature and sea-level response of an EMIC to a range of sunshade geoengineering scenarios

The climate effects of sunshade geoengineering would depend not only on the CO_2 level and the level of reduction of insolation but also on the rate at which these factors are changed. Appendix C presents a study that was carried out by me and my collaborators on the global mean surface air temperature and sea-level response to a range of sunshade geoengineering scenarios (Irvine *et al.*, 2012). The results of this study are discussed in brief here. The EMIC UVic (Weaver *et al.*, 2001) was used in conjunction with the sea-level methodology used in the IPCC AR4 (IPCC, 2007; Wigley and Raper, 2005; Gregory and Huybrechts, 2006) to calculate the surface air temperature (SAT) and sea-level rise (SLR) response to a range of sunshade geoengineering schemes with a variety of reductions in insolation, phase-in times, and phase-out times. The worst-case RCP 8.5 scenario was used as a baseline (Meinshausen *et al.*, 2011). A tension was found between the goals of mitigating SAT and SLR, as a larger reduction in insolation with a faster phase-in time is required to halt SLR than was required to halt SAT change. SAT responds more quickly to changes in insolation which can cause a rapid cooling after the insolation reduction is phased in. It was also found that if sunshade geoengineering was phased out in just a few years, a rapid warming would ensue, at a rate up to five times greater than the peak rate under the business-as-usual scenario. The larger the insolation reduction, the longer sunshade geoengineering is maintained, and the faster the phase-out is conducted, the greater the rate of temperature change on phase-out. These results imply a long commitment to SRM geoengineering and the potential for great damage if geoengineering were to fail.

2.8 Summary and conclusion

The purpose of this chapter has been to describe the modelling and analysis approach followed in this thesis and to demonstrate this approach by analysing sunshade geoengineering. This chapter informs the approach taken in Chapter 3 where

an in-depth analysis is made of three surface albedo geoengineering schemes (Irvine *et al.*, 2011) and Chapter 4 where a method to assess parametric uncertainty in SRM geoengineering results is made. The choice of the GCMs HadCM3 and HadCM3L, and the use of the equilibrium simulation approach were explained. The overall experimental design was developed; applying simple SRM geoengineering modifications and launching multiple simulations for each study. The results of this chapter were presented in the form of three published studies, two as central to the chapter and a third as an appendix with additional work comparing the models and analyzing the sunshade geoengineering response to different CO_2 concentrations presented as a separate section. Section 2.5 explored the effects of different reductions in insolation at $4 \times CO_2$ with the HadCM3L model (Irvine *et al.*, 2010); Section 2.6 applied the results of Section 2.5 to an off-line ice-sheet model to investigate the effects on the Greenland Ice sheet (Irvine *et al.*, 2009); and Section 2.7.3 provided analysis of sunshade geoengineering at different CO_2 concentrations and compared the performance of HadCM3 and HadCM3L (Irvine *et al.*, 2010). Appendix C covered the response of global-mean surface air temperature and sea-level rise to a wide range of sunshade geoengineering scenarios.

Overall the results of this chapter and a review of the literature suggest that sunshade geoengineering would mitigate many aspects of climate change significantly; reducing global temperatures, increasing the stability of the Greenland ice-sheet and reducing sea-level rise (Irvine *et al.*, 2009, 2010, 2011, 2012; Bala *et al.*, 2010a; Lunt *et al.*, 2008b; Govindasamy *et al.*, 2003; Schmidt *et al.*, 2012). However in a number of key ways these results suggest that the climate of a world with elevated CO_2 levels, a reduction in insolation and pre-industrial global-mean temperature would differ significantly from the pre-industrial; with a large reduction in global precipitation, a reduced meridional temperature gradient, and no reduction in ocean acidification (Bala *et al.*, 2010a; Schmidt *et al.*, 2012; Irvine *et al.*, 2010; Matthews *et al.*, 2009). Many of the climate effects of sunshade geoengineering are shown to vary linearly with the reduction in insolation and with the CO_2 forcing which sunshade geoengineering counteracts (Irvine *et al.*, 2010; Ricke *et al.*, 2010). It is also shown that regional responses to sunshade geoengineering can differ greatly, particularly for precipitation with some regions getting drier and others getting wetter for the larger reductions in insolation (Irvine *et al.*, 2010; Ricke *et al.*, 2010). Many of these

regional changes are found to be novel, i.e. the climate changes are of the opposite sign to the global warming signal, and thus present problems that would not be faced with global warming (Irvine *et al.*, 2010). Modes of variability may also be altered; ENSO may be reduced relative to the pre-industrial by sunshade geoengineering but further study is required to confirm this. If sunshade geoengineering was phased out sometime after deployment it would produce a rapid warming which implies that a slow phase out, and thus a long commitment to geoengineering, would be necessary (Irvine *et al.*, 2012; Matthews and Caldeira, 2007). These results suggest that sunshade geoengineering would mitigate many of the effects of global warming but would introduce new problems that may have serious consequences.

CHAPTER 3

Climatic effects of surface albedo geoengineering

3.1 Cover sheet

Surface albedo geoengineering would involve modifying the local albedo of the land surface and as each scheme proposed would have a limited area of application, these schemes will produce a heterogeneous forcing on the climate. There have been few GCM studies of crop and urban geoengineering (Ridgwell *et al.*, 2009; Singarayer *et al.*, 2009; Oleson *et al.*, 2010), and no studies of desert albedo geoengineering, and so the climate consequences of these schemes are uncertain. This chapter presents the first intercomparison of multiple SRM geoengineering schemes using the same model setup, investigating the effects of urban, crop and desert geoengineering and comparing these to sunshade geoengineering. The methodological and analysis approach developed in Chapter 2 is applied and extended in the work in this chapter. The results of this chapter provide a clear way to compare the climate effects of SRM geoengineering schemes and make conclusions about their relative benefits and risks. The rest of this chapter presents a study that I was lead author on, in its entirety.

This study finds that the highly heterogeneous forcing of surface albedo geoengineering produces a number of important changes in regional and seasonal climate. Urban and crop albedo geoengineering schemes both produce a local cooling that is strongest in summer but have little effect on the global-mean temperature or on precipitation. Desert albedo geoengineering produces a substantial global-mean cooling and a large reduction in continental precipitation but has a much smaller effect on global-mean precipitation. The regional impacts of desert albedo geoengineering are substantial; the local cooling in areas of application can be greater than 15K and there are large changes in precipitation patterns world-wide with dramatic reductions in monsoon precipitation in some regions. Comparisons with sunshade geoengineering suggest that homogeneous forcing may be the better option for ame-

liorating the impacts of global climate change but that small-scale schemes such as urban and crop geoengineering could provide significant local benefits.

This chapter presents the results of (Irvine *et al.*, 2011), a study of the climate effects of three land surface albedo schemes using the HadCM3 model. I developed and produced the boundary condition modifications for the simulations, ran the model, conducted the analysis and wrote the first draft. Prof. Andy Ridgwell, Dr. Dan Lunt and I jointly developed the goals of the project and chose the specific analysis included in the paper. Dr. Dan Lunt made suggestions for changes to the manuscript text and Prof. Andy Ridgwell provided input on the structure and wording of the text. I arranged the corrections to the text and figures, and prepared the article for submission. Three anonymous reviewers are to be thanked for their comments and suggestions. The reviews were jointly discussed by all authors, but answers to the reviews were written by me, as were changes implemented in the manuscript. The published article is available at the following DOI:

DOI:10.1029/2011JD016281

3.2 Abstract

Various surface albedo modification geoengineering schemes such as those involving desert, urban, or agricultural areas have been proposed as potential strategies for helping counteract the warming caused by greenhouse gas emissions. However, such schemes tend to be inherently limited in their potential and would create a much more heterogeneous radiative forcing than propositions for space-based 'reflectors' and enhanced stratospheric aerosol concentrations. Here we present results of a series of Atmosphere-Ocean General Circulation Model (GCM) simulations to compare three surface albedo geoengineering proposals: urban, crop-land, and desert albedo enhancement. We find that the cooling effect of surface albedo modification is strongly seasonal and mostly confined to the areas of application. For urban and crop-land geoengineering, the global effects are minor but, due to being co-located with areas of human activity, they may provide some regional benefits. Global desert geoengineering, which is associated with significant global-scale changes in circulation and the hydrological cycle, causes a smaller reduction in global precipitation per degree of cooling than sunshade geoengineering, 1.1 $\%K^{-1}$ and 2.0 $\%K^{-1}$ respec-

tively, but a far greater reduction in the precipitation over land 3.9 $\%K^{-1}$ compared to 1.0 $\%K^{-1}$. Desert geoengineering also causes large regional scale changes in precipitation with a large reduction in the intensity of the Indian and African monsoons in particular. None of the schemes studied reverse the climate changes associated with a doubling of CO_2; with desert geoengineering profoundly altering the climate and with urban and crop-land geoengineering only providing some regional amelioration at most.

3.3 Introduction

The IPCC's 4th Assessment Report concluded that the global temperature change by 2100 would likely range from 1.1°C to 6.4°C, depending on the climate sensitivity of the Earth and on the emissions pathway followed Solomon *et al.* (2007). To limit global warming to 2°C or less, a target proposed by the European Union (CEC, 2007), some authors predict that emissions reductions of 90% by 2050 would be required (Weaver *et al.*, 2007). However, efforts to mitigate carbon emissions so far have been relatively ineffectual; global emissions of greenhouse gases increased by 29% between 2000 and 2008 to 8.7 $PgCyr^{-1}$, reduced in 2009 by 1.3% as a result of the economic crisis and are projected to have grown during 2010 by more than 3% (Friedlingstein *et al.*, 2010; Le Quere *et al.*, 2009).

Solar Radiation Management (SRM) geoengineering, or 'climate engineering', a proposed means to tackle future climate change (Shepherd *et al.*, 2009), involves increasing the upwards (towards space) reflection of sunlight and reducing the fraction of shortwave radiation absorbed at the surface, hence cooling the climate and potentially countering the warming effects of increased CO_2 (and other greenhouse gases). Increasing the outgoing shortwave radiation can, in theory, be achieved through increasing the albedo at a number of different heights in the atmosphere, at the surface, or even in space. This flexibility over which mediums could be modified and over which areas the modification could be applied has led to a wide variety of SRM schemes being proposed, such as of the creation of a sunshade in space (Angel, 2006), cloud albedo modification (Salter *et al.*, 2008), and stratospheric injection of sulphate aerosols (Crutzen, 2006), together with a number of surface albedo geoengineering schemes, including crop albedo enhancement (Ridgwell *et al.*, 2009),

urban albedo enhancement (Akbari *et al.*, 2009), and desert albedo geoengineering (Gaskill, 2004).

Most attention to date has been on cloud and aerosol SRM schemes because of their potential to be deployed on a quasi-global scale and to exert sufficient forcing to cancel anthropogenic greenhouse warming of up to a doubling of CO_2 (Shepherd *et al.*, 2009). Space-based reflectors also fall into this category, but because of the high cost and very long deployment timescale they have attracted less serious consideration (Angel, 2006). In contrast, surface albedo modification (SAM) geoengineering schemes would generally be deployed rather more heterogeneously across the Earth's surface and, because of their more limited potential for global impact (Shepherd *et al.*, 2009), have been less well studied. In this paper we address the climate consequences of the three principal SAM schemes, of: urban areas, croplands, and deserts, which were introduced in sections 1.3.4, 1.3.5 and 1.3.6, respectively.

3.3.1 Summary and chapter outline

The three different proposals for surface albedo modification (SAM) geoengineering schemes considered here have been previously compared using 0-D or 1-D radiative forcing calculations (for example: Lenton and Vaughan (2009) and Hamwey (2007)). However, unlike other climate engineering schemes, SAM geoengineering schemes would be deployed heterogeneously across the Earth's surface. Hence one would expect important regional scale impacts and potential side-effects that may not be revealed by annual and global-scale averaging. While there have been several GCM analyses made for urban albedo enhancement (Oleson *et al.*, 2010) and crop albedo enhancement (Ridgwell *et al.*, 2009; Singarayer *et al.*, 2009), these were made using different models and used different experimental and analysis methodologies (e.g., integration time), preventing direct comparison of their projections.

To address this, we have carried out a GCM analysis of all three main SAM schemes, using the same model and the same methodology, presenting GCM results for desert geoengineering for the first time. This allows us to directly compare the three schemes side by side and to explore the relative seasonal and regional impacts which will be very important for these spatially heterogeneous schemes.

To compare the different schemes we analyze the global, local and remote climate effects of regional surface albedo modification and assess the extent and 'quality' of

the climate change amelioration achieved. For an initial comparison we conduct an analysis of the effects of the schemes on precipitation and temperature at the global scale. To analyze the local cooling effect we focus on Europe, a region with large urban and crop areas, which is located near to the Sahara (and hence may be expected to be cooled significantly by desert albedo geoengineering). We also analyze the effect of the schemes on regional precipitation, focussing particularly on monsoon regions, and analyzing some of the changes in circulation. For remote effects we focus on Arctic snow and sea-ice changes; the Arctic is a region remote from any of the regions affected by SAM but one which has been a focus for previous climate engineering studies (Caldeira, 2008; Irvine and Ridgwell, 2009; Robock *et al.*, 2008). It must be noted that, whilst the results presented here are illustrative of the types of changes that could be expected, GCM models do not, in general, simulate precipitation or regional climate changes well (Cox *et al.*, 2000; IPCC, 2007).

This paper continues with a methodology, results section, and a discussion and conclusion section. The results section is split into global effects, European summer changes, monsoon changes and Arctic changes. The discussion and conclusion will deal with the implications of the results presented.

3.4 Methodology

HadCM3, the fully coupled atmosphere-ocean global circulation model (GCM) used in this paper (Gordon *et al.*, 2000), has been used in the IPCC third and fourth assessment reports (IPCC, 2007) and performs well in a number of tests relative to other global GCMs (Covey *et al.*, 2003; IPCC, 2007). Although it has been superseded by HadGEM2 (Collins *et al.*, 2011) for the 5th IPCC assessment and can no longer be considered 'state-of-the-art', HadCM3 does have the advantages of being relatively computationally efficient which allows more and/or longer runs to be conducted than would be possible with a more recent, higher resolution model.

The horizontal resolution of the atmospheric model is 2.5° in latitude by 3.75° in longitude, with 19 vertical layers. The atmospheric model has a time step of 30 min and includes many parameterizations representing sub grid-scale effects, such as convection (Gregory and Rowntree, 1990) and boundary-layer mixing (Gordon *et al.*, 2000). The land surface scheme includes the representation of the freezing

and melting of soil moisture. The spatial resolution in the ocean is 1.25° by 1.25°, with 20 vertical layers. The ocean model component uses the Gent and McWilliams (1990) mixing scheme, and there is no explicit horizontal tracer diffusion. The sea-ice model uses a simple thermodynamic scheme and contains parameterizations of sea-ice drift and leads (Cattle and Crossley, 1995). HadCM3 has a climate sensitivity of 3.3°C for a doubling of CO_2, which falls in the mid-range of the estimate of the likely climate sensitivity reported in the IPCC AR4 (2.0°C to 4.5°C) (Solomon *et al.*, 2007).

We employ the MOSES 1 land surface scheme (Cox *et al.*, 1999) which accounts for terrestrial surface fluxes of temperature, moisture and radiation. Although later versions of MOSES are available, for example Essery and Clark (2003). The combination of HadCM3 with MOSES 1 is the most widely used and is the most robustly tested (Gordon *et al.*, 2000; Johns *et al.*, 2003; Martin *et al.*, 2006) and for this reason we employ this combination. MOSES includes: 4 soil layers, recording temperature, moisture and phase changes; a canopy layer; and a representation of snow cover. The representation of evaporation includes the dependence of stomatal resistance on temperature, vapour pressure and CO_2 concentration (Cox *et al.*, 1999). Each grid cell has surface properties; roughness length, snow-free albedo, etc., which reflect the vegetation cover present, as derived from the Wilson and Henderson-Sellers (1985) dataset.

In the simulations presented here we modified the albedo properties in MOSES, i.e., snow-free albedo and deep-snow albedo, in areas which would be affected by the different surface albedo geoengineering schemes considered. All other surface properties were left fixed at pre-industrial conditions for all experiments. We carried out 11 different model simulations using HadCM3: a pre-industrial simulation, a simulation with doubled pre-industrial CO_2 concentration ($2 \times CO_2$), plus nine simulations with increased surface albedo and doubled CO_2, consisting of three simulations with increased albedo for each of the three geoengineering schemes (urban, crop, and desert albedo geoengineering). An additional simulation, with $2 \times CO_2$ and a reduction in incoming solar radiation sufficient to return global average temperature to pre-industrial levels (referred to as sunshade geoengineering), was run for comparison. This sunshade geoengineering was achieved by reducing the solar constant by a fraction sufficient to return the global average temperature to the

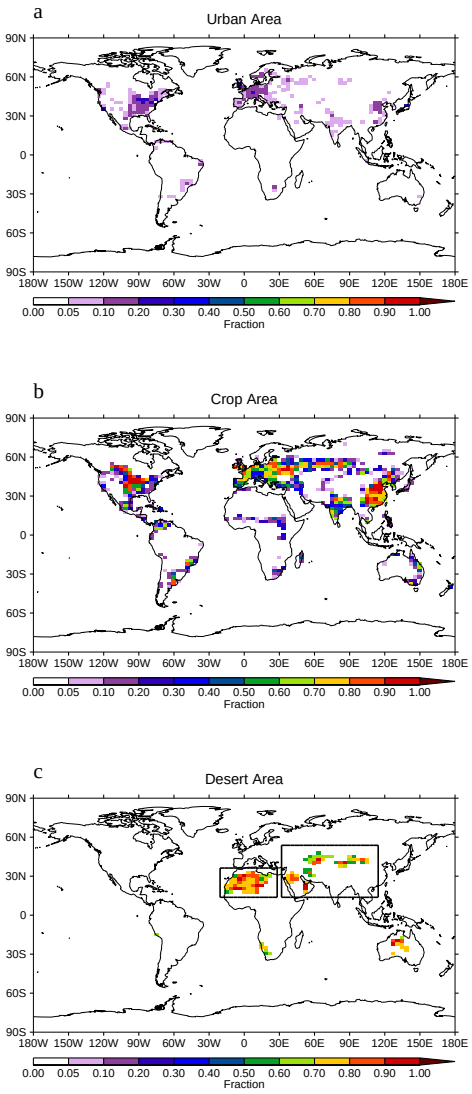

Figure 3.1: Maps showing the fractional coverage of urban (a), crop (b) and desert (c) to which albedo increases were applied. The boxes in (c) show the limited domains of albedo enhancement for the Asian and Saharan Desert schemes.

pre-industrial value, in our case a 2.1% reduction in incoming sunlight was required (this is the same method implemented in Lunt *et al.* (2008b) and Irvine and Ridgwell (2009)).

The regions over which the increases in albedo were applied for each of the schemes are shown in figure 3.1. The area for the urban and crop albedo schemes remained the same for each simulation, with the degree of albedo increase varying. For the desert geoengineering simulations, the albedo increase remained the same for all simulations but the area modified were varied in figure 3.1. Table 3.1 summarizes the albedo modifications and area coverage of all the different geoengineering

Geoengineering	Fractional global area (%)	Snow-free albedo increase	Deep snow albedo increase
Urban High	0.556	0.175	0.113
Urban Mid	0.556	0.1	0.0646
Urban Low	0.556	0.0725	0.046
Crops High	3.08	0.08	0
Crops Mid	3.08	0.04	0
Crops Low	3.08	0.02	0
Global Deserts	1.78	Set to 0.8	0
Asian Deserts	0.66	Set to 0.8	0
Sahara Desert	0.84	Set to 0.8	0

Table 3.1: Area affected and albedo increase for geoengineering schemes.

scenarios considered here. In most of our analysis we focus on the maximum implementation of each scheme. We do not suggest that these are the most feasible or likely implementations, but were chosen to give the strongest and hence most statistically significant change in order to help identify any subtle effects. All model runs were initialized from a pre-industrial spin-up totalling more than 1000 years with each simulation being run for a total of 400 years, using the final 100 years for averaging.

3.4.1 Urban albedo modification

Urban albedo geoengineering has the smallest potential radiative forcing of the three different SRM interventions considered here, and in a previous GCM analysis no statistically significant changes in the climate were recorded (Oleson *et al.*, 2010). To test whether any feasible implementation of urban albedo enhancement would even be observable (let alone provide significant climate mitigation), and to allow us to fully elucidate the characteristics of the resulting changes in climate, we assumed an upper estimate of the area to which increased albedo could be applied. In this, we used the Global Rural-Urban Mapping Project (GRUMP) dataset of urban extent (GRUMP, 2005) to determine the fraction of each model grid-cell that is 'urban'. The total urban area recorded in the GRUMP urban extent map is 3.5×10^6 km^2, or 0.68% of the Earth's area, which after regridding onto the HadCM3 land grid (Figure 3.1b), becomes 2.8×10^6 km^2, or 0.56% of the Earth's area (and 1.9% of total land area). The difference is a consequence of the relatively low resolution of HadCM3 and consequent loss of some coastal urban areas in the gridding process.

We followed the methodology of (Akbari *et al.*, 2009), assuming 35% of the

urban area is paved and 25% is roofing, and applying albedo enhancement to these two surfaces, leaving the other 40% unchanged. Based on the estimates of Akbari *et al.* (2009), we tested three levels of albedo increases to roofing and paving (which on average have an albedo estimated at around 0.2 and 0.1, respectively); (1) a maximum increase of 0.35 and 0.25, respectively, (2) a moderate increase of 0.25 and 0.15, respectively, and (3) a small increase of 0.15 and 0.1, respectively. The overall increase in snow-free albedo applied is shown in table 3.1.

Urban areas at higher latitudes are often snow covered in winter months and so a change to the deep-snow albedo in the model was also applied (table 3.1). The effect of albedo increases in urban areas will affect the deep-snow albedo but only insofar as the underlying surface is exposed. Although the MOSES 1 land surface scheme (Cox *et al.*, 1999) used here does not have an urban land type, MOSES 2.2 does (Essery and Clark, 2003). We hence used the values for snow-free and deep snow albedo from MOSES 2.2 to calculate the exposed fraction:

$$\alpha_{us} = f \cdot \alpha_u + (1 - f) \cdot \alpha_s \tag{3.1}$$

where α_{us} is the recorded deep snow albedo of urban areas, f is the fraction of exposed urban surface and $1 - f$ is the fraction of snow coverage, α_u is the snow-free urban albedo and α_s is the deep-snow albedo in the open. In MOSES 1 deep-snow, α_s, has an albedo of 0.8, the urban albedo values from MOSES 2.2 are, 0.4 for α_{us} and 0.18 for α_u (Wiscombe and Warren, 1980). On this basis f was found to be 0.645 and so the deep snow albedo increase applied to urban areas is $f \cdot \Delta\alpha_{us}$; the full list of albedo modifications can be found in table 3.1.

3.4.2 Crop albedo modification

Crop albedo geoengineering has been tested in HadCM3 by Ridgwell *et al.* (2009) and Singarayer *et al.* (2009) and in CAM 3.0 by Doughty *et al.* (2011). We follow a similar methodology to both Ridgwell *et al.* (2009) and Singarayer *et al.* (2009), apart from using the MOSES 1 land surface scheme rather than MOSES 2.1, used in these studies, in order to provide consistency with the other simulations presented in this paper. We adopt the same definition of crop extent, with the crop area being defined as C3 or C4 grasses that are within human controlled or disturbed areas as defined by the Wilson and Henderson-Sellers (1985) land type dataset. The total

area covered by crops is 15.7×10^6 km^2, 3.1% of the Earth's surface area or 10.6% of the land area (Figure 3.1a). To these areas we apply an increase in snow-free albedo dependent on the fractional crop coverage in the grid cell.

We test the same albedo increases as in Ridgwell *et al.* (2009): +0.02, +0.04, +0.08, so as to provide a point of direct comparison. (Ridgwell *et al.*, 2009) argue that these levels span the range of changes of what could be possible within existing inter-variety albedo variability. This range is consistent with measurements of the leaf albedo of wheat and sorghum that exhibit variations of 0.05 and 0.16, respectively between varieties (Grant *et al.*, 2003; Uddin and Marshall, 1988). An average canopy albedo increase of 0.04 in commercially grown varieties may thus be at least partially achievable using traditional plant breeding techniques. However, in the analysis of a number of soybean isolines, Doughty *et al.* (2011) found differences in albedo no greater than our lowest tested assumption (+0.02). The deep snow albedo was not modified as crop coverage is at very low levels in snowy conditions, assuming that either crop plants are not present (or exist as planted seeds) or have minimal canopy during the winter months.

3.4.3 Desert albedo modification

Desert geoengineering represents the most extreme local albedo modification of the surface albedo modification schemes considered, and we explore the effects of different spatial extents instead of exploring different levels (intensities) of implementation. In an account of a US Department of Energy (DOE) meeting on geoengineering, Gaskill (2004) estimates a possible albedo of 0.8 for commercially available coverings and that an estimated 11.7×10^6 km^2 would be suitable for this application. We take these estimates as the basis for our extreme case of what is possible for desert geoengineering.

We generated a definition for desert areas, based on a combination of observed precipitation and fractional vegetation cover at the resolution of HadCM3, designed to roughly match the estimated total area of Gaskill (2004). If a gridcell receives on average less than 250 $mmyr^{-1}$, as calculated from the CRU (Climate Research Unit, University of East Anglia) reanalysis data for the period 1961-1990, then it is classed as desert. We also specified that a gridcell must be less than 50% covered in vegetation, as defined by the Wilson and Henderson-Sellers land-type dataset

(Wilson and Henderson-Sellers, 1985) before it was considered suitable for desert geoengineering (Fig 3.1c). This simple method does not capture all desert regions - notably, no deserts are identified in North America - but our method does produce a total area (9.1 million km^2) close to the estimate (11.7 million km^2) of Gaskill (2004). The albedo of the desert grid cells are adjusted to:

$$\alpha = f \cdot \alpha_0 + (1 - f) \cdot 0.8 \tag{3.2}$$

where the albedo α is dependent on the vegetated fraction f, α_0 is the original albedo of the gridcell, and 0.8 is the albedo of the reflective covering. The deep-snow albedo was not changed as the properties of snow deposited on a reflective coating would be similar to those of snow on desert regions.

Three experiments were run to explore the effect of applying desert albedo geoengineering in different regions (see figure 3.1c): (1) in which all desert regions were modified ('Global'), (2) modification only of the Sahara desert ('Sahara'), (3) in which only Asian deserts, i.e., from Saudi Arabia and the Middle East eastward, are modified ('Asian').

3.5 Results

We present results of the global, local and remote climate effects of SAM geoengineering, splitting the results into four parts; Global Effects (Section 3.5.1), European Summertime Changes (3.5.2), Monsoon System changes (3.5.3), and Arctic Changes (3.5.4). The global effects section gives an overview of the major changes in temperature and precipitation that arise due to the different geoengineering schemes.

In addition to this global assessment of climate effects, a number of specific changes are investigated: Europe is an illustrative region as there is a high crop and urban density in the region and it is also relatively close to the Sahara, suggesting that we might expect some effect on European climate from each of the SAM geoengineering schemes. Monsoon systems are associated with seasonal atmospheric overturning circulations driven by land-sea temperature differences, and play a central role in continental hydrology (Trenberth and Caron, 2000). We can expect that SAM geoengineering will change the seasonal land-sea temperature difference that plays a key role in monsoon circulations, making this an essential part of our analysis. Climate change in the Arctic is expected to be greater than elsewhere due to

the action of local positive climate feedbacks, e.g., the melting of snow and ice and the consequent albedo decrease which leads to greater local warming (IPCC, 2007); we examine the effect of SAM geoengineering schemes on the Arctic to assess their effectiveness at reversing the amplified climate change there. All values reported in the text have passed a 5% student T-test significance test unless otherwise stated. Throughout the results sections we focus on a common subset of the simulations, i.e., the simulations with largest albedo modification for each surface albedo geoengineering scheme. This is because the weaker crop and urban geoengineering schemes induce relatively small changes in climate that can be difficult to distinguish from the model's internal variability. However, in focussing on the extreme urban and crop geoengineering implementations, we do not claim that these changes in climate would necessarily be linear with respect to the magnitude of SAM albedo increase. For desert geoengineering the global implementation is shown in all figures and the Asian and Saharan implementations shown when space allows.

In this study we mostly calculate climate anomalies relative to the $2 \times CO_2$ simulation rather than the Pre-industrial ('Pre-ind') simulation. This makes it easy to see the small changes in climate brought about by urban and crop geoengineering, without them being dwarfed by the changes from $2 \times CO_2$ to Pre-ind. For desert and sunshade geoengineering we also compare to Pre-ind, as the climate changes that these schemes can cause are large enough to reverse the effects of doubling CO_2 in some cases.

3.5.1 Global effects

The impacts on global and land averaged temperature and precipitation for each geoengineering scheme, as well as the effect of unmitigated global warming, are summarized in table 3.2. At doubled CO_2 there is a global average increase in surface air temperature of +3.0C and an increase in precipitation of +4.0%. On land, the annual average temperature change is amplified (+4.2°C) whereas the precipitation enhancement is reduced (down to +1.8%). Global average warming is not completely reversed by any SAM scheme, with urban geoengineering having the potential to cool on a global annual average basis by a maximum of 0.11°C, crop geoengineering by 0.23°C, and (global) desert geoengineering by 1.12°C, with the amount of cooling determined by the assumed degree of geoengineering intervention.

	Global		Land	
Experiments	SAT (°C)	Precip (%)	SAT (°C)	Precip (%)
$2 \times CO_2$- Pre-ind	**3.03**	**3.99**	**4.16**	**1.84**
Urban High - $2 \times CO_2$	**-0.11**	-0.07	**-0.21**	0.18
Urban Mid - $2 \times CO_2$	**-0.06**	-0.03	**-0.12**	0.33
Urban Low - $2 \times CO_2$	-0.05	-0.04	**-0.10**	0.20
Crops High - $2 \times CO_2$	**-0.23**	-0.20	**-0.42**	-0.07
Crops Mid - $2 \times CO_2$	**-0.14**	0.09	**-0.26**	0.17
Crops Low - $2 \times CO_2$	-0.05	0.01	**-0.11**	0.12
Global Deserts - $2 \times CO_2$	**-1.12**	**-1.19**	**-2.20**	**-4.33**
Sahara Desert - $2 \times CO_2$	**-0.52**	**-0.69**	**-1.06**	**-3.38**
Asian Deserts - $2 \times CO_2$	**-0.53**	-0.34	**-1.02**	1.13
Sunshade - $2 \times CO_2$	**-2.91**	**-5.71**	**-3.86**	**-2.87**
Bold-typed values passed a 5% student T-test for statistical significance.				

Table 3.2: Annual average aurface air temperature and precipitation change.

Changes in the radiative forcing of the planet affect the hydrological cycle in two ways; there is a 'slow' or temperature-driven component which does not depend on the details of the radiative forcing mechanism, and there is a 'fast' atmospheric adjustment component that differs between radiative forcing mechanisms (Andrews *et al.*, 2010). The 'slow' temperature response has been found to cause around a 2-3% change in precipitation for every degree Kelvin of temperature change, with precipitation increasing with rising temperatures (Lambert and Webb, 2008). Our simulations show that sunshade geoengineering caused a $2.0\%K^{-1}$ reduction in precipitation, whereas global desert geoengineering caused only a $1.1\%K^{-1}$ reduction (we exclude urban and crop geoengineering as a statistically significant change in global average precipitation was not found). For comparison, a study on cloud albedo geoengineering (which increases albedo over ocean areas only) caused a $2.5\%K^{-1}$ reduction in global average precipitation (Bala *et al.*, 2010a). The different global precipitation responses of these geoengineering schemes is a result of the differing availability of moisture for evaporation in the regions affected, i.e. ocean regions have an infinite supply of water for evaporation whereas the continents do not. Thus the effect of a reduction in incoming sunlight on the surface energy budget of the ocean will consist of a change in the latent and sensible heat fluxes, leading to a large reduction in evaporation, whereas over the land this will consist mainly of a change in sensible heat flux, with a smaller reduction in global evaporation.

However the change in continental precipitation shows an opposite result to this global picture; desert geoengineering has the largest reduction at $3.9\%K^{-1}$, sunshade

geoengineering shows $1\%K^{-1}$, and cloud albedo geoengineering shows $0.9\%K^{-1}$. This difference in continental precipitation arises from changes in circulation which redistribute the precipitation. This change in distribution has a greater effect on continental precipitation than the change in the atmospheric moisture availability that controls global precipitation.

The patterns of annual mean surface temperature change are shown in figure 3.2. For unmitigated climate change (Figure 3.2a) warming occurs everywhere, with greater warming towards the poles and over the land areas. As one would expect, SAM geoengineering does not produce a uniform cooling. Furthermore, in some areas, statistically significant warming (in addition to the impact of $2 \times CO_2$) occurs under each of the different geoengineering interventions, probably as a result of changes in circulation patterns, i.e., diverting warm currents of air to high latitude areas. An example of this is the Southern Ocean around Tasmania which is warmer for all three SAM geoengineering schemes. In contrast, sunshade geoengineering produces a relatively uniform cooling across the world compared to the surface albedo geoengineering schemes, with land areas and high-latitude areas cooled more than others, reversing most of the warming from $2 \times CO_2$.

For urban geoengineering, we find a statistically significant cooling across most continental areas. This is in contrast to the results of Oleson *et al.* (2010) who did not find any statistically significant cooling as a result of a global reduction in urban albedo. This difference is likely to be partly due to the more extreme implementation we have assumed (and focussed on the results of), together with the greater urban coverage assumed in our dataset. We have also employed a longer averaging period: 100 years here compared to 58 years in the simulations of Oleson *et al.* (2010) and hence we are better able to identify small changes in climate against the background of modelled inter-annual variability. We find the largest cooling in Europe, North America and in the Arctic a consequence of the relatively large urban coverage of both Europe and North America (figure 3.2b). This regional cooling is amplified by positive cryospheric feedbacks operating in the high latitudes, particularly due to changes in sea-ice extent (see Section 3.5.4).

Crop albedo geoengineering exhibits a pattern of cooling (Figure 3.2c) to a first order similar to urban geoengineering (Figure 3.2b), with most of the cooling occurring in the northern hemisphere. This similarity between crop and urban albedo

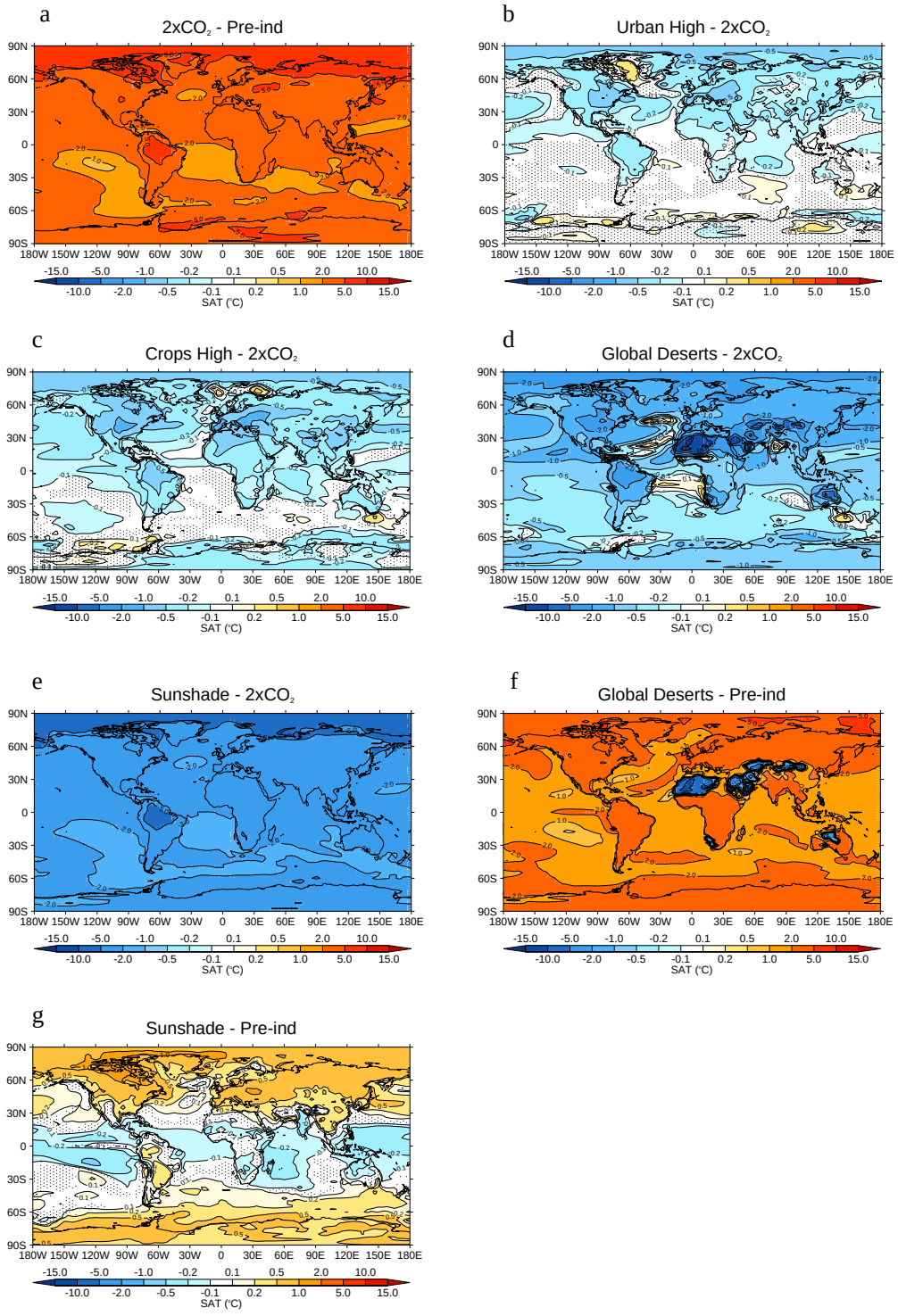

Figure 3.2: This shows the surface air temperature (SAT) anomaly between $2 \times CO_2$ and Pre-industrial (a), and between the various geoengineering schemes and $2 \times CO_2$. Areas which failed a 5% student T-test are stippled.

is due to the co-existence of greatest crop cover and urban fraction (population) in most regions (figure 3.2 a and b). Consistent with the results of Singarayer *et al.* (2009), we find that crop albedo geoengineering results in the greatest cooling across Eurasia and North America. We also find less cooling than may be expected in south and east Asia, an area with significant crop coverage a result of an associated reduction in cloud cover in the region (Doughty *et al.*, 2011; Singarayer *et al.*, 2009). Some warm anomalies are also induced, for example in the Barents Sea, but are not found consistently in the moderate or weak implementations of crop geoengineering and are therefore perhaps a result of long-term climate variability.

Although global desert geoengineering has the potential to generate the largest global average cooling effect, this average masks the fact that most of the 1.12°C cooling is highly concentrated over the desert regions where the albedo increase is applied (compare Figure 3.2 d and Figure 3.1 c). For example, global desert geoengineering causes some areas of the Sahara to be greater than 10°C cooler than in the pre-industrial (Figure 3.2 f). A pronounced general cooling of most continental areas, of between 1.5°C and 2°C over most of Eurasia and North America also occurs, with the notable exception being India which becomes slightly warmer despite being proximal to a number of desert areas. This warming in India can be explained by the ∼10% reduction in cloud cover in the region (not shown). As with crop and urban geoengineering, the Northern Hemisphere tends to be cooled more than the Southern Hemisphere: a simple consequence of the presence of much greater land coverage in the north.

Sunshade geoengineering produces a much more uniform cooling than the SAM schemes, with noticeably greater cooling in the Northern Hemisphere and Arctic (figure 3.2 e), but does not reproduce the pre-industrial temperature distribution; with the low latitudes cooler than in the pre-industrial and the high latitudes warmer (Figure 3.2 g). This difference in temperature is due to the greenhouse forcing acting to slow the loss of heat, which warms the Arctic more, and the reduced solar forcing, which has a greater role in the energy budget at low latitudes, acting to cool the Tropics.

In contrast to the response of surface air temperature, which is strongest at the sites of SAM geoengineering, changes in precipitation are much more heterogeneous (figure 3.3). Doubling CO_2 leads to large regional changes in precipitation, with

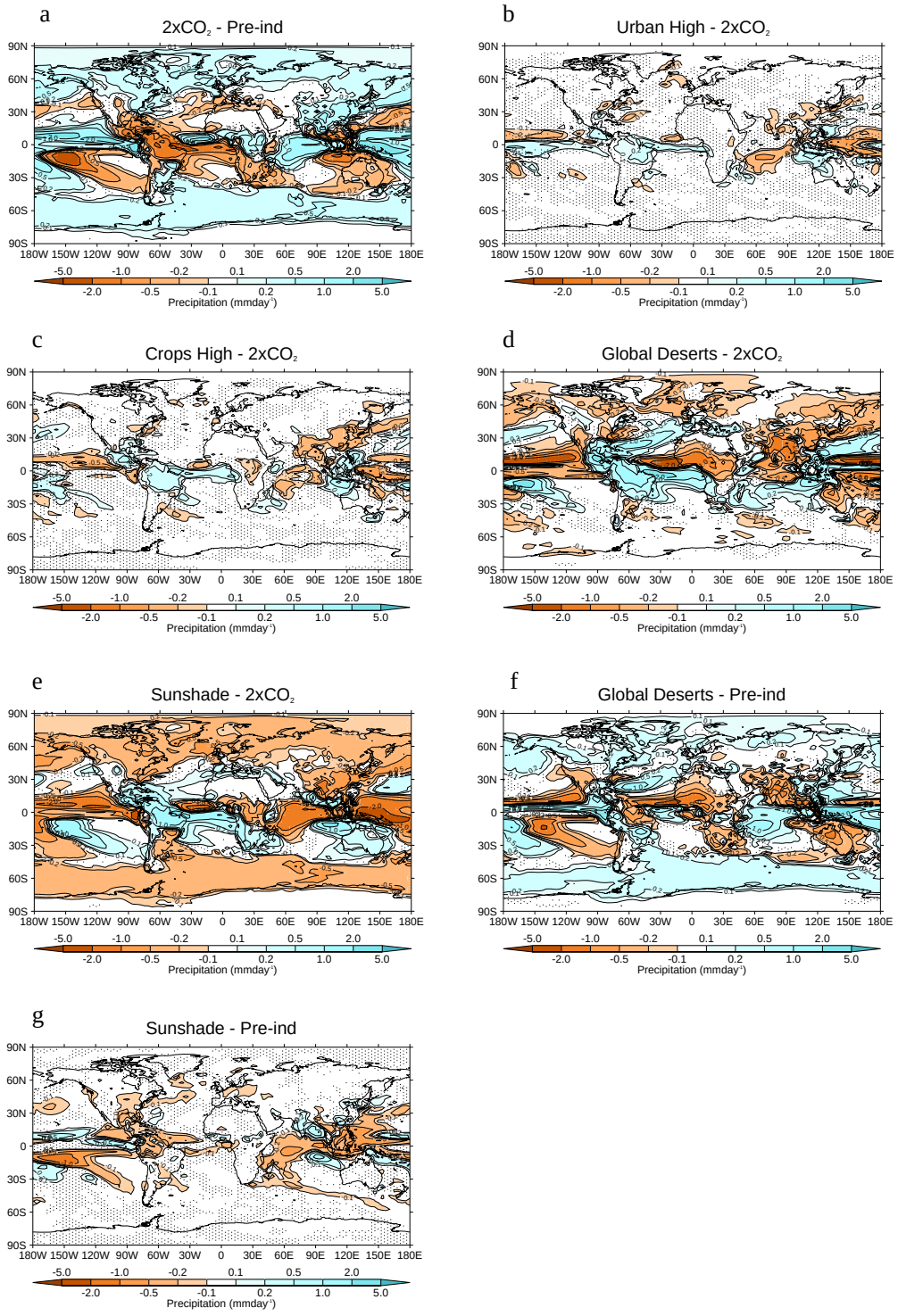

Figure 3.3: This shows the precipitation anomaly between $2 \times CO_2$ and pre-industrial (a), and between the various geoengineering schemes and $2 \times CO_2$. Areas which failed a 5% student T-test are stippled.

some areas becoming much drier, e.g., the Amazon, South Africa and Australia, and others becoming much wetter, e.g., South-Asia and Equatorial Africa, but with an overall increase in precipitation see figure 3.3 a and table 3.2. For both urban and crop albedo geoengineering only minimal shifts in precipitation occur, with the exception of Equatorial Pacific regions (Figure 3.3 b and c), whereas desert geoengineering induces quite extreme changes in precipitation patterns throughout the tropics and sub-tropics (Figure 3.3 d).

Urban and crop albedo techniques generally induce only small changes in precipitation with few areas that exhibit a statistically significant change (Figure 3.3 b and c). The changes in precipitation that do occur are consistent with a small southward shift of the ITCZ which is induced by an unequal change in the temperature between the Northern and Southern Hemispheres. Both schemes also result in slightly altered precipitation patterns around south-east Asia, the Indian Ocean and around Australasia, changes that are more marked with crop albedo geoengineering than urban. These changes in precipitation are due to changes in evaporation which occurs locally and changes in circulation which redistribute rainfall.

Our prescribed enhancement of desert albedo induces shifts in precipitation patterns (Figure 3.3 d) of comparable magnitude to those that arise from doubling CO_2 levels alone (i.e., unmitigated climate change) (figure 3.3 a). The most prominent changes occur in monsoonal regions such as sub-Saharan Africa, South-east Asia and Australia, where the decrease in rainfall leaves these regions drier than in the Pre-industrial simulation (figure 3.3 f). Northern South America and Central America experience increases in precipitation that are sufficient to reverse the drying caused by doubling CO_2.

In comparison, sunshade geoengineering produces a reduction in precipitation in most regions relative to $2 \times CO_2$, with some large positive and negative anomalies in the tropics (figure 3.3 e). When compared with pre-industrial, few regions experience statistically different precipitation, with exceptions occurring mostly in the tropics (Figure 3.3g).

The climatology of the HadCM3 model employed here reproduces many of the first-order features of the global climate system but, as with all models, is not perfect and HadCM3 has some specific deficiencies which should be borne in mind when considering the results presented here. Although HadCM3 reproduces the

global patterns of surface air temperature it exhibits a cold bias at high latitudes in the Northern Hemisphere which is particularly pronounced in Russia, east of Scandinavia, and the coarse resolution orography leads to local and remote biases (Gordon *et al.*, 2000). The performance for precipitation is generally less good; the observed global patterns are captured but significant biases exist: the South Pacific Convergence Zone extends farther and in a more easterly direction than observed (the 'double ITCZ' problem), there is a strong wet bias around the maritime continent and a dry bias in India and the northern Amazon region (Solomon *et al.*, 2007). HadCM3, as with other GCMs, also fails to reproduce the temporal structure of observed precipitation with simulated precipitation occurring too frequently and at lower intensity than observed.

3.5.2 European summertime changes

Europe is a highly urbanised region with significant areas of agricultural land. It is also a region which experiences periodic damaging heatwaves, with the 2003 heatwave causing an estimated 70,000 deaths (Robine *et al.*, 2008). Climate model projections suggest that average European summer temperatures as warm as in 2003 may become the mean state by the end of the 21st century, with significant implications for human health, energy consumption (air conditioning), and agriculture in the region (Stott *et al.*, 2004). Thus, Europe is one of the regions which may potentially benefit most from the application of land albedo geoengineering (Singarayer *et al.*, 2009) with the strongest cooling effect tending to be exerted over the summer months which should ameliorate some of the effects of extremely warm summers. Because of the relatively large fraction of the land occupied by urban area and cropland, Europe will experience a cooling significantly greater than the global average (e.g., Ridgwell *et al.* (2009)) under these albedo modification schemes.

To examine the effect of SAM geoengineering on the climate of Europe we examine results for inter-annual variability in average annual, and summer (June, July and August), temperature across the region of Western Europe (defined as in figure 3.3 e). Table 3.3 summarizes the annual and summer temperature anomalies for the different geoengineering schemes for this region. At $2 \times CO_2$ there is an increase of 4.18°C in the annual temperature across the region, with a larger increase in summer (5.03°C).

	SAT (°C)	
Experiments	Annual	JJA
$2 \times CO_2$- Pre-ind	**4.18**	**5.03**
Urban High - $2 \times CO_2$	**-0.50**	**-0.57**
Urban Mid - $2 \times CO_2$	**-0.14**	**-0.20**
Urban Low - $2 \times CO_2$	**-0.26**	**-0.22**
Crops High - $2 \times CO_2$	**-0.83**	**-1.26**
Crops Mid - $2 \times CO_2$	**-0.49**	**-0.80**
Crops Low - $2 \times CO_2$	**-0.27**	**-0.44**
Global Deserts - $2 \times CO_2$	**-1.55**	**-1.53**
Sahara Desert - $2 \times CO_2$	**-0.74**	**-0.98**
Asian Deserts - $2 \times CO_2$	**-1.20**	**1.49**
Sunshade - $2 \times CO_2$	**-3.47**	**-4.01**
All values passed a 5% student T-test for statistical significance.		

Table 3.3: Surface air temperature change in Western Europe

Against the greenhouse warming of $2 \times CO_2$, urban geoengineering produces a cooling of 0.50°C annually and 0.57°C in summer for maximum deployment. For both moderate and low urban geoengineering there is a statistically significant cooling both annually and in summer, however low urban geoengineering has a greater cooling than moderate urban geoengineering. This small deviation, of around 0.2°C from the expected moderate signal of 0.4 °C, could be a result of decadal to centennial variability in the model. A previous study of crop albedo geoengineering using HadCM3 found that a century-scale variation in sea-ice concentration and SSTs in the north atlantic affected their european temperature results and produced a deviation from the anticipated results of a similar magnitude (Singarayer *et al.*, 2009). Crop albedo geoengineering is more effective than urban geoengineering in Europe, with a maximum deployment cooling by 0.83°C annually and 1.26°C in summer. Desert albedo geoengineering, applied globally, exerts a cooling of 1.55°C annually and 1.53°C in summer across the region.

Rather counter-intuitively, desert geoengineering restricted to the Sahara has less of a cooling effect in Europe than when it is restricted to Asia. Desert geoengineering cools air locally but this air does not simply diffuse from the desert regions, instead it is advected in a complicated manner by the patterns of circulation which in turn are also modified by desert geoengineering.

Figure 3.4 shows how the frequency distribution of summer average temperatures over Western Europe is affected by SAM geoengineering. At $2 \times CO_2$ there is a much warmer summer ($\sim$5°C warmer than the preindustrial on average) and during the

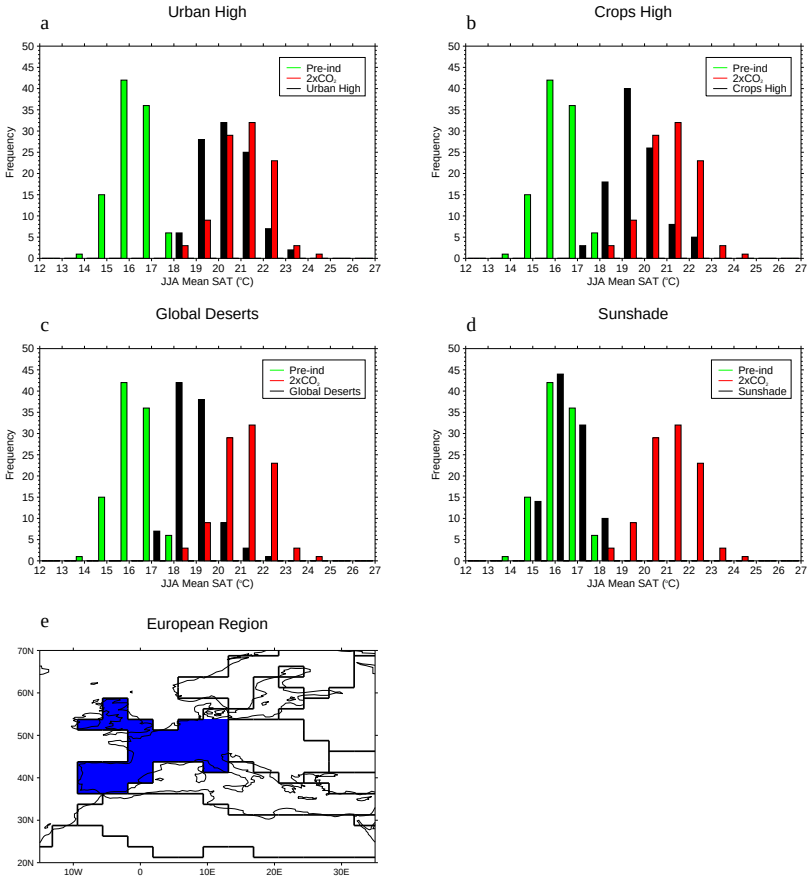

Figure 3.4: The panels a-d show the average summer (JJA) surface air temperature in the region shown in panel e and the frequency with which each temperature occurs over a 100 year period for Pre-ind, $2 \times CO_2$, and $2 \times CO_2$ with geoengineering. The Urban High (a), Crops High (b), Global Deserts (c) and Sunshade (d) results are shown.

100 year period analysed all summers were warmer than the warmest pre-industrial summer. A number of particularly warm summers also occur; four times with an average temperature above 23°C and once with an average temperature between 24 and 25°C. High urban geoengineering (Figure 3.3 a) lowers the average summer temperature by ∼0.6°C, reducing the number of extremely warm summers. Crop albedo geoengineering (Figure 3.3 b) is more effective and the greatest intervention lowers average summer temperatures by 1.3°C. With global desert geoengineering (Figure 3.3 c) there is a cooling in the summer of 1.5°C and a reduction in the number of extremely warm summers.

The simulation of European surface air temperature in HadCM3 suffers from a cold bias of around one to two degrees Celsius in this region. Stott *et al.* (2004) found that internal variability in European summer temperatures in HadCM3 is similar to observed values but the model might overestimate variability somewhat

(note however that the region they defined differs from ours). In simulations of European climate with Regional climate models driven by HadAM3H (a high-resolution atmosphere-only version of HadCM3) it was found that higher resolution orography could improve the spatial patterns of surface air temperature but that problems with land surface schemes and the driving GCM's representation of blocking highs affected the surface air temperature variability (Jacob *et al.*, 2007). These problems with the land surface schemes and with blocking highs affect our model, and hence our results. However, despite these problems these results reveal the important local and seasonal effects of these SAM geoengineering schemes.

3.5.3 Monsoon changes

As was noted earlier, global desert geoengineering may cause large changes in precipitation patterns around the world, particularly in monsoon regions such as India, Sub-Saharan Africa, and Australia, due to the mechanism which drives monsoon circulations; seasonal land-sea temperature differences. In the normal sequence of events, during the summer months continental areas warm faster than ocean areas, creating a pressure difference: this causes air to circulate, with warm, dry air rising over the continents being replaced by cooler, moist air from the ocean. In winter the opposite occurs as the oceans retain the heat collected over the summer for longer than the land. With desert geoengineering, there is a large change in albedo of the continental land surface, resulting in cooler summer temperatures, which reduce monsoon circulation locally and lead to significant changes in regional precipitation patterns and also changes in global circulation patterns.

Figures 3.5 a shows the difference between June, July, August (JJA) and December, January, February (DJF) rainfall for the pre-industrial. The monsoon systems have a positive difference in precipitation in the North and a negative difference in the South, i.e. greater rainfall in the summer relative to the winter in their respective hemispheres. Figure 3.5 b shows the changes in precipitation seasonality between $2 \times CO_2$ and pre-industrial; there is an intensification of the seasonality of rainfall in South-East Asia and the Indonesia and a reduction in the Amazon region and around the Caribbean. For both urban and crop geoengineering we find few statistically significant changes in the seasonality of rainfall and so these results are not shown here. For global desert geoengineering there is a large reduction in

monsoonal rains in areas neighbouring the modified desert areas (Figures 3.5 c-e). Global desert geoengineering reduces the intensity of the Indian, East Asian, North African and Australian monsoons but intensifies seasonal rains in Central and South America relative to $2\times CO_2$ (Figure 3.5 c). On the whole there is a large reduction in summer continental rainfall across the tropics compared to the pre-industrial (figure 3.5 g).

Restricting desert albedo modification to the Sahara (figure 3.5 d) reduces the intensity of the North African monsoon and to a lesser extent the Asian monsoon, whereas Asian desert geoengineering (Figure 3.5 e) reduces the intensity of the Asian monsoon and, perhaps surprisingly, strengthens the North African monsoon, and both schemes increase summer rainfall over Central and South America.

In comparison: sunshade geoengineering reverses most of the effects that doubling CO_2 has on precipitation seasonality (figure 3.5 f), returning the seasonality of precipitation very close to the pre-industrial with few statistically significant changes (figure 3.5 h).

In figure 3.6 we show the seasonal changes in 850 hPa winds for global desert geoengineering, alongside the changes in precipitation. Desert geoengineering profoundly changes the atmospheric circulation (figure 3.6 a,b), with the most extreme changes occurring in the Northern Hemisphere summer, when the desert albedo changes have their greatest effect. The altered patterns of precipitation (figure 3.6 c,d) correlate well with changes in 850 hPa wind, i.e., there are changes in moisture advection driven by the changes in the winds. This can be seen, for example, along the Ivory Coast where a large reduction in JJA rainfall coincides with a seaward wind anomaly (i.e., a reduction in monsoonal, landward winds) and in Central America where the increase in JJA rainfall coincides with an increase in Pacific to Atlantic winds over the isthmus (figures 3.6 a,c). In Australia, where there are reductions in precipitation, an anti-cyclonic anomaly in 850 hPa wind during Austral summer (DJF) acts to reduce the advection of moisture into the north of the continent (figures 3.6 b,d). In general, desert albedo geoengineering leads to disruption of precipitation locally and remotely through changes in circulation and therefore in moisture advection.

We identify six different areas of interest which may be affected significantly by desert geoengineering (Figure 3.7 g). The percentage change in average annual

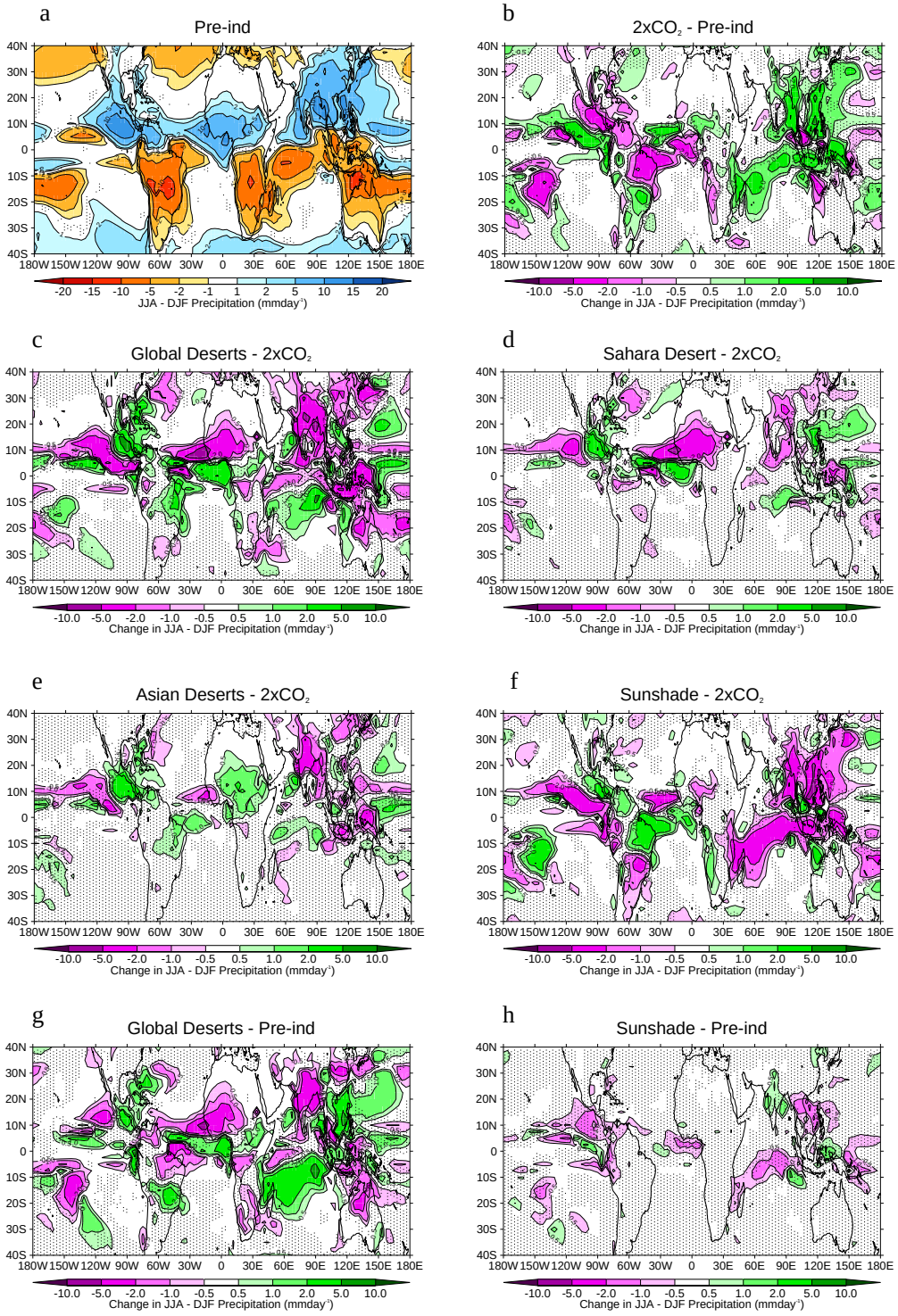

Figure 3.5: Panel a shows JJA-DJF precipitation, i.e. the seasonality of precipitation, for the pre-industrial. Panels b-g show the change in seasonality, i.e., the difference in absolute JJA-DJF precipitation, with negative numbers showing a decrease in seasonality. For $2 \times CO_2$ the anomaly is taken with the pre-industrial (b) and for the geoengineering schemes the anomaly is taken with the $2 \times CO_2$ case (c-g). Areas which failed a 5% student T-test are stippled.

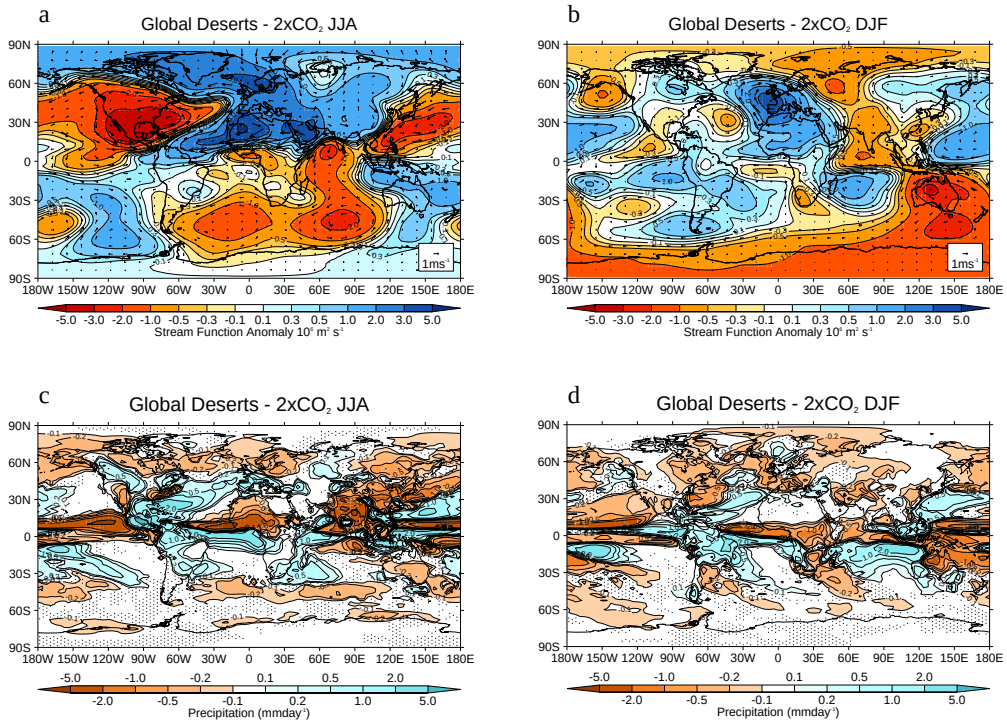

Figure 3.6: This shows the changes between Global Desert geoengineering and $2 \times CO_2$ for the wind speed and stream function at 850hPa during JJA (a) and DJF (b) and for precipitation during the same periods, panels c and d respectively. For precipitation, areas which failed a 5% student T-test are stippled.

precipitation for each of these six regions under different geoengineering scenarios are summarized in table 3.4. Brazil experiences a large decrease in precipitation at $2 \times CO_2$, compared to pre-industrial, and all the geoengineering schemes increase precipitation in Brazil, with global desert geoengineering returning precipitation to just above the pre-industrial value.

In the two African regions considered there are small increases in precipitation at $2 \times CO_2$, and for crop and urban geoengineering there is little effect on average

	Precipitation Change (%)					
Experiments	Brazil	Sahel	Ivory Coast	India	SE Asia	Australia
$2 \times CO_2$- Pre-ind	**-21.7**	**5.2**	**6.6**	**14.8**	**7.5**	**-14.3**
Urban High - $2 \times CO_2$	**4.6**	0.7	-0.2	**-3.8**	-1.7	4.7
Crops High - $2 \times CO_2$	**6.8**	0.5	-0.4	**-9.8**	**-2.3**	2.3
Global Deserts - $2 \times CO_2$	**28.8**	**-30.6**	**-17.4**	**-45.0**	**-12.8**	**-18.2**
Sahara Desert - $2 \times CO_2$	**10.8**	**-33.4**	**-19.1**	**-12.5**	**-4.8**	-2.8
Asian Deserts - $2 \times CO_2$	**10.5**	**19.0**	**2.0**	**-28.7**	**-5.0**	**8.7**
Sunshade - $2 \times CO_2$	**24.9**	**-5.1**	**-5.7**	**-6.6**	**-10.3**	**17.7**
Bold-typed values passed a 5% student T-test for statistical significance.						

Table 3.4: Precipitation change in monsoon regions.

precipitation. Global and Saharan desert geoengineering cause large decreases in precipitation in the Sahel and Ivory Coast regions, whereas Asian desert geoengineering causes a large increase in the Sahel band.

In India and South-East Asia there are moderate increases in precipitation at $2 \times CO_2$; both crops and urban geoengineering reduce rainfall in these regions, particularly in India, although it remains above the pre-industrial value. Global desert geoengineering decreases rainfall in India significantly and in Southeast Asia to some extent, with a 37% reduction in rainfall, relative to pre-industrial in India, and a 6% decrease in south-east Asia.

Australia experiences a reduction in precipitation at $2 \times CO_2$ and most geoengineering schemes considered increase precipitation in Australia, whereas global desert geoengineering (which includes an Australian component) produces an 18% reduction in rainfall compared to the pre-industrial.

Variability in monsoon rainfall is also an important indicator of change; figure 3.7 shows frequency plots for annual precipitation over India (in figure 3.7 g the Indian region is shaded blue). The rainfall distribution changes from pre-industrial to $2 \times CO_2$ with average rainfall up 15% and fewer dry years. Figure 3.7 a shows that urban geoengineering reduces the rainfall over India slightly, returning the distribution somewhat closer to its pre-industrial state. Crop geoengineering has a larger impact, returning the mean rainfall over India close to pre-industrial but broadening the distribution (Figure 3.7 b).

The desert geoengineering schemes applied globally, in the Sahara and in Asia, all reduce Indian rainfall, resulting in a 37% reduction, no statistically significant change, and an 18% reduction relative to the pre-industrial respectively (figures 3.7 c-e). For global desert geoengineering the wettest years are below the pre-industrial mean and, in the driest years, India receives less than 300 mm of rain, down from more than 500 mm in the pre-industrial. Asian desert geoengineering has a significant drying effect, whereas Sahara desert geoengineering returns the distribution close to the pre-industrial state.

Jiang *et al.* (2005) assessed some of the models used in the CMIP3 for their performance at reproducing the East-Asian monsoon and found that all models had difficulties reproducing the observed behaviour but that HadCM3 was one of the better models. They found that whilst HadCM3 overestimated precipitation

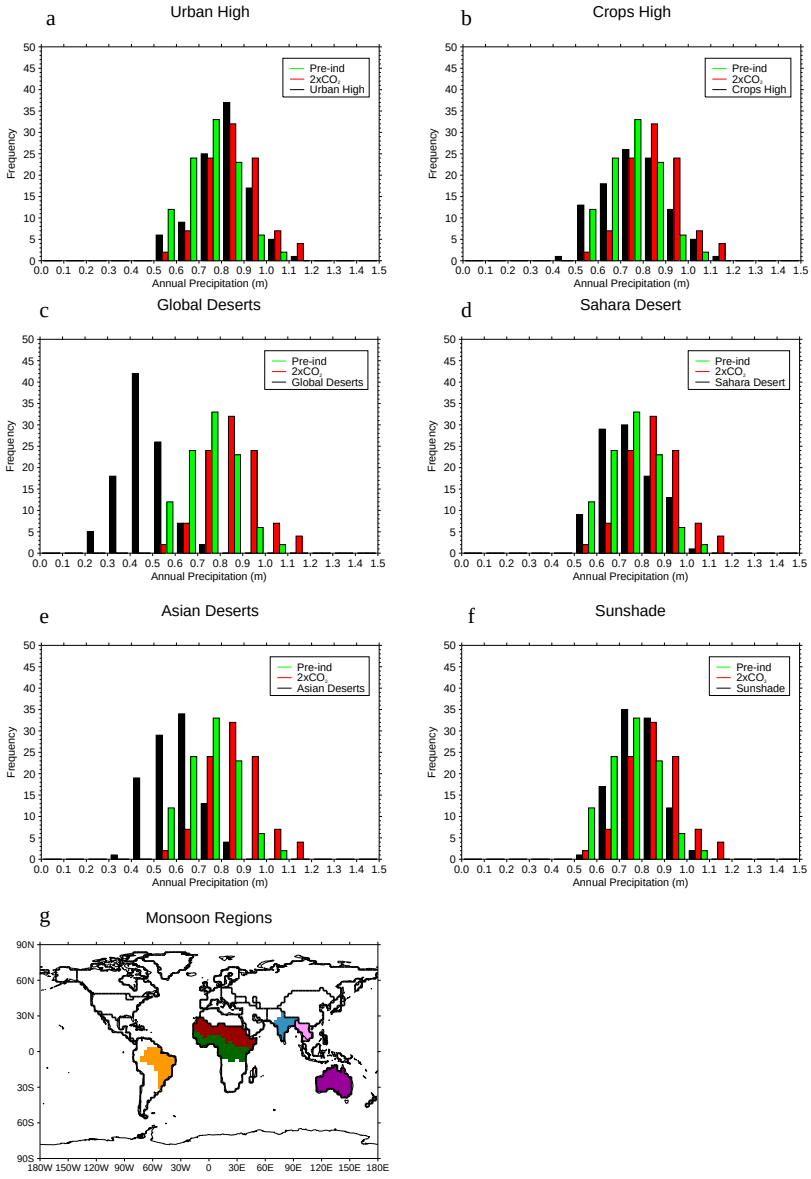

Figure 3.7: The panels a-f show the average annual precipitation in India (see panel g) and the frequency with which the volumes of precipitation occur over a 100 year period for Pre-ind, $2\times CO_2$, and $2 \times CO_2$ with geoengineering. The Urban High (a), Crops High (b), Global, Asian and Sahara Deserts (c-e) and Sunshade (f) results are shown. Panel g shows the regions which were used to calculate the area-averaged changes in precipitation, these are based on the regions in the FUND model (Anthoff *et al.*, 2009)

in all seasons, the distribution of precipitation was similar to observations, and although the winter was too cold, the surface air temperature was well reproduced. These problems and others affect the quality of the monsoon results shown and so the details of the results must be viewed with caution. However, due to desert geoengineering directly affecting the seasonal land-sea temperature difference, the driver of monsoon circulation, the general result of reduced rainfall near to modified desert regions is likely to be robust.

3.5.4 Arctic changes

The Arctic is a region which is warming faster than the rest of the world, as a result of global warming (IPCC, 2007). Although the exact mechanisms are uncertain, retreating sea-ice and, to a lesser extent, changes in snow cover are likely to be involved (Screen and Simmonds, 2010). The Arctic is home to large reservoirs of stored carbon, as decayed plant matter in permafrost and methane reserves in hydrates, which could provide an additional (carbon cycle) positive feedback (Archer, 2007). We focus on the Arctic here for these reasons as well as the fact that it is remote from all the SAM schemes and hence illustrates the potential for non-local impacts (and teleconnections) arising from land albedo geoengineering.

Figure 3.8 shows the simulated pre-industrial sea-ice and snow coverage for the Northern Hemisphere and the effects of doubling CO_2 and geoengineering on sea-ice and snow. Comparing figures 3.8 a and b, it can be seen that the sea-ice extent and thickness are reduced at $2 \times CO_2$ compared to pre-industrial, with minimum sea-ice cover (September average) reduced by 71% (Figure 3.8 c). The change in snow depth is more spatially heterogeneous, with snow loss at mid-latitudes but an increase in snow depth at high latitude. At high latitudes the increase in snow accumulation outweighs the increased losses due to higher temperatures and with a greater fraction of the Arctic Ocean ice free there will be more evaporation and consequently greater snowfall (the increase in precipitation is shown in Figure 3.3 a). The snow depth projections for Greenland are omitted as the model does not include an ice-sheet module and so cannot simulate changes in this region reasonably, i.e. mass loss by iceberg calving, etc. is not represented.

Figures 3.8 c and d show that urban and crop-land geoengineering induce a slight recovery of annual mean sea-ice thickness, with a 13% and 20% increase in minimum

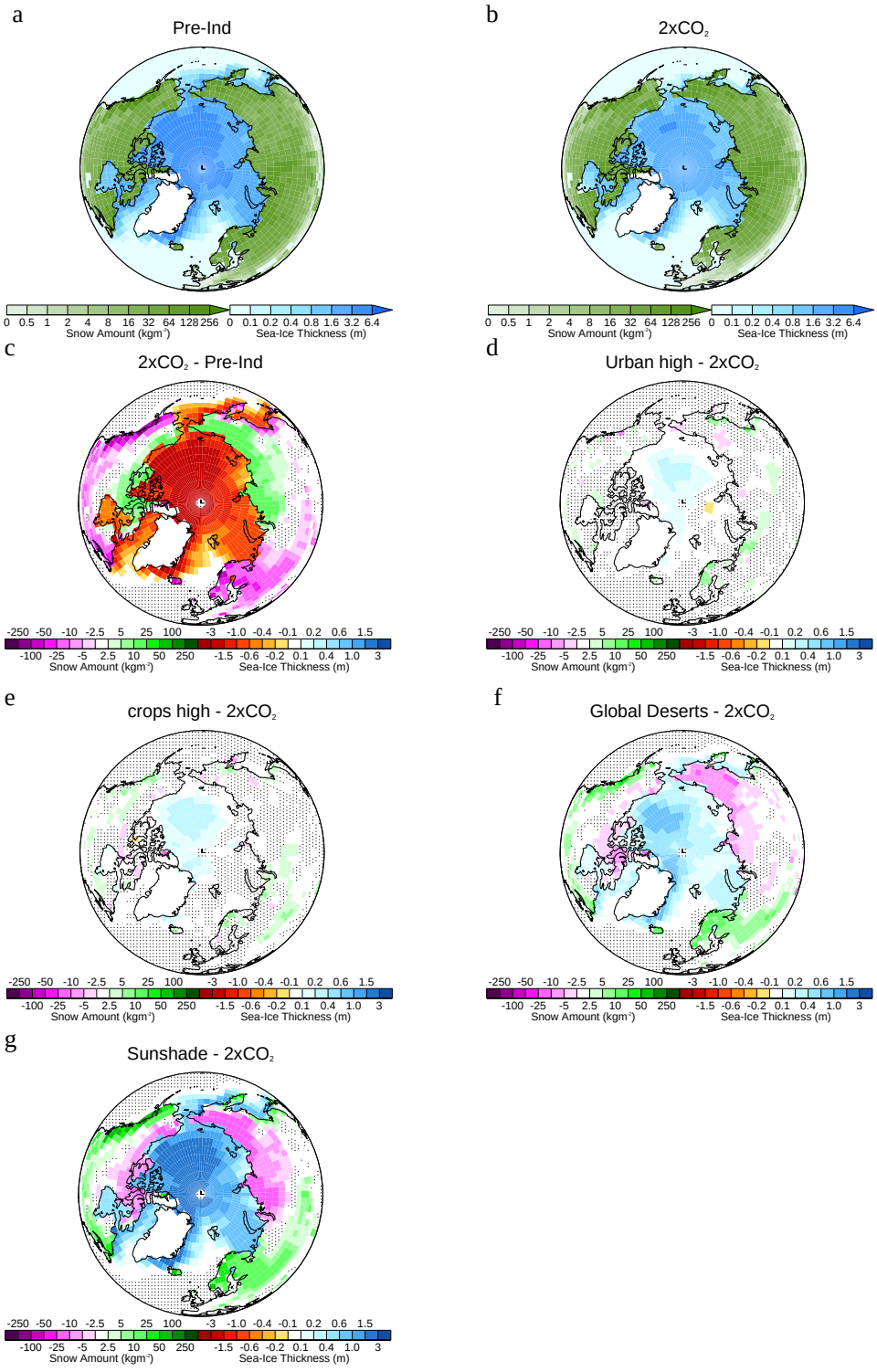

Figure 3.8: Panels a and b show the pre-industrial and $2 \times CO_2$ simulated snow and sea-ice cover. Panel c shows the difference in snow and sea-ice cover between $2 \times CO_2$ and pre-industrial, Panels d-g show the difference between the geoengineering experiments and $2 \times CO_2$; Urban High geoengineering (c), Crops High geoengineering (d), Global desert geoengineering (e), Sunshade geoengineering (f). The results for Greenland have been masked out as the model does not include a representation of ice-sheet processes. Areas which fail a 5% student T-test are stippled.

sea-ice cover (September average) relative to $2 \times CO_2$, and a very small effect on snow depth. Desert geoengineering exerts a more substantial effect on annual mean sea-ice thickness, with a 65% increase in minimum sea-ice cover relative to $2 \times CO_2$ which remains 53% lower than the pre-industrial coverage. Desert geoengineering also has a large impact on snow depth, with almost the opposite spatial pattern to that of $2 \times CO_2$ i.e., desert geoengineering cools and dries the Northern Hemisphere, partly reversing the trend induced by global warming.

Again, projections of effects of geoengineering on climate must be viewed in the context of the degree of fidelity of the climate model used: HadCM3 has a number of biases in the climate state of high northern latitudes which will affect the results shown in this section, the most important of which is a cold bias (Gregory *et al.*, 2002). HadCM3 also has a wet bias at high latitudes which will affect the quality of the snow cover results (Solomon *et al.*, 2007). There are problems in the sea-ice climatology of HadCM3 but the model does roughly reproduce the 20th century trend in sea-ice (Gregory *et al.*, 2002) and matches the projections of other AOGCMs, predicting a large decline in summer sea-ice extent over the course of the 21^{st} century (Johannessen *et al.*, 2004). However, the results shown are consistent with the cooling of the SAM schemes being concentrated in the Northern Hemisphere and show that SAM geoengineering may help to reduce Arctic climate change somewhat.

3.6 Discussion and conclusion

Global average measures of climate change alone are insufficient in the assessment of the effectiveness and particularly, side-effects of surface albedo geoengineering. Analysis of regional and seasonal changes in temperature, precipitation, and other variables, are critical to elucidating whether any particular proposed geoengineering scheme may be a suitable means to ameliorate climate change. In this study we have used a fully coupled general circulation model (GCM) to project the climatic effects of different surface albedo modification (SAM) geoengineering schemes. However, GCMs are far from perfect representations of the Earth's climate and, although they perform relatively well on the large scale, they do not match observations well on small spatial and temporal scales (IPCC, 2007). GCMs are particularly poor at reproducing regional precipitation observations and so any specific patterns

of precipitation change should be viewed with caution (IPCC, 2007). In addition to these considerations, and as well as deficiencies specific to the HadCM3 model discussed in earlier sections, the MOSES 1 land surface scheme we use assumes fixed vegetation and so does not allow adjustments to changed climatological conditions. Vegetation-climate feedbacks will hence not be captured in our simulations.

Our treatment of surface albedo geoengineering is relatively simplistic and there are no explicit urban, crop or desert surface land types in the MOSES 1 land surface scheme (Cox *et al.*, 1999) we employ here. Areas to which we applied surface albedo geoengineering could also have been alternatively defined. For instance, our definition of desert was based on grid-scale sized areas, excluding smaller deserts and hence our distribution of desert geoengineering could be revised. Given the extreme nature of desert albedo modification, a different distribution of modified desert would likely produce a significantly different regional response, which can be seen by comparing the very different responses from our three different areas of application. The assumed magnitudes of geoengineering we deployed for each scheme and in particular for urban geoengineering, are generally at the upper end of estimates and do not necessarily represent 'realistic' scenarios. We chose to mostly test relatively large magnitude albedo modifications in order to obtain a sufficient signal to noise ratio and thus to enable us to more fully explore the potential climatic consequences of highly concentrated changes in albedo. Overall, however, we believe the distributions we used capture the essential properties of these schemes and at a minimum our study provides a unique sensitivity test for the climate impacts of the three main proposals for surface albedo geoengineering.

Surface albedo modification (SAM) geoengineering gives rise to both nearfield and farfield changes in climate. We find small to insignificant changes in global average temperature from urban and crop geoengineering, consistent with other studies (Lenton and Vaughan, 2009; Ridgwell *et al.*, 2009), and a more significant cooling with desert geoengineering. For all the SAM schemes we find a local cooling around the region with modified albedo, which is greatest in summer; although we found this effect can be reduced somewhat by changes in cloud cover and advection, as has been found in other studies of SAM geoengineering (Doughty *et al.*, 2011; Ridgwell *et al.*, 2009).

On a global scale we find that the cooling effect of the SAM geoengineering

schemes is greater over land and in the Northern Hemisphere due to the greater fraction of suitable regions being in the Northern Hemisphere. We find that the Arctic is cooled somewhat by all schemes, despite being remote from any areas of application, and there is some recovery of sea-ice and snow cover but even desert geoengineering is insufficient to return the Arctic sea-ice and snow to its pre-industrial condition. We find that very large changes in precipitation patterns can occur for desert geoengineering, with much smaller changes for urban and crop geoengineering. We compared desert geoengineering to sunshade geoengineering and to the results of a cloud albedo study and found that, although desert geoengineering produces a smaller reduction in global average precipitation per change in temperature, it causes a much greater reduction in the land-average precipitation (Bala *et al.*, 2010a). This is consistent with, but opposite to, the results found in the cloud albedo study of (Bala *et al.*, 2010a), where they found a large reduction in global average precipitation but a much smaller reduction in land-average precipitation. This is explained in their study by the warmer region (the land in their case, or ocean in ours) having an increase in upward motion in the atmosphere giving rise to increased precipitation, with the opposite being true for the colder region (Bala *et al.*, 2010a). Similarly we find, for urban and crop geoengineering, that the relative cooling of the Northern Hemisphere leads to a slight southward shift of the ITCZ that for desert geoengineering is hard to distinguish due to the dramatic changes in circulation arising from the extreme local cooling.

Desert geoengineering causes large changes to continental rainfall in regions neighbouring deserts and more broadly causes significant changes in tropical rainfall patterns. These changes arise, in part, due to the seasonal nature of the cooling exerted by SAM geoengineering, with the greatest cooling occurring in summer, when the air over the continents would normally warm faster than the ocean creating an updraft, which draws in moist air from the oceans bringing seasonal rainfall. This monsoon circulation is reduced by desert geoengineering, leading to a reduction in precipitation across a wide area. We find that precipitation across the Tropics is radically shifted with some areas becoming much drier than in the pre-industrial, particularly India, and others becoming wetter.

SAM geoengineering schemes do not offer anything like a full solution to the problems arising from rising greenhouse gas concentrations and, desert geoengineering in

particular, may prove to be detrimental. Our simulations show that urban and crop geoengineering may have little effect on global climate and primarily only offer local amelioration of some climate change effects. Desert geoengineering, on the other hand, produces strong local cooling in desert regions and results in large changes in circulation and precipitation world-wide. Not only are land albedo geoengineering schemes unable to correct fully for greenhouse gas induced climate changes (as is the case for all SRM schemes investigated so far, e.g., Lunt *et al.* (2008b), Irvine *et al.* (2010), Jones *et al.* (2011a) and Ban-Weiss and Caldeira (2010)), they would not address ocean acidification (Cao and Caldeira, 2008; Matthews *et al.*, 2009). Only mitigation of CO_2 emissions, or removal of CO_2 from the atmosphere by some carbon dioxide removal scheme (Shepherd *et al.*, 2009), would provide a correction for both the climatic and ocean chemistry impacts of elevated CO_2 concentrations. Future work on SAM geoengineering could look in more detail at the impacts of these schemes with a higher resolution GCM or a regional climate model, or consider combinations of surface albedo modification and other climate engineering schemes as a way to 'optimize' the climate modification.

CHAPTER 4

Development of a perturbed parameter ensemble with an application to SRM geoengineering

4.1 Cover sheet

The previous chapters have presented results of studies which used a single General Circulation Model (GCM) but as all models have structural and parametric uncertainty the specific results of these studies must be treated with caution. The impact of these uncertainties can be assessed by using many different GCMs or using perturbed parameter ensembles (PPE). This chapter develops and tests a perturbed parameter ensemble of HadCM3 and applies this to two sunshade geoengineering experiments. This work provides a measure of the uncertainty in the results of sunshade geoengineering; helping to identify which aspects of the results of Chapters 2 and 3 are robust. This chapter consists of a study which will be submitted to the journal Geoscientific Model Development which I will be first author on and some additional material on sunshade geoengineering that will be included in a later study published elsewhere. These initial sunshade geoengineering results are included within the text of this section to make the work relevant to the thesis and to improve the flow of the presentation.

The perturbed parameter ensemble (PPE) of HadCM3 developed in this chapter uses a coupled ocean and does not use flux adjustment. Most perturbed parameter ensembles of GCMs use flux adjustment and a simplified ocean model which allows the models to stay in equilibrium. After generating an initial ensemble of 200 members, 27 members are selected and compared to the third Climate Model Intercomparison Project (CMIP3) ensemble. Most members of the PPE perform

similarly to the CMIP3 ensemble members in the pre-industrial control although a few members are either too warm or too cold. At elevated CO_2 levels some members of the ensemble are found to behave unrealistically and some of these begin a runaway climate warming. The PPE is applied to two sunshade geoengineering experiments and finds that many of the results of Chapter 2 are robust. However, this analysis indicates that the results of Section 2.6 may over-estimate the stability of the Greenland Ice-Sheet under sunshade geoengineering. Other implications of these PPE results for the thesis are also discussed in this chapter.

Prof. Paul Valdes, Dr. Dan Lunt, and I chose the methodological approach and defined the goals for the PPE. The methodology for producing and managing the hundreds of simulations was developed by Dr. Lauren Gregoire (Gregoire *et al.*, 2010), and extended and applied to HadCM3 by me. I produced all the simulations, conducted the analysis, and drafted manuscript. Prof. Andy Ridgwell, Dr. Dan Lunt and I selected the final analysis included in the chapter and suggested changes to the manuscript. The final text I drafted is based on these suggestions.

4.2 Abstract

Flux adjustment was used in early GCMs to correct for biases in the control climatology and has been used in PPE studies to correct for biases introduced into the energy budget by the parameter perturbations. We present the first PPE to use a fully-coupled atmosphere-ocean CMIP3-era GCM, HadCM3, without flux adjustment, with the aim of developing a research tool for climate modelling studies. Seven atmospheric parameters and an ocean parameter were jointly perturbed within a reasonable range to generate an initial group of 200 members. A 20 year pre-industrial control simulation was run and members whose projected global mean temperature fell outside of a range of temperatures near to the observed pre-industrial mean of 13.6 $\pm$ 2 °C were discarded (Jones *et al.*, 1999; Brohan *et al.*, 2006). Twenty seven members, including the standard model, were accepted, covering almost the entire span of the 8 parameters, challenging the argument that without flux adjustment, parameter ranges would be unduly restricted (Collins *et al.*, 2006). For the remaining members (the PPE) an 800 year pre-industrial, a 150 year quadrupled CO_2 simulation, and a 150 year 1% CO_2 rise per annum simulation were run. The

behaviour of the PPE for the pre-industrial control was compared to the CMIP3 ensemble for a number of surface and atmospheric column variables and few members of the PPE were outside the range of behaviour seen in the CMIP3 ensemble (Meehl *et al.*, 2007b). However as has been noted in previous studies (Joshi *et al.*, 2010; Sanderson *et al.*, 2010), we find that members of the PPE with low values of the entrainment rate coefficient show very large increase in upper tropospheric and stratospheric water vapour levels in response to elevated CO_2 and some show very high climate sensitivities. In fact some of the members seem to be entering a runaway greenhouse warming, failing to converge on an equilibrium temperature response. This lends support to the assessment of Joshi *et al.* (2010) that the response of the members with a low entrainment coefficient to elevated CO_2 levels may be unrealistic and suggest revising the range for the entrainment rate coefficient in HadCM3 from 0.6 - 9.0 to 2.0 - 9.0 . An example application of the PPE to sunshade geoengineering is consistent with many results of other studies and the spread in the climate response across the ensemble covers the range of response seen in a sunshade study with 4 GCMs (Schmidt *et al.*, 2012).

4.3 Introduction

PPEs of GCMs are becoming more common as a means to assess the range of uncertainty in climate model projections (Murphy *et al.*, 2004; Stainforth *et al.*, 2005; Collins *et al.*, 2006; Sanderson, 2011; Yokohata *et al.*, 2010). This PPE approach is a complement to the Multi-Model Ensemble (MME) approach notably applied in the IPCC assessments (Solomon *et al.*, 2007; Meehl *et al.*, 2007b). These two approaches address two aspects of model uncertainty; the structural uncertainty associated with the understanding, discretization and parameterization of the climate system as a GCM and the parametric uncertainty associated with the uncertain values of the parameters within a GCM. Although these two methods sample uncertainty in climate model results and can be used to get a clearer idea of the range of possible response, they are not substitutes as they address different kinds of uncertainty. MMEs sample a range of different modelling approaches and thus sample structural uncertainty, and PPEs sample the parametric uncertainty of a given model. The multi-model approach has the advantage of having independent modelling schemes (although the

fact there is a somewhat common heritage amongst models and they are developed by a group of experts sharing similar knowledge limits the independence (Masson and Knutti, 2011)), but as the number of possible models is indefinable, any MME will represent a haphazard sampling of the structural uncertainty in climate model predictions (Meehl *et al.*, 2007b). The PPE approach has the advantage that the space of all the parameters to be perturbed is known and a sample of parameter combinations can be taken with a known coverage of this parameter space. It is not possible to generate a large number of models with different structures, unless a long program of model development is begun, however it is possible to generate a very large number of different versions of one model by perturbing parameters, with the availability of computing resources being the only effective limit. For these reasons PPE experiments are a useful tool for assessing uncertainty in climate model projections.

As greater computing resources have become available, larger and more complex PPEs of GCMs have become possible (Frame *et al.*, 2009). There are many hundreds of uncertain parameters in a GCM and so expert elicitation is needed to select which parameters are important and to indicate a reasonable range for these parameters (Murphy *et al.*, 2004). The early PPEs consisted of single-parameter perturbations, in effect a sensitivity test of parametric uncertainty (Murphy *et al.*, 2004). However, many parameters in a GCM will interact in complex non-linear ways, and so parameters must be perturbed simultaneously to explore the full range of response implied by the prior parametric uncertainty (Stainforth *et al.*, 2005). The space of all uncertain parameters can be very large indeed for GCMs and so many studies have taken subsets of the most important parameters to try and achieve a thorough coverage of the parameter space (Stainforth *et al.*, 2005; Knight *et al.*, 2007).

Most PPEs to date have used atmosphere-only or slab-ocean versions of GCMs as these take between a few years and a few decades to reach equilibrium as opposed to the millennia required to fully spin-up a fully dynamic coupled atmosphere-ocean GCM, although some parametric sensitivity studies have used coupled oceans (Collins *et al.*, 2007; Brierley *et al.*, 2010). All PPE studies that the authors are aware of have used flux adjustment to keep the ensemble members in radiative balance. This flux adjustment is applied as a heat flux into the ocean surface designed to correct for model biases in the sea-surface temperature, and these are either cal-

culated at each grid cell or as an average over the whole ocean (Collins *et al.*, 2006). Top-of-atmosphere (TOA) radiative balance is an emergent property in GCMs and the fact that the models of the IPCC AR4 did not need flux adjustment was seen as an improvement over earlier models (Solomon *et al.*, 2007).

When using climate models to estimate the climate response to a forcing some assessment of the suitability and quality of the models must be made. Climate sensitivity, i.e. the equilibrium temperature response to doubling CO_2, is one example of an uncertain aspect of the climate system and one on which models disagree on. The approach outlined in the IPCC AR4 to assess the climate sensitivity is to take a number of suitable models (GCMs) with a range of different model structures and sub-gridscale parameterizations, and assess the performance of these models in simulating observed climate (IPCC, 2007). The models which most closely resemble the observed climate are then believed to have reasonable estimates of climate sensitivity and thus the estimate of climate sensitivity presented in the IPCC AR4 is then a survey of all these reasonable models (Meehl *et al.*, 2007b; IPCC, 2007). The idea that all models, passing some quality control test, should be considered equal for the purposes of assessing climate sensitivity has been challenged as some models perform better at reproducing observed climates than others (Knutti, 2010). Model equality is also problematic for PPEs as they are likely to include versions of the model which are much poorer at simulating observed climate that the standard version of the model. In many PPE studies a formal quality test is applied such as the climate prediction index and poorly performing models are excluded or given much less weight than better performing models in ensemble-mean statistics (Murphy *et al.*, 2004). Flux adjustment means that SSTs are adjusted to observations, which excludes the inherent radiative balance constraint that acts on the fully-coupled models of MMEs.

Equilibrium climate sensitivity, the equilibrium temperature response to a doubling of CO_2 concentrations, is an important tool in estimating the temperature response of the Earth to anthropogenic GHG emissions. The GCMs investigated by the IPCC AR4 had a range of equilibrium climate sensitivities of between 2.1°C and 4.4°C, with a mean value of 3.2°C (IPCC, 2007). These GCM results, along with other evidence, led to the IPCC stating that climate sensitivity was 'likely to be in the range 2.0°C to 4.5°C with a best estimate of about 3°C', i.e. greater

than 66% probability of being in this range (IPCC, 2007). It was also noted that values of climate sensitivity substantially higher than 4.5°C cannot be ruled out but no well-performing models were found at these higher climate sensitivities (IPCC, 2007). This 'fat-tail', or skew to higher values, of the probability distribution of climate sensitivity is an inherent property of systems with an uncertain, net positive feedback (Roe and Baker, 2007). This is due to the fact that a unit increase in the total feedback factor causes a greater change in the equilibrium climate sensitivity than a unit decrease does, due to the action of the positive feedback. PPEs have reported much broader ranges of climate sensitivity than those in the IPCC AR4 MME, e.g. Stainforth *et al.* (2005) found acceptable model versions with climate sensitivities from 2.0 - 11.0 °C, and Piani *et al.* (2005) found that their ensemble had a mean climate sensitivity of 3.3 °C, with 5% and 95% confidence bounds of 2.2 and 6.8 °C, respectively. MMEs consist of the best performing parameterization of each participant model whereas PPEs consist of a large number of different model parameterizations, some of which perform rather poorly compared to observations (Murphy *et al.*, 2004; IPCC, 2007). Part of the argument in the IPCC AR4 against very high climate sensitivities comes from the fact that models with climate sensitivities higher than 4.5 °C perform poorly compared to observations and so the step of filtering or weighting members in PPEs is key to constraining the climate sensitivity estimate produced (Murphy *et al.*, 2004; Piani *et al.*, 2005). The choice of priors for the parameter ranges plays an important role, as does the choice of using a uniform prior on the climate sensitivity or feedback parameter (Frame *et al.*, 2005).

In this study we develop the first PPE using the fully-coupled Atmosphere-Ocean GCM (AOGCM) HadCM3 without applying fluxadjustments (although similar work has been done with FAMOUS, a low-resolution version of HadCM3 (Gregoire *et al.*, 2010)). This ensemble is developed with the goal of creating a relatively computationally efficient modelling tool for investigating parametric uncertainty in climate and paleo-climate experiments where the use of a flux adjusted PPE is inappropriate. We test the ensemble behaviour on the TOA radiative balance of the ensemble members and a number of other basic metrics and assess the range of response to elevated CO_2 experiments. The rest of the paper is laid out as: methodology in Section 4.4, basic performance in Section 4.5.1, pre-industrial control performance in Section 4.5.2, $4 \times CO_2$ and 1% CO_2 per annum experiments in Section 4.5.3, and

two solar insolation geoengineering experiments which cancel the forcing of $4 \times CO_2$ and 1% CO_2 per annum G1 and G2 in Section 4.5.4 and discussion in Section 4.6.

4.3.1 Motivation for SRM geoengineering application

Solar radiation management (SRM) geoengineering has been proposed as a means to ameliorate the effects of rising greenhouse gas concentrations and the climate effects of some of these SRM schemes have been investigated with GCMs (Jones *et al.*, 2009; Lunt *et al.*, 2008b; Irvine *et al.*, 2010; Ban-Weiss and Caldeira, 2010). There is a project underway to investigate SRM geoengineering using a range of GCM climate models called the geoengineering model intercomparison project (geoMIP) (Kravitz *et al.*, 2011). Two experiments from the geoMIP ensemble deal with sunshade geoengineering and these are used as an example application of the PPE developed in this study.

4.4 Methodology

4.4.1 HadCM3 model description

The fully coupled AOGCM used in this paper is HadCM3 (Gordon *et al.*, 2000). HadCM3 has been used in the IPCC third and fourth assessment reports (IPCC, 2007) and performs well in a number of tests relative to other global GCMs (Covey *et al.*, 2003; IPCC, 2007), although since the development of new models in preparation for the 5th IPCC assessment (e.g. HadGEM2 the latest model from the Met Office (Collins *et al.*, 2011)), it can no longer be considered 'state-of-the-art' for century-scale integrations. The horizontal resolution of the atmospheric model is 2.5° in latitude by 3.75° in longitude, with 19 vertical layers. The atmospheric model has a time step of 30 minutes and includes many parameterizations representing sub grid-scale effects, such as convection (Gregory and Rowntree, 1990) and boundary-layer mixing (Gordon *et al.*, 2000). The spatial resolution in the ocean is 1.25° by 1.25°, with 20 vertical layers. The ocean model component uses the (Gent and McWilliams, 1990) mixing scheme, and there is no explicit horizontal tracer diffusion. The sea-ice model uses a simple thermodynamic scheme and contains parameterizations of sea-ice drift and leads (Cattle and Crossley, 1995). We employ the MOSES 1 land surface scheme (Cox *et al.*, 1999), which accounts for

terrestrial surface fluxes of temperature, moisture and radiation. MOSES includes; 4 soil layers, recording temperature, moisture and phase changes; a canopy layer; and a representation of lying snow. The representation of evaporation includes the dependence of stomatal resistance on temperature, vapour pressure and CO_2 concentration (Cox *et al.*, 1999). Each grid cell has surface properties; roughness length, snow-free albedo, etc., which reflect the vegetation cover present, as derived from the Wilson and Henderson-Sellers (1985) dataset.

4.4.2 Ensemble design

As we are using a fully-coupled AOGCM a considerable spinup of the model will be required and only a relatively small number of simulations are possible, so to allow for a reasonable coverage of parameter space only a small number of parameters are chosen. The greater the number of parameters included in an ensemble the more aspects of the parametric uncertainty in the model can be assessed, however, with a greater number of parameters there is a larger parameter space. One way to quantify the coverage of parameter space that a given ensemble represents is to divide each parameter range into two halves, 'low' and 'high', thus there are 2^p combinations of 'low' and 'high' for p parameters. If we start with an ensemble of 200 members 78% of the 'halves' of an 8 parameter space can be covered but only 20% of the 'halves' of a 10 parameter space and only 5% of a 12 parameter space. We chose to start with an initial ensemble of 200 members and chose to modify only 8 parameters to strike a balance between coverage of parameter space and the number of important parameters.

Table 1 outlines the 8 continuously varying parameters that were jointly modified; these include the 6 atmospheric parameters modified in Stainforth et al. (2005), the entrainment rate coefficient (ENTCOEF), the ice-fall speed (VF1), the critical relative humidity (RHCRIT), the droplet to rain conversion rate (CT), the droplet to rain conversion threshold over land and sea (CW_LAND/SEA, modified together), the empirically adjusted cloud fraction (EACF); the sea-ice low albedo (ALPHAM); and the background vertical ocean diffusivity parameter (VDIFF) used in Collins *et al.* (2007). The 6 parameters modified in Stainforth *et al.* (2005) were chosen for the large impact that these parameters have on climate sensitivity (Rougier *et al.*, 2009). The sea-ice low albedo (ALPHAM) parameter was added as it is

expected that this ensemble will be used for paleo-climate simulations of glacial periods where sea-ice parameters may play a more important role than today or in the future. The vertical ocean diffusivity parameter was added, as this was the ocean parameter found to have the most significant effect on the transient climate response of HadCM3 (Collins *et al.*, 2007; Brierley *et al.*, 2010). The range for all parameters except for VDIFF were taken from the expert elicitation in Murphy *et al.* (2004), however the lower ranges of EACF and ALPHAM were extended by 20% as the standard version of HadCM3 sits at the lower limit for these parameters. It was reasoned that if the parameter values of the standard version of HadCM3 are reasonable, small deviations from these values should be reasonable too. The VDIFF parameter consists of the initial surface background diffusivity and a rate of increase of diffusivity with depth which were varied together as in Collins *et al.* (2007) and Brierley *et al.* (2010). All parameters are sampled using a uniform prior on parameter value except for VDIFF for which uses a uniform prior on the power of the parameter value, i.e. the initial diffusivity and the rate of increase of diffusivity vary as 2^x and 4^x respectively, where x varies uniformly from -1 to 1. This choice for the VDIFF parameter was made after discussions with the author of a study which presented an expert elicited range for this parameter (Brierley, C. personal communications (Brierley *et al.*, 2010)).

To select parameter combinations a maximin latin hypercube sampling technique was used and 200 combinations of the 8 parameters drawn (Tang, 1994; Gregoire *et al.*, 2010). To generate a latin hypercube each parameter range is divided into 200 sections with one point drawn from each of the sections of each parameter, ensuring that there is no repetition. There are many possible latin hypercubes which satisfy these conditions and a better sampling is possible with the maximin latin hypercube approach. Maximin latin hypercube sampling adds the requirement that each point drawn must be as far from previous points as possible, thus ensuring a greater coverage of the parameter space. At this stage each point is defined as a small region of parameter space between the minima and maxima of its respective parameter sections. To get a definitive value for each of the point's parameter co-ordinates a random value between the minimum and maximum of each section of each parameter is found in turn. Thus we have 200 well-spaced parameter value drawn from across the 8 dimensional parameter space.

Parameter name	Standard value	Minimum value	Maximum value	Description
ENTCOEF	3.0	0.6	9.0	Entrainment rate coefficient (N/A)
VF1	1.0	0.5	2.0	Ice-fall speed (ms^{-1})
CT	1.0×10^{-4}	5.0×10^{-5}	4.0×10^{-4}	Cloud droplet to rain conversion rate (s^{-1})
CW (Land / Sea)	2.0×10^{-4} / 5.0×10^{-5}	1.0×10^{-4} / 2.0×10^{-5}	2.0×10^{-3} / 5.0×10^{-4}	Cloud droplet to rain conversion threshold (Kgm^{-3})
EACF	0.5	0.47[1]	0.65	Empirically adjusted cloud fraction at saturation (N/A)
RHCRIT	0.7	0.6	0.9	Threshold of relative humidity for cloud formation (N/A)
ALPHAM	0.5	0.47[1]	0.65	Sea-ice albedo at 0°C (N/A)
VDIFF[2] (Min / Max)	1.0 - 15.0	0.5 - 4.0	2.0 - 58.0	Background vertical diffusivity ($10^{-5}m^2s^{-1}$)

Table 4.1: Parameter values for PPE members. [1] - lower range extended, [2] - non-uniform distribution, see text for details.

4.4.3 Experimental setup

Initially 200 members were created and 20 year pre-industrial control simulations were run, continuing from a many thousand year long pre-industrial spin-up of the standard version of hadCM3, i.e. with standard parameter values. Many simulations failed to complete the first 20 years as HadCM3 is not entirely stable across its parameter space (Rougier *et al.*, 2009), and without flux adjustment some otherwise stable simulations have been found to give a simulation so unrealistic that they eventually became numerically unstable (Murphy *et al.*, 2004). Around half of the simulations failed and these failed simulations could not be used for the sensitivity simulations and so are discounted. To select which of the remaining members of the ensemble to retain, a projection of the equilibrium temperature response is made assuming that the change in parameters causes an instantaneous change in TOA radiative forcing, an approach which has previously been applied to PPEs (Joshi *et al.*, 2010). The projection of temperature and the initial TOA radiative forcing is made from a linear fit of the temperature plotted against the TOA radiative imbalance, after Gregory *et al.* (2004a). Those members which were projected to have equilibrium pre-industrial global-mean temperature within $\pm$ 2.0°C of the estimated pre-industrial temperature of 13.6 °C (Jones *et al.*, 1999) were retained and form the PPE (Brohan *et al.*, 2006). The range of $\pm$ 2.0 °C was decided upon as being similar to the spread in the pre-industrial absolute temperature of the World Climate Research Program's (WCRP's) Coupled Model Intercomparison Project phase 3 (CMIP3) multi-model dataset, which has a spread of 2.9 °C (Meehl *et al.*, 2007b). As we are modifying the ocean and atmosphere of the model we follow the procedure outlined in Collins *et al.* (2007), of running a 500 year spin-up to allow the model's temperature to approach close to the equilibrium value but not so long as to allow the ocean state to drift too far from the temperatures and salinities of the standard configuration. After the spin-up 5 further simulations per PPE member were started, a 300 year pre-industrial control run, a 150 year simulation with an instantaneous quadrupling of CO_2 ($4 \times CO_2$), a 150 year simulation with CO_2 rising by 1% per annum (1%CO_2), and two 70 year simulations with $4 \times CO_2$ and 1%CO_2 and radiative-imbalance-offsetting reductions in insolation (G1 and G2).

The setup of the G1 and G2 experiments of the geoengineering model inter-

comparison project (geoMIP) are described in (Kravitz *et al.*, 2011). The G1 experiment consists of an instantaneous quadrupling of CO_2 levels and a reduction in insolation sufficient to return within 0.1 Wm^{-2} of the TOA radiative balance of the pre-industrial. As all members of the PPE will deviate somewhat from perfect TOA radiative balance in the pre-industrial, the target radiative balance will be set from each ensemble member's pre-industrial control run. The solar insolation reduction required for each ensemble member's G1 experiment was estimated from a simple energy balance calculation and then iterated by testing the TOA radiative imbalance with a 10 year simulation and altering the insolation reduction until the simulations were within 0.1 Wm^{-2} of the radiative balance of the pre-industrial. We find that a calculation of the required insolation reduction found by equating the change in solar forcing to the CO_2 forcing fails to balance the radiative budget and a larger reduction in insolation is required. This has been seen in previous sunshade geoengineering experiments (Schmidt *et al.*, 2012; Govindasamy *et al.*, 2003) and can be explained by the fact that solar forcing has been found to produce a smaller temperature change for the same TOA radiative forcing, when compared to CO_2 forcing, i.e. solar forcing is less effective that CO_2 forcing (Hansen *et al.*, 2005). The individual insolation reductions found for the G1 experiment are scaled to produce the ramping-up of the G2 insolation reduction, as suggested in the geoMIP experimental description (Kravitz *et al.*, 2011). The G1 and G2 experiments were both run for 50 years with the solar insolation reduction described above and then after 50 years the geoengineering ceases and the simulations run for a further 20 years.

4.5 Results

4.5.1 Basic performance

Figure 4.1 a and b shows the projected temperature and estimated initial TOA radiative imbalance of the 200 initial members of the PPE. A large number of the simulations failed to complete but there was no clear relation between failure to complete this first 20 years and any individual parameter. Many of the simulations which completed the first 20 years had very large changes in TOA radiative balance and were projected to warm or cool rapidly, deviating greatly from the observed global-mean pre-industrial temperature. Figure 4.1c shows the projected tempera-

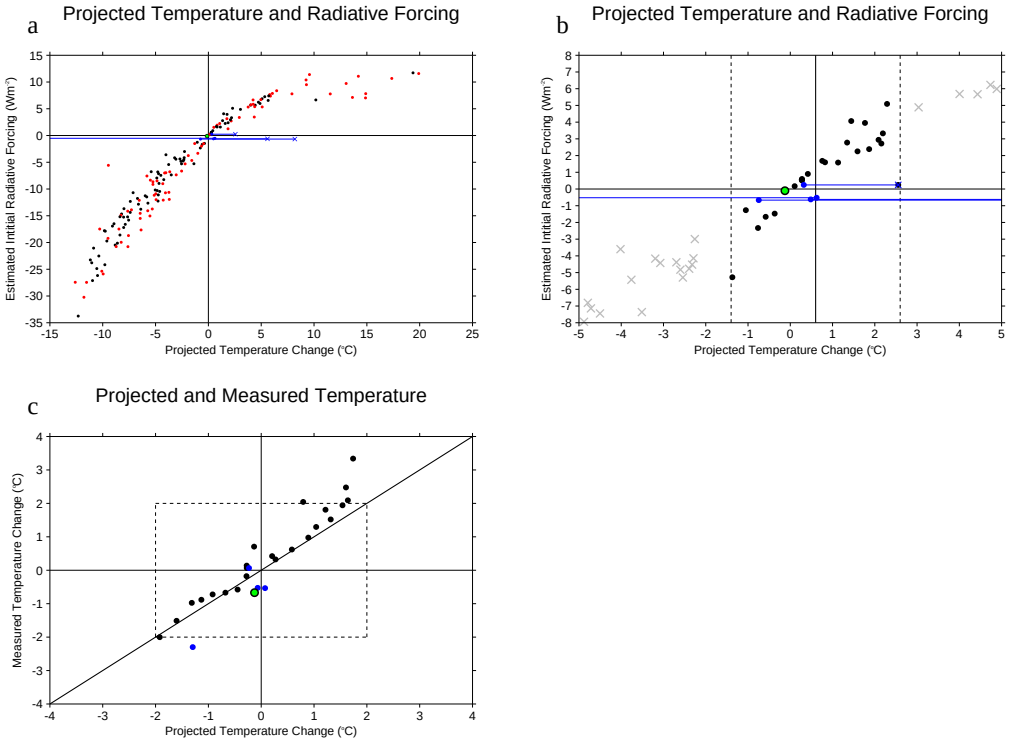

Figure 4.1: Shows the projections of equilibrium temperature and initial TOA radiative forcing for the ensemble (a and b) and shows a comparison between the projected temperature and the simulated temperature at the end of the control run (c). Simulations which completed the first 20 years are shown in black and those which failed to complete are shown in red, the green and black point is for the standard model. The projection method failed for some runs shown in blue with a cross at the projected temperature and a dot for the temperature of the 20th simulated year. Panel b and c show the acceptable range of temperatures with dashed lines, i.e. within ± 2 °C of the observed pre-industrial temperature of 13.6 °C. The projections of equilibrium temperature and initial TOA radiative imbalance are made by applying the Gregory plot method to the initial 20 years of simulation (Gregory *et al.*, 2004a), see the main text for more details.

ture from the first 20 years and the temperature after 800 years of pre-industrial control run for each of the 27 members of the PPE which were projected to be within ± 2.0 °C of the pre-industrial observed temperature, hence referred to as the ensemble. Most members of the PPE are close to their respective projected temperatures but a number of the warmer members, and a single cold member, are outside of the range, this is because the assumption that the parameter perturbation acts like an instantaneous TOA radiative forcing perturbation does not hold completely and breaks down for some parameter perturbations (Joshi *et al.*, 2010). These failed runs are retained to help understand the role of the parameters in the PPE response.

4.5.2 Pre-industrial control

The 27 members of the ensemble, including the standard configuration, simulated 800 years of pre-industrial conditions. Figure 4.2 shows the evolution of a number of variables over the course of these runs. Figures 4.2 a and b show that most members of the PPE behave as if an instantaneous TOA radiative forcing had been applied, i.e. they follow an asymptotic approach to a new equilibrium temperature and the TOA radiative imbalance is decaying to zero. However a number of the members have large TOA radiative imbalances, greater than 1 Wm^{-2}, at the end of the control run and the warmest member shows a near-linear rise in temperature, indicating that the response of these members to the parameter perturbations is not as simple as an adjustment to an instantaneous TOA radiative forcing change. The change in precipitation, figure 2, shows both fast and slow changes in precipitation, i.e. a rapid adjustment to the altered atmospheric conditions followed by a temperature driven change in precipitation (Bala et al., 2010). The sea-ice area, figure 4.2d, changes quite significantly, with the warmer members losing up to a third of their sea-ice, and some members gaining sea-ice area. Figure 4.2 e shows the ocean temperature at a depth of 2.7 km; all the members of the ensemble, including the standard simulation which shows a slight cooling, show a roughly linear trend in temperature which is not diminished at the end of the 800 years. Figure 4.2 f shows the evolution of the maximum meridional circulation in the Atlantic; most members remain close to the standard model's condition with an overturning strength of ∼18 Sv but a number of members show increased overturning of up to ∼30 Sv and some also show a large increase in variability. Although the surface variables appear to be near equilibrium after 800 years of the pre-industrial control, the ocean temperature is not and it is not clear whether the overturning strength has reached equilibrium. The results of the rest of the paper should be viewed keeping in mind that the ocean has not yet reached equilibrium.

The parameters that have previously been found to have the largest role in controlling climate sensitivity in the HadCM3 model are also found to exert significant control over the equilibrium pre-industrial temperature (Rougier *et al.*, 2009; Sanderson *et al.*, 2008a). The entrainment rate coefficient (ENTCOEF) and the ice fall speed (VF1) have the greatest influence on pre-industrial temperature, with low

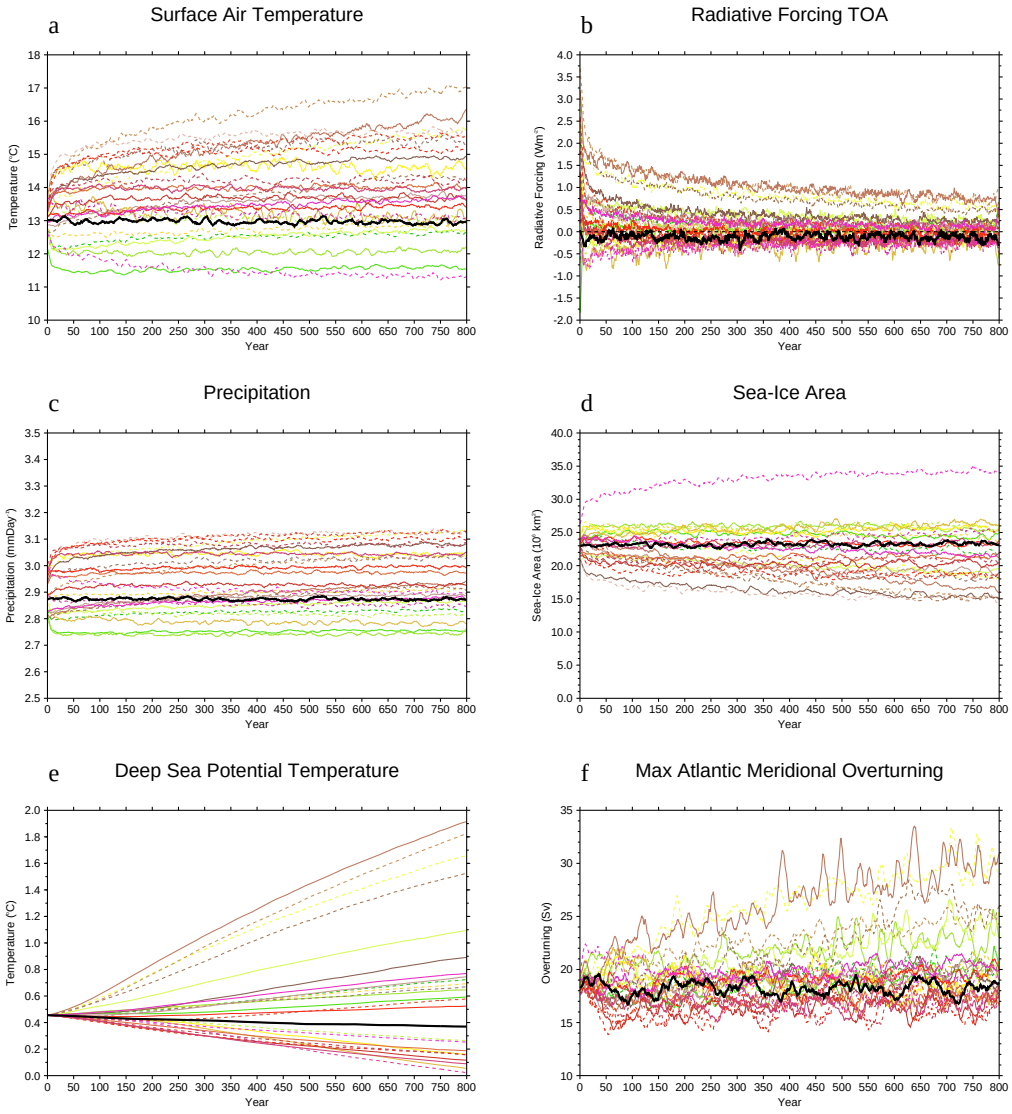

Figure 4.2: Shows the evolution of surface air temperature (a), TOA radiative balance (b), precipitation (c), annual-mean sea-ice area (d), potential temperature at 2700m (e), maximum Atlantic overturning (f), over the course of the 800 year pre-industrial control simulation. All variables are calculated at the global and annual mean. The standard version of HadCM3 is plotted with a black line.

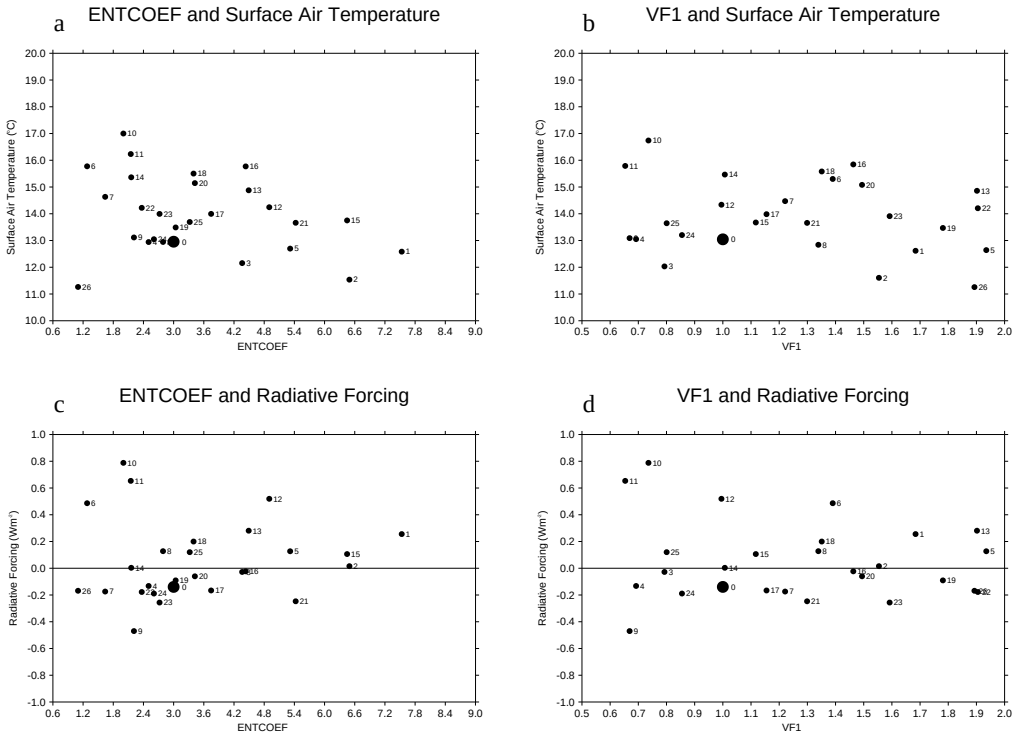

Figure 4.3: Shows scatter plots of the pre-industrial control temperature (a, b) and the TOA radiative forcing at the end of the control run against the entrainment coefficient (ENTCOEF) and the ice fall speed (VF1), respectively.

values of both parameters tending to give warmer conditions, see figure 4.3. However the coldest member of the PPE has the lowest value of ENTCOEF and one of the highest value of VF1, consistent with the results of Sanderson *et al.* (2008a) who found that this combination led to a member with very low climate sensitivity. VF1 also exerts a strong control over the cloud fraction in the control runs with lower values of VF1 having a cloud fraction greater than 55% and the highest values of VF1 having a cloud fraction lower than 50% as seen in other studies, see figure 4.4 (Wu, 2002; Sanderson *et al.*, 2008a). Surface air temperature plays a much more significant role in determining the sea-ice fraction than ALPHAM (not shown). The effect of these and other atmospheric parameters on the HadCM3 model have been explored in detail by a number of other studies and so the interested reader should refer to these for further information (Collins *et al.*, 2006; Murphy *et al.*, 2004; Sanderson *et al.*, 2008a; Knight *et al.*, 2007).

In scatter plots of ocean vertical diffusivity (VDIFF) against the pre-industrial TOA radiative imbalance after 800 years we find that higher values of VDIFF are associated with more positive radiative imbalance (see figure 4.5). For high values

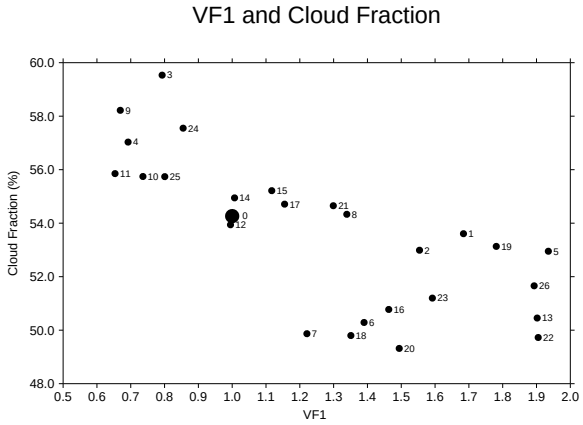

Figure 4.4: Shows the control global cloud fraction after 800 years as a function of the ice fall speed parameter. The standard run is plotted with a larger point and labelled with a zero.

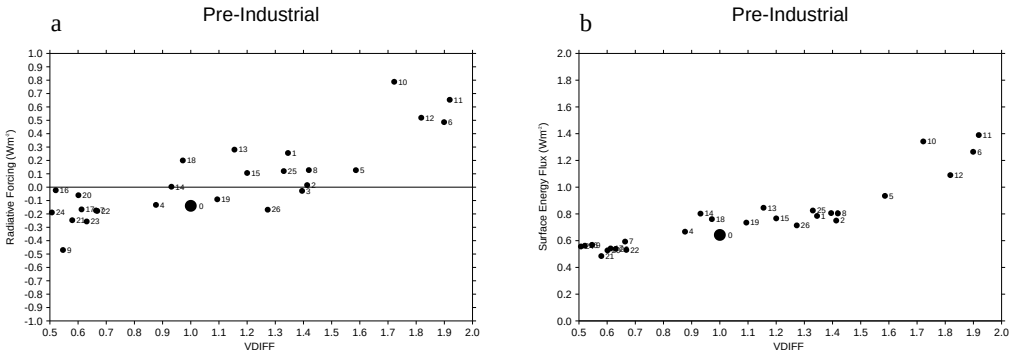

Figure 4.5: Shows the control global mean temperature after 800 years (a) and the global mean heat flux into the ocean (b), as a function of the vertical diffusivity parameter. The standard run is plotted with a larger point and labelled with a zero.

of the VDIFF parameter much more energy is absorbed by the ocean, up to ∼0.8 Wm^{-2} more than the standard model's ∼0.6 Wm^{-2}, absorbing energy that would otherwise have warmed the model surface (the opposite is also true for low values of VDIFF with up to ∼0.15 Wm^{-2} less energy absorbed by the ocean). However, VDIFF on its own has been found to have the opposite effect, raising global mean temperatures but by only a few tenths of a degree (Collins *et al.*, 2007; Brierley *et al.*, 2010). It is likely that this association between high values of VDIFF and higher pre-industrial temperatures is due to VDIFF mitigating the initial rate of temperature change (Brierley, C. personal communications). It has been found that high/low values of VDIFF cause an increase/decrease in the flux of energy in/out of the oceans in the initial years and so may act to keep members, that would have otherwise warmed/cooled too fast, close to the observed pre-industrial temperature (Brierley *et al.*, 2010).

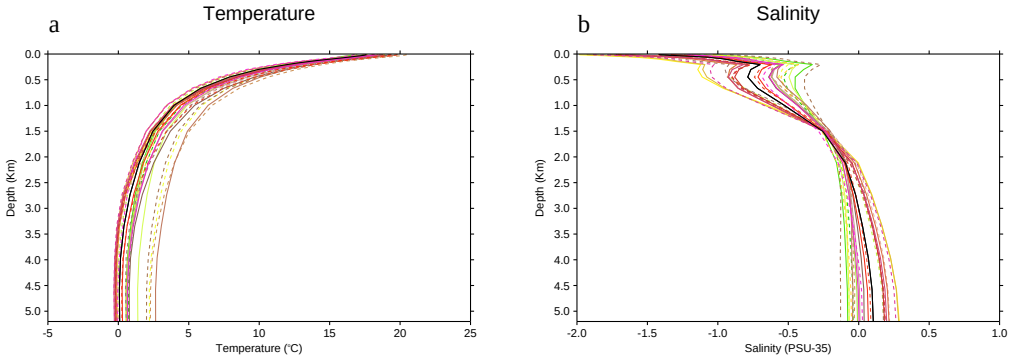

Figure 4.6: Shows the annual and ocean area average temperature (a) and salinity (b) of the ocean with depth. The standard version of HadCM3 is plotted with a black line.

Although the ocean has not fully adjusted to the parameter perturbations after 800 years; significant changes in the ocean have occurred. Figure 4.6 shows the depth profile of the ocean potential temperature and salinity, showing that the condition of the ocean has changed markedly across the ensemble. VDIFF has a small effect on the ocean temperature at depth whilst the other atmospheric variables have a greater effect (not shown). Figure 4.7a shows that Atlantic overturning strength is associated with VDIFF, with the members with the highest values of VDIFF showing a large increase in overturning whereas the members with a standard or low value of VDIFF show little change; this is consistent with the results of Brierley *et al.* (2010). This is despite the fact that members of the PPE with the highest values of VDIFF also have the warmest control run simulations and a warmer climate is expected to weaken overturning due to the increased freshwater flux at high latitudes and reduced sea-ice formation, see figure 4.7 (IPCC, 2007).

Figure 4.8 shows the annual and zonal mean state of the pre-industrial climate in the PPE and compares this with the CMIP3 ensemble (Meehl *et al.*, 2007b). Figures 4.8 a-b show that the zonal mean temperatures of the PPE and the CMIP3 ensemble show a similar distribution however there are PPE members that are a few degrees warmer in the tropics than any of the CMIP3 ensemble. The zonal precipitation, figure 4.8 c-d, of the PPE shows a similar overall structure but much less variance than the CMIP3 ensemble and the ensemble members have shared biases that the members of the CMIP3 ensemble do not have. The TOA radiative imbalance, figure 4.8 e-f, of the PPE is similar to the CMIP3 ensemble except near the equator where there is a greater spread than in the CMIP3 ensemble. Overall the PPE shares similar features with the CMIP3 ensemble and few of the members would stand out

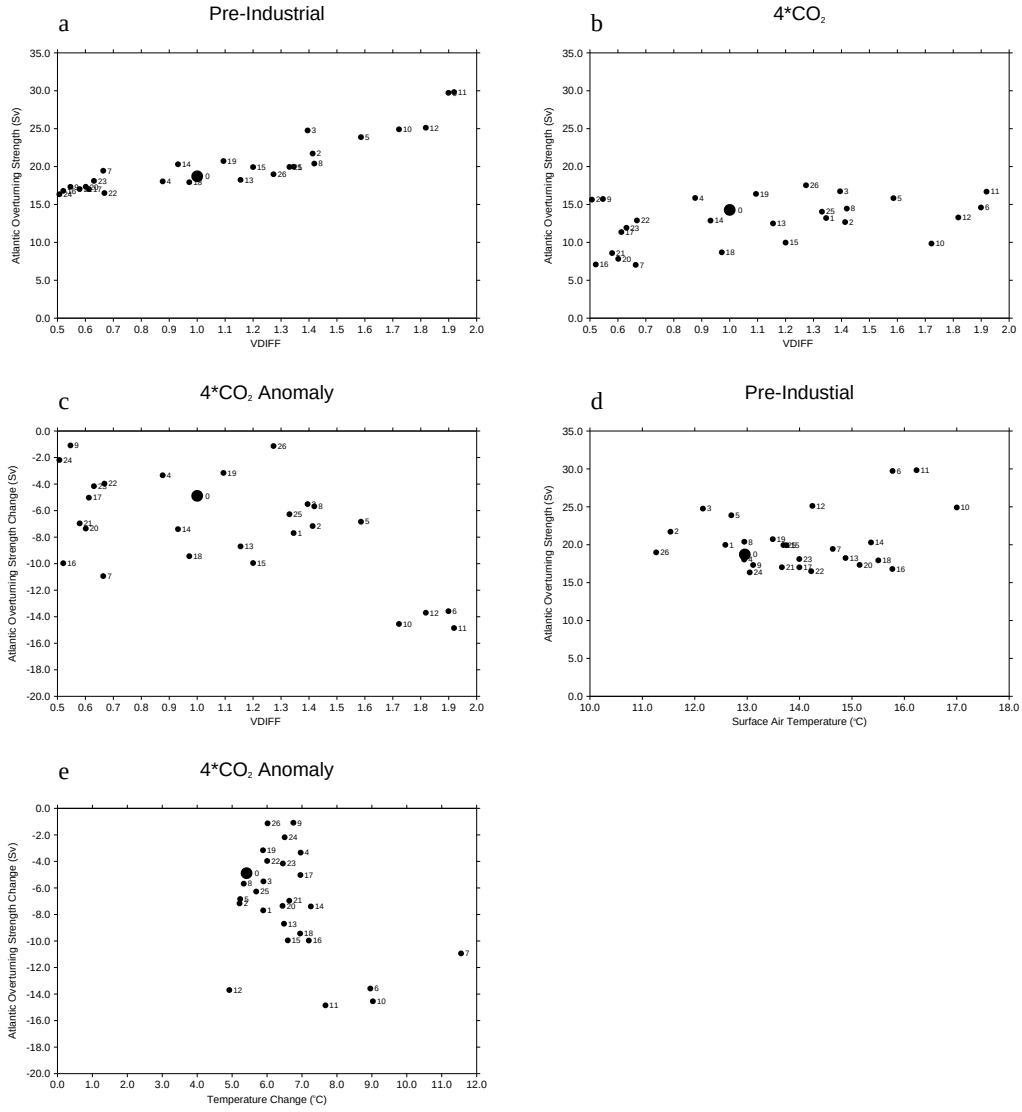

Figure 4.7: Shows the relationship between the maximum Atlantic overturning and both the background vertical diffusivity parameter and global-mean temperature for the ensemble. Panels a-c show how vertical diffusivity affects the control overturning (a), the overturning at $4 \times CO_2$ (b) and the change in overturning between $4 \times CO_2$ and the control (c). Panels d and e show the effect of pre-industrial global-mean temperature (d) and the effect of warming to $4 \times CO_2$ (e) on Atlantic overturning.

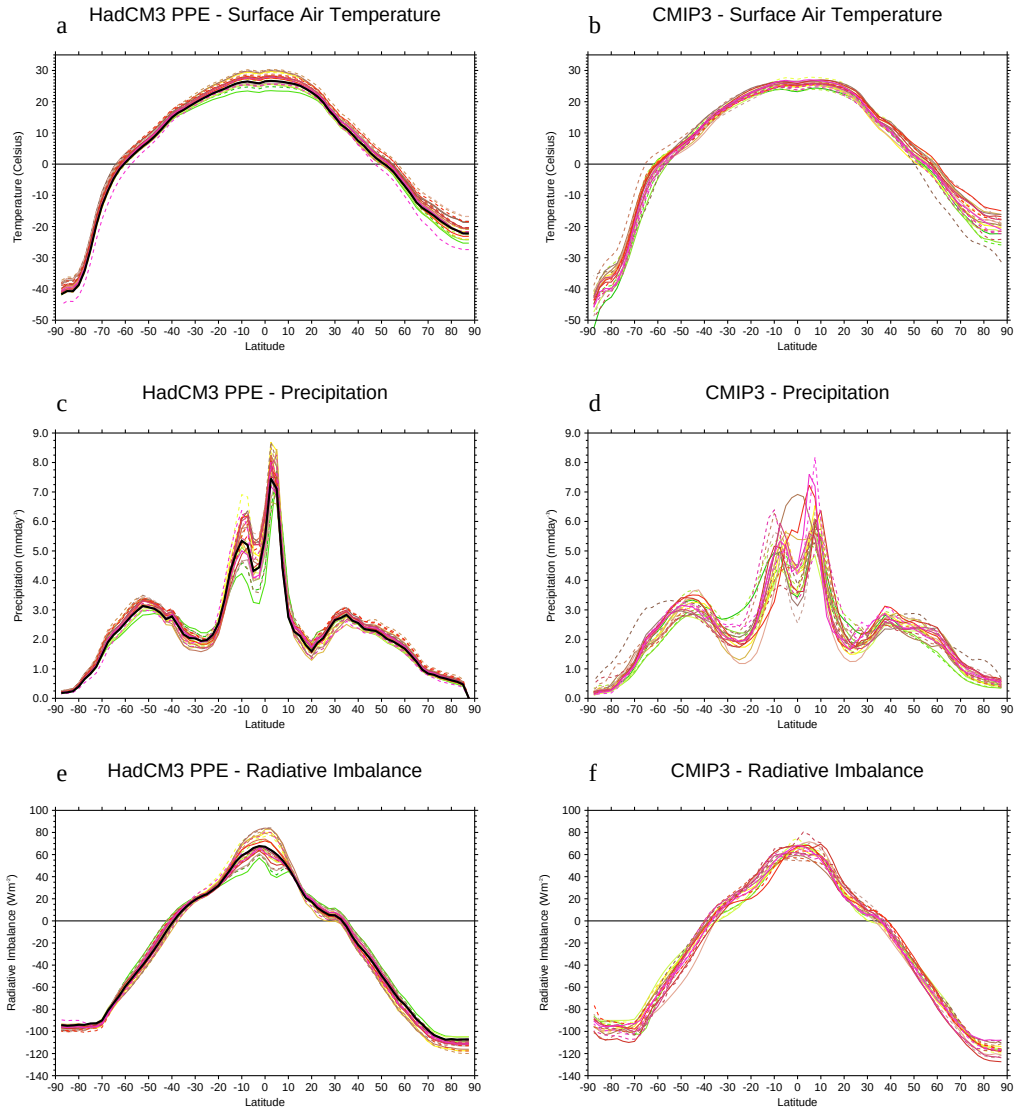

Figure 4.8: Shows the surface air temperature (a, b), precipitation (c, d), and TOA radiative balance (e, f) for the PPE simulations and for the CMIP3 ensemble. The standard version of HadCM3 is plotted in black for the PPE simulations.

within the CMIP3 ensemble except perhaps for the warmest runs.

Most of the parameters that were perturbed in the PPE were uncertain atmospheric properties, particularly related to convection and clouds, and so differences within the ensemble are expected to be greatest in the atmospheric column. Figure 4.9 shows a comparison between the vertical temperature and specific humidity profile of the PPE and the CMIP3 ensemble (Meehl *et al.*, 2007b), note that data above 30 mb is unavailable for most members of the CMIP3 ensemble. The PPE shows little spread in the vertical temperature profile except at the surface in contrast to the CMIP3 ensemble which shows the opposite, with general agreement at

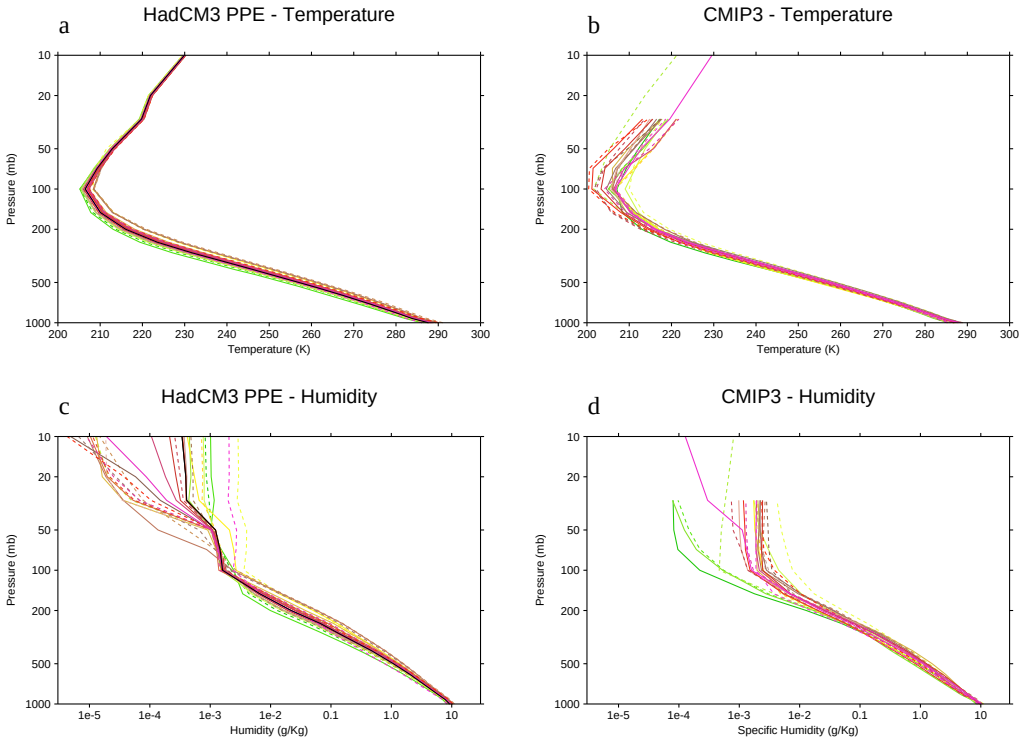

Figure 4.9: Shows the temperature (a, b) and specific humidity (c, d) throughout the atmospheric column for the PPE simulations and the CMIP3 ensemble. The standard version of HadCM3 is plotted in black for the PPE simulations. Note that for the PPE cells below ground level the values are extrapolated and included in the level mean.

the surface and a large spread of temperatures at higher altitudes. Figure 4.9 a and b show that this must, in part, be due to the wider spread in pre-industrial surface air temperatures in the PPE and indicates that the PPE has not substantially perturbed the dynamics that control upper atmosphere temperatures. The PPE shows a broad spread of behaviour in the humidity profile, with the greatest spread at the highest altitudes (Figure 4.9c; note that humidity is plotted on a logarithmic scale). Most members of the CMIP3 ensemble show humidity varying smoothly with altitude whereas the standard version of HadCM3 and most members of the PPE show a sharp change above 100 mb. These changes indicate that although 6 key atmospheric parameters have been perturbed, the PPE does not cover the range of different upper atmospheric behaviour seen in the CMIP3 ensemble, as has been shown for other HadCM3 ensembles (Collins *et al.*, 2010b).

Water vapour is the most important natural greenhouse gas and its absorption of longwave radiation scales with the logarithm of concentration, thus changes in water vapour at the drier high altitudes are more significant than at the moist lower

altitudes (Forster and Shine, 2002; IPCC, 2007). As the planet warms in response to elevated CO_2 concentrations the water vapour concentration in the atmosphere is expected to rise, increasing the water vapour greenhouse effect, and warming the planet further; this water vapour feedback is believed to be one of the most important positive feedbacks in the climate system (IPCC, 2007). The control concentration of high altitude water vapour along with other conditions determines the control greenhouse effect of a model but is not so important in determining the climate sensitivity of a model, however any changes in high altitude humidity would exert a strong greenhouse effect (IPCC, 2007; Held and Soden, 2000). For the PPE there is a large range of specific humidity concentrations at high altitudes which constitutes a large range of changes in humidity from the standard model configuration and so a large change in the water vapour greenhouse effect (Held and Soden, 2000; Forster and Shine, 2002; Joshi *et al.*, 2010). Despite these large changes in the water vapour greenhouse effect across the PPE most members have remained within 2 °C of the pre-industrial observed global-mean temperature.

4.5.3 Elevated CO_2 experiments

Figure 4.10 shows the change in the vertical profile of some atmospheric variables with height in response to the instant quadrupling of CO_2 levels. All members of the PPE show a broadly similar response to warming in line with the CMIP3 models (IPCC, 2007), i.e. a warming in the troposphere, a rise in the tropopause, and a cooling of the stratosphere. There is a wide spread in the temperature response but all members show the warming signal in the mid-troposphere as an amplification of the surface warming signal. At higher altitudes most members of the PPE show the same cooling of ∼12 °C despite the spread of ∼6 °C in the surface temperature signals, however 3 of members show a greater cooling of >15 °C. Figures 4.10 c-d show the changes in specific humidity; up to 100 mb the humidity increases for all members in a similar way, with the warmer runs showing a greater increase in humidity; at higher altitudes there is a very broad range of response with many members, including the standard model, showing a large drying and others showing a large increase in humidity. The specific humidity is plotted as the logarithm of the change from the pre-industrial, as the radiative effect of a 100-fold increase in moisture content is equal to twice the effect of a 10-fold increase (IPCC, 2007). Most

models of the CMIP3 ensemble show a doubling or tripling of upper level humidity on doubling CO_2 concentrations (although this excludes the HadCM3 model which shows a drying) (Meehl *et al.*, 2007b), much smaller than the 10 to 100 fold increase of some members of the PPE. Figure 4.10 e-f shows that for most members over most of the atmospheric column the absolute change in relative humidity is less than 5% (excluding around 150 mb, where changes in tropopause height are evident) but some of the members show a large increase in relative humidity in the stratosphere where most members have very low concentrations of water vapour (∼100 ppbv).

The entrainment rate coefficient (ENTCOEF) plays the greatest role of any of the parameters in controlling high altitude humidity, as it controls the mixing of warm, moist, convecting air packets with their surroundings (Sanderson *et al.*, 2008a; Rougier *et al.*, 2009; Murphy *et al.*, 2004), and thus the mechanism by which water vapour can reach the upper atmosphere. These changes in upper atmospheric humidity constitute a radiative feedback which could amplify the warming from raised CO_2 levels (Sanderson *et al.*, 2008a; Forster and Shine, 2002; Joshi *et al.*, 2010). Figures 4.11 a-c show the specific and relative humidity in the pre-industrial control simulations vary as a function of ENTCOEF; low values of ENTCEOF are associated with the highest specific humidities at high altitude as has been shown in other studies (Joshi *et al.*, 2010; Sanderson *et al.*, 2008a). Figures 4.11 d-f show how ENTCOEF is associated with high altitude humidity in the $4 \times CO_2$ simulation; very large increases in high altitude humidity are seen only for members of the ensemble with the lowest values of ENTCOEF, whereas for moderate and high values of ENTCOEF humidity remains relatively unchanged. Figures 4.11 g-h shows that only the members with the largest rises in temperature at $4 \times CO_2$ have very large changes in high altitude humidity. Such large changes in humidity at high altitude will increase the member's greenhouse effect and will therefore act as a positive feedback generating further warming (Held and Soden, 2000; Forster and Shine, 2002; IPCC, 2007; Joshi *et al.*, 2010). These amplified changes in high altitude humidity seem to occur at values of ENTCOEF of 2.5 or less with the largest changes occurring in members with an ENTCOEF value of 2.0 of less. The climate sensitivity of HadCM3 has been found to be much greater for these low values of ENTCOEF, rising rapidly for levels below the standard value of 3.0 (see Figure 6 of Sanderson *et al.* (2008a) and Figure 6 of Rougier *et al.* (2009)), seemingly agreeing with the

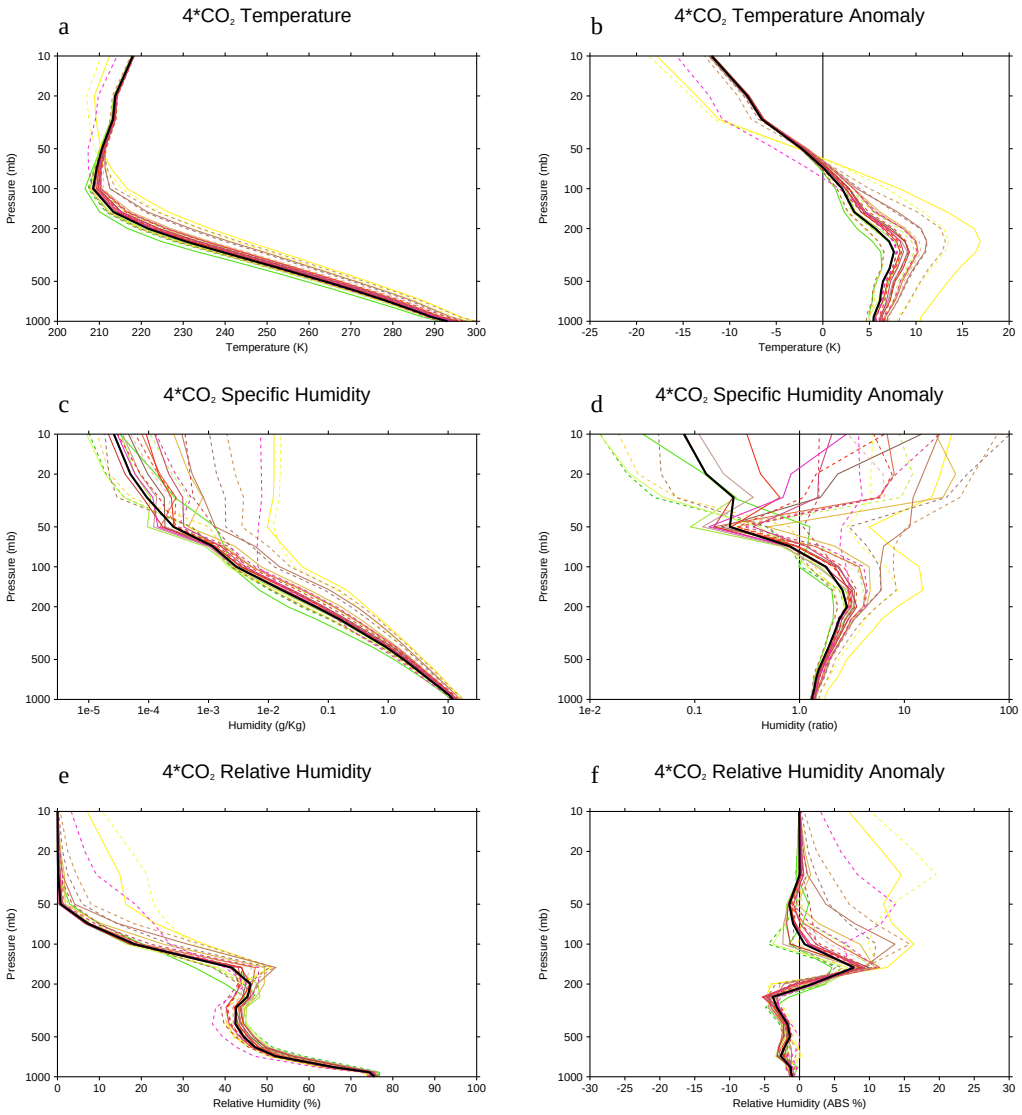

Figure 4.10: Shows the mean $4 \times CO_2$ and the anomaly between $4 \times CO_2$ and the pre-industrial control for temperature (a, b), specific humidity (c, d) and relative humidity (e, f) for the PPE simulations. The standard version of HadCM3 is shown in black for the PPE plots. Note that cells below ground level the values are extrapolated and included in the level mean.

suggestion of Joshi *et al.* (2010) that the high altitude humidity of a low ENTCOEF HadCM3 simulation was responsible for its extremely high climate sensitivity.

In the quadrupled CO_2 simulations all members of the PPE are still warming somewhat after 140 years with the warmest runs showing a rate of warming of > 0.3 K per decade in the last 50 years, see figure 4.12 a. These warmest runs have a residual TOA radiative imbalance more than 1 Wm^{-2} greater than the ensemble mean of $\sim$1.6 Wm^{-2} after 140 years. A similar trend can be seen in the 1% CO_2 per annum experiment, figures 4.12 b and d, with the warmest runs building up a greater radiative imbalance by the end of the run than the rest of the PPE and showing a slightly super-linear trend in temperature rather than the linear response seen in the other members. For both the $4 \times CO_2$ and 1% CO_2 experiments the precipitation response roughly follows the temperature trend (figure 4.12 e and f), with the $4 \times CO_2$ members showing an initial sharp reduction in ensemble mean precipitation to around -0.12 $mmday^{-1}$ which recovers to around 0.2 $mmday^{-1}$ by the end of the run (Bala *et al.*, 2010a). We also find that the members with the highest pre-industrial temperature are also the members which warm the most at $4 \times CO_2$, see figure 4.13a for details.

Estimates of the equilibrium temperature response and initial radiative forcing of the $4 \times CO_2$ simulations are possible by following the method of Gregory *et al.* (2004b) and applying a linear fit over the first 50 years, as was applied for the pre-industrial pre-calibration. Fitting a line to the joint evolution of temperature and TOA radiative imbalance is expected to provide an estimate of the initial radiative forcing perturbation and a final equilibrium temperature. This approach works for most members of the PPE, which show some deviation from the 50 year linear fit, but for a number of the low ENTCOEF members this relationship breaks down. Some of the low ENTCOEF members deviate substantially from the initial 50 year linear fit and in the later years of the simulation show increases in temperature without the expected reduction in radiative forcing, see figure 4.14. This trend appears to indicate that these low ENTCOEF members have begun a runaway greenhouse warming and if so these members will continue to warm until they reach a temperature at which the model is numerically unstable. The exact mechanism for this runaway greenhouse warming is not certain but may be due to the very large increases in humidity in the upper atmosphere of these low ENTCOEF members in response to

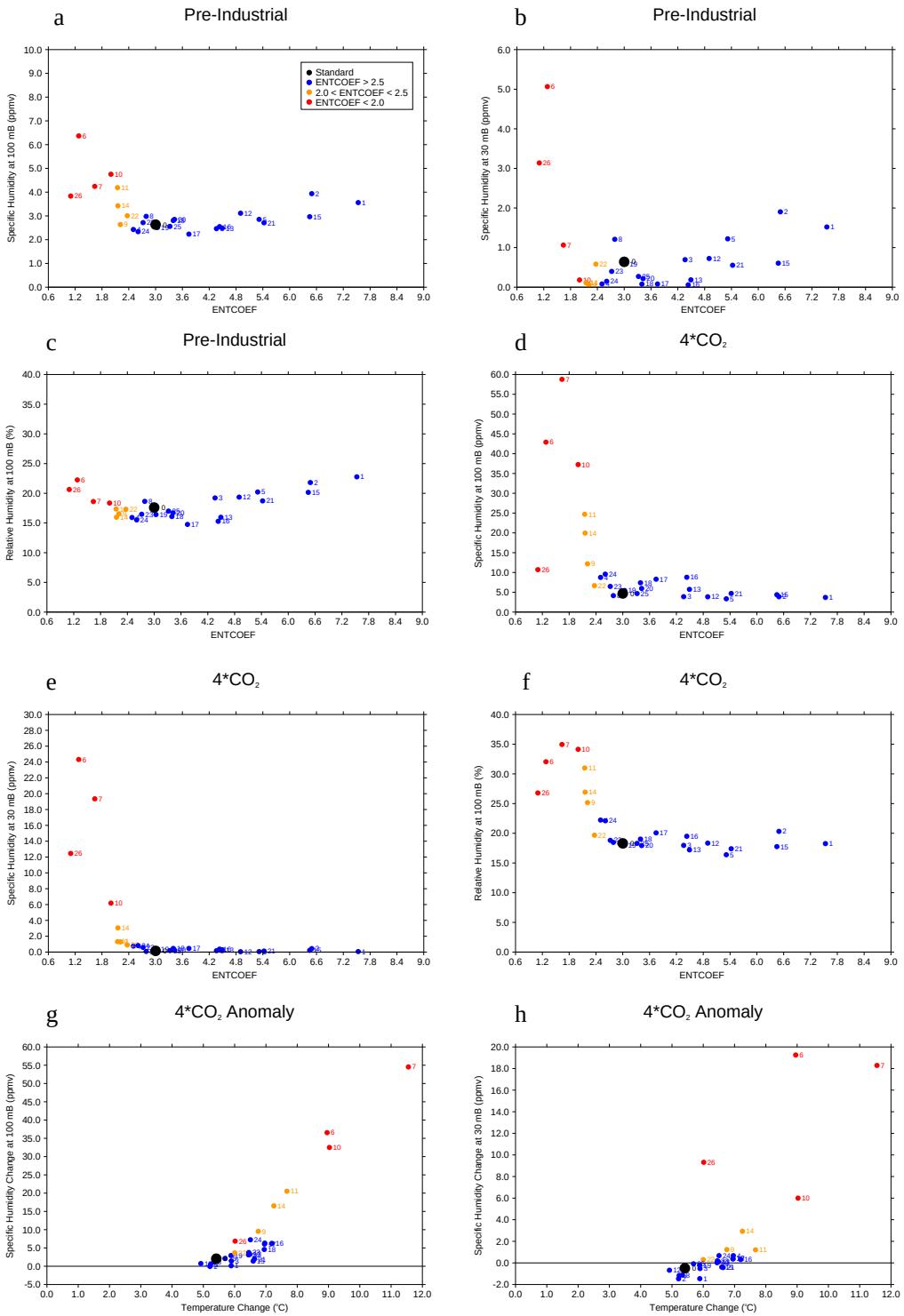

Figure 4.11: Shows how specific humidity (in ppmv) and relative humidity at stratospheric levels varies with the entrainment rate coefficient (a-f) and with changes in temperature (g, h). Panels a-f show for the pre-industrial (a-c) and $4 \times CO_2$ (d-f) the relationship between the entrainment rate coefficient and specific humidity at 100 mb and 30 mb, and relative humidity at 100 mb respectively. Panels g and h show the relationship between the surface air temperature anomaly between $4 \times CO_2$ and the pre-industrial and the change in specific humidity at 100 mb (g) and 30 mb (h).

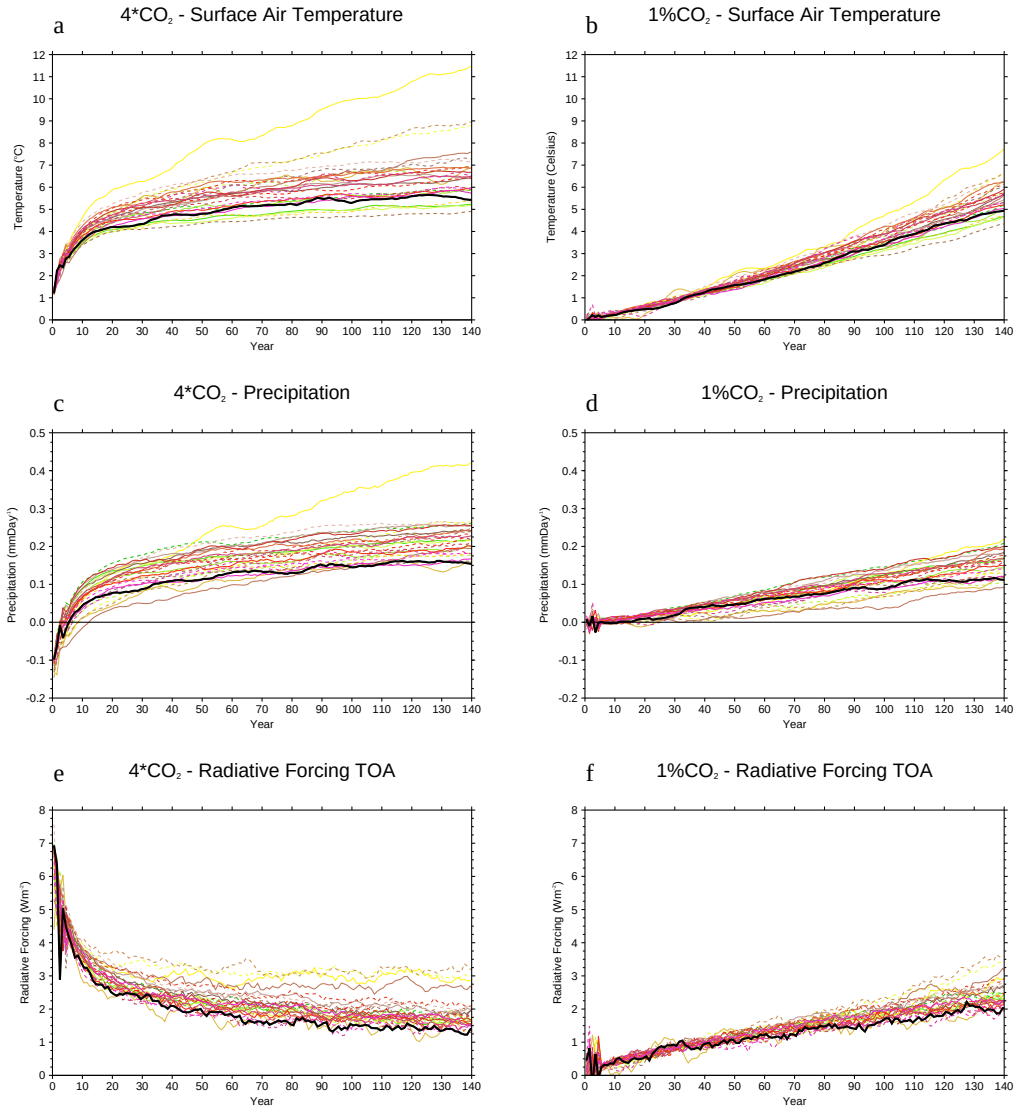

Figure 4.12: Shows the evolution of temperature (a and b), TOA radiative forcing (c and d), and precipitation (e and f), for the $4 \times CO_2$ and $1\%CO_2$ simulations. The variables are plotted as anomalies from the start of the runs, i.e. the end of each of the pre-industrial spin-ups. The standard run is plotted in black. A ten year running mean is applied to the data without extrapolation at the beginning of the run.

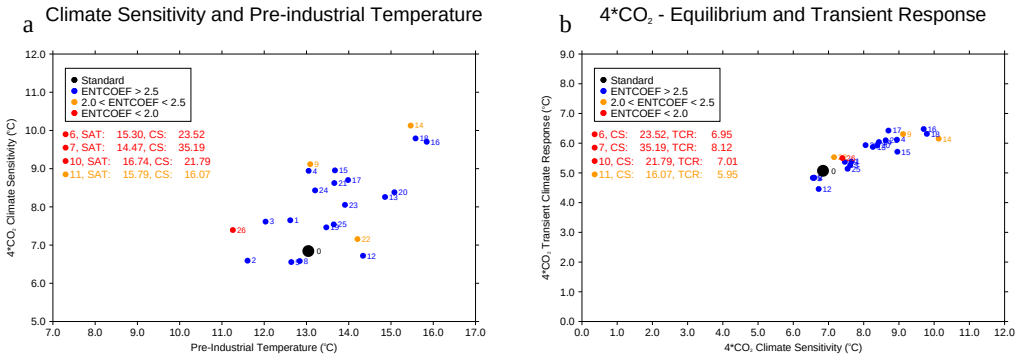

Figure 4.13: Shows a scatter plot of the pre-industrial control temperature against the change in temperature at $4 \times CO_2$. The values are global means averaging over the last 10 years of the 150 year $4 \times CO_2$ simulations and the same point in the control simulations. The standard run is plotted with a larger point and labelled with a zero.

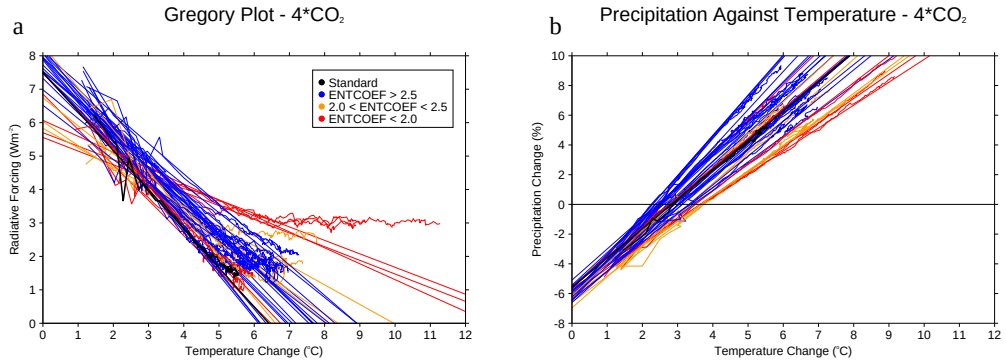

Figure 4.14: shows the evolution of TOA radiative imbalance against temperature change (a) and of precipitation change against temperature change (b) for all PPE members during the $4 \times CO_2$ simulation. A ten year running average is applied to the data and a line showing the 50 year linear fit from the beginning of the simulation are shown.

warming. One of the low ENTCOEF members appears to be showing a runaway process in the pre-industrial control simulation with the temperature rising almost linearly over time, rather than asymptotically approaching an equilibrium temperature as expected (see figure 4.1a). Some of these low ENTCOEF runs, which appear to be beginning runaway global warming, are outside of the pre-industrial target temperature window after the 800 year pre-industrial control run but others are close to the target temperature. Applying a similar method it is possible to estimate the initial precipitation response and an equilibrium 'hydrological sensitivity' by following the method outlined in Bala *et al.* (2010a), for these calculations a 50 year linear fit is made to the joint evolution of precipitation and temperature, see figure 4.14.

The projected equilibrium temperatures of the $4 \times CO_2$ simulations, 4*CS, are shown in figure 4.15 a. These are found from a 150 year linear fit applied in the same

way as in the temperature and TOA radiative imbalance evolution shown in figure 4.14. Most ensemble members have a 4*CS in the range of 6.5 - 10.5 °C, with a few members having estimates of 4*CS of > 20 °C due to the breakdown of the linear relation between increasing temperatures and decreasing TOA radiative imbalance. The temperature of the 1%CO_2 simulations at the time at which CO_2 levels have quadrupled (year 140), 4*TCR, is shown in figure 4.15 b. We find that most PPE members have a ratio of roughly 2:3 between their 4*TCR and 4*CS values, see figure 4.13. This comparison does not work for some of the low ENTCOEF runs due to the breakdown of the 'Gregory plot', linear relationship between temperature and TOA radiative imbalance (Gregory *et al.*, 2004a). If the low ENTCOEF runs are excluded, there is a clear relation between low values of 4*TCR and high values of VDIFF and vice versa despite there being no correlation between VDIFF and 4*CS (again excluding the low ENTCOEF members; not shown). This follows from the fact that higher values of VDIFF should lead to a greater transport of heat to depth and is consistent with the results of an earlier study into the effects of VDIFF and other ocean parameters (Collins *et al.*, 2007).

The response of precipitation to changes in radiative forcing has been considered to consist of a fast component or precipitation adjustment, corresponding to a change in the patterns of latent and specific heating particular to the type of forcing, and a more or less independent slow component, that depends on the global mean temperature (Andrews *et al.*, 2010; Bala *et al.*, 2010b). This slow, temperature-driven, component has been called the hydrological sensitivity and is measured in percentage change per degree of warming (Andrews *et al.*, 2010; Bala *et al.*, 2010b). The PPE shows a range of both fast and slow behaviour to the $4 \times CO_2$ forcing with a 'fast' reduction in precipitation of $\sim 6 \pm 1\%$, and a hydrological sensitivity of $\sim 2.0 \pm 0.3$ %°C $^{-1}$, see figures 4.15 c and d. At $2 \times CO_2$ Andrews *et al.* (2009) showed an ensemble mean hydrological sensitivity of 2.8 %°C $^{-1}$ and a mean precipitation adjustment of 2.5% for the CMIP3 models they considered, but more in line with our PPE results they find a hydrological sensitivity of 2.2 %°C $^{-1}$ and a precipitation adjustment of 3.0% (roughly half the $4 \times CO_2$ value shown here as expected) for the HadSM3 model.

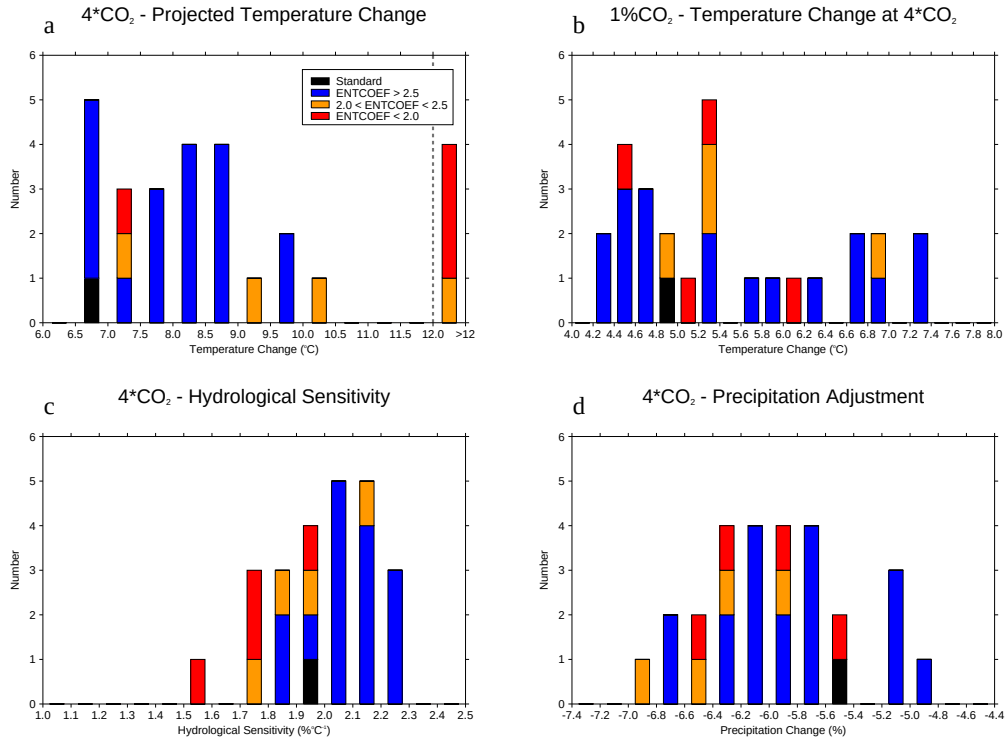

Figure 4.15: Shows histograms of the projected temperature change of the $4 \times CO_2$ simulations (a), the temperature change of the $1\%CO_2$ simulations at year 140 (b), and the hydrological sensitivity (c) and precipitation adjustment (d) of the $4 \times CO_2$ simulations. All changes are relative to the pre-industrial control simulations.

4.5.4 Sunshade geoengineering results

We now present PPE results on the G1 and G2 experiments from geoMIP to investigate the inter-member differences in response to geoengineering (Kravitz *et al.*, 2011). The mean insolation reduction required for the G1 experiment was 4.1% with most members tightly clustered around this values, however some were as low as 3.7% and others as high as 4.3%. Schmidt *et al.* (2012) found a broader range with the 4 GCM models they investigated requiring 3.5%, 3.9%, 4.0% and 4.7%. Figures 4.16 a and c, show that the solar insolation reductions used for the G1 and G2 simulations are appropriate, as surface air temperatures do not deviate far from the pre-industrial mean in the first 50 years and the inter-member spread is of the order of internal model variability. After the geoengineering forcing ceases at the end of year 50, the global mean temperature rises rapidly in both G1 and G2 experiments, rising by between 3.6 to 6.0 °C and 1.7 to 2.7 °C, respectively, in 20 years. In the first 50 years of the G1 simulation the PPE shows a precipitation adjustment, or fast hydrological response, of between -0.12 mmday^{-1} to -0.15 mmday^{-1} which

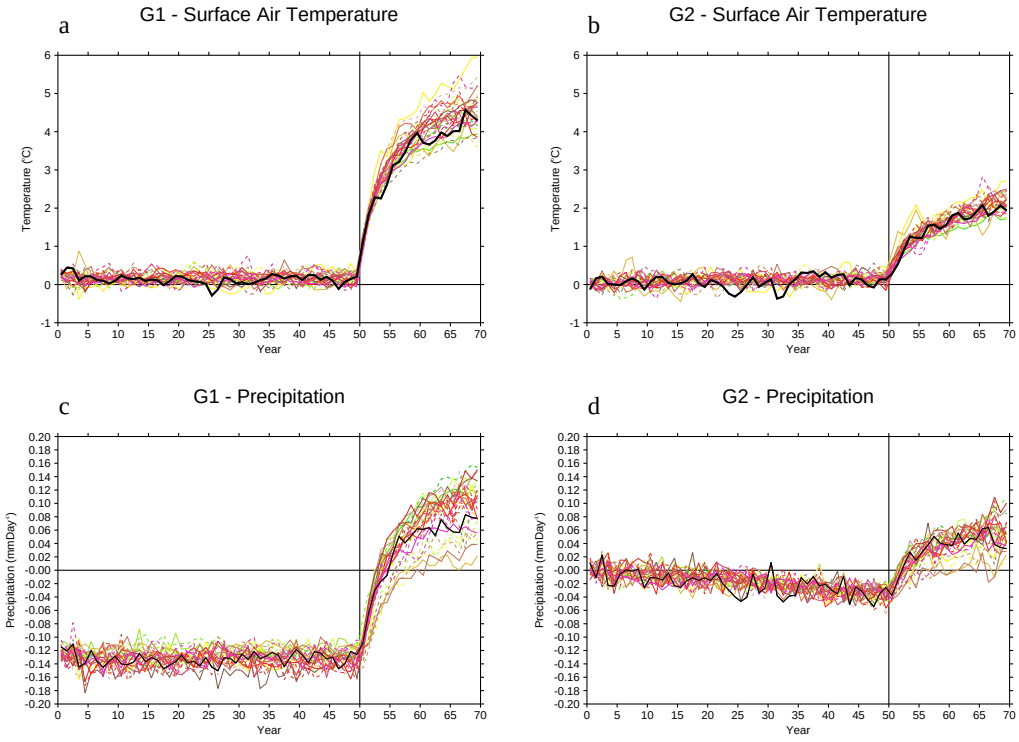

Figure 4.16: Time evolution of annual global mean temperature and precipitation for the G1, a and c, and G2, b and d, simulations. Insolation reduction for both G1 and G2 ceases at the end of the 50^{th} year. The standard HadCM3 model simulation is indicated by a thick black line.

is mostly complete within the first year of simulation. For the G2 simulation the PPE shows a gradual reduction in precipitation, reaching -0.02 mmday^{-1} to -0.04 mmday^{-1} by year 50. After the geoengineering forcing ceases, the precipitation in both rises as the global mean temperature increases. The reduction in precipitation seen whilst the geoengineering forcing is on, reflects the 'fast', dynamic, adjustment to elevated CO_2 levels and after the geoengineering forcing ceases the 'slow', temperature-driven, hydrological sensitivity to warming occurs (Bala *et al.*, 2010b).

Figure 4.17 shows zonal mean plots of temperature and precipitation for the G1 and G2 simulations. As seen in other G1-style experiments the pre-industrial temperature distribution is not reproduced; there is an overcooling in the tropics and at high latitudes there is a residual warming (Schmidt *et al.*, 2012; Lunt *et al.*, 2008b; Irvine *et al.*, 2010). The same is true for most of the G2 simulations, although some members cool at high northern latitudes, and the temperature changes are of a much smaller magnitude. There is fairly good agreement between the PPE members on which latitudes warm and cool but the magnitude of the temperature changes differ substantially, especially at high northern latitudes. There is some

shared structure to the G1 zonal mean precipitation anomaly of the PPE members, with all models showing a reduction in precipitation in the mid-latitudes and a more significant reduction between 10° S and 5° N, however there is a wide range of different magnitudes for these changes within the PPE. Some members show an increase in precipitation in non-equatorial tropical regions and at high northern latitudes and most members of the PPE seem to show a northward shift in the ITCZ accompanying the overall reduction in equatorial precipitation, resulting in a large positive anomaly north of the equator for some members and a small negative anomaly for others. These positive anomalies in the Northern hemisphere may be due to the substantial polar warming in some members increasing evaporation and precipitation at high northern latitudes and drawing the ITCZ northwards. The zonal precipitation changes in the G2 simulations are of a much smaller magnitude than those of the G1 simulations and it is hard to draw conclusions, however there are large differences in the precipitation anomaly in the tropics. For both G1 and G2 simulations all members of the PPE show a large reduction in evaporation for most latitudes, however the zonal responses differ substantially within the PPE.

Figure 4.18 shows plots of the ensemble-mean annual anomalies of temperature, precipitation and total evaporation for the $4\times CO_2$ and G1 simulations relative to the pre-industrial. In the $4 \times CO_2$ simulation there is a global increase in temperature, which is larger over continental regions and at high latitudes. In the G1 simulation the PPE generally shows a cooling the in the tropics and a warming at high latitudes and over most continental regions. There is agreement on the sign of the change in most regions, including over most tropical continental regions, some of which show a cooling and others which show a warming; however there is disagreement within the PPE over the sign of the Atlantic temperature response and in regions with small magnitude changes. In the $4 \times CO_2$ simulation there is consensus within the PPE on the large-scale precipitation changes, with some disagreement at the boundaries between positive and negative anomalies. The same is true for the G1 simulation with all models generally agreeing on the mean precipitation changes, although there is a substantial area of disagreement in areas with an ensemble mean change of less than 0.1 mmday^{-1}, it is not known whether this is due to the small magnitude of the changes or the cancelling out of larger anomalies. The evaporation response in the $4 \times CO_2$ simulation shows the same kind of behaviour as the precipitation response

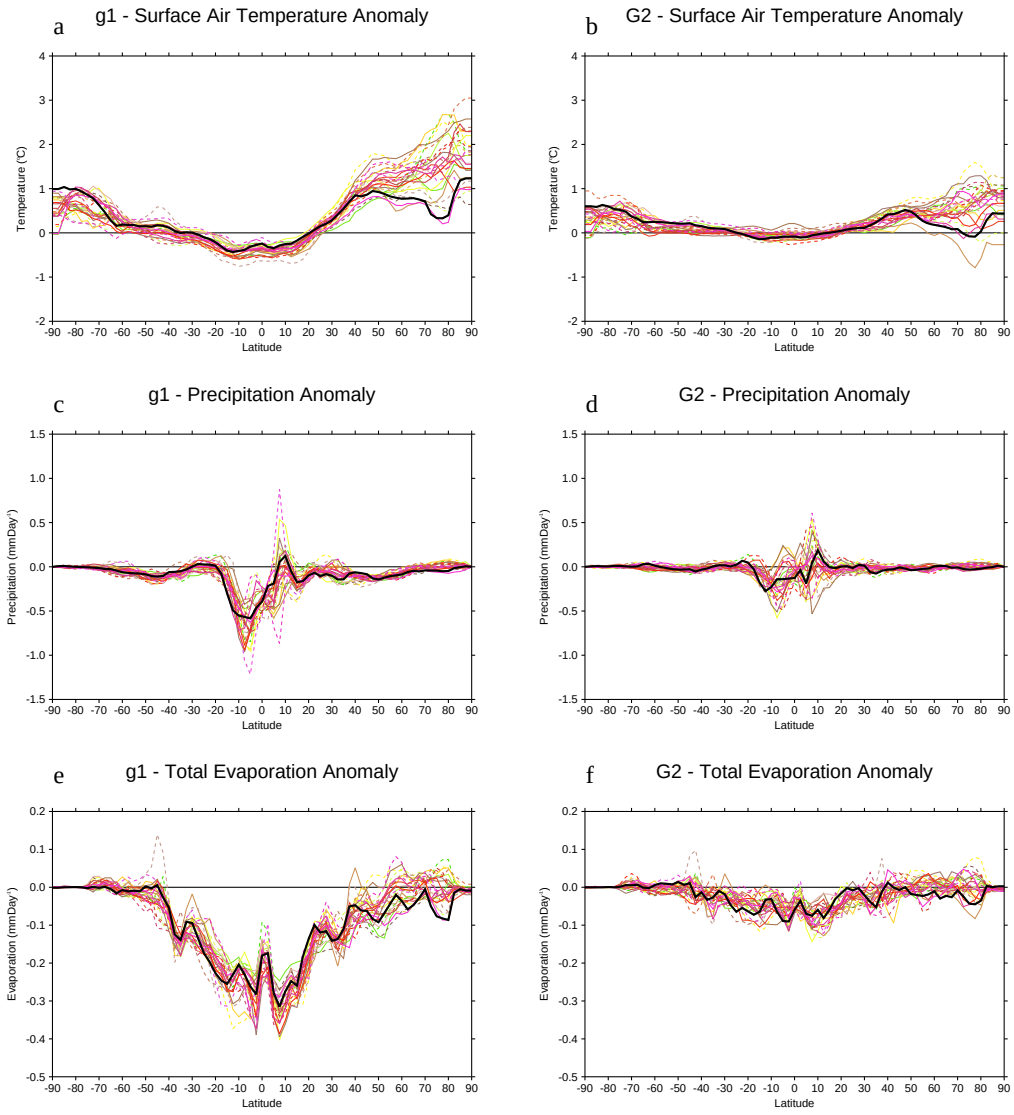

Figure 4.17: Annual zonal mean anomaly plots of surface air temperature (a and b), precipitation (c and d), and total evaporation (e and f), for G1 and G2 simulations. Anomalies are calculated from years 31-49 of the pre-industrial control and the G1 and G2 simulations. The standard HadCM3 model simulation is indicated by a thick black line.

with general agreement between the PPE members on the regional response. There is also close agreement between all PPE members in the G1 total evaporation response with large reductions across the tropics and in some mid-latitude regions; however there are disagreements in regions with an ensemble mean change of less than 0.1 mmday^{-1}.

4.6 Discussion

This study has presented the methodology used to generate the first PPE using the fully-coupled AOGCM HadCM3 without flux adjustment and presented some analysis of these results. The goal has been to develop a research tool that can be used to explore the role of parametric uncertainty in climate studies where flux adjustment is not appropriate. Flux adjustment corrects for sea-surface temperature biases and the TOA radiative imbalance of climate models, this prevents the global mean temperature of a model, or a member of an ensemble, deviating too far from observations (Collins *et al.*, 2006). However by not allowing models to drift, arguably unrealistic members of an ensemble will be maintained; for the ENTCOEF parameter in HadCM3 this has arguably led to exaggerated climate sensitivity estimates (Murphy *et al.*, 2004; Sanderson *et al.*, 2008a; Joshi *et al.*, 2010). By removing flux adjustment, an additional physical constraint is applied and by only preserving models or ensemble members that are close to the observed pre-industrial temperature, unrealistic model versions can be excluded. This line of reasoning has been challenged on the grounds that it is an overly strong constraint and would limit the range of parameters too much (Collins *et al.*, 2006); however, we find that our ensemble spans most of the range of the 8 parameters perturbed, challenging this assertion. Figure 4.19 shows a list of the parameter values and some key results for the 27 members of the ensemble.

We find that the ocean perturbation affected the energy flux into the ocean and may have altered the projected temperatures and thus the target pre-industrial temperature pre-selection process we applied. In this study we perturbed atmospheric parameters which control climate sensitivity as well as a highly uncertain background ocean diffusivity parameter that has a large effect on the condition of the ocean in HadCM3 (Collins *et al.*, 2007). We find that the 500 year spin-up

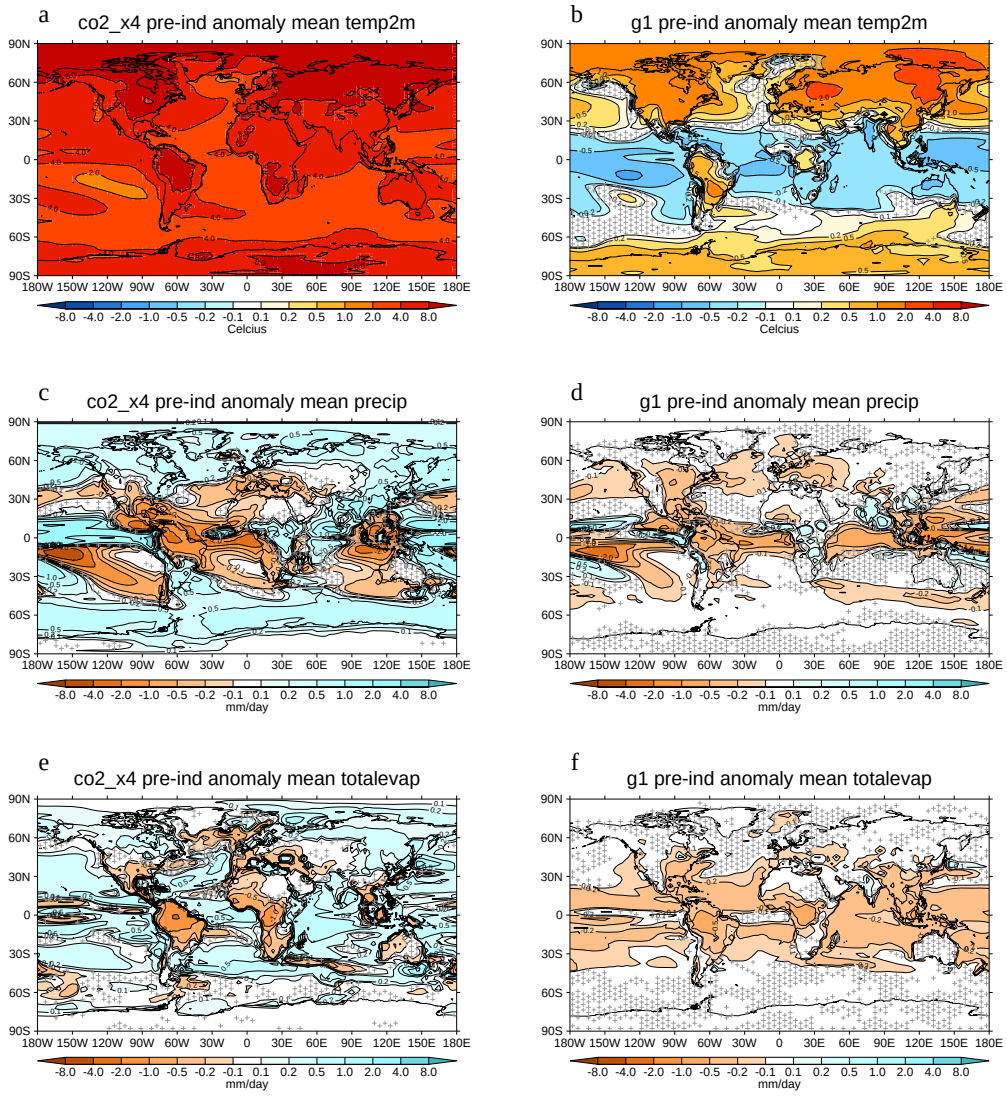

Figure 4.18: Ensemble mean plots of the annual mean anomalies of surface air temperature (a and b), precipitation (c and d), and total evaporation (e and f) for the $4 \times CO_2$ and G1 experiments. Anomalies are calculated from years 31-49 of the pre-industrial control and the G1 and G2 simulations. Stippling indicates regions where less than 66% of ensemble members agree on the sign of the anomaly.

Experiments	ENTCOEF	EACF	RHCRIT	VF1	CT	CW_LAND	CW_SEA	ALPHAM	KAPPA0_SI	DKAPPA_DZ_SI	A	B	C	D	E	F
0 (STD)	3.0000	0.5000	0.7000	1.0000	1.0000E-04	2.0000E-04	5.0000E-05	5.0000E-01	1.0000E-05	2.8000E-08	18.72	12.95	2.63	4.70	6.84	4.92
1	7.5340	0.5096	0.8903	1.6840	2.6130E-04	3.1460E-04	7.4220E-05	6.4950E-01	1.3450E-05	5.0640E-08	19.98	12.58	3.56	3.70	7.65	4.73
2	6.4940	0.4793	0.6791	1.5540	3.2470E-04	2.6170E-04	6.0840E-05	5.6610E-01	1.4130E-05	5.5920E-08	21.72	11.54	3.94	3.87	6.59	4.30
3	4.3620	0.6006	0.8013	0.7928	2.5190E-04	1.0500E-03	2.5990E-04	6.0960E-01	1.3950E-05	5.4520E-08	24.77	12.16	2.46	3.89	7.61	4.44
4	2.5030	0.4981	0.6874	0.6921	1.4860E-04	1.4850E-03	3.7000E-04	5.4950E-01	8.7640E-06	2.1510E-08	18.05	12.94	2.43	8.75	8.94	4.63
5	5.3160	0.4819	0.8936	1.9350	2.2910E-04	1.2190E-03	3.0280E-04	4.8430E-01	1.5860E-05	7.0390E-08	23.89	12.70	2.85	3.35	6.56	6.68
6	1.2800	0.5706	0.7816	1.3900	1.7740E-04	1.8840E-03	4.7060E-04	6.1970E-01	1.8990E-05	1.0100E-07	29.73	15.77	6.37	42.91	23.52	5.13
7	1.6390	0.4702	0.7884	1.2210	6.1930E-05	5.9150E-04	1.4420E-04	6.4360E-01	6.6370E-06	1.2330E-08	19.45	14.63	4.24	58.78	35.19	6.04
8	2.7890	0.6108	0.6352	1.3390	2.6900E-04	1.6060E-04	3.5310E-05	6.0740E-01	1.4190E-05	5.6380E-08	20.39	12.95	2.98	4.15	6.58	6.75
9	2.2110	0.5431	0.8690	0.6691	8.9290E-05	1.5030E-03	3.7450E-04	5.8000E-01	5.4640E-06	8.3600E-09	17.33	13.11	2.64	12.18	9.12	6.92
10	2.0010	0.5849	0.7113	0.7360	1.4740E-04	4.6160E-04	1.1130E-04	6.3570E-01	1.7220E-05	8.3080E-08	24.92	17.00	4.75	37.25	21.79	4.58
11	2.1480	0.4904	0.7838	0.6535	1.1220E-04	1.7070E-03	4.2590E-04	5.9010E-01	1.9190E-05	1.0310E-07	29.83	16.23	4.19	24.71	16.07	5.35
12	4.9010	0.5093	0.6616	0.9950	3.6590E-04	2.5750E-04	5.9780E-05	5.8750E-01	1.8180E-05	9.2540E-08	25.13	14.24	3.11	3.86	6.72	5.85
13	4.4920	0.4882	0.8513	1.9020	3.7690E-04	1.4520E-03	3.6150E-04	4.7050E-01	1.1550E-05	3.7380E-08	18.25	14.88	2.49	5.73	8.26	5.32
14	2.1570	0.6160	0.8669	1.0070	2.0280E-04	1.5850E-03	3.9500E-04	5.0310E-01	9.3130E-06	2.4280E-08	20.30	15.36	3.42	19.95	10.13	4.89
15	6.4480	0.5587	0.8348	1.1170	3.4750E-04	4.0090E-04	9.6010E-05	6.4020E-01	1.2000E-05	4.0300E-08	19.93	13.75	2.97	4.38	8.96	7.21
16	4.4320	0.5031	0.8124	1.4630	3.9430E-04	1.0720E-03	2.6570E-04	5.0020E-01	5.2070E-06	7.5910E-09	16.80	15.77	2.55	8.79	9.70	4.64
17	3.7450	0.5530	0.8831	1.1550	3.2480E-04	1.6350E-03	4.0780E-04	5.4140E-01	6.1230E-06	1.0500E-08	17.02	14.00	2.23	8.30	8.70	7.35
18	3.3960	0.4937	0.6904	1.3510	3.5960E-04	6.7350E-04	1.6490E-04	6.4630E-01	9.7170E-06	2.6440E-08	17.94	15.50	2.81	7.40	9.79	4.60
19	3.0400	0.5928	0.8494	1.7810	2.2510E-04	1.3110E-03	3.2590E-04	5.8280E-01	1.0940E-05	3.3510E-08	20.73	13.49	2.51	5.44	7.46	6.90
20	3.4220	0.4783	0.6808	1.4940	2.3670E-04	2.7530E-04	6.4290E-05	5.6230E-01	6.0120E-06	1.0120E-08	17.34	15.15	2.85	5.97	8.38	4.57
21	5.4260	0.5646	0.8443	1.2990	2.4400E-04	3.3220E-04	7.8660E-05	5.6360E-01	5.7930E-06	9.3960E-09	17.03	13.66	2.71	4.71	8.62	6.30
22	2.3660	0.5368	0.6765	1.9050	2.6230E-04	9.9640E-04	2.4650E-04	4.7490E-01	6.6800E-06	1.2490E-08	16.51	14.22	3.01	6.67	7.16	5.33
23	2.7200	0.5423	0.7032	1.5920	2.9640E-04	1.0940E-03	2.7120E-04	5.6500E-01	6.3050E-06	1.1130E-08	18.11	13.99	2.72	6.48	8.05	5.39
24	2.6080	0.5999	0.8766	0.8549	1.8590E-04	1.8140E-03	4.5290E-04	5.4310E-01	5.0690E-06	7.1950E-09	16.35	13.05	2.34	9.58	8.43	5.78
25	3.3200	0.5044	0.6392	0.8006	1.8900E-04	3.8880E-04	9.2960E-05	5.8690E-01	1.3300E-05	4.9500E-08	19.95	13.69	2.56	4.68	7.54	4.37
26	1.1000	0.6283	0.6445	1.8930	1.7420E-04	1.3490E-03	3.3550E-04	6.0040E-01	1.2730E-05	4.5390E-08	18.99	11.26	3.84	10.71	7.39	5.38
A	Overturning (Sv)				C	Pre-ind 100 mB Humidity (ppmv)				E	4*CO2 Projected Temp					
B	Pre-ind Temp (°C)				D	4*CO2 100 mB humidity (ppmv)				F	4*CS TCR					

Figure 4.19: List of the parameter values and some key climate indicators for the 27 members of the PPE of HadCM3.

and full 800 year control are not long enough for the oceans of the members of the PPE to adjust fully to these new conditions and so both the pre-industrial experiments and the raised CO_2 experiments were run with an ocean that is not in equilibrium. These results may not perfectly match those that would be obtained after a several millenia spin-up; however this ensemble will still be useful in assessing the parametric uncertainty in climate studies. We found that for the initial short pre-industrial integrations there is a strong interaction between the ocean diffusivity changes and the initial temperature selection, in that for high values of the VDIFF parameter much more energy is absorbed by the ocean preventing the atmosphere from warming as much as it would have. This short-term energy imbalance masks the long-term equilibrium value of the warming for these members and may bias the equilibrium temperature projection which forms the basis for selection for inclusion in the ensemble. High values of VDIFF have been found to be associated with increased absorption of energy into the oceans and lower values of TCR (Collins *et al.*, 2007), and in this ensemble there is a correlation between higher pre-industrial temperatures and higher values of climate sensitivity (see figure 4.13), thus due to the artifical association of pre-industrial temperature and VDIFF the PPE may have a narrower range of TCR than would be the case if this selection artifact was not present. Such interactions between atmospheric and ocean parameter perturbations should be considered for future non-flux-adjusting fully-coupled PPE experiments with simulation times shorter than the time required to spin the ocean up fully.

Numerous methods to test the 'realism' of members of a PPE of a GCM have been developed (Edwards *et al.*, 2010; Murphy *et al.*, 2004; Rodwell and Palmer, 2007), but as far as the authors are aware this study is the first to test members on their projected equilibrium pre-industrial temperature, i.e. to run a PPE of a GCM model without using flux adjustment. Murphy *et al.* (2004) created and analyzed a PPE of HadCM3 using the climate prediction index, a method which applies a set of comparisons to observational data that gives each member a weight, which has also been applied to other PPE studies (Collins *et al.*, 2010b). The climate prediction index aggregates a large number of different tests of model 'realism', or similarity to observations, and so highly unrealistic behaviour in one aspect can be counteracted by reasonably realistic behaviour in others. For example, the LOW ENTCOEF (ENTCOEF = 0.6) model version was kept in the ensemble of Murphy et

al. (2004) despite being numerically unstable without flux adjustment and showed a stratospheric water vapour response to warming that was substantially larger than the observed response, and hence unrealistic (Joshi *et al.*, 2010). An alternative approach is to run the GCM in meteorology mode, i.e. starting from observed initial atmospheric conditions, and measure the deviation of the simulated atmospheric column from observations over the course of a few days of simulation (Rodwell and Palmer, 2007). If the PPE member changes the structure of the variables throughout the atmospheric column substantially from observations the member can be ruled unrealistic and excluded, although defining an appropriate multi-variate measure that appropriately excludes unrealistic models but retains an appropriate fraction of the ensemble may be challenging. Edwards *et al.* (2010) outlined an approach for testing the 'feasibility' of model output; a set of lenient physical criteria are defined such that the member should be deemed unsuitable if it fails to satisfy any of these loose criteria and those members which remain should be considered 'feasible' representations of the system.

The behaviour of the HadCM3 PPE used in this study will now be considered with the 'feasibility' approach of Edwards *et al.* (2010) in mind, and we can judge which aspects of the ensemble behaviour are unfeasible and so which members of the ensemble can be excluded. Running the GCM without flux adjustment and projecting the equilibrium temperature response to check whether it was within 2°C of the observed pre-industrial temperature of 13.6°C (Brohan *et al.*, 2006; Jones *et al.*, 1999), was the first 'feasibility' test applied to the members of the PPE. We thus generated the 27 members of the PPE 6 of which were found to fall beyond ±2°C although three of those were within 10% of this threshold, see figure 4.1 . If we take the Atlantic overturning circulation after 800 years as another constraint we find that all but 6 members of the PPE are within 3 Sv of the observed overturning strength of ∼18 Sv (Ganachaud and Wunsch, 2000), which compares with the year-to-year standard deviation of overturning strength at 26.5 N in the Atlantic of 4.8 Sv (Rayner *et al.*, 2011).The greatest overturning strength in the PPE of ∼30 Sv is still lower than the 40 - 50 Sv of the GISS-AOM, one of the members of the CMIP3 ensemble (IPCC, 2007), see figure 4.2 f. A crude comparison of the zonal mean climatology of the PPE and the CMIP3 ensemble shows that the behaviour of most of the members of the PPE is within the range seen in the CMIP3 ensemble and

so could be judged to be consistent with previous work, see figure 4.8. Exceptions to this are found in the zonal temperature plots where some members of the PPE have peak tropical temperatures up to ∼3°C warmer than the warmest run in the CMIP3 ensemble, although these are the same members that have global mean temperatures more than 2°C warmer than the observed pre-industrial temperature of 13.6°C (Jones *et al.*, 1999; Brohan *et al.*, 2006; Meehl *et al.*, 2007b).

We find the greatest range of behaviour in the PPE for high-altitude humidity, for this variable there is a large spread in the pre-industrial control humidity profile and a large spread in the changes in the humidity profile in response to quadrupling CO_2 levels. Selection on the basis of the pre-industrial humidity profile has not been made due to the roughly 2 orders of magnitude range in the specific humidity at 30 mB in both the PPE and the CMIP3 ensemble, see figure 4.9. We find that ENTCOEF has the greatest effect on specific humidity at altitudes above 100 mb in the pre-industrial; members of the PPE with low values of ENTCOEF have specific humidity values many times higher than the standard version of HadCM3, see figures 4.9 and 4.11. At elevated CO_2 levels the low ENCOEF members have have specific humidity values up to 10 - 100 times higher than the standard model version between 100 and 10 mb which has a large effect on the TOA radiative balance (Forster and Shine, 2002; IPCC, 2007). The very high climate sensitivities of the low ENTCOEF runs is linked to these temperature driven increases in upper tropospheric and stratospheric humidity (Joshi *et al.*, 2010; Sanderson *et al.*, 2008a). However, most GCMs simulate a weak stratospheric humidity response to warming and small changes in relative humidity throughout the atmospheric column (Colman, 2001; Stuber *et al.*, 2005) which is backed up by observations of recent warming (IPCC, 2007); this suggests that the very high climate sensitivities of the low ENTCOEF members may be unrealistic (Joshi *et al.*, 2010).

We find that no members of the ensemble have obviously inconsistent specific and relative humidity profiles in the pre-industrial when compared to the CMIP3 models, however we find arguably 'unrealistic' responses to quadrupling CO_2 levels in the low ENTCOEF members, as the increase in humidity per degree of warming is much higher than that observed (Joshi *et al.*, 2010). In fact some of the low ENTCOEF members of the ensemble appear not to be converging to an equilibrium temperature but instead to be beginning a runaway greenhouse warming, with temperatures rising

without reducing the TOA radiative imbalance, see figure 4.14. The mechanism behind this runaway greenhouse warming has not been definitively identified but one plausible hypothesis is that the large increases in upper atmospheric humidity in response to warming in the low ENTCOEF runs, constitutes a very large, positive, longwave feedback which comes to dominate at higher temperatures. For some of the low ENTCOEF runs this upper level humidity feedback appears to be strong enough to prevent the TOA radiative imbalance from dropping, despite the rapidly rising temperature. We find that our results for low entrainment rate members are consistent with those of Joshi *et al.* (2010) and that we agree with their assessment that this kind of response is unrealistic and as such the very high climate sensitivities produced by these members should be viewed with extreme caution, see figure 4.15 and figure 4.14. On these grounds we suggest revising the range for ENTCOEF from 0.6 - 9.0 to 2.0 - 9.0, for future perturbed parameter studies with HadCM3.

Applying the PPE to the geoMIP G1 and G2 geoengineering experiments we find a general agreement on the large scale changes in temperature, precipitation and evaporation but substantial differences in the details of the responses. The PPE shows that there would be an overcooling in the tropics and a residual warming at high latitudes, particularly in the north, relative to the pre-industrial (see figure 4.17 and 4.18); this is in agreement with the results of Schmidt et al. (2012) (compare figure 4 in their study with figure 4.17 a in this study) who compared the response of four GCMs to the G1 simulation. The PPE shows a more complicated zonal precipitation response with reductions in the mid-latitudes and south of the equator for all members and evidence of a northward shift in the ITCZ resulting in some members showing a large increase in precipitation north of the equator. The zonal precipitation results of Schmidt *et al.* (2012) show a similar general result and a similar range of response with some models showing that large northward shift in the ITCZ and others not (compare figure 7 in their study with figure 4.17 c in this study). The regional temperature response of the PPE G1 experiment, figure 4.18 b, is again similar to the results of Schmidt *et al.* (2012), showing similar patterns of positive and negative anomalies and even a similar pattern of agreement within each ensemble. The regional precipitation response of the PPE, figure 4.18 d, and figure 8 of Schmidt *et al.* (2012) also show similar results, with a similar pattern of drier and wetter regions although both studies show large areas where the ensemble

members disagree on the sign of the change.

This comparison with the Schmidt *et al.* (2012) study demonstrates that the PPE covers a reasonable range of climate model behaviour and can be used to provide an assessment of the uncertainty in climate model response to changes in forcing. The results presented here, when compared with Schmidt et al. (2012), reinforce some of the conclusions of previous sunshade geoengineering (or G1) experiments (Lunt *et al.*, 2008b; Govindasamy *et al.*, 2003; Irvine *et al.*, 2010). In fact there is agreement on many of the regional climate responses to geoengineering, e.g. that continental south America will warm despite the general cooling in the tropics and the large reductions in European and North American precipitation. However the results also show the aspects on which there is some uncertainty, such as by how much will the ITCZ shift northwards and how will the continental precipitation response vary from region to region in the tropics?

4.7 Conclusion

This study presents the methodology and some initial results from the first PPE of a non-flux adjusted, fully-coupled CMIP3-era GCM. The purpose has been to create a modestly-sized PPE to explore the effects of parametric uncertainty on climate and paleo-climate experiments. Two hundred different versions of the HadCM3 model were generated with 8 continuous parameters varied. 27 ensemble members of the HadCM3 model (Gordon *et al.*, 2000), including the standard configuration, were selected from these 200 using an estimation of the equilibrium pre-industrial temperature to constrain the ensemble, i.e. models with projected temperatures within 13.6 ± 2°C were kept (Brohan *et al.*, 2006; Jones *et al.*, 1999). Despite the ocean not reaching equilibrium after 800 years the pre-industrial control surface climatology of the ensemble compares well on the whole to the CMIP3 ensemble (Meehl *et al.*, 2007b). However some members of the ensemble were either warmer or colder after the 800 year control than the temperature projections and fell outside the target range. We find that not using flux adjustment and instead constraining our ensemble on the pre-industrial equilibrium temperature has not led to a serious curtailment of parameter space as has been suggested previously (Collins *et al.*, 2006). In fact some members of the ensemble with low values of the entrainment

coefficient remain close to pre-industrial TOA radiative balance despite the fact that at quadrupled CO_2 levels they show an unrealistic increase in stratospheric and upper tropospheric humidity levels and some members show a runaway climate response.

An example application of the PPE is made, investigating uncertainty in SRM geoengineering by simulating the G1 and G2 experiments of the geoMIP project (Kravitz *et al.*, 2011). Agreement within the PPE is found on a number of key climate responses to the solar insolation reductions specified in the G1 and G2 experiments. The ensemble response is consistent with many of the results of Schmidt *et al.* (2012) who compared the response of 4 GCMs to the G1 experiment, and has a similar spread of zonal-mean climate response. These results suggest that the PPE should be useful in assessing climate model uncertainty.

4.8 Implications for thesis

The results of the PPE for the G1 and G2 simulations have implications for the robustness of the results of Chapter 2 and 3. The basic climate effects of sunshade geoengineering seen in simulations by both HadCM3 and HadCM3L in Chapters 2 and 3 are seen in the PPE, i.e. a cooler equator and warmer poles than in the pre-industrial; a global reduction in precipitation, a northward shift of the ITCZ, and drier mid-latitudes; and a strong reduction in evaporation world-wide but with the largest reductions in the tropics. The results of the sunshade geoengineering simulations with the PPE and a comparison with the MME sunshade assessment of Schmidt *et al.* (2012), suggest that many of the regional trends in temperature and precipitation seen in Chapter 2 are robust but that the magnitude of the change may not necessarily be robust.

The sunshade geoengineering results of the PPE have some implications for the specific results and claims of the preceding chapters, which I now review. Firstly, the PPE results for the G2 experiment provide some additional evidence for the linearity of the global response to sunshade geoengineering at different CO_2 concentrations. An assessment of whether this linearity holds at the regional level is not possible with the PPE G2 simulations as the climate signal is weak due to the small changes in the CO_2 concentration and only 50 years of a single transient run for each member

are available. As such the PPE does not provide much additional evidence for the linearity of the response to sunshade geoengineering. However, the PPE does provide confirmation of the specific regional responses to sunshade geoengineering seen in Section 2.5; there is agreement that North America is drier than the pre-industrial; Australia and China are both close to the pre-industrial precipitation values, reversing the dry and wet signal seen at $4 \times CO_2$, respectively; Brazil remains dry but less dry than at $4 \times CO_2$; and Western Europe has a similar precipitation anomaly at $4 \times CO_2$ and with sunshade geoengineering. As the overall climate response to sunshade geoengineering for the PPE seems similar to the results in Section 2.5, it seems reasonable to assume that similar 'novel' climate change results would be found with the PPE.

The results of Section 2.6 of Chapter 2 deal with the response of the Greenland ice-sheet to sunshade geoengineering for different reductions in insolation. This Greenland analysis uses the HadCM3L model but the HadCM3 PPE results of this chapter are still relevant as he standard configurations of HadCM3 and HadCM3L have similar climate responses over Greenland to sunshade geoengineering as can be seen from figure 2.12 of Section 2.7. The PPE shows a similar mean temperature change as was found in Section 2.6 for Greenland but the PPE shows a wide range of temperature anomalies from the pre-industrial in the latitudes of Greenland, with the standard version of HadCM3 as one of the coldest ensemble members in this latitude band. There is disagreement over the sign of precipitation change over Greenland for the PPE and the magnitude of change from the pre-industrial is relatively small. As most PPE members have a warmer Greenland climate than the standard HadCM3 model version under sunshade geoengineering, this suggests that the stability of the Greenland ice-sheet may have been over-estimated in Section 2.6. Interestingly the opposite is true in Antarctica where the standard HadCM3 model is warmer than most of the PPE members for sunshade geoengineering, which suggests that if a study of the Antarctic ice-sheet had been conducted with HadCM3, the stability of that ice-sheet could have been under-estimated.

The implications the PPE sunshade geoengineering results for Chapter 3 are limited as no regional geoengineering schemes were investigated. It cannot be predicted from these results whether the PPE response to regional geoengineering would show more or less agreement than the response to sunshade geoengineering. However, the

similarity of the PPE sunshade geoengineering results reinforces the contrast between the relatively homogeneous climate response of sunshade geoengineering and the highly heterogeneous response to the desert geoengineering scheme.

CHAPTER 5

Conclusion

5.1 Introduction

Evaluating the climate consequences of SRM geoengineering interventions is a key first step in deciding whether these schemes may help ameliorate the effects of dangerous climate change. The aim of this thesis was to investigate the climate effects of a number of Solar Radiation Managment (SRM) geoengineering schemes using a General Circulation Model (GCM) and some of the indirect climate effects using an off-line ice sheet model. Section 5.2 summarizes the achievements and findings of the thesis with respect to the objectives outlined in Section 1.6. A brief description of the overall contribution of this thesis to the field of SRM geoengineering research is given in Section 5.3. Section 5.4 identifies further research that would test the findings of this work and future directions for SRM geoengineering research. Section 5.5 presents some final thoughts on SRM geoengineering.

5.2 Summary of work

5.2.1 Sunshade geoengineering

Sunshade geoengineering is arguably the conceptually simplest form of SRM geoengineering as the reduction in absorption of solar energy would be achieved by reducing the solar insolation reaching the Earth. Many groups have simulated the effects of having elevated CO_2 levels with a reduction in insolation sufficient to maintain pre-industrial temperature or radiation balance (Lunt *et al.*, 2008b; Govindasamy *et al.*, 2003; Schmidt *et al.*, 2012). This simple type of geoengineering experiment is a useful analogy to other more feasible schemes, specifically the stratospheric aerosol geoengineering scheme, and can provide an easy means to compare the response of different models to geoengineering (Kravitz *et al.*, 2011). The simplicity of the scheme makes it relatively straightforward to investigate interesting variations of the equilibrium CO_2-cancelling sunshade geoengineering experiment. In Chapter 2, two aspects of sunshade geoengineering scenarios are investigated using the HadCM3 and

HadCM3L models (Gordon *et al.*, 2000; Cox *et al.*, 2000); the differences between partial and full CO_2-cancelling sunshade geoengineering and the differences between sunshade geoengineering at different CO_2 levels. These simulations were used to analyze the regional and seasonal climate response to sunshade geoengineering and to investigate the impact on the El Niño Southern Oscillation (ENSO). The HadCM3L results were also used in the investigation into the effect of sunshade geoengineering on the Greenland Ice Sheet, summarized in the next section.

The partial sunshade geoengineering results of Section 2.5 show that the global and regional climate effects vary linearly, or near-linearly with the reduction in insolation applied by sunshade geoengineering. Sunshade geoengineering is found to bring some regions very close to their pre-industrial mean climate whereas other regions are left with a climate that is roughly the same temperature but much drier than in the pre-industrial. An assessment of the fraction of the planet affected by 'novel' climate conditions, i.e. a regional climate anomaly with a sign different from the regional global warming climate anomaly, shows that at all insolation reductions some regions would experience novel precipitation conditions (generally drier than pre-industrial) and at large insolation reductions a large fraction would also experience novel temperature conditions (cooler than pre-industrial). These results suggest that partial sunshade geoengineering, of perhaps 60%, may offer a better solution than full sunshade geoengineering, returning pre-industrial global mean precipitation and significantly mitigating the effects of climate change whilst exposing only a few regions to novel climate conditions.

However, the specific regional climate signals reported in Chapter 2 must be treated with caution as GCMs do not perform very well at reproducing regional climatology, particularly for precipitation, and there are differences in regional projections of climate change (Min *et al.*, 2004; Johannessen *et al.*, 2004). In fact, the HadCM3 and HadCM3l climate responses differ substantially even though they only differ in their ocean resolution and land surface scheme. This raises difficulties as it is hard to tell how the model results would have differed if, for example HadCM3 had been used instead of HadCM3L to model the partial sunshade geoengineering simulations. However, it does seem reasonable to assume that both HadCM3 and HadCM3L would have shown a similar linear response to both the CO_2 forcing and the sunshade insolation reduction, as they share the same atmospheric model,

HadAM3 (Gordon *et al.*, 2000). There appears to be no non-linear changes in the climate response to different insolation reductions or CO_2 forcing over the 400 years simulated however these simulations do not include vegetation feedbacks which could introduce non-linearities and for longer integration times changes in the meridional overturning circulation have been shown to exhibit tipping points (Keller and McInerney, 2008), which would affect these results. Additionally there are difficulties with the ENSO results as the century-long timeseries were too short to draw robust conclusions due to the large decadal variability in the ENSO 3.4 sea-surface temperature series.

5.2.2 Greenland Ice Sheet and sea-level rise response to sunshade geoengineering

SRM geoengineering would not only affect the climate but also would indirectly affect other important aspects of the Earth system; in Chapter 2 the effects of different sunshade geoengineering scenarios on the Greenland ice sheet and on the global mean sea-level were investigated. The sea level rise over the next century will be driven by a number of different factors: the thermal expansion of the oceans; the changes in surface mass balance of glaciers and ice-caps; and the changes in the surface mass balance and outflow from the Greenland and Antarctic ice sheets (IPCC, 2007; Wigley and Raper, 2005; Cazenave *et al.*, 2009). Over the longer term the sea-level response is likely to be dominated by the response of the Greenland and Antarctic ice sheets due to the very large volumes of water these contain (IPCC, 2007), which could raise sea-levels by around 70m if both completely melted (Alley *et al.*, 2005). SRM geoengineering is expected to reduce sea-level rise by lowering ocean temperatures and reducing ablation of ice mass (Wigley, 2006; Moore *et al.*, 2010), however it may also change the accumulation of ice due to reductions in precipitation (Lunt *et al.*, 2008b).

The equilibrium Greenland Ice Sheet response to sunshade geoengineering for a range of insolation reductions was simulated using output from the partial sunshade experiments with the HadCM3L model and the off-line Glimmer ice sheet model (Cox *et al.*, 2000; Rutt *et al.*, 2009). The climate of Greenland at quadrupled CO_2 concentrations with a full sunshade was warmer and wetter than the pre-industrial climate, and was warmer and wetter still for smaller reductions in insolation. The

Glimmer model simulated a near complete collapse of the Greenland Ice Sheet at quadrupled CO_2 concentrations and for 20% or less sunshade geoengineering, for 30%-50% sunshade a partial Greenland Ice Sheet was maintained, and for 60% or more sunshade geoengineering the Greenland Ice Sheet maintained its full pre-industrial mass.

The results for the Greenland Ice Sheet response have two sources of problems; the input regional climate response, and the ice sheet model response. GCM models have biases in their control climatology which can be fairly large on a regional basis, in the case of HadCM3L there is a cold bias in the area of concern. Regional climate projections by GCMs for future changes differ substantially, particularly in the Arctic (Meehl *et al.*, 2007b; IPCC, 2007), which is expected to warm much more than the global mean (Arndt *et al.*, 2011; IPCC, 2007), and thus there is a large amount of uncertainty in the inputs to the ice sheet model. In particular, the perturbed parameter ensemble used in Chapter 4 found that the standard version of HadCM3 was one of the coldest members of the ensemble at the latitudes of Greenland. This suggests that the results in Section 2.6 are likely an over-estimate of the ability of sunshade geoengineering to stabilize the Greenland Ice Sheet. The ice sheet model (Glimmer) also has limitations (Rutt *et al.*, 2009); due to the use of the shallow-ice approximation (Hutter, 1983), it does not well simulate fast-flowing ice streams and has a relatively simple treatment of basal sliding, basal hydrology, and calving at marine margins. The pre-industrial ice volume is overestimated by Glimmer (Rutt *et al.*, 2009), which is a common deficiency in current generation ice sheet models due to the lack of an accurate representation of ice dynamics (Ridley *et al.*, 2005; Huybrechts and de Wolde, 1999; Ritz *et al.*, 1997; Greve, 2000). Despite these GCM and ice sheet model limitations, including the likely over-estimation of effectiveness, it seems clear from these results that sunshade geoengineering could help stabilize the Greenland Ice Sheet.

5.2.3 Comparison of surface albedo modification and sunshade geoengineering

There are many different SRM geoengineering schemes that act in different ways and could help to ameliorate the effects of rising greenhouse gas concentrations; however a comparison of multiple schemes using the same modelling framework had

not been done before. Chapter 3 compares the highly heterogeneous urban, crop and desert geoengineering schemes with the homogeneous sunshade geoengineering scheme at double the pre-industrial CO_2 concentration, using the HadCM3 model with the MOSES 1 land surface scheme. Increasing urban and crop albedo would make only a small difference to the global energy budget but on a regional scale could make a more significant change (Oleson *et al.*, 2010; Ridgwell *et al.*, 2009). Desert geoengineering on the other hand would make a much larger change in albedo over a relatively large fraction of the land surface, and could have a significant global effect (Gaskill, 2004). The sunshade geoengineering scheme was included to tie this work in with the work of Chapter 2 and to contrast the differences between a homogeneous forcing with the heterogeneous forcings of the surface albedo modification schemes. A range of analysis building on the work in Chapter 2 was applied to investigate the climate effects of these schemes.

Surface albedo geoengineering produces a much more heterogeneous forcing than sunshade geoengineering and this is reflected in the highly regional nature of the cooling that these schemes produce. Urban and crop albedo geoengineering produced a global mean cooling of only a few tenths of a degree Kelvin but produced a much larger regional and local cooling, which peaked in the summer. Desert albedo geoengineering was found to substantially cool the planet but caused intense local cooling in areas of application. Desert albedo geoengineering also caused major shifts in precipitation with a magnitude roughly equal to doubled CO_2 but of a different kind, i.e. not reversing the effects of doubled CO_2. Although desert albedo geoengineering caused a smaller reduction in global mean precipitation per degree of cooling than sunshade geoengineering, it causes a much greater reduction in precipitation over land. Desert geoengineering also reduces the intensity of monsoon precipitation dramatically in some regions, e.g. Indian average precipitation dropped by 37% relative to the pre-industrial. These results suggest that urban and crop albedo geoengineering are of limited use as a means to ameliorate global climate change but might play a significant role at limiting climate change impacts locally, e.g. reducing the intensity of heatwaves in urban and agrarian regions. Desert albedo geoengineering does have a global cooling effect which could partially offset the warming produced by a doubling of CO_2 however it introduces large changes in precipitation patterns world-wide, reduces the intensity of monsoon precipitation and overall ap-

pears to create more problems than it solves. In comparison the more homogeneous forcing of sunshade geoengineering seems to reverse the effects of doubled CO_2 more effectively and causes fewer side effects.

Regional climate results of a single GCM are not wholly reliable as detailed in the sections above which means that the climate effects seen for surface albedo geoengineering must be treated with caution. Unlike with the sunshade geoengineering results there have been few other studies of surface albedo geoengineering and the perturbed parameter ensemble was not used to study surface albedo geoengineering in this thesis. However, the large local and seasonal cooling in the areas modified seems logical, as solar forcing is at a maximum in summer and thus the change in albedo will make a greater difference at this time. Desert albedo geoengineering showed a reduction in the fraction of precipitation that fell over the continents and some confirmation of this can be found from a study investigating cloud albedo increase over the ocean, i.e. it created the opposite land-sea temperature contrast, which showed a larger fraction of precipitation falling on the continents (Bala *et al.*, 2010a). The large impact of desert albedo geoengineering on monsoon rainfall seems robust as well, as a reduction in the warming of the continents in the summer will reduce the monsoon circulation as has been found for high-latitude Northern Hemisphere volcanic eruptions (Oman *et al.*, 2005).

5.2.4 Development and testing of a perturbed parameter ensemble of HadCM3

All the results in Chapters 2 and 3 are from single simulations of individual GCMs but there are many possible valid versions of a single GCM and many entirely different GCM models. GCMs are not perfect simulators of the climate system and so caution must be taken when drawing conclusions from the results of a single GCM, such as HadCM3. To assess the uncertainty in the climate results I generated a perturbed parameter ensemble (PPE) of HadCM3, varying 8 uncertain parameters in the model code to create many *a priori* equally likely versions of the same model, e.g. Murphy *et al.* (2004), Stainforth *et al.* (2005), Knight *et al.* (2007). Chapter 4 presented the development and testing of a non-flux-adjusting PPE of the HadCM3 model. An initial ensemble of 200 members was created without using flux-adjustment, so the ensemble members drifted from their initial (stan-

dard model) conditions, and after an initial 20 year pre-industrial control only the ensemble members which with projected temperatures close to the pre-industrial global-mean temperature were kept.

An ensemble of 27 different versions of the HadCM3 model was kept and after an 800 year pre-industrial control most members were within 2°C of the observed pre-industrial temperature of 13.6°C (Brohan *et al.*, 2006; Jones *et al.*, 1999). Comparisons to the CMIP3 ensemble showed that most members of the PPE produced a reasonable pre-industrial climate within the range of behaviour seen in the CMIP3 ensemble (Meehl *et al.*, 2007b). However, the PPE had some shared biases and a number of members had global-mean temperatures and upper atmosphere humidities beyond the range seen in the CMIP3 ensemble. The PPE showed a range of climate sensitivities on the high side, with most members having a range of 3.25 - 5.25°C and four members having climate sensitivities > 8°C and appeared to be begining a runaway greenhouse warming, with temperatures increasing rapidly without a decrease in TOA radiative imbalance. At high CO_2, low values of the entrainment rate coefficient (ENTCOEF) were associated with large increases in stratospheric humidity as the members warm, which will increase the water vapour climate feedback and leads to high climate sensitivities and potentially runaway greenhouse warming (Forster and Shine, 2002; Held and Soden, 2000; Joshi *et al.*, 2010). This increase in stratospheric water vapour in response to warming is not backed up by observations and is arguably an unrealistic response (Joshi *et al.*, 2010), however some of these runaway models showed no indication of unrealistic behaviour in the pre-industrial simulation.

The non-flux-adjusted PPE of HadCM3 developed in Chapter 4 produced many reasonable versions of the HadCM3 model, spanning a range of behaviour broader than the CMIP3 ensemble but with some common biases. The ensemble is not in equilibrium as the time to spin up the ocean of GCM models can be thousands of years and so the results will differ from those found after the model has fully spun up. The joint perturbation of atmospheric and oceanic parameters lead to an artificial association between the ocean parameter and stmospheric paramters due to the pre-selection approach adopted. The PPE does not represent a full sampling of parametric uncertainty as only eight parameters were varied and only 27 final ensemble members were kept. The ensemble also shares the same land-surface model

and overall model structure and so cannot replace multi-model ensembles as a tool for assessing model uncertainty. Overall the PPE seems to be suitable for assessing parametric uncertainty in geoengineering model studies and in other future climate studies.

5.2.5 Sunshade geoengineering parametric uncertainty

SRM geoengineering research has so far been carried out by many different groups conducting experiments in different ways; the Geoengineering Model Intercomparison Project (geoMIP) has defined a set of standard geoengineering experiments so comparisons between different GCMs can be facilitated. Chapter 4 applied the PPE to two of the geoMIP experiments to investigate the role of parametric uncertainty in sunshade geoengineering and to compare these results with the results of other GCMs. This thesis presented initial geoMIP sunshade geoengineering results from the PPE, which will be developed further as a separate study in due course. There was some spread in the insolation reduction required to achieve the pre-industrial TOA radiative balance at $4 \times CO_2$, with a range of 3.7% to 4.3% for the PPE, narrower than the range of 3.5% to 4.7% found for 4 different GCMs (Schmidt *et al.*, 2012). The PPE showed substantial regional differences in the response to sunshade geoengineering with the PPE showing disagreement on the sign of change over large areas of the globe. However, a comparison with the results of Schmidt *et al.* (2012) shows that the PPE has a very similar mean response and, more strikingly, a very similar pattern of intra-ensemble disagreement over the sign of change. A rapid warming and increase in precipitation on the shutdown of sunshade forcing was found, with a rate that reflected the climate sensitivity of the models.

The sunshade geoengineering results of the PPE confirmed the main findings on the global and regional climate effects of sunshade geoengineering shown in Chapter 2 and previous sunshade geoengineering work (Lunt *et al.*, 2008b; Govindasamy *et al.*, 2003; Schmidt *et al.*, 2012). Additionally, support is found for the finding that the global climate effects of sunshade geoengineering vary linearly with the CO_2 forcing. The PPE results do suggest that the Greenland Ice Sheet results of HadCM3 in Chapter 2 may over-estimate the stability of the Greenland Ice Sheet because almost all members of the PPE were warmer in the latitudes of Greenland than HadCM3.

This study suggests that the PPE has a reasonable mean climate response and represents GCM uncertainty fairly well, and as such will be a useful modelling tool for assessing uncertainty in climate model projections. Further development of this work will help identify, with some confidence, the aspects of the climate response to sunshade geoengineering that are robust and those that are uncertain.

5.3 Contribution of thesis

This thesis has presented work I conducted since January 2009, during a time when research into SRM geoengineering was expanding rapidly. Before this thesis little was known about SRM geoengineering apart from estimates of the effectiveness of some schemes and some global-scale analysis of the climate effects. This section details the contribution of myself and collaborators to the understanding of SRM geoengineering.

At the time Irvine *et al.* (2010) was written, Section 2.5 of this thesis, there had been no analysis of how the climate effects of sunshade geoengineering, or any other scheme, varied from region to region or with the strength of the forcing applied. However, the first analysis of this kind was published a few months before Irvine *et al.* (2010), by Ricke *et al.* (2010) who conducted a similar style of study but without either set of authors being aware of the fact. Irvine *et al.* (2010) did provide the first attempt to analyze SRM geoengineering with a subjective measure of quality of mitigation; the 'novel' climate analysis showed the fraction of the planet which experienced a novel change in climate, i.e. the sign of the geoengineering climate change differed from the sign of the CO_2-induced climate change. The analysis in Irvine *et al.* (2010) provided some insight into the difficulties that control over SRM geoengineering may cause, as some regions seem to be better off with one level of sunshade geoengineering and others better off under a different level.

Irvine *et al.* (2009), Section 2.6 of this thesis, has provided the first and only assessment of SRM geoengineering on the cryosphere, investigating the stability of the Greenland Ice Sheet. This work showed that sunshade geoengineering could help stabilize the Greenland ice sheet despite elevated CO_2 concentrations and that other reduced but still stable configurations of the Greenland ice sheet are possible with weaker sunshade geoengineering. Irvine *et al.* (2012), appendix C, showed how there

is a tension between the goals of mitigating surface air temperature and sea-level rise for a range of possible controls over sunshade geoengineering. Together with Irvine *et al.* (2010), these results suggest that determining an 'optimal' way to implement sunshade geoengineering that would please all regions and actors, would be fraught with difficulties.

The first intercomparison of surface albedo geoengineering schemes using the same model setup was conducted in Irvine *et al.* (2011), Chapter 3 of this thesis, and this was the first time desert geoengineering had been simulated with a GCM. The results of this study highlighted the need for a focus on the regional and seasonal effects of SRM geoengineering and presented worrying results about the effects of desert geoengineering on global precipitation, particularly monsoon precipitation. This study highlighted the risks posed by highly heterogeneous SRM geoengineering schemes, such as desert albedo and cloud albedo geoengineering, which offer control over regional forcing with complex consequences for the climate.

Chapter 4 presents results that will form two papers (yet to be submitted); one on the development and testing of the perturbed parameter ensemble (PPE), and one on sunshade geoengineering with the PPE. The development and testing study will show a PPE that performs similarly to the CMIP3 ensemble which does not include flux-adjustment as most PPEs do. This ensemble should be useful for exploring the role of parametric uncertainty in future climate studies and will provide insight into the consequences of not using flux-adjustment with a PPE. The sunshade geoengineering results of the PPE presented in this thesis, along with the work of Schmidt *et al.* (2012), helped to draw conclusions about which elements of the climate response to sunshade geoengineering are robust and which are uncertain. This work will also contribute to the work of the geoMIP Intercomparison of sunshade geoengineering results to improve our understanding of the consequences of SRM geoengineering.

5.4 Future work

This thesis has investigated the climate effects of a number of SRM geoengineering schemes. A considerable amount of research into SRM geoengineering is ongoing, however there is much to learn. The feasibility and climate consequences of sulphate aerosol and cloud albedo geoengineering schemes have received particular attention

(Niemeier *et al.*, 2011; Rasch *et al.*, 2008a; Korhonen *et al.*, 2010; Pringle *et al.*, 2012). Work is also beginning on testing the robustness of SRM geoengineering GCM results with a multi model ensemble and with the perturbed parameter work in Chapter 4 of this thesis. Despite all this progress, there are many areas of SRM geoengineering that have received little attention. Research into the indirect climate effects of SRM geoengineering, such as on ice sheets and agriculture, is critically important as this provides information on the impacts of SRM geoengineering. Questions remain over the effects of the highly regional climate forcing that some geoengineering schemes can produce, such as desert or cloud albedo geoengineering, and how such regional control over forcing could be used to fine-tune climate (Ban-Weiss and Caldeira, 2010; Jones *et al.*, 2009; Irvine *et al.*, 2011). This section presents a number of extensions to this thesis and other potential research projects that will help improve our understanding of SRM geoengineering.

Coral reefs are under threat from both rising ocean temperatures and the acidification of the ocean (Hoegh-Guldberg *et al.*, 2007); SRM geoengineering may alleviate the threat from rising temperatures but will have little effect on ocean acidification and so may or may not help to preserve coral reefs (Matthews *et al.*, 2009). I am currently collaborating with colleagues at the University of Bristol on the impacts of SRM geoengineering on coral reefs using the UVic model to simulate a range of different sunshade geoengineering scenarios and a model developed by one of my collaborators, which determines the viability of coral reef communities based on environmental conditions (Weaver *et al.*, 2001). The study is not complete but early results suggest that sunshade geoengineering may significantly reduce the threat to coral reefs in vulnerable areas. This work will be continued and published in due course.

As discussed in Section 5.4 the geoMIP G1 and G2 work with the PPE will be developed further and prepared as a separate paper. This work will expand on the initial analysis presented in Chapter 4, exploring what the more or less certain aspects of the sunshade response are. Additional analysis on specific regional responses will also be conducted in a similar manner to the surface albedo geoengineering analysis in Chapter 3, e.g. analyzing the monsoon, Arctic, or European summer time responses. A more thorough comparison between the PPE and the other geoMIP GCMs will be conducted as well to determine how well the results agree and to

test the value of the PPE developed in this thesis as a tool for simulating GCM uncertainty.

Participation in the geoMIP project will allow access to the growing geoMIP multi-model dataset which will be a great resource for investigating the climate effects and other consequences of sunshade and sulphate aerosol geoengineering. The project will produce a number of group papers analyzing the response of the entire ensemble and will also provide an opportunity for in-depth analysis of specific impacts and to apply off-line models. Off-line ice sheet modelling combined with glacier surface mass balance modelling and an analysis of the GCM thermosteric sea-level rise would build on the sea-level rise and Greenland Ice Sheet analysis in Chapter 2, providing a thorough assessment of the potential for SRM geoengineering to mitigate sea-level rise. Assessments of the effects of SRM geoengineering on Net Primary Productivity, vegetation, and on agriculture are also important in determining the impacts on ecosystems and human populations. The geoMIP dataset will allow a detailed examination of the changes in extremes in climate, e.g. dry spells, cold snaps, etc., using the same models that will be used in the IPCC AR5 to assess the effects of global warming induced changes in these extremes. GeoMIP could also be used to help answer the question of how easy it would be to determine whether SRM geoengineering had changed the climate or not. Using pseudo-observations of a 'perfect model' from the ensemble and comparing these to the ensemble predictions would allow a mock detection and attribution study to be conducted.

An investigation into the limits of SRM geoengineering using idealized studies is necessary to reveal the consequences of the potential highly regional control over forcing that schemes such as desert geoengineering and cloud albedo geoengineering could offer. To understand the limits of SRM geoengineering the question of how the effects of regional schemes combine is important and whether they would combine linearly as some studies seem to suggest (Jones *et al.*, 2009). Whether or not regional geoengineering forcings combine in a simple way, they may offer a large degree of control over the regional climate response across the world. This begs the question of whether it would be possible to reverse-engineer particular climate outcomes, another question which further idealized SRM geoengineering studies may help to answer. Uncertainty in the response to globally uniform geoengineering is being investigated but a similar effort is also needed to help understand the consequences

of highly heterogeneous geoengineering forcing. The desert albedo geoengineering results of Chapter 3 suggest that very large regional changes in precipitation would occur with a general drying of the continents but research is needed to find out how much these results would differ in a multi-model ensemble.

The potential for SRM geoengineering as a means to address climate change has drawn a lot of attention and it is vital to provide solid scientific inputs into the debates about the economic, social and political consequences of SRM geoengineering. Some work to provide a social context to SRM geoengineering results has been made with studies investigating cost-functions to determine the 'quality' of the climate mitigation of SRM geoengineering (Moreno-Cruz *et al.*, 2011). In Chapter 2 the 'novel' climate metric and the population weighting of climate changes were also attempts to provide a social science context to the climate model data. More work can be done to develop cost-functions and metrics to provide insight into the consequences of geoengineering, for example a metric which distinguishes between increases and decreases in precipitation in dry regions would help to explore how the politics of SRM geoengineering may shape up. Work can also be done to frame issues for ethical discussion, for example I conducted work with an ethicist on the ethical and technical problems posed by trying to develop a just system of compensation for the harms of SRM geoengineering. Ethical and other considerations can also help define the inputs for scientific and economic assessments of SRM geoengineering, as will be detailed by a study being prepared which I have contributed to. As the issues raised by SRM geoengineering are not solely scientific, inter-disciplinary research is essential to provide a complete picture of the consequences of this radical approach to addressing climate change.

5.5 Final thoughts

SRM geoengineering seems to offer a partial solution to the problems of anthropogenic greenhouse gas emissions, potentially ameliorating some of the worst effect of global warming but leaving some problems unaddressed and introducing new problems. However, SRM geoengineering will not exist in a vacuum; some suggest SRM geoengineering could be used instead of mitigation as it would be cheaper (Barrett, 2008), and some worry that there may be international tension over the

type and scale of SRM geoengineering (Schneider, 2008; Victor, 2008; Virgoe, 2009). This temptation to use SRM geoengineering as an easy way out may prove too much for policy makers and these partial solutions for the climate change may be relied on heavily to the detriment of the natural and human environment. More worryingly, the potential for international tension over the management of the planet's climate may make the political dangers of SRM geoengineering far greater than the physical risks that these schemes pose. If it came to the worst, the direct effects and subsequent climate impacts of an all-out nuclear war are far scarier than the climate effects of SRM geoengineering (Robock *et al.*, 2007).

SRM geoengineering is not a single option but potentially offers a range of choices over the type of geoengineering deployed, the strength, and the region affected by the forcing. Regional geoengineering schemes which offer control over radiative forcing over a large and flexible area, and which could be turned on or off quickly, such as cloud albedo modification, cirrus-cloud geoengineering (or 'smart' aerosols if they are possible); offer a large amount of influence over the climate. If our understanding of the climate and of these technologies improves sufficiently, SRM geoengineering is likely to offer much more control than simply the ability to set the global mean temperature and precipitation. These technologies, combined with an advanced understanding of the climate, may make it possible to tweak regional and seasonal climate across the planet, thus controlling who benefits and who loses out as a result. Advanced SRM geoengineering has the potential to radically alter our relationship with the planet and put enormous power into the hands of those with the controls.

If such SRM technology is possible, the old military adage 'capabilities affect intentions' bears consideration. Will the capability to modify the climate, change our intentions from the narrow goal of ameliorating the effects of global warming to something else? If we could choose between a climate very similar to the pre-industrial and an unnatural one which has less risk of floods, droughts, hurricanes, etc. than the pre-industrial, would we have a moral responsibility to protect people and choose the less harmful but more unnatural climate? A broader argument for further meddling could be made about the need for a climate better suited to greater agricultural productivity or economic growth. Many people rail against this idea of 'playing god' with the climate and believe we should deal responsibly with CO_2 emissions despite the cost and face up to the consequences as they come.

Consideration of the implications of SRM geoengineering brings to the fore the very important question: How do we want to live on this planet?

Climate research, like that in this thesis, can help identify the physical risks and benefits of SRM geoengineering and inform the kinds of geo-political hazards and moral choices that control over the climate may pose. It seems to me, that the potential for control over the climate raises more pressing ethical and political questions than scientific questions. However, it must be borne in mind that SRM geoengineering is a potential response to a failure to address anthropogenic emissions of greenhouse gases that has not yet occurred. A concerted effort to reduce the human footprint on the planet still offers the most complete solution to global warming and should be pursued vigorously.

Bibliography

Akbari, H., Menon, S., and Rosenfeld, A. (2009). Global cooling: increasing world-wide urban albedos to offset co2. *Climatic Change*, **94**(3), 275–286.

Albrecht, B. A. (1989). Aerosols, cloud microphysics, and fractional cloudiness. *Science*, **245**(4923), 1227–1230.

Alley, R. B., Clark, P. U., Huybrechts, P., and Joughin, I. (2005). Ice-sheet and sea-level changes. *Science*, **310**(5747), 456–460.

Ammann, C. M., Washington, W. M., Meehl, G. A., Buja, L., and Teng, H. Y. (2010). Climate engineering through artificial enhancement of natural forcings: Magnitudes and implied consequences. *Journal of Geophysical Research-Atmospheres*, **115**.

Andreae, M. O., Jones, C. D., and Cox, P. M. (2005). Strong present-day aerosol cooling implies a hot future. *Nature*, **435**(7046), 1187–1190.

Andrews, T., Forster, P. M., and Gregory, J. M. (2009). A surface energy perspective on climate change. *Journal of Climate*, **22**(10), 2557–2570.

Andrews, T., Forster, P. M., Boucher, O., Bellouin, N., and Jones, A. (2010). Precipitation, radiative forcing and global temperature change. *Geophys. Res. Lett.*, **37**(14), L14701.

Angel, R. (2006). Feasibility of cooling the earth with a cloud of small spacecraft near the inner lagrange point (l1). *Proceedings of the National Academy of Sciences of the United States of America*, **103**(46), 17184–17189.

Anthoff, D., Hepburn, C., and Tol, R. S. J. (2009). Equity weighting and the marginal damage costs of climate change. *Ecological Economics*, **68**(3), 836–849.

Archer, D. (2007). Methane hydrate stability and anthropogenic climate change. *Biogeosciences*, **4**(4), 521–544.

Archer, D., Eby, M., Brovkin, V., Ridgwell, A., Cao, L., Mikolajewicz, U., Caldeira, K., Matsumoto, K., Munhoven, G., Montenegro, A., and Tokos, K. (2009). *Atmospheric Lifetime of Fossil Fuel Carbon Dioxide*, volume 37 of *Annual Review of Earth and Planetary Sciences*, pages 117–134.

Arndt, D. S., Blunden, J., and Baringer, M. O. (2011). State of the climate in 2010. *Bulletin of the American Meteorological Society*, **92**(6), S17–+.

Azar, C., Lindgren, K., Obersteiner, M., Riahi, K., van Vuuren, D. P., den Elzen, K. M. G. J., Moellersten, K., and Larson, E. D. (2010). The feasibility of low co(2) concentration targets and the role of bio-energy with carbon capture and storage (beccs). *Climatic Change*, **100**(1), 195–202.

Bala, G., Duffy, P. B., and Taylor, K. E. (2008). Impact of geoengineering schemes on the global hydrological cycle. *Proceedings of the National Academy of Sciences of the United States of America*, **105**(22), 7664–7669.

Bala, G., Caldeira, K., Nemani, R., Cao, L., Ban-Weiss, G., and Shin, H.-J. (2010a). Albedo enhancement of marine clouds to counteract global warming: impacts on the hydrological cycle. *Climate Dynamics*, pages 1–17.

Bala, G., Caldeira, K., and Nemani, R. (2010b). Fast versus slow response in climate change: implications for the global hydrological cycle. *Climate Dynamics*, **35**(2), 423–434.

Bamber, J. L., Layberry, R. L., and Gogineni, S. (2001). A new ice thickness and bed data set for the greenland ice sheet 1. measurement, data reduction, and errors. *Journal of Geophysical Research-Atmospheres*, **106**(D24), 33773–33780.

Ban-Weiss, G. A. and Caldeira, K. (2010). Geoengineering as an optimization problem. *Environmental Research Letters*, **5**(3).

Bao, L. and Trachtenberg, M. C. (2006). Facilitated transport of co2 across a liquid membrane: Comparing enzyme, amine, and alkaline. *Journal of Membrane Science*, **280**(1-2), 330–334.

Barrett, S. (2008). The incredible economics of geoengineering. *Environmental & Resource Economics*, **39**(1), 45–54.

Bengtsson, L., Hodges, K., Roeckner, E., and Brokopf, R. (2006). On the natural variability of the pre-industrial european climate. *Climatic Dynamics*, **27**(7-8), 743–760.

Betts, R. A., Falloon, P. D., Goldewijk, K. K., and Ramankutty, N. (2007a). Biogeophysical effects of land use on climate: Model simulations of radiative forcing and large-scale temperature change. *Agricultural and Forest Meteorology*, **142**(2-4), 216–233.

Betts, R. A., Boucher, O., Collins, M., Cox, P. M., Falloon, P. D., Gedney, N., Hemming, D. L., Huntingford, C., Jones, C. D., Sexton, D. M. H., and Webb, M. J. (2007b). Projected increase in continental runoff due to plant responses to increasing carbon dioxide. *Nature*, **448**(7157), 1037–U5.

Boucher, O., Jones, A., and Betts, R. A. (2009). Climate response to the physiological impact of carbon dioxide on plants in the met office unified model hadcm3. *Climate Dynamics*, **32**(2-3), 237–249.

Bougamont, M., Bamber, J. L., Ridley, J. K., Gladstone, R. M., Greuell, W., Hanna, E., Payne, A. J., and Rutt, I. (2007). Impact of model physics on estimating the surface mass balance of the greenland ice sheet. *Geophysical Research Letters*, **34**(17), L17501.

Boyd, P. W. (2008). Implications of large-scale iron fertilization of the oceans. *Marine Ecology Progress Series*, **364**, 213–218.

Boyd, P. W., Jickells, T., Law, C. S., Blain, S., Boyle, E. A., Buesseler, K. O., Coale, K. H., Cullen, J. J., de Baar, H. J. W., Follows, M., Harvey, M., Lancelot, C., Levasseur, M., Owens, N. P. J., Pollard, R., Rivkin, R. B., Sarmiento, J., Schoemann, V., Smetacek, V., Takeda, S., Tsuda, A., Turner, S., and Watson, A. J. (2007). Mesoscale iron enrichment experiments 1993-2005: Synthesis and future directions. *Science*, **315**(5812), 612–617.

Bretz, S., Akbari, H., and Rosenfeld, A. (1998). Practical issues for using solar-reflective materials to mitigate urban heat islands. *Atmospheric Environment*, **32**(1), 95–101.

Brierley, C. M., Collins, M., and Thorpe, A. J. (2010). The impact of perturbations to ocean-model parameters on climate and climate change in a coupled model. *Climate Dynamics*, **34**(2-3), 325–343.

Brohan, P., Kennedy, J. J., Harris, I., Tett, S. F. B., and Jones, P. D. (2006). Uncertainty estimates in regional and global observed temperature changes: A new data set from 1850. *Journal of Geophysical Research-Atmospheres*, **111**(D12).

Brovkin, V., Petoukhov, V., Claussen, M., Bauer, E., Archer, D., and Jaeger, C. (2009). Geoengineering climate by stratospheric sulfur injections: Earth system vulnerability to technological failure. *Climatic Change*, **92**(3-4), 243–259.

Bryden, H. L., Candela, J., and Kinder, T. H. (1994). Exchange through the strait of gibraltar. *Progress in Oceanography*, **33**(3), 201–248.

Burke, E. J. and Brown, S. J. (2008). Evaluating uncertainties in the projection of future drought. *Journal of Hydrometeorology*, **9**(2), 292–299.

Burke, E. J., Brown, S. J., and Christidis, N. (2006). Modeling the recent evolution of global drought and projections for the twenty-first century with the hadley centre climate model. *Journal of Hydrometeorology*, **7**(5), 1113–1125.

Caldeira, K. (2008). Geoengineering: Perhaps palliative medicine. *Geotimes*, **53**(7), 59–59.

Canadell, J. G. and Raupach, M. R. (2008). Managing forests for climate change mitigation. *Science*, **320**(5882), 1456–1457.

Cao, L. and Caldeira, K. (2008). Atmospheric co2 stabilization and ocean acidification. *Geophysical Research Letters*, **35**(19).

Cao, L. and Caldeira, K. (2010). Atmospheric carbon dioxide removal: long-term consequences and commitment. *Environmental Research Letters*, **5**(2).

Cao, L., Bala, G., Caldeira, K., Nemani, R., and Ban-Weiss, G. (2010). Importance of carbon dioxide physiological forcing to future climate change. *Proceedings of the National Academy of Sciences of the United States of America*, **107**(21), 9513–9518.

Cattle, H. and Crossley, J. (1995). Modeling arctic climate-change. *Philosophical Transactions of the Royal Society of London Series a-Mathematical Physical and Engineering Sciences*, **352**(1699), 201–213.

Cazenave, A., Dominh, K., Guinehut, S., Berthier, E., Llovel, W., Ramillien, G., Ablain, M., and Larnicol, G. (2009). Sea level budget over 2003-2008: A reevaluation from grace space gravimetry, satellite altimetry and argo. *Global and Planetary Change*, **65**(1-2), 83–88.

CEC (2007). Limiting global climate change to 2 degrees celcius: The way ahead for 2020 and beyond.

Chen, T., Rossow, W. B., and Zhang, Y. C. (2000). Radiative effects of cloud-type variations. *Journal of Climate*, **13**(1), 264–286.

Chen, W. T., Nenes, A., Liao, H., Adams, P. J., Li, J. L. F., and Seinfeld, J. H. (2010). Global climate response to anthropogenic aerosol indirect effects: Present day and year 2100. *Journal of Geophysical Research-Atmospheres*, **115**.

Cole-Dai, J., Ferris, D., Lanciki, A., Savarino, J., Baroni, M., and Thiemens, M. H. (2009). Cold decade (ad 1810-1819) caused by tambora (1815) and another (1809) stratospheric volcanic eruption. *Geophysical Research Letters*, **36**, 6.

Collins, M., Booth, B. B. B., Harris, G. R., Murphy, J. M., Sexton, D. M. H., and Webb, M. J. (2006). Towards quantifying uncertainty in transient climate change. *Climate Dynamics*, **27**(2-3), 127–147.

Collins, M., Brierley, C. M., MacVean, M., Booth, B. B. B., and Harris, G. R. (2007). The sensitivity of the rate of transient climate change to ocean physics perturbations. *Journal of Climate*, **20**(10), 2315–2320.

Collins, M., Booth, B., Bhaskaran, B., Harris, G., Murphy, J., Sexton, D., and Webb, M. (2010a). Climate model errors, feedbacks and forcings: a comparison of perturbed physics and multi-model ensembles. *Climate Dynamics*, pages 1–30.

Collins, M., An, S. I., Cai, W. J., Ganachaud, A., Guilyardi, E., Jin, F. F., Jochum, M., Lengaigne, M., Power, S., Timmermann, A., Vecchi, G., and Wittenberg, A. (2010b). The impact of global warming on the tropical pacific ocean and el nino. *Nature Geoscience*, **3**(6), 391–397.

Collins, W. J., Bellouin, N., Doutriaux-Boucher, M., Gedney, N., Halloran, P., Hinton, T., Hughes, J., Jones, C. D., Joshi, M., Liddicoat, S., Martin, G., O'Connor, F., Rae, J., Senior, C., Sitch, S., Totterdell, I., Wiltshire, A., and Woodward, S. (2011). Development and evaluation of an earth-system model hadgem2. *Geosci. Model Dev. Discuss.*, **4**(2), 997–1062.

Colman, R. A. (2001). On the vertical extent of atmospheric feedbacks. *Climate Dynamics*, **17**(5-6), 391–405.

Costa, M. H., Yanagi, S. N. M., Souza, P., Ribeiro, A., and Rocha, E. J. P. (2007). Climate change in amazonia caused by soybean cropland expansion, as compared to caused by pastureland expansion. *Geophysical Research Letters*, **34**(7).

Costello, A., Abbas, M., Allen, A., Ball, S., Bell, S., Bellamy, R., Friel, S., Groce, N., Johnson, A., Kett, M., Lee, M., Levy, C., Maslin, M., McCoy, D., McGuire, B., Montgomery, H., Napier, D., Pagel, C., Patel, J., Antonio, J., de Oliveira, P., Redclift, N., Rees, H., Rogger, D., Scott, J., Stephenson, J., Twigg, J., Wolff, J., and Patterson, C. (2009). Managing the health effects of climate change. *Lancet*, **373**(9676), 1693–1733.

Covey, C., AchutaRao, K. M., Cubasch, U., Jones, P., Lambert, S. J., Mann, M. E., Phillips, T. J., and Taylor, K. E. (2003). An overview of results from the coupled model intercomparison project. *Global and Planetary Change*, **37**(1-2), 103–133.

Cox, P. M., Betts, R. A., Bunton, C. B., Essery, R. L. H., Rowntree, P. R., and Smith, J. (1999). The impact of new land surface physics on the gcm simulation of climate and climate sensitivity. *Climate Dynamics*, **15**(3), 183–203.

Cox, P. M., Betts, R. A., Jones, C. D., Spall, S. A., and Totterdell, I. J. (2000). Acceleration of global warming due to carbon-cycle feedbacks in a coupled climate model. *Nature*, **408**(6809), 184–187.

Crutzen, P. J. (2006). Albedo enhancement by stratospheric sulfur injections: A contribution to resolve a policy dilemma? *Climatic Change*, **77**(3-4), 211–219.

Dessler, A. (2009). Energy for air capture. *Nature Geoscience*, **2**(12), 811–811.

Dockery, D. W., Pope, C. A., Xu, X. P., Spengler, J. D., Ware, J. H., Fay, M. E., Ferris, B. G., and Speizer, F. E. (1993). An association between air-pollution and

mortality in 6 united-states cities. *New England Journal of Medicine*, **329**(24), 1753–1759.

Domingues, C. M., Church, J. A., White, N. J., Gleckler, P. J., Wijffels, S. E., Barker, P. M., and Dunn, J. R. (2008). Improved estimates of upper-ocean warming and multi-decadal sea-level rise. *Nature*, **453**(7198), 1090–U6.

Doney, S. C., Fabry, V. J., Feely, R. A., and Kleypas, J. A. (2009). Ocean acidification: The other co2 problem. *Annual Review of Marine Science*, **1**, 169–192.

Doughty, C., Field, C., and McMillan, A. (2011). Can crop albedo be increased through the modification of leaf trichomes, and could this cool regional climate? *Climatic Change*, **104**(2), 379–387.

Dowsett, H. J., Haywood, A. M., Valdes, P. J., Robinson, M. M., Lunt, D. J., Hill, D., Stoll, D. K., and Foley, K. M. (2011). Sea surface temperatures of the mid-piacenzian warm period: A comparison of prism3 and hadcm3. *Palaeogeography Palaeoclimatology Palaeoecology*, **309**(1-2), 83–91.

Edwards, N. R., Cameron, D., and Rougier, J. (2010). Precalibrating an intermediate complexity climate model. *Climate Dynamics*, page (In Press).

Eliseev, A. V. and Mokhov, I. (2009). Estimating the efficiency of mitigating and preventing global warming with scenarios of controlled aerosol emissions into the stratosphere. *Izvestiya Atmospheric and Oceanic Physics*, **45**(2), 221–232.

Essery, R. and Clark, D. B. (2003). Developments in the moses 2 land-surface model for pilps 2e. *Global and Planetary Change*, **38**(1-2), 161–164.

Etheridge, D. M., Steele, L. P., Francey, R. J., and Langenfelds, R. L. (1998). Atmospheric methane between 1000 ad and present: Evidence of anthropogenic emissions and climatic variability. *Journal of Geophysical Research-Atmospheres*, **103**(D13), 15979–15993.

Fahey, T. J., Woodbury, P. B., Battles, J. J., Goodale, C. L., Hamburg, S. P., Ollinger, S. V., and Woodall, C. W. (2010). Forest carbon storage: ecology, management, and policy. *Frontiers in Ecology and the Environment*, **8**(5), 245–252.

Febrero, A., Fernandez, S., Molina-Cano, J. L., and Araus, J. L. (1998). Yield, carbon isotope discrimination, canopy reflectance and cuticular conductance of barley isolines of differing glaucousness. *Journal of Experimental Botany*, **49**(326), 1575–1581.

Feichter, J. and Leisner, T. (2009). Climate engineering: A critical review of approaches to modify the global energy balance. *European Physical Journal-Special Topics*, **176**, 81–92.

Ferraro, A. J., Highwood, E. J., and Charlton-Perez, A. J. (2011). Stratospheric heating by potential geoengineering aerosols. *Geophysical Research Letters*, **38**.

Forster, P. M. D. and Shine, K. P. (2002). Assessing the climate impact of trends in stratospheric water vapor. *Geophysical Research Letters*, **29**(6).

Frame, D. J., Booth, B. B. B., Kettleborough, J. A., Stainforth, D. A., Gregory, J. M., Collins, M., and Allen, M. R. (2005). Constraining climate forecasts: The role of prior assumptions. *Geophysical Research Letters*, **32**(9).

Frame, D. J., Aina, T., Christensen, C. M., Faull, N. E., Knight, S. H. E., Piani, C., Rosier, S. M., Yamazaki, K., Yamazaki, Y., and Allen, M. R. (2009). The climateprediction.net bbc climate change experiment: design of the coupled model ensemble. *Philosophical Transactions of the Royal Society a-Mathematical Physical and Engineering Sciences*, **367**(1890), 855–870.

Friedlingstein, P., Houghton, R. A., Marland, G., Hackler, J., Boden, T. A., Conway, T. J., Canadell, J. G., Raupach, M. R., Ciais, P., and Le Quere, C. (2010). Update on co2 emissions. *Nature Geosci*, **3**(12), 811–812.

Ganachaud, A. and Wunsch, C. (2000). Improved estimates of global ocean circulation, heat transport and mixing from hydrographic data. *Nature*, **408**(6811), 453–457.

Gaskill, A. (2004). Summary of meeting with us doe to discuss geoengineering options to prevent long-term climate change.

Gent, P. R. and McWilliams, J. C. (1990). Isopycnal mixing in ocean circulation models. *Journal of Physical Oceanography*, **20**(1), 150–155.

Glibert, P. M., Azanza, R., Burford, M., Furuya, K., Abal, E., Al-Azri, A., Al-Yamani, F., Andersen, P., Anderson, D. M., Beardall, J., Berg, G. M., Brand, L., Bronk, D., Brookes, J., Burkholder, J. M., Cembella, A., Cochlan, W. P., Collier, J. L., Collos, Y., Diaz, R., Doblin, M., Drennen, T., Dyhrman, S., Fukuyo, Y., Furnas, M., Galloway, J., Graneli, E., Ha, D. V., Hallegraeff, G., Harrison, J., Harrison, P. J., Heil, C. A., Heimann, K., Howarth, R., Jauzein, C., Kana, A. A., Kana, T. M., Kim, H., Kudela, R., Legrand, C., Mallin, M., Mulholland, M., Murray, S., O'Neil, J., Pitcher, G., Qi, Y. Z., Rabalais, N., Raine, R., Seitzinger, S., Salomon, P. S., Solomon, C., Stoecker, D. K., Usup, G., Wilson, J., Yin, K. D., Zhou, M. J., and Zhu, M. Y. (2008). Ocean urea fertilization for carbon credits poses high ecological risks. *Marine Pollution Bulletin*, **56**(6), 1049–1056.

Goes, M., Tuana, N., and Keller, K. (2011). The economics (or lack thereof) of aerosol geoengineering. *Climatic Change*, pages 1–26.

Gordon, C., Cooper, C., Senior, C. A., Banks, H., Gregory, J. M., Johns, T. C., Mitchell, J. F. B., and Wood, R. A. (2000). The simulation of sst, sea ice extents and ocean heat transports in a version of the hadley centre coupled model without flux adjustments. *Climate Dynamics*, **16**(2-3), 147–168.

Govindasamy, B. and Caldeira, K. (2000). Geoengineering earth's radiation balance to mitigate co2-induced climate change. *Geophysical Research Letters*, **27**(14), 2141–2144.

Govindasamy, B., Caldeira, K., and Duffy, P. B. (2003). Geoengineering earth's radiation balance to mitigate climate change from a quadrupling of co2. *Global and Planetary Change*, **37**(1-2), 157–168.

Grant, R. H., Heisler, G. M., Gao, W., and Jenks, M. (2003). Ultraviolet leaf reflectance of common urban trees and the prediction of reflectance from leaf surface characteristics. *Agricultural and Forest Meteorology*, **120**(1-4), 127–139.

Gray, M. L., Champagne, K. J., Fauth, D., Baltrus, J. P., and Pennline, H. (2008). Performance of immobilized tertiary amine solid sorbents for the capture of carbon dioxide. *International Journal of Greenhouse Gas Control*, **2**(1), 3–8.

Gregoire, L., Valdes, P., Payne, A., and Kahana, R. (2010). Optimal tuning of a gcm using modern and glacial constraints. *Climate Dynamics*, pages 1–15.

Gregory, D. and Rowntree, P. (1990). A mass flux convection scheme with representation of cloud ensemble characteristics and stability-dependent closure. *Monthly Weather Review*, **118**(7), 1483–1506.

Gregory, J. M. and Huybrechts, P. (2006). Ice-sheet contributions to future sea-level change. *Philosophical Transactions of the Royal Society a-Mathematical Physical and Engineering Sciences*, **364**(1844), 1709–1731.

Gregory, J. M., Stott, P. A., Cresswell, D. J., Rayner, N. A., Gordon, C., and Sexton, D. M. H. (2002). Recent and future changes in arctic sea ice simulated by the hadcm3 aogcm. *Geophysical Research Letters*, **29**(24).

Gregory, J. M., Huybrechts, P., and Raper, S. C. B. (2004a). Climatology - threatened loss of the greenland ice-sheet. *Nature*, **428**(6983), 616–616.

Gregory, J. M., Ingram, W. J., Palmer, M. A., Jones, G. S., Stott, P. A., Thorpe, R. B., Lowe, J. A., Johns, T. C., and Williams, K. D. (2004b). A new method for diagnosing radiative forcing and climate sensitivity. *Geophysical Research Letters*, **31**(3).

Greve, R. (2000). On the response of the greenland ice sheet to greenhouse climate change. *Climatic Change*, **46**(3), 289–303.

GRUMP (2005). Center for international earth science information network (ciesin), columbia university; international food policy research institute (ipfri); the world bank; centro internacional de agricultura tropical (ciat).

Gu, L. H., Baldocchi, D. D., Wofsy, S. C., Munger, J. W., Michalsky, J. J., Urbanski, S. P., and Boden, T. A. (2003). Response of a deciduous forest to the mount pinatubo eruption: Enhanced photosynthesis. *Science*, **299**(5615), 2035–2038.

Hamwey, R. (2007). Active amplification of the terrestrial albedo to mitigate climate change: An exploratory study. *Mitigation and Adaptation Strategies for Global Change*, **12**(4), 419–439.

Hansen, J., Sato, M., and Ruedy, R. (1997). Radiative forcing and climate response. *Journal of Geophysical Research-Atmospheres*, **102**(D6), 6831–6864.

Hansen, J., Sato, M., Ruedy, R., Nazarenko, L., Lacis, A., Schmidt, G. A., Russell, G., Aleinov, I., Bauer, M., Bauer, S., Bell, N., Cairns, B., Canuto, V., Chandler, M., Cheng, Y., Del Genio, A., Faluvegi, G., Fleming, E., Friend, A., Hall, T., Jackman, C., Kelley, M., Kiang, N., Koch, D., Lean, J., Lerner, J., Lo, K., Menon, S., Miller, R., Minnis, P., Novakov, T., Oinas, V., Perlwitz, J., Rind, D., Romanou, A., Shindell, D., Stone, P., Sun, S., Tausnev, N., Thresher, D., Wielicki, B., Wong, T., Yao, M., and Zhang, S. (2005). Efficacy of climate forcings. *Journal of Geophysical Research-Atmospheres*, **110**(D18).

Hansen, J., Sato, M., Ruedy, R., Lo, K., Lea, D. W., and Medina-Elizade, M. (2006). Global temperature change. *Proceedings of the National Academy of Sciences of the United States of America*, **103**(39), 14288–14293.

Hansen, J., Sato, M., Ruedy, R., Kharecha, P., Lacis, A., Miller, R., Nazarenko, L., Lo, K., Schmidt, G. A., Russell, G., Aleinov, I., Bauer, S., Baum, E., Cairns, B., Canuto, V., Chandler, M., Cheng, Y., Cohen, A., Del Genio, A., Faluvegi, G., Fleming, E., Friend, A., Hall, T., Jackman, C., Jonas, J., Kelley, M., Kiang, N. Y., Koch, D., Labow, G., Lerner, J., Menon, S., Novakov, T., Oinas, V., Perlwitz, J., Perlwitz, J., Rind, D., Romanou, A., Schmunk, R., Shindell, D., Stone, P., Sun, S., Streets, D., Tausnev, N., Thresher, D., Unger, N., Yao, M., and Zhang, S. (2007). Dangerous human-made interference with climate: a giss modele study. *Atmospheric Chemistry and Physics*, **7**(9), 2287–2312.

Hansen, M. C., Defries, R. S., Townshend, J. R. G., and Sohlberg, R. (2000). Global land cover classification at 1km spatial resolution using a classification tree approach. *International Journal of Remote Sensing*, **21**(6-7), 1331–1364.

Harris, B. M. and Highwood, E. J. (2011). A simple relationship between volcanic sulfate aerosol optical depth and surface temperature change simulated in an atmosphere-ocean general circulation model. *Journal of Geophysical Research-Atmospheres*, **116**.

Harvey, L. D. D. (2008). Mitigating the atmospheric co2 increase and ocean acidi-

fication by adding limestone powder to upwelling regions. *Journal of Geophysical Research-Oceans*, **113**(C4).

Hatfield, J. L. and Carlson, R. E. (1979). Light quality distributions and spectral albedo of 3 maize canopies. *Agricultural Meteorology*, **20**(3), 215–226.

Heckendorn, P. and et al. (2009). The impact of geoengineering aerosols on stratospheric temperature and ozone. *Environmental Research Letters*, **4**(4), 045108.

Held, I. M. and Soden, B. J. (2000). Water vapor feedback and global warming. *Annual Review of Energy and the Environment*, **25**, 441–475.

Held, I. M., Delworth, T. L., Lu, J., Findell, K. L., and Knutson, T. R. (2005). Simulation of sahel drought in the 20th and 21st centuries. *Proceedings of the National Academy of Sciences of the United States of America*, **102**(50), 17891–17896.

Hinzman, L. D., Bettez, N. D., Bolton, W. R., Chapin, F. S., Dyurgerov, M. B., Fastie, C. L., Griffith, B., Hollister, R. D., Hope, A., Huntington, H. P., Jensen, A. M., Jia, G. J., Jorgenson, T., Kane, D. L., Klein, D. R., Kofinas, G., Lynch, A. H., Lloyd, A. H., McGuire, A. D., Nelson, F. E., Oechel, W. C., Osterkamp, T. E., Racine, C. H., Romanovsky, V. E., Stone, R. S., Stow, D. A., Sturm, M., Tweedie, C. E., Vourlitis, G. L., Walker, M. D., Walker, D. A., Webber, P. J., Welker, J. M., Winker, K., and Yoshikawa, K. (2005). Evidence and implications of recent climate change in northern alaska and other arctic regions. *Climatic Change*, **72**(3), 251–298.

Hoegh-Guldberg, O., Mumby, P. J., Hooten, A. J., Steneck, R. S., Greenfield, P., Gomez, E., Harvell, C. D., Sale, P. F., Edwards, A. J., Caldeira, K., Knowlton, N., Eakin, C. M., Iglesias-Prieto, R., Muthiga, N., Bradbury, R. H., Dubi, A., and Hatziolos, M. E. (2007). Coral reefs under rapid climate change and ocean acidification. *Science*, **318**(5857), 1737–1742.

Hohenegger, C., Brockhaus, P., and Schar, C. (2008). Towards climate simulations at cloud-resolving scales. *Meteorologische Zeitschrift*, **17**(4), 383–394.

Holmes, M. G. and Keiller, D. R. (2002). Effects of pubescence and waxes on the re-

flectance of leaves in the ultraviolet and photosynthetic wavebands: a comparison of a range of species. *Plant Cell and Environment*, **25**(1), 85–93.

Hutter, K. (1983). *Theoretical Glaciology: Mathematical Approaches to Geophysics*. D. Reidel, Dordrecht, Netherlands.

Huybrechts, P. and de Wolde, J. (1999). The dynamic response of the greenland and antarctic ice sheets to multiple-century climatic warming. *Journal of Climate*, **12**(8), 2169–2188.

IPCC (2007). *Climate Change 2007: The Physical Science Basis*, page 996 pp. Cambridge University Press, Cambridge.

Irvine, P. and Ridgwell, A. (2009). 'geoengineering' - taking control of our planet's climate. *Science Progress*, **92**(2), 139–162.

Irvine, P. J., Lunt, D. J., Stone, E. J., and Ridgwell, A. (2009). The fate of the greenland ice sheet in a geoengineered, high co2 world. *Environmental Research Letters*, **4**(4).

Irvine, P. J., Ridgwell, A., and Lunt, D. J. (2010). Assessing the regional disparities in geoengineering impacts. *Geophysical Research Letters*, **37**.

Irvine, P. J., Ridgwell, A., and Lunt, D. J. (2011). Climatic effects of surface albedo geoengineering. *J. Geophys. Res.*, **116**(D24), D24112.

Irvine, P. J., Sriver, R. L., and Keller, K. (2012). Tension between reducing sea-level rise and global warming through solar radiation management. *Nature Clim. Change*, **advance online publication**.

Jacob, D., Barring, L., Christensen, O. B., Christensen, J. H., de Castro, M., Deque, M., Giorgi, F., Hagemann, S., Lenderink, G., Rockel, B., Sanchez, E., Schar, C., Seneviratne, S. I., Somot, S., van Ulden, A., and van den Hurk, B. (2007). An inter-comparison of regional climate models for europe: model performance in present-day climate. *Climatic Change*, **81**, 31–52.

Jamieson, D. (1996). Ethics and intentional climate change. *Climatic Change*, **33**(3), 323–336.

Jiang, D. B., Wang, H. J., and Lang, X. M. (2005). Evaluation of east asian climatology as simulated by seven coupled models. *Advances in Atmospheric Sciences*, **22**(4), 479–495.

Johannessen, O. M., Bengtsson, L., Miles, M. W., Kuzmina, S. I., Semenov, V. A., Alekseev, G. V., Nagurnyi, A. P., Zakharov, V. F., Bobylev, L. P., Pettersson, L. H., Hasselmann, K., and Cattle, A. P. (2004). Arctic climate change: observed and modelled temperature and sea-ice variability. *Tellus Series a-Dynamic Meteorology and Oceanography*, **56**(4), 328–341.

Johns, T. C., Gregory, J. M., Ingram, W. J., Johnson, C. E., Jones, A., Lowe, J. A., Mitchell, J. F. B., Roberts, D. L., Sexton, D. M. H., Stevenson, D. S., Tett, S. F. B., and Woodage, M. J. (2003). Anthropogenic climate change for 1860 to 2100 simulated with the hadcm3 model under updated emissions scenarios. *Climate Dynamics*, **20**(6), 583–612.

Johnson, B. D. and Cooke, R. C. (1981). Generation of stabilized microbubbles in seawater. *Science*, **213**(4504), 209–211.

Jones, A., Haywood, J., and Boucher, O. (2009). Climate impacts of geoengineering marine stratocumulus clouds. *Journal of Geophysical Research-Atmospheres*, **114**, 9.

Jones, A., Haywood, J., Boucher, O., Kravitz, B., and Robock, A. (2010). Geoengineering by stratospheric so2 injection: results from the met office hadgem(2) climate model and comparison with the goddard institute for space studies modele. *Atmospheric Chemistry and Physics*, **10**(13), 5999–6006.

Jones, A., Haywood, J., and Boucher, O. (2011a). A comparison of the climate impacts of geoengineering by stratospheric so2 injection and by brightening of marine stratocumulus cloud. *Atmospheric Science Letters*, **12**(2), 176–183.

Jones, C. D., Hughes, J. K., Bellouin, N., Hardiman, S. C., Jones, G. S., Knight, J., Liddicoat, S., O'Connor, F. M., Andres, R. J., Bell, C., Boo, K. O., Bozzo, A., Butchart, N., Cadule, P., Corbin, K. D., Doutriaux-Boucher, M., Friedlingstein, P., Gornall, J., Gray, L., Halloran, P. R., Hurtt, G., Ingram, W. J., Lamarque, J. F., Law, R. M., Meinshausen, M., Osprey, S., Palin, E. J., Parsons Chini, L.,

Raddatz, T., Sanderson, M. G., Sellar, A. A., Schurer, A., Valdes, P., Wood, N., Woodward, S., Yoshioka, M., and Zerroukat, M. (2011b). The hadgem2-es implementation of cmip5 centennial simulations. *Geoscientific Model Development*, **4**(3), 543–570.

Jones, P. D., New, M., Parker, D. E., Martin, S., and Rigor, I. G. (1999). Surface air temperature and its changes over the past 150 years. *Reviews of Geophysics*, **37**(2), 173–199.

Joseph, R. and Nigam, S. (2006). Enso evolution and teleconnections in ipcc's twentieth-century climate simulations: Realistic representation? *Journal of Climate*, **19**(17), 4360–4377.

Joseph, R. and Zeng, N. (2011). Seasonally modulated tropical drought induced by volcanic aerosol. *Journal of Climate*, **24**(8), 2045–2060.

Joshi, M. M., Webb, M. J., Maycock, A. C., and Collins, M. (2010). Stratospheric water vapour and high climate sensitivity in a version of the hadsm3 climate model. *Atmospheric Chemistry and Physics*, **10**(15), 7161–7167.

Keith, D. W. (2000). Geoengineering the climate: History and prospect. *Annual Review of Energy and the Environment*, **25**, 245–284.

Keith, D. W. (2009). Why capture co2 from the atmosphere? *Science*, **325**(5948), 1654–1655.

Keith, D. W. (2010). Photophoretic levitation of engineered aerosols for geoengineering. *Proceedings of the National Academy of Sciences of the United States of America*, **107**(38), 16428–16431.

Keith, D. W., Ha-Duong, M., and Stolaroff, J. K. (2006). Climate strategy with co2 capture from the air. *Climatic Change*, **74**(1-3), 17–45.

Keller, K. and McInerney, D. (2008). The dynamics of learning about a climate threshold. *Climate Dynamics*, **30**(2-3), 321–332.

Khairoutdinov, M., Randall, D., and DeMott, C. (2005). Simulations of the atmospheric general circulation using a cloud-resolving model as a superparameterization of physical processes. *Journal of the Atmospheric Sciences*, **62**(7), 2136–2154.

Kiehl, J. T. (2007). Twentieth century climate model response and climate sensitivity. *Geophys. Res. Lett.*, **34**(22), L22710.

Kimoto, M., Yasutomi, N., Yokoyama, C., and Emori, S. (2005). Projected changes in precipitation characteristics around japan under the global warming. *SOLA*, **1**, 85–88.

Kirchner, I., Stenchikov, G. L., Graf, H. F., Robock, A., and Antuna, J. C. (1999). Climate model simulation of winter warming and summer cooling following the 1991 mount pinatubo volcanic eruption. *Journal of Geophysical Research-Atmospheres*, **104**(D16), 19039–19055.

Knight, C. G., Knight, S. H. E., Massey, N., Aina, T., Christensen, C., Frame, D. J., Kettleborough, J. A., Martin, A., Pascoe, S., Sanderson, B., Stainforth, D. A., and Allen, M. R. (2007). Association of parameter, software, and hardware variation with large-scale behavior across 57,,000 climate models. *Proceedings of the National Academy of Sciences of the United States of America*, **104**(30), 12259–12264.

Knutti, R. (2010). The end of model democracy? *Climatic Change*, **102**(3-4), 395–404.

Korhonen, H., Carslaw, K. S., and Romakkaniemi, S. (2010). Enhancement of marine cloud albedo via controlled sea spray injections: a global model study of the influence of emission rates, microphysics and transport. *Atmospheric Chemistry and Physics*, **10**(9), 4133–4143.

Krabill, W., Hanna, E., Huybrechts, P., Abdalati, W., Cappelen, J., Csatho, B., Frederick, E., Manizade, S., Martin, C., Sonntag, J., Swift, R., Thomas, R., and Yungel, J. (2004). Greenland ice sheet: Increased coastal thinning. *Geophysical Research Letters*, **31**(24), L24402.

Kravitz, B., Robock, A., Oman, L., Stenchikov, G., and Marquardt, A. B. (2009). Sulfuric acid deposition from stratospheric geoengineering with sulfate aerosols. *Journal of Geophysical Research-Atmospheres*, **114**, 7.

Kravitz, B., Robock, A., Boucher, O., Schmidt, H., Taylor, K. E., Stenchikov, G.,

and Schulz, M. (2011). The geoengineering model intercomparison project (geomip). *Atmospheric Science Letters*, pages n/a–n/a.

Kravitz, B., Robock, A., Shindell, D. T., and Miller, M. A. (in press). Sensitivity of stratospheric geoengineering with black carbon to aerosol size and altitude of injection. *J. Geophys. Res.*

Kripalani, R. H., Oh, J. H., and Chaudhari, H. S. (2007). Response of the east asian summer monsoon to doubled atmospheric co2: Coupled climate model simulations and projections under ipcc ar4. *Theoretical and Applied Climatology*, **87**(1-4), 1–28.

Kyle, J. L. and Harris, E. (2008). *Global Spread and Persistence of Dengue*, volume 62 of *Annual Review of Microbiology*, pages 71–92.

Lackner, K. S. (2009). Capture of carbon dioxide from ambient air. *European Physical Journal-Special Topics*, **176**, 93–106.

Lambert, F. H. and Webb, M. J. (2008). Dependency of global mean precipitation on surface temperature. *Geophysical Research Letters*, **35**(16).

LandScanTM (2007). Global population database.

Latham, J. (1990). Control of global warming. *Nature*, **347**(6291), 339–340.

Latham, J., Rasch, P., Chen, C. C., Kettles, L., Gadian, A., Gettelman, A., Morrison, H., Bower, K., and Choularton, T. (2008). Global temperature stabilization via controlled albedo enhancement of low-level maritime clouds. *Philosophical Transactions of the Royal Society a-Mathematical Physical and Engineering Sciences*, **366**(1882), 3969–3987.

Le Quere, C., Raupach, M. R., Canadell, J. G., Marland, G., Bopp, L., Ciais, P., Conway, T. J., Doney, S. C., Feely, R. A., Foster, P., Friedlingstein, P., Gurney, K., Houghton, R. A., House, J. I., Huntingford, C., Levy, P. E., Lomas, M. R., Majkut, J., Metzl, N., Ometto, J. P., Peters, G. P., Prentice, I. C., Randerson, J. T., Running, S. W., Sarmiento, J. L., Schuster, U., Sitch, S., Takahashi, T., Viovy, N., van der Werf, G. R., and Woodward, F. I. (2009). Trends in the sources and sinks of carbon dioxide. *Nature Geoscience*, **2**(12), 831–836.

Leemans, R. and Eickhout, B. (2004). Another reason for concern: regional and global impacts on ecosystems for different levels of climate change. *Global Environmental Change-Human and Policy Dimensions*, **14**(3), 219–228.

Lehmann, J., Gaunt, J., and Rondon, M. (2006). Bio-char sequestration in terrestrial ecosystems a review. *Mitigation and Adaptation Strategies for Global Change*, **11**(2), 395–419.

Lenton, T. M. and Vaughan, N. E. (2009). The radiative forcing potential of different climate geoengineering options. *Atmospheric Chemistry and Physics*, **9**(15), 5539–5561.

Lenton, T. M., Williamson, M. S., Edwards, N. R., Marsh, R., Price, A. R., Ridgwell, A. J., Shepherd, J. G., Cox, S. J., and team, G. (2006). Millennial timescale carbon cycle and climate change in an efficient earth system model. *Climate Dynamics*, **26**(7-8), 687–711.

Lenton, T. M., Held, H., Kriegler, E., Hall, J. W., Lucht, W., Rahmstorf, S., and Schellnhuber, H. J. (2008). Tipping elements in the earth's climate system. *Proceedings of the National Academy of Sciences of the United States of America*, **105**(6), 1786–1793.

Likens, G. E., Driscoll, C. T., and Buso, D. C. (1996). Long-term effects of acid rain: Response and recovery of a forest ecosystem. *Science*, **272**(5259), 244–246.

Liu, H. L., Zhang, X. H., Li, W., Yu, Y. Q., and Yu, R. C. (2004). An eddy-permitting oceanic general circulation model and its preliminary evaluation. *Advances in Atmospheric Sciences*, **21**(5), 675–690.

Lobell, D. B. and Field, C. B. (2007). Global scale climate - crop yield relationships and the impacts of recent warming. *Environmental Research Letters*, **2**(1).

Lohmann, U. and Feichter, J. (2005). Global indirect aerosol effects: a review. *Atmospheric Chemistry and Physics*, **5**, 715–737.

Loveland, T. R., Reed, B. C., Brown, J. F., Ohlen, D. O., Zhu, Z., Yang, L., and Merchant, J. W. (2000). Development of a global land cover characteristics database and igbp discover from 1 km avhrr data. *International Journal of Remote Sensing*, **21**(6-7), 1303–1330.

Lunt, D. J., Ross, I., Hopley, P. J., and Valdes, P. J. (2007). Modelling late oligocene c-4 grasses and climate. *Palaeogeography Palaeoclimatology Palaeoecology*, **251**(2), 239–253.

Lunt, D. J., Foster, G. L., Haywood, A. M., and Stone, E. J. (2008a). Late pliocene greenland glaciation controlled by a decline in atmospheric co2 levels. *Nature*, **454**(7208), 1102–U41.

Lunt, D. J., Ridgwell, A., Valdes, P. J., and Seale, A. (2008b). "sunshade world": A fully coupled gcm evaluation of the climatic impacts of geoengineering. *Geophysical Research Letters*, **35**(12), L12710.

Lunt, D. J., Haywood, A. M., Foster, G. L., and Stone, E. J. (2009). The arctic cryosphere in the mid-pliocene and the future. *Philosophical Transactions of the Royal Society a-Mathematical Physical and Engineering Sciences*, **367**(1886), 49–67.

Machida, T., Nakazawa, T., Fujii, Y., Aoki, S., and Watanabe, O. (1995). Increase in the atmospheric nitrous-oxide concentration during the last 250 years. *Geophysical Research Letters*, **22**(21), 2921–2924.

MacMynowski, D. G., Shin, H.-J., and Caldeira, K. (2011). The frequency response of temperature and precipitation in a climate model. *Geophys. Res. Lett.*, **38**(16), L16711.

Mahmoudkhani, M. and Keith, D. W. (2009). Low-energy sodium hydroxide recovery for co(2) capture from atmospheric air-thermodynamic analysis. *International Journal of Greenhouse Gas Control*, **3**(4), 376–384.

Manabe, S. and Stouffer, R. J. (1996). Low-frequency variability of surface air temperature in a 1000-year integration of a coupled atmosphere-ocean-land surface model. *Journal of Climate*, **9**(2), 376–393.

Mann, M. E. and Park, J. (1994). Global-scale modes of surface-temperature variability on interannual to century timescales. *Journal of Geophysical Research-Atmospheres*, **99**(D12), 25819–25833.

Martin, G. M., Ringer, M. A., Pope, V. D., Jones, A., Dearden, C., and Hinton, T. J. (2006). The physical properties of the atmosphere in the new hadley centre global

environmental model (hadgem1). part i: Model description and global climatology. *Journal of Climate*, **19**(7), 1274–1301.

Masson, D. and Knutti, R. (2011). Climate model genealogy. *Geophys. Res. Lett.*, **38**(8), L08703.

Matthews, H. D. and Caldeira, K. (2007). Transient climate-carbon simulations of planetary geoengineering. *Proceedings of the National Academy of Sciences of the United States of America*, **104**(24), 9949–9954.

Matthews, H. D., Weaver, A. J., Eby, M., and Meissner, K. J. (2003). Radiative forcing of climate by historical land cover change. *Geophysical Research Letters*, **30**(2).

Matthews, H. D., Cao, L., and Caldeira, K. (2009). Sensitivity of ocean acidification to geoengineered climate stabilization. *Geophysical Research Letters*, **36**, 5.

Meehl, G. A. and Tebaldi, C. (2004). More intense, more frequent, and longer lasting heat waves in the 21st century. *Science*, **305**(5686), 994–997.

Meehl, G. A., Stocker, W. D., Friedlingstein, P., Gaye, A. T., Gregory, J. M., Kitoh, A., Knutti, R., Murphy, J. M., Noda, A., Raper, S. C. B., Watterson, I. G., Weaver, A. J., and Zhao, Z. C. (2007a). *Global Climate Projections.* Cambridge University Press, Camridge, United Kingdom and New York, NY, USA.

Meehl, G. A., Covey, C., Delworth, T., Latif, M., McAvaney, B., Mitchell, J. F. B., Stouffer, R. J., and Taylor, K. E. (2007b). The wcrp cmip3 multimodel dataset - a new era in climate change research. *Bulletin of the American Meteorological Society*, **88**, 1383–+.

Meier, M. F., Dyurgerov, M. B., Rick, U. K., O'Neel, S., Pfeffer, W. T., Anderson, R. S., Anderson, S. P., and Glazovsky, A. F. (2007). Glaciers dominate eustatic sea-level rise in the 21st century. *Science*, **317**(5841), 1064–1067.

Meinshausen, M., Smith, S. J., Calvin, K., Daniel, J. S., Kainuma, M. L. T., Lamarque, J. F., Matsumoto, K., Montzka, S. A., Raper, S. C. B., Riahi, K., Thomson, A., Velders, G. J. M., and van Vuuren, D. P. P. (2011). The rcp greenhouse gas concentrations and their extensions from 1765 to 2300. *Climatic Change*, **109**(1-2), 213–241.

Mercado, L. M., Bellouin, N., Sitch, S., Boucher, O., Huntingford, C., Wild, M., and Cox, P. M. (2009). Impact of changes in diffuse radiation on the global land carbon sink. *Nature*, **458**(7241), 1014–1017.

Min, S. K., Park, E. H., and Kwon, W. T. (2004). Future projections of east asian climate change from multi-aogcm ensembles of ipccsres scenario simulations. *Journal of the Meteorological Society of Japan*, **82**(4), 1187–1211.

Mitchell, D. L. and Finnegan, W. (2009). Modification of cirrus clouds to reduce global warming. *Environmental Research Letters*, **4**(4), 045102.

Monteith, J. L. and Unsworth, M. H. (1990). *PRINCIPLES OF ENVIRONMENTAL PHYSICS SECOND EDITION*. Monteith, J. L. And M. H. Unsworth. Principles of Environmental Physics, Second Edition. Xii+291p. Routledge, Chapman and Hall: New York, New York, USA. Illus. Paper.

Moore, J. C., Jevrejeva, S., and Grinsted, A. (2010). Efficacy of geoengineering to limit 21st century sea-level rise. *Proceedings of the National Academy of Sciences of the United States of America*, **107**(36), 15699–15703.

Moreno-Cruz, J., Ricke, K., and Keith, D. (2011). A simple model to account for regional inequalities in the effectiveness of solar radiation management. *Climatic Change*, pages 1–20.

Murphy, D. M. (2009). Effect of stratospheric aerosols on direct sunlight and implications for concentrating solar power. *Environmental Science & Technology*, **43**(8), 2784–2786.

Murphy, J. M., Sexton, D. M. H., Barnett, D. N., Jones, G. S., Webb, M. J., and Collins, M. (2004). Quantification of modelling uncertainties in a large ensemble of climate change simulations. *Nature*, **430**(7001), 768–772.

Nelson, E., Mendoza, G., Regetz, J., Polasky, S., Tallis, H., Cameron, D. R., Chan, K. M. A., Daily, G. C., Goldstein, J., Kareiva, P. M., Lonsdorf, E., Naidoo, R., Ricketts, T. H., and Shaw, M. R. (2009). Modeling multiple ecosystem services, biodiversity conservation, commodity production, and tradeoffs at landscape scales. *Frontiers in Ecology and the Environment*, **7**(1), 4–11.

Niemeier, U., Schmidt, H., and Timmreck, C. (2011). The dependency of geo-engineered sulfate aerosol on the emission strategy. *Atmospheric Science Letters*, **12**(2), 189–194.

Obersteiner, M., Azar, C., Kauppi, P., Mollersten, K., Moreira, J., Nilsson, S., Read, P., Riahi, K., Schlamadinger, B., Yamagata, Y., Yan, J., and van Ypersele, J. P. (2001). Managing climate risk. *Science*, **294**(5543), 786–787.

Oleson, K. W., Bonan, G. B., and Feddema, J. (2010). Effects of white roofs on urban temperature in a global climate model. *Geophys. Res. Lett.*, **37**, L03701.

Oman, L., Robock, A., Stenchikov, G., Schmidt, G. A., and Ruedy, R. (2005). Climatic response to high-latitude volcanic eruptions. *Journal of Geophysical Research-Atmospheres*, **110**(D13).

Oman, L., Robock, A., Stenchikov, G. L., and Thordarson, T. (2006). High-latitude eruptions cast shadow over the african monsoon and the flow of the nile. *Geophysical Research Letters*, **33**(18).

Oppenheimer, M. and Alley, R. B. (2005). Ice sheets, global warming, and article 2 of the unfccc. *Climatic Change*, **68**(3), 257–267.

Pall, P., Aina, T., Stone, D. A., Stott, P. A., Nozawa, T., Hilberts, A. G. J., Lohmann, D., and Allen, M. R. (2011). Anthropogenic greenhouse gas contribution to flood risk in england and wales in autumn 2000. *Nature*, **470**(7334), 382–385.

Palmer, M. A., Liermann, C. A. R., Nilsson, C., Floerke, M., Alcamo, J., Lake, P. S., and Bond, N. (2008). Climate change and the world's river basins: anticipating management options. *Frontiers in Ecology and the Environment*, **6**(2), 81–89.

Paquette, A. and Messier, C. (2010). The role of plantations in managing the world's forests in the anthropocene. *Frontiers in Ecology and the Environment*, **8**(1), 27–34.

Parizek, B. R. and Alley, R. B. (2004). Implications of increased greenland surface melt under global-warming scenarios: ice-sheet simulations. *Quaternary Science Reviews*, **23**(9-10), 1013–1027.

Parker, D. E., Legg, T. P., and Folland, C. K. (1992). A new daily central england temperature series, 1772-1991. *International Journal of Climatology*, **12**(4), 317–342.

Pattyn, F. (2003). A new three-dimensional higher-order thermomechanical ice sheet model: Basic sensitivity, ice stream development, and ice flow across subglacial lakes. *Journal of Geophysical Research-Solid Earth*, **108**(B8), 2382.

Pattyn, F., Huyghe, A., De Brabander, S., and De Smedt, B. (2006). Role of transition zones in marine ice sheet dynamics. *Journal of Geophysical Research-Earth Surface*, **111**(F2), F02004.

Payne, A. J. (1999). A thermomechanical model of ice flow in west antarctica. *Climate Dynamics*, **15**(2), 115–125.

Peltier, W. R. (2009). Closure of the budget of global sea level rise over the grace era: the importance and magnitudes of the required corrections for global glacial isostatic adjustment. *Quaternary Science Reviews*, **28**(17-18), 1658–1674.

Penner, J. E., Xu, L., and Wang, M. (2011). Satellite methods underestimate indirect climate forcing by aerosols. *Proceedings of the National Academy of Sciences*, **108**(33), 13404–13408.

Pfeffer, W. T., Harper, J. T., and O'Neel, S. (2008). Kinematic constraints on glacier contributions to 21st-century sea-level rise. *Science*, **321**(5894), 1340–1343.

Philip, S. Y., Collins, M., van Oldenborgh, G. J., and van den Hurk, B. (2010). The role of atmosphere and ocean physical processes in enso in a perturbed physics coupled climate model. *Ocean Science*, **6**(2), 441–459.

Piani, C., Frame, D. J., Stainforth, D. A., and Allen, M. R. (2005). Constraints on climate change from a multi-thousand member ensemble of simulations. *Geophysical Research Letters*, **32**(23).

Piani, C., Sanderson, B., Giorgi, F., Frame, D. J., Christensen, C., and Allen, M. R. (2007). Regional probabilistic climate forecasts from a multithousand, multimodel ensemble of simulations. *Journal of Geophysical Research-Atmospheres*, **112**(D24).

Pierce, J. R., Weisenstein, D. K., Heckendorn, P., Peter, T., and Keith, D. W. (2010). Efficient formation of stratospheric aerosol for climate engineering by emission of condensible vapor from aircraft. *Geophysical Research Letters*, **37**.

Pomerantz, M., Akbari, H., Berdahl, P., Konopacki, S. J., Taha, H., and Rosenfeld, A. H. (1999). Reflective surfaces for cooler buildings and cities. *Philosophical Magazine B-Physics of Condensed Matter Statistical Mechanics Electronic Optical and Magnetic Properties*, **79**(9), 1457–1476.

Pongratz, J., Reick, C. H., Raddatz, T., Caldeira, K., and Claussen, M. (2011). Past land use decisions have increased mitigation potential of reforestation. *Geophysical Research Letters*, **38**.

Price, S. F., Conway, H., Waddington, E. D., and Bindschadler, R. A. (2008). Model investigations of inland migration of fast-flowing outlet glaciers and ice streams. *Journal of Glaciology*, **54**(184), 49–60.

Pringle, K. J., Carslaw, K. S., Fan, T., Mann, G. W., Hill, A., Stier, P., Zhang, K., and Tost, H. (2012). A multi-model assessment of the efficacy of sea spray geoengineering. *Atmos. Chem. Phys. Discuss.*, **12**(3), 7125–7166.

Quaas, J., Ming, Y., Menon, S., Takemura, T., Wang, M., Penner, J. E., Gettelman, A., Lohmann, U., Bellouin, N., Boucher, O., Sayer, A. M., Thomas, G. E., McComiskey, A., Feingold, G., Hoose, C., Kristjansson, J. E., Liu, X., Balkanski, Y., Donner, L. J., Ginoux, P. A., Stier, P., Grandey, B., Feichter, J., Sednev, I., Bauer, S. E., Koch, D., Grainger, R. G., Kirkevag, A., Iversen, T., Seland, O., Easter, R., Ghan, S. J., Rasch, P. J., Morrison, H., Lamarque, J. F., Iacono, M. J., Kinne, S., and Schulz, M. (2009). Aerosol indirect effects - general circulation model intercomparison and evaluation with satellite data. *Atmospheric Chemistry and Physics*, **9**(22), 8697–8717.

Radic, V. and Hock, R. (2011). Regionally differentiated contribution of mountain glaciers and ice caps to future sea-level rise. *Nature Geoscience*, **4**(2), 91–94.

Ramanathan, V., Crutzen, P. J., Lelieveld, J., Mitra, A. P., Althausen, D., Anderson, J., Andreae, M. O., Cantrell, W., Cass, G. R., Chung, C. E., Clarke, A. D., Coakley, J. A., Collins, W. D., Conant, W. C., Dulac, F., Heintzenberg,

J., Heymsfield, A. J., Holben, B., Howell, S., Hudson, J., Jayaraman, A., Kiehl, J. T., Krishnamurti, T. N., Lubin, D., McFarquhar, G., Novakov, T., Ogren, J. A., Podgorny, I. A., Prather, K., Priestley, K., Prospero, J. M., Quinn, P. K., Rajeev, K., Rasch, P., Rupert, S., Sadourny, R., Satheesh, S. K., Shaw, G. E., Sheridan, P., and Valero, F. P. J. (2001). Indian ocean experiment: An integrated analysis of the climate forcing and effects of the great indo-asian haze. *Journal of Geophysical Research-Atmospheres*, **106**(D22), 28371–28398.

Rasch, P. J., Crutzen, P. J., and Coleman, D. B. (2008a). Exploring the geoengineering of climate using stratospheric sulfate aerosols: The role of particle size. *Geophysical Research Letters*, **35**(2).

Rasch, P. J., Tilmes, S., Turco, R. P., Robock, A., Oman, L., Chen, C. C., Stenchikov, G. L., and Garcia, R. R. (2008b). An overview of geoengineering of climate using stratospheric sulphate aerosols. *Philosophical Transactions of the Royal Society a-Mathematical Physical and Engineering Sciences*, **366**(1882), 4007–4037.

Rasch, P. J., Latham, J., and Chen, C. C. (2009). Geoengineering by cloud seeding: influence on sea ice and climate system. *Environmental Research Letters*, **4**(4).

Rau, G. H. (2008). Electrochemical splitting of calcium carbonate to increase solution alkalinity: Implications for mitigation of carbon dioxide and ocean acidity. *Environmental Science & Technology*, **42**(23), 8935–8940.

Rayner, D., Hirschi, J. J. M., Kanzow, T., Johns, W. E., Wright, P. G., Frajka-Williams, E., Bryden, H. L., Meinen, C. S., Baringer, M. O., Marotzke, J., Beal, L. M., and Cunningham, S. A. (2011). Monitoring the atlantic meridional overturning circulation. *Deep-Sea Research Part Ii-Topical Studies in Oceanography*, **58**(17-18), 1744–1753.

Ricke, K. L., Morgan, M. G., and Allen, M. R. (2010). Regional climate response to solar-radiation management. *Nature Geosci*, **3**(8), 537–541.

Ridgwell, A. (2011). Evolution of the ocean's "biological pump". *Proceedings of the National Academy of Sciences of the United States of America*, **108**(40), 16485–16486.

Ridgwell, A., Singarayer, J. S., Hetherington, A. M., and Valdes, P. J. (2009). Tackling regional climate change by leaf albedo bio-geoengineering. *Current Biology*, **19**(2), 146–150.

Ridley, J. K., Huybrechts, P., Gregory, J. M., and Lowe, J. A. (2005). Elimination of the greenland ice sheet in a high co2 climate. *Journal of Climate*, **18**(17), 3409–3427.

Rignot, E., Bamber, J. L., Van Den Broeke, M. R., Davis, C., Li, Y. H., Van De Berg, W. J., and Van Meijgaard, E. (2008). Recent antarctic ice mass loss from radar interferometry and regional climate modelling. *Nature Geoscience*, **1**(2), 106–110.

Rignot, E., Velicogna, I., van den Broeke, M. R., Monaghan, A., and Lenaerts, J. (2011). Acceleration of the contribution of the greenland and antarctic ice sheets to sea level rise. *Geophys. Res. Lett.*, **38**(5), L05503.

Ritz, C., Fabre, A., and Letreguilly, A. (1997). Sensitivity of a greenland ice sheet model to ice flow and ablation parameters: Consequences for the evolution through the last climatic cycle. *Climate Dynamics*, **13**(1), 11–24.

Robine, J.-M., Cheung, S. L. K., Le Roy, S., Van Oyen, H., Griffiths, C., Michel, J.-P., and Herrmann, F. R. (2008). Death toll exceeded 70,000 in europe during the summer of 2003. *Comptes Rendus Biologies*, **331**(2), 171–178.

Robock, A. (2008). 20 reasons why geoengineering may be a bad idea. *Bulletin of the Atomic Scientists*, **64**(2), 14–+.

Robock, A., Oman, L., Stenchikov, G. L., Toon, O. B., Bardeen, C., and Turco, R. P. (2007). Climatic consequences of regional nuclear conflicts. *Atmospheric Chemistry and Physics*, **7**(8), 2003–2012.

Robock, A., Oman, L., and Stenchikov, G. L. (2008). Regional climate responses to geoengineering with tropical and arctic so2 injections. *Journal of Geophysical Research-Atmospheres*, **113**(D16), D16101.

Robock, A., Marquardt, A., Kravitz, B., and Stenchikov, G. (2009). Benefits, risks, and costs of stratospheric geoengineering. *Geophysical Research Letters*, **36**, 9.

Rodwell, M. J. and Palmer, T. N. (2007). Using numerical weather prediction to assess climate models. *Quarterly Journal of the Royal Meteorological Society*, **133**(622), 129–146.

Roe, G. H. and Baker, M. B. (2007). Why is climate sensitivity so unpredictable? *Science*, **318**(5850), 629–632.

Rougier, J., Sexton, D. M. H., Murphy, J. M., and Stainforth, D. (2009). Analyzing the climate sensitivity of the hadsm3 climate model using ensembles from different but related experiments. *Journal of Climate*, **22**(13), 3540–3557.

Rutt, I. C., Hagdorn, M., Hulton, N. R. J., and Payne, A. J. (2009). The glimmer community ice sheet model. *J. Geophys. Res.*, **114**, F02004.

Sakamoto, T. T., Sumi, A., Emori, S., Nishimura, T., Hasumi, H., Suzuki, T., and Kimoto, M. (2004). Far-reaching effects of the hawaiian islands in the ccsr/nies/frcgc high-resolution climate model. *Geophysical Research Letters*, **31**(17).

Salter, S., Sortino, G., and Latham, J. (2008). Sea-going hardware for the cloud albedo method of reversing global warming. *Philosophical Transactions of the Royal Society a-Mathematical Physical and Engineering Sciences*, **366**(1882), 3989–4006.

Sanderson, B. M. (2011). A multimodel study of parametric uncertainty in predictions of climate response to rising greenhouse gas concentrations. *Journal of Climate*, **24**(5), 1362–1377.

Sanderson, B. M., Knutti, R., Aina, T., Christensen, C., Faull, N., Frame, D. J., Ingram, W. J., Piani, C., Stainforth, D. A., Stone, D. A., and Allen, M. R. (2008a). Constraints on model response to greenhouse gas forcing and the role of subgrid-scale processes. *Journal of Climate*, **21**(11), 2384–2400.

Sanderson, B. M., Piani, C., Ingram, W. J., Stone, D. A., and Allen, M. R. (2008b). Towards constraining climate sensitivity by linear analysis of feedback patterns in thousands of perturbed-physics gcm simulations. *Climate Dynamics*, **30**(2-3), 175–190.

Sanderson, B. M., Shell, K. M., and Ingram, W. (2010). Climate feedbacks determined using radiative kernels in a multi-thousand member ensemble of aogcms. *Climate Dynamics*, **35**(7-8), 1219–1236.

Schar, C., Vidale, P. L., Luthi, D., Frei, C., Haberli, C., Liniger, M. A., and Appenzeller, C. (2004). The role of increasing temperature variability in european summer heatwaves. *Nature*, **427**(6972), 332–336.

Schmidt, H., Alterskjr, K., Bou Karam, D., Boucher, O., Jones, A., Kristjansson, J. E., Niemeier, U., Schulz, M., Aaheim, A., Benduhn, F., Lawrence, M., and Timmreck, C. (2012). Can a reduction of solar irradiance counteract co2-induced climate change? results from four earth system models. *Earth Syst. Dynam. Discuss.*, **3**(1), 31–72.

Schneider, S. H. (2001). What is 'dangerous' climate change? *Nature*, **411**(6833), 17–19.

Schneider, S. H. (2008). Geoengineering: could we or should we make it work? *Philosophical Transactions of the Royal Society a-Mathematical Physical and Engineering Sciences*, **366**(1882), 3843–3862.

Schoof, C. (2006). A variational approach to ice stream flow. *Journal of Fluid Mechanics*, **556**, 227–251.

Schoof, C. (2007). Ice sheet grounding line dynamics: Steady states, stability, and hysteresis. *Journal of Geophysical Research-Earth Surface*, **112**(F3), F03S28.

Screen, J. A. and Simmonds, I. (2010). The central role of diminishing sea ice in recent arctic temperature amplification. *Nature*, **464**(7293), 1334–1337.

Seager, R., Kushnir, Y., Herweijer, C., Naik, N., and Velez, J. (2005). Modeling of tropical forcing of persistent droughts and pluvials over western north america: 1856-2000. *Journal of Climate*, **18**(19), 4065–4088.

Seitz, F. (1958). On the theory of the bubble chamber. *Physics of Fluids*, **1**(1), 2–13.

Seitz, R. (2011). Bright water: hydrosols, water conservation and climate change. *Climatic Change*, **105**(3-4), 365–381.

Serreze, M. C., Walsh, J. E., Chapin, F. S., Osterkamp, T., Dyurgerov, M., Romanovsky, V., Oechel, W. C., Morison, J., Zhang, T., and Barry, R. G. (2000). Observational evidence of recent change in the northern high-latitude environment. *Climatic Change*, **46**(1-2), 159–207.

Shepherd, J., Caldeira, K., Cox, P., Haigh, J., Keith, D., Launder, B., Mace, G., MacKerron, G., Pyle, J., Rayner, S., Redgwell, C., Watson, A., Garthwaite, R., Heap, R., Parker, A., and Wilsdon, J. (2009). Geoengineering the climate: science, governace and uncertainty,. Technical report, The Royal Society.

Singarayer, J. S., Ridgwell, A., and Irvine, P. (2009). Assessing the benefits of crop albedo bio-geoengineering. *Environmental Research Letters*, **4**(4), 8.

Smith, J. B., Schneider, S. H., Oppenheimer, M., Yohe, G. W., Hare, W., Mastrandrea, M. D., Patwardhan, A., Burton, I., Corfee-Morlot, J., Magadza, C. H. D., Fuessel, H. M., Pittock, A. B., Rahman, A., Suarez, A., and van Ypersele, J. P. (2009). Assessing dangerous climate change through an update of the intergovernmental panel on climate change (ipcc) "reasons for concern". *Proceedings of the National Academy of Sciences of the United States of America*, **106**(11), 4133–4137.

Solomon, S., Qin, D., Manning, M., Chen, Z., Marquis, M., Averyt, K., Tignor, M., and Miller, H. (2007). *Climate Change 2007: The Physical Science Basis*, page 996 pp. Cambridge University Press, Cambridge.

Stainforth, D. A., Aina, T., Christensen, C., Collins, M., Faull, N., Frame, D. J., Kettleborough, J. A., Knight, S., Martin, A., Murphy, J. M., Piani, C., Sexton, D., Smith, L. A., Spicer, R. A., Thorpe, A. J., and Allen, M. R. (2005). Uncertainty in predictions of the climate response to rising levels of greenhouse gases. *Nature*, **433**(7024), 403–406.

Steffen, W., Crutzen, P. J., and McNeill, J. R. (2007). The anthropocene: Are humans now overwhelming the great forces of nature. *Ambio*, **36**(8), 614–621.

Stenke, A., Grewe, V., and Ponater, M. (2008). Lagrangian transport of water vapor and cloud water in the echam4 gcm and its impact on the cold bias. *Climate Dynamics*, **31**(5), 491–506.

Stothers, R. B. (1984). The great tambora eruption in 1815 and its aftermath. *Science*, **224**(4654), 1191–1198.

Stott, P. A., Stone, D. A., and Allen, M. R. (2004). Human contribution to the european heatwave of 2003. *Nature*, **432**(7017), 610–614.

Strand, S. E. and Benford, G. (2009). Ocean sequestration of crop residue carbon: Recycling fossil fuel carbon back to deep sediments. *Environmental Science & Technology*, **43**(4), 1000–1007.

Stuber, N., Ponater, M., and Sausen, R. (2005). Why radiative forcing might fail as a predictor of climate change. *Climate Dynamics*, **24**(5), 497–510.

Taha, H., Konopacki, S., and Gabersek, S. (1999). Impacts of large-scale surface modifications on meteorological conditions and energy use: A 10-region modeling study. *Theoretical and Applied Climatology*, **62**(3-4), 175–185.

Tang, B. X. (1994). A theorem for selecting oa-based latin hypercubes using a distance criterion. *Communications in Statistics-Theory and Methods*, **23**(7), 2047–2058.

Taylor, C. M., Lambin, E. F., Stephenne, N., Harding, R. J., and Essery, R. L. H. (2002). The influence of land use change on climate in the sahel. *Journal of Climate*, **15**(24), 3615–3629.

Tebaldi, C., Hayhoe, K., Arblaster, J. M., and Meehl, G. A. (2006). Going to the extremes. *Climatic Change*, **79**(3-4), 185–211.

Terray, L. and Cassou, C. (2002). Tropical atlantic sea surface temperature forcing of quasi-decadal climate variability over the north atlantic-european region. *Journal of Climate*, **15**(22), 3170–3187.

Thordarson, T. and Self, S. (2003). Atmospheric and environmental effects of the 1783-1784 laki eruption: A review and reassessment. *Journal of Geophysical Research-Atmospheres*, **108**(D1).

Tilmes, S., Muller, R., and Salawitch, R. (2008). The sensitivity of polar ozone depletion to proposed geoengineering schemes. *Science*, **320**(5880), 1201–1204.

Tilmes, S., Garcia, R. R., Kinnison, D. E., Gettelman, A., and Rasch, P. J. (2009). Impact of geoengineered aerosols on the troposphere and stratosphere. *Journal of Geophysical Research-Atmospheres*, **114**, 22.

Tol, R. S. J., Bohn, M., Downing, T. E., Guillerminet, M. L., Hizsnyik, E., Kasperson, R., Lonsdale, K., Mays, C., Nicholls, R. J., Olsthoorn, A. A., Pfeifle, G., Poumadere, M., Toth, F. L., Vafeidis, A. T., Van der Werff, P. E., and Yetkiner, I. H. (2006). Adaptation to five metres of sea level rise. *Journal of Risk Research*, **9**(5), 467–482.

Trenberth, K. E. (1997). The definition of el nino. *Bulletin of the American Meteorological Society*, **78**(12), 2771–2777.

Trenberth, K. E. (2011). Changes in precipitation with climate change. *Climate Research*, **47**(1-2), 123–138.

Trenberth, K. E. and Caron, J. M. (2000). The southern oscillation revisited: Sea level pressures, surface temperatures, and precipitation. *Journal of Climate*, **13**(24), 4358–4365.

Trenberth, K. E. and Dai, A. (2007). Effects of mount pinatubo volcanic eruption on the hydrological cycle as an analog of geoengineering. *Geophysical Research Letters*, **34**(15).

Trenberth, K. E., Stepaniak, D. P., and Caron, J. M. (2002). Interannual variations in the atmospheric heat budget. *Journal of Geophysical Research-Atmospheres*, **107**(D7-8).

Twomey, S. (1977). Influence of pollution on shortwave albedo of clouds. *Journal of the Atmospheric Sciences*, **34**(7), 1149–1152.

Uddin, M. N. and Marshall, D. R. (1988). Variation in epicuticular wax content in wheat. *Euphytica*, **38**(1), 3–9.

van den Broeke, M., Bamber, J., Ettema, J., Rignot, E., Schrama, E., van de Berg, W. J., van Meijgaard, E., Velicogna, I., and Wouters, B. (2009). Partitioning recent greenland mass loss. *Science*, **326**(5955), 984–986.

Vaughan, N. E., Lenton, T. M., and Shepherd, J. G. (2009). Climate change mitigation: trade-offs between delay and strength of action required. *Climatic Change*, **96**(1-2), 29–43.

Victor, D. G. (2008). On the regulation of geoengineering. *Oxford Review of Economic Policy*, **24**(2), 322–336.

Virgoe, J. (2009). International governance of a possible geoengineering intervention to combat climate change. *Climatic Change*, **95**(1-2), 103–119.

Wang, H., Rasch, P. J., and Feingold, G. (2011). Manipulating marine stratocumulus cloud amount and albedo: a process-modelling study of aerosol-cloud-precipitation interactions in response to injection of cloud condensation nuclei. *Atmospheric Chemistry and Physics*, **11**(9), 4237–4249.

Watson, R., Noble, I., Bolin, B., Ravindranath, N., Verardo, D., and Dokken, J. (2000). Special report: Land use, land-use change, and forestry. Technical report, Intergovernmental Report on Climate Change.

Weaver, A. J., Eby, M., Wiebe, E. C., Bitz, C. M., Duffy, P. B., Ewen, T. L., Fanning, A. F., Holland, M. M., MacFadyen, A., Matthews, H. D., Meissner, K. J., Saenko, O., Schmittner, A., Wang, H. X., and Yoshimori, M. (2001). The uvic earth system climate model: Model description, climatology, and applications to past, present and future climates. *Atmosphere-Ocean*, **39**(4), 361–428.

Weaver, A. J., Zickfeld, K., Montenegro, A., and Eby, M. (2007). Long term climate implications of 2050 emission reduction targets. *Geophysical Research Letters*, **34**, L19703.

Wigley, T. M. L. (2006). A combined mitigation/geoengineering approach to climate stabilization. *Science*, **314**(5798), 452–454.

Wigley, T. M. L. and Raper, S. C. B. (2005). Extended scenarios for glacier melt due to anthropogenic forcing. *Geophysical Research Letters*, **32**(5).

Wilson, M. F. and Henderson-Sellers, A. (1985). A global archive of land cover and soils data for use in general-circulation climate models. *Journal of Climatology*, **5**(2), 119–143.

Wiscombe, W. J. and Warren, S. G. (1980). A model for the spectral albedo of snow .1. pure snow. *Journal of the Atmospheric Sciences*, **37**(12), 2712–2733.

Wu, X. Q. (2002). Effects of ice microphysics on tropical radiative-convective-oceanic quasi-equilibrium states. *Journal of the Atmospheric Sciences*, **59**(11), 1885–1897.

Xu, K. M. and Randall, D. A. (1999). A sensitivity study of radiative-convective equilibrium in the tropics with a convection-resolving model. *Journal of the Atmospheric Sciences*, **56**(19), 3385–3399.

Yokohata, T., Webb, M. J., Collins, M., Williams, K. D., Yoshimori, M., Hargreaves, J. C., and Annan, J. D. (2010). Structural similarities and differences in climate responses to co(2) increase between two perturbed physics ensembles. *Journal of Climate*, **23**(6), 1392–1410.

Yoshimura, J., Sugi, M., and Noda, A. (2006). Influence of greenhouse warming on tropical cyclone frequency. *Journal of the Meteorological Society of Japan*, **84**(2), 405–428.

Zeman, F. (2007). Energy and material balance of co2 capture from ambient air. *Environmental Science & Technology*, **41**, 7558–7563.

Appendix A

A.1 IRVINE, P. & RIDGWELL, A. 2009. 'Geoengineering' - taking control of our planet's climate. Science Progress, 92, 139-162.

This appendix presents a review of geoengineering for a general science audience. Some sections of this work were adapted and included in Chapter 1. I reviewed the material for the study and prepared a draft of the manuscript. Prof. Andy Ridgwell and I produced or reworked the figures included in the paper. Prof. Andy Ridgwell provided input on the structure and wording of the text, changing the language to be more suitable for a general audience. The final preparations and corrections to the manuscript were arranged by me before submission. The published review is available here:

DOI:10.3184/003685009X461495

Appendix B

B.1 SINGARAYER, J. S., RIDGWELL, A. & IRVINE, P. 2009. Assessing the benefits of crop albedo bio-geoengineering. Environmental Research Letters, 4, 8.

This study explores the climate effects of crop albedo geoengineering to determine whether it would help to ameliorate the effects of global warming. It is found that although there is a small global effect of crop albedo geoengineering there is a substantial regional cooling which is greatest in summer in Europe and greatest in winter in South-East Asian regions. A positive impact on soil moisture and net primary productivity is found in Europe. There are difficulties in detecting and verifying the climate signal due to interdecadal variability in North Atlantic sea-ice cover and sea surface temperatures. These interdecadal variability results are presented and discussed in Section 2.4. Overall it is concluded that crop albedo geoengineering may play a significant role in mitigating regional climate change impacts.

This study was conceived and directed by Dr. Joy Singarayer and Prof. Andy Ridgwell. Dr. Joy Singarayer led the modelling, analysis and writing of the study. Dr. Joy Singarayer and Prof. Andy Ridgwell jointly prepared the text of the final submission. I contributed the interdecadal variability analysis work, proof-read the manuscript and assisted in answering reviewer's comments. The published study is available here:

DOI:10.1088/1748-9326/4/4/045110

Appendix C

C.1 IRVINE, P. J., SRIVER, R. L. & KELLER, K. 2012. Tension between reducing sea-level rise and global warming through solar radiation management. Nature Clim. Change, 2, 2.

If sunshade geoengineering is deployed there are many controls over how this could be done; this appendix presents a study which analysed of the consequences of these choices on the global-mean surface air temperature (SAT) and Sea-level rise (SLR). This Appendix presents the results of a study that I was first author on that dealt with SAT and SLR responses to sunshade geoengineering (Irvine *et al.*, 2012). A number of sunshade geoengineering scenarios with different phase-in rates, forcing strengths, and phase-out rates were studied using the UVic Earth system model of intermediate complexity (EMIC) (Weaver *et al.*, 2001). The results indicate that halting sea-level rise would require a faster phase-in rate and a greater forcing strength than would be required to halt the temperature rise. It is also found that phasing out sunshade geoengineering can result in a rapid warming of the planet and implies that there a long commitment to sunshade geoengineering is necessary. These results suggest that there may be tensions between the goals to mitigate SLR and SAT over which is the best way to implement SRM geoengineering and the exposure to the risk of failure of geoengineering.

The project goals and the specific focus of the paper were decided by Klaus Keller, Ryan Sriver and I in discussion. I conducted the simulations, analysis and produced the figures. The first draft was written by me but all authors assisted in editing the text. Two anonymous reviewers are to be thanked for their comments and suggestions. I arranged the final preparation of the manuscript and submission.

DOI:10.1038/nclimate1351